Doctoral Thesis

Aspects of some physical processes around compact objects in theories of gravity

By
Saraswati Devi
Roll No: 196121027
Department of Physics
Indian Institute of Technology Guwahati

Supervisor: **Dr. Sayan Chakrabarti**

A thesis submitted in fulfillment of the requirements for the degree of Doctor of Philosophy in the Department of Physics at Indian Institute of Technology Guwahati

May 6, 2025

भारतीय प्रौद्योगिकी संस्थान गुवाहाटी
Indian Institute of Technology Guwahati

Saraswati Devi
Research Scholar
Roll No: 196121027
Department of Physics
IIT Guwahati
Guwahati, India
email:sdevi@iitg.ac.in

Declaration

I hereby declare that the work presented in the thesis entitled ***"Aspects of some physical processes around compact objects in theories of gravity"*** is a record of the original work carried out by me under the supervision of Dr. Sayan Chakrabarti at the Department of Physics, Indian Institute of Technology Guwahati, India. The thesis has not been submitted anywhere else for any degree. Works presented in the thesis are all my own unless referenced to the contrary in the thesis.

Saraswati Devi

Saraswati Devi

Date: May 6, 2025

भारतीय प्रौद्योगिकी संस्थान गुवाहाटी
Indian Institute of Technology Guwahati

Dr. Sayan Chakrabarti
Associate Professor
Department of Physics
IIT Guwahati
Guwahati, India
email:sayan.chakrabarti@iitg.ac.in

Certificate

It is to certify that the work incorporated in the thesis entitled "***Aspects of some physical processes around compact objects in theories of gravity***", submitted by Ms. ***Saraswati Devi*** (Roll No - 196121027), a PhD student in the Department of Physics, Indian Institute of Technology Guwahati, in fulfillment of the requirements for the award of the degree of ***Doctor of Philosophy*** embodies original research work carried out by the student under my supervision and has not been submitted elsewhere for the award of any other degree.

Sayan Chakrabarti

Date: May 6, 2025

भारतीय प्रौद्योगिकी संस्थान गुवाहाटी
Indian Institute of Technology Guwahati

Abstract

Although Einstein's theory of general relativity (GR) is regarded as one of the most successful theories for comprehending gravity both from an experimental as well as from theoretical perspective, numerous pathologies are known to exist in the theory. Among those, the most significant one is the existence of spacetime singularities, which cannot be avoided in GR. The fact that GR is plagued with singularities, present unique mathematical challenges as it does not represent any physical object in nature, neither is it classically avoidable. A number of alternatives to GR are proposed with a hope to remove such pathologies and to also provide hint about the regimes of spacetimes where physics is not clearly understood at present. Such alternatives are expected to reduce to GR as a low energy effective theory. On the other hand, the hunt for unravelling the mysteries of the universe is an unending process and it provides us with a number of platforms where the theories of gravity can be put to test to check their validity. Among them, black holes (BH) provide a perfect test bed to explore and understand different physical processes as well as different theories of gravity. Other compact objects like naked singularities (NS), wormholes, etc. are also further helpful in carrying out the above investigations. Such compact spacetimes have been studied in literature in different theories of gravity in an attempt to find observational signatures or any distinctive features, if any. The progress in the observational arena, both in the gravitational and electromagnetic channel via the gravitational wave (GW) detectors and the event horizon telescope (EHT) have provided indirect and direct ways to probe the universe and has further pushed the frontiers of research in alternative theories and compact objects. The present thesis is aligned with this area and tries to focus in brief on the study of some aspects of the physical processes like shadows, quasinormal modes (QNMs), superradiance and stability of solutions in two different types of alternative theories of gravity: the novel four dimensional Einstein-Gauss-Bonnet ($4D$-EGB) gravity and the Loop Quantum Gravity (LQG). The former one contains higher order curvature corrections in the action, in addition to the Einstein-Hilbert term, while, the later was developed with a view to circumvent the loopholes of GR, such as notion of discreteness, thereby, rendering the spacetime regular. The QNMs and greybody factors of asymptotically de Sitter $4D$-EGB BH have been studied by the perturbation technique using test scalar, electromagnetic and Dirac fields. The parameter of the $4D$-EGB theory modifies these quantities, thereby providing us with an opportunity to check for these modifications in the observed data and comment on the nature of the compact object or the theory of gravity. The NS solution in $4D$-EGB theory has also been explored and its stability has been checked. Since it acts as a BH mimicker for various reasons, the thesis discusses the distinguishable features exhibited by the NS solution in $4D$-EGB theory in the time evolution of the test fields against which the response of the background has been studied. The presence of echoes in the time domain evolution of the test fields in case of the NS solution was found, which is a distinctive feature as it is not expected in case of the BH solution in this theory. It was also found that such spacetimes are unstable against perturbation by test scalar, electromagnetic and Dirac fields, thereby respecting the cosmic censorship conjecture

and restricting the parameter space of the Gauss-Bonnet coupling constant. On the other hand, in order to understand the implications of quantum parameters on some astrophysical processes, the thesis discussed the shadows and superradiance in a quantum-corrected BH in the domain of LQG and found that even if the effects at present, are not within the domain of any observational techniques, interesting physical insights could still be found to take place at the scale of Planckian regimes, which might help in understanding the primordial BHs. The studies discussed in the thesis are important in understanding the nature of effects due to modifications in the theories of gravity, thereby providing a window to understand the nature of the background spacetime and check for distinctive observational features, if any.

Keywords: *general relativity, Gauss-Bonnet, quasinormal modes, shadows, naked singularities, echoes, stability, super-radiance*

Acknowledgements

Since childhood, I have always been fascinated by the sky. As I reached high school, I went through a couple of books by Stephen Hawking and kept ruminating on the origin of the universe, what would exist without it, how gravity behaves, what are these mysterious objects like Black holes, and many other things, some of which (my thoughts) do not make sense to me even today. My interest in Physics was further deepened by the teachings of my Physics tutor in high school, the Late Amarendra Dey Sir, to whom, I owe a debt of gratitude and it was because of him that I was encouraged to pursue Physics Honors during my Bachelor's degree. Consequently to have a better understanding and to taste more of my thoughts I took a specialization in this area during my Masters and got to learn the basics of this subject in the most fundamental way from Dr. Sanjeev Kalita, Assistant Professor, Gauhati University. The way he taught in the classroom, explained difficult topics in layman's language, planted the seeds of curiosity in our minds to understand the cosmos which further ignited my interest in the field of research which finally led me to embrace the path of Ph.D. thus landing me here in IIT Guwahati. The journey of a research life is never easy, it comes with a package full of ups and downs. One should not be daunted by the exhausting times rather collect the experiences and keep advancing. Despite all the hindrances and setbacks at certain moments, my PhD journey has been a successful and memorable one due to the encouragement, support and mentoring of some incredible people around me. I want to thank these people and give them due acknowledgement for their contributions and support throughout the journey of my PhD work.

First and foremost I would like to express my deepest gratitude to my PhD supervisor Dr. Sayan Chakrabarti for providing me with such a nice opportunity to work under his proficient guidance. He has always been compassionate and was always ready to clear my doubts even in case of small queries. His breadth of knowledge, enthusiasm and abundant experience in the subject have inspired me in both my daily life and my academic pursuits. I am very much grateful for his guidance, patience, encouragement and support throughout my research work and for allowing me the freedom to find how I work best. It is because of the information and instructions he provided that I was able to avail additional academic opportunities like attending various schools, conferences and workshops, which, in many ways have greatly enhanced my knowledge, research skills, and comprehension of the ongoing work in my field of study.

I would also like to thank Dr. Bibhas Ranjan Majhi for his useful suggestions, fruitful discussions and valuable comments over regular meetings throughout my work in Chapter (4) which played a vital role in accomplishing my Ph.D. thesis work. Your expertise was invaluable in getting the search up and running. Your immense knowledge, profuse experience and dedication towards your work have been an inspiration for me.

I would also like to thank my other Doctoral committee members, Dr. Debaprasad Maity (Chairperson) and Dr. Sovan Chakraborty for providing valuable suggestions, feedback and scientific opinions while assessing presentations of my

Doctoral work which helped in further refining my knowledge and content of my thesis.

Thanks to Mr. Abhinove Nagarajan S., ex-M.Sc. student at IIT Guwahati and presently a PhD Researcher at the University of Sheffield.). I learnt a lot from you while working on our project on shadows. I will miss the late-night discussions and codings we had in the library.

Thanks to Dr. Avijit Chowdhury, a postdoctoral fellow at IIT Guwahati for useful discussions with various aspects of the study throughout my work on naked singularities. You were always very patient in answering my queries whenever I had a doubt anytime, anywhere. I appreciate your instant responses to my emails and calls in spite of your busy days.

Thanks to my seniors Mr. Rajesh Karmakar and Dr. Sumit Dey for the useful and fine discussions on some topics that helped me really understand some underlying concepts related to my work.

Thanks to my sister Dr. Lakhi Sharma for always being there during my bad days. You have always inspired me in every aspect of my life and I must say that I have been able to reach upto this place in my life mainly because of your constant love, support, care and motivation.

To my family, where I always find unconditional support, I cannot thank enough in words. Of course, peace of mind is important when doing research but I am characterised by extreme mood swings. At these times there were only a few people apart from my family I could rely on. Thanks to Gyandhriti, Sagarika, Pranab, Shyam (patting on my shoulder for having friends like you – you are my family members too) for always being able to put up with my continuous non-sense, and still smile for me. Thanks for always believing in me, encouraging me to follow my dreams and always being there no matter why, what and when.

It is very natural to get stressed and exasperated at certain times during one's PhD life owing to failures at the workplace or other bureaucratic issues. To keep me sane during this journey I have been lucky enough to have batchmates Anupam, Shafeeque, Alolika, Esha, Amalika, Sonali, Gargi and Pooja who have always been reassuring. Thanks for your love, encouragement and counselling to overcome occasional pessimism and chilling out during bored times. I will miss the late-night walks, "*addaaas and gappppes*".

It would be hard to mention everyone on the long list of persons who have influenced my work, but I am incredibly grateful to them all since, despite many challenges, my doctoral path has been amazing because of them. Above all, earning a PhD is a roller coaster trip with highs and lows as well as WOW moments. It's not a walk in the park. It teaches self-motivation, autonomous creative thought, and time management, so learning should continue to advance. Finally, I want to express my gratitude to the Almighty for giving me the wisdom, capacity, and endurance to start this trip to persist and accomplish it satisfactorily.

I love you all!

I will always keep pushing myself to progress more and gain more knowledge in the journey of research.

List of Publications

(1) **Quasinormal modes and greybody factors of the novel four dimensional Gauss–Bonnet black holes in asymptotically de Sitter space time: scalar, electromagnetic and Dirac perturbations**

Saraswati Devi, Rittick Roy and Sayan Chakrabarti

Eur. Phys. J. C **80** *no.8, 760(2020)* [arXiv: 2004.14935 [gr-qc]]

(2) **Naked singularity in 4D Einstein-Gauss-Bonnet novel gravity: Echoes and instability**

Avijit Chowdhury, **Saraswati Devi** and Sayan Chakrabarti

Phys. Rev. D ***106****, no.2, 024023 (2022)* [arXiv: 2202.13698 [gr-qc]].

(3) **Shadow of quantum extended Kruskal black hole and its superradiance property**

Saraswati Devi, Abhinove Nagarajan S., Sayan Chakrabarti and Bibhas Ranjan Majhi

Phys. Dark Univ. ***39****, 101173 (2023)* [arXiv: 2105.11847 [gr-qc]].

Contents

List of Figures

List of Tables

List of Symbols

- G - Gravitational constant
- c - Speed of light
- $h = 2\pi\hbar$ - Planck's constant
- r_* - Tortoise coordinate
- α - Gauss-Bonnet coupling constant
- $\mathcal{G}$ - Gauss-Bonnet combination term
- Λ - Cosmological constant
- γ_l - Greybody factor
- R - Reflection coefficient
- I - Incident coefficient
- T - Transmission coefficient
- λ - Affine parameter
- $\tilde{\gamma}$ - Barbero-Immirzi parameter
- $\wp$ - Lyapunov exponent
- $\mathcal{Q}$ - Carter's constant
- ℓ_{Pl} - Planck's length

Notations and conventions

We adopt the metric signature $(-,+,+,+)$ and work in $D = 4$ spacetime dimensions. The bulk spacetime indices are designated by the Greek alphabets $\mu, \nu, \alpha, \beta \cdots$.

भारतीय प्रौद्योगिकी संस्थान गुवाहाटी
Indian Institute of Technology Guwahati

List of Abbreviations

- BH - Black Hole
- GR - General Relativity
- GW - Gravitational Wave
- QNM - Quasinormal Mode
- QNF - Quasinormal Frequency
- NS - Naked singularity
- AOS - Ashtekar-Olmedo-Singh
- LQG - Loop Quantum Gravity
- EGB - Einstein-Gauss-Bonnet
- 4D-EGB - Four dimension Einstein-Gauss-Bonnet
- LIGO - Laser Interferometer Gravitational-Wave Observatory
- CFT - Conformal Field Theory
- QFT - Quantum field theory
- AdS - Anti-de Sitter
- KAGRA - Kamioka Gravitational Wave Detector
- EHT - Event Horizon Telescope
- WKB - Wentzel–Kramers–Brillouin
- ADM - Arnowitt–Deser–Misner
- NJA - Newman-Janis Algorithm

भारतीय प्रौद्योगिकी संस्थान गुवाहाटी
Indian Institute of Technology Guwahati

Dedicated to my family . . .

भारतीय प्रौद्योगिकी संस्थान गुवाहाटी
Indian Institute of Technology Guwahati

Objective and chapter-wise outline of the thesis:

The study of black holes (BH) provides deep intuitions about the core concepts of gravity. It is the simplest object described by a minimum number of parameters and therefore, sometimes referred to as the hydrogen atom of General Relativity (GR) (see [1] and references therein). Lot of research had been and presently being done on this very active area of BH physics. In particular, topics like the motion of particles around BHs, gravitational waves (GW) from BH-BH or BH-neutron star mergers, BH shadow, BH perturbation, BH thermodynamics, quantum aspects of BHs are the focus areas of research nowadays. In this context, a part of this thesis focuses on BH perturbation theory. The perturbation technique provides an excellent tool to analyse different alternative theories of gravity going beyond GR. Different processes, such as quasinormal modes (QNMs), greybody factors, shadows, super-radiance, stability, and echoes can be studied in the context of the solutions to these alternative theories to uncover new aspects of our universe's fundamental structure.

Below, we briefly describe the astrophysical processes that are the subject of our work. A detailed discussion on these processes as well as on the different alternative gravity backgrounds discussed in this thesis will be provided later in chapter (1).

Quasinormal modes are often associated with compact objects like BHs or neutron stars, while they also arise in a variety of other physical systems like waveguides, optical fibers etc. However, for the purpose of this thesis, we will concentrate on compact objects. It is known that the ringing part of a binary merger event is dominated by QNMs. This part of the GW signal emitted by the perturbed geometry has been studied extensively in the literature [2, 3]. The QNMs allow us not only to validate a theory of gravity but also to gather information about the intrinsic parameters of a BH. Such modes reflect the imprints of the underlying gravitational theory and are crucial for interpreting the stability and dynamics of BHs. QNMs of BHs and other extreme compact objects are widely studied as they carry unique information about the parameters of these objects. Despite their classical origin, it was found that QNMs also may provide a hint into the quantum nature of the BHs, in turn shedding some light on the quantum nature of gravity [4], which is so far not very well understood. On the other hand, the concept of greybody factors [5, 6] is essential for calculating the spectrum of the emitted radiation, and therefore directly probing Hawking's theory for BH thermodynamics. Another important signature apart from the QNMs, expected to be found in the GW signal arising from certain specific exotic compact objects (ECO) is echo. ECOs are extremely dense and compact theoretical astrophysical objects characterized by the absence of an event horizon or having unusual properties upon comparison with BHs that deviate from the predictions of GR. ECOs like gravastars, boson stars, wormholes, fuzzballs and others, offer horizonless alternatives to BHs. They hold the promise to test whether there are true analogues for classical horizons or not such as a reflective or nearly absorptive surfaces in case of gravastars, boson stars, or fuzzballs that imitate a horizon's behavior without fully trapping signals or information. The study

of echoes can hint at the nature of new physics expected to be present in the vicinity of an event horizon of a BH or near a naked singular (NS) spacetime. They also can serve as a window to understand quantum gravity effects as well as probe into the nature of ECOs [7]. A part of this thesis is dedicated to the study of QNMs, greybody factors [8] and echoes [9] related to a particular alternative theory of gravity, known as the novel $4D$-Einstein-Gauss-Bonnet ($4D$-EGB) gravity [10].

Shadows are another observational feature that one can rely on to gather information about the different types of compact objects [11, 12]. They serve as an important tool to distinguish between different types of BHs from each other (thereby confronting standard GR with alternative theories of gravity), and also for distinguishing BHs from BH mimickers [13] like wormholes, NSs, boson stars etc., that can sometimes mimic the shadow of a BH.

Super-radiance is another phenomenon, that has recently gained renewed interest with the ongoing advancement in the electromagnetic and GW detection facilities [14]. In this process, waves are amplified upon scattering by a rotating BH, which can induce instabilities and promote the growth of test fields that provide a unique avenue to test different gravity theories. Such advancements in the observational arena have elevated the searches for direct evidence of BH super-radiance, thus providing a new tool to test gravitational theories as well as particle physics in curved spacetime. In our work [15], we have extensively studied the shadow and super-radiance properties of a quantum gravity motivated BH solution [16].

Checking the stability of any background spacetime under perturbation is a must before carrying out any realistic astrophysical studies in that particular spacetime. Together, the study of QNMs, greybody factors, super-radiance, and echoes can shed light on the perturbative stability of a background spacetime on one hand and the study of shadows, on the other hand, can provide important information about testing the boundaries of our current understanding of gravity, potentially revealing new physics at astrophysical scales. The thesis explores the effects that will be pronounced on the QNMs, greybody factors, shadow and super-radiance in two different theories of gravity - the novel $4D$-EGB theory and Loop Quantum Gravity (LQG). It is expected that the presence of the Gauss-Bonnet coupling term in the case of $4D$-EGB theory and the quantum parameters in the case of LQG will modify the quasinormal frequencies (QNFs), greybody factors, shadow contour and super-radiance amplification factors. Thus throughout the thesis, our main objective has been to probe those aspects of physical processes for which one can verify a particular theory of gravity with the data provided by observations. Such studies are further motivated by the fact that they can also help put constraints on the parameters of the alternative theories of gravity. The entire thesis is divided into five chapters including the introduction and conclusion along with the future outlooks:

- **Chapter 1**

  In chapter (1), we provide the introduction and the motivation leading to the thesis work. This chapter explains in brief the status of Einstein's theory of gravity and its success in explaining plethora of observations and provides a brief introduction to the different background alternative theories of gravity along with the different astrophysical processes around the solutions of these

theories. The methodologies adopted to compute various quantities have also been briefly mentioned in this chapter.

- **Chapter 2**

Chapter (2) of the thesis explores the novel $4D$-EGB gravity obtained by rescaling the Gauss–Bonnet coupling constant α as $\frac{\alpha}{D-4}$. Consequently, flurry of works followed since its proposal by Glavan and Lin [10]. This theory in four spacetime dimensions, defined as a $D \to 4$ limit of the higher dimensional Gauss-Bonnet theory at the level of equations of motion admits BH solutions in asymptotically flat and (anti)-de Sitter spacetimes. While most of the works in this area have focused on constructing different BH solutions, and the consistency of the theory, not much effort has gone into figuring out the QNMs of spherically symmetric BHs (particularly in non-asymptotically flat spacetimes) with a few exceptions [17–20]. Our aim is to fill up this gap in the literature by studying the QNMs of spherically symmetric BHs in novel $4D$-EGB gravity in asymptotically de Sitter spacetime. Towards this direction, in this chapter, we have studied the low-lying QNMs of scalar, electromagnetic and Dirac perturbations and greybody factors of a spherically symmetric BH in novel $4D$-EGB gravity in asymptotically dS spacetime using the third order WKB approximation as well as Padé approximation, as an improvement over WKB. We figure out the effect of α and the cosmological constant Λ on the real and imaginary parts of the QNM frequencies. We also study the greybody factors and eikonal limits in the above background for all the three different types of perturbations. It is seen that the presence of α tends to alter the values of the QNMs as compared to GR. It is to be noted that our analysis does not give preference to any particular version of the consistent $4D$-EGB theory and, as such, can be regarded as more general. More details about the limitations of the regularization scheme used in the original work [10] and the procedure to overcome it, is provided in chapter (1). A brief overview of QNMs and the WKB and Padé method that we have used to compute the QNMs has also been provided in chapter (1) before discussing the work.

- **Chapter 3**

Chapter (3) discusses an NS solution in the novel $4D$-EGB theory of gravity and attempts to answer the question, "Whether such a solution is astrophysically viable or not?". It is seen that for large values of the Gauss-Bonnet coupling constant α, we get an asymptotically flat, static, spherically symmetric NS solution. If such solutions exist, then the question that follows is "What are the different distinct signatures which NS solutions in novel $4D$-EGB gravity have, that can help distinguish them from BHs in the same theory?". To seek answers to these questions, we have checked the stability and response of such a background under scalar, electromagnetic and Dirac perturbations by studying the time domain evolution of these test fields. We found that close to the singularity, the potential diverges for an NS, unlike the case of a BH. Also for $l = 1$ modes of scalar, electromagnetic perturbation, and $l = 0, 1$ modes of Dirac perturbation, the time-domain profiles give rise

to distinct echoes. Such echoes are not expected for the case of a BH in this theory, because the effective potential of the BH background is not suitable to give rise to echoes. However, as the coupling constant increases, the echoes align, and the QNM structure of the $4D$-EGB NS spacetime becomes prominent. It was also observed that for higher values of the multipole number l, the spacetime becomes unstable, thereby restricting the parameter space of the coupling parameter α.

- **Chapter 4**

LQG is one of the attempts to formulate a quantum theory of gravity that tries to overcome the difficulties faced by GR and gives way to solutions free from singularities. Chapter (4) briefly highlights one such quantum-corrected BH solution first proposed by Ashtekar, Olmedo and Singh (AOS BH) [16, 21, 22]. We then make an effort to see what role the quantum parameters play, or, how its effect is pronounced on any astrophysical phenomenon taking place around such AOS BH. For this, we study the effect of the quantum parameters on the shadow and super-radiance in this background. For the first time we have constructed the rotating version of the AOS BH solution using the modified Newman-Janis Algorithm (NJA) [23, 24] and studied the shadow contour for the rotating and the non-rotating case. The quantum parameters are found to modify the contours of the shadow in both cases when compared to their counterparts in GR i.e., Kerr and Schwarzschild BH respectively. The super-radiance phenomenon has also been studied in the LQG-motivated rotating AOS BH solution and the quantum parameters are found to modify the super-radiance amplification factors and the angular velocity of the horizon. We observe that the quantum effects are found to be more pronounced for smaller masses and extremely rotating BHs. Thus, the LQG-inspired corrections can provide a noticeable effect only when the BH is of the order of Planck size. Thus, with the present observational techniques, in all practical situations, the quantum effects shall remain non-detectable. Nevertheless, new physics can appear at different length scales in the theory. Having said this from the theoretical perspective, the shadows and super-radiance at Planck scales have been investigated in this chapter. On the other hand, the microscopic BHs are important at the primordial level. Therefore, understanding these LQG-inspired BHs might be relevant in understanding a few important aspects of the inflationary era during the early stages of our universe.

- **Chapter 5**

We dedicate the final chapter (5) of our thesis to the possible extensions of the work related to the thesis as well as we provide some more future directions. We have also highlighted several important conclusions related to our work.

Chapter 1

Introduction

Einstein's General Theory of Relativity to date is the most accepted theory of gravity. The field equations provide the correct modern description of the macroscopic behavior of spacetime. At the same time, it is the most successful theory of gravity that correctly predicts and explains a significant portion of observations starting from solar system scales to the astrophysical [25] as well as cosmological scales [26]. Starting from perihelion precession of Mercury at the solar system scale to the observation of the black hole (BH) image by the Event Horizon Telescope (EHT) [27], from the generation and propagation of gravitational waves (GW) [28] to the cosmic expansion and structure formation at cosmological scales [29], General Relativity (GR) has remained a consistent theory altogether. It is only at the strong field regime and at the quantum level that GR lacks propriety. However, no consistent method of connecting the macroscopic theory of GR to a quantum field theory (QFT) exists in the literature as yet. Such a unification is believed to help resolve some of the long-standing pathologies that GR encompasses. It is well known that GR predicts spacetime singularities [30] and they do have mathematical problems of their own, as the laws of physics break down at the singularities. This problem is probably the outcome of the fact that GR does not take into account the quantum nature of gravity [31]. On another front, the shortcomings of GR have been brought to light by the 'dark universe' scenario. On one hand, there have been evidence that for gravity to comply with Einstein's field equations, the presence of a vast amount of 'dark matter' is required in galaxies [32, 33] and on the other, 'dark energy' is necessary to explain the universe's accelerated expansion [34, 35]. These ideas point towards the possibility that GR may require modifications to explain the nature of our universe. In addition, it is commonly thought that the predictions of GR may not hold when spacetime curvature enters the Planck regime, since the quantum gravity modifications to Einstein's equations would dominantly come into play. In particular, if a theory of quantum gravity resolves singularities of classical GR, then classical solutions with naked singularities might be regarded as the window to new physics [36–39]. Thus alternatives to GR were introduced for a variety of mathematical, philosophical, and observational reasons, but almost all have the common goal to generalize the theory that Einstein initially proposed.

Recently, investigations of the strong and dynamical region of gravity surrounding BHs in previously unheard-of ways have become a reality due to two significant experimental projects. The first major accomplishment came from the observations made by the Laser Interferometer Gravitational-Wave Observatory (LIGO) in the

US in the year 2015 [28], which succeeded in directly detecting the GWs from the merging of two BHs. Quickly, the observational efforts were joined by the Virgo observatory in Italy in the year 2017, followed by the KAGRA observatory in Japan in the year 2020 observing almost hundred compact binary mergers, all in agreement with the coalescence of stellar mass BHs and neutron stars as described by GR [40, 41]. It should be noted that GWs are "ripples" in spacetime, caused by some of the most violent and energetic phenomena in our universe. The waves are produced by BH-BH or BH-neutron star or neutron star-neutron star binaries that orbit each other (inspiral) and finally collide to merge (merger) into a single object that rings down before settling. GWs are emitted through all the different stages of inspiral, merger, and ringdown, as described above. With an immense amount of hard work carried on for decades, theoretical predictions of GW waveforms for the entire processes have been worked out, following the fundamental methodologies prescribed by Einstein's theory. These predictions were used to translate the patterns of detected GWs into an understanding of what produced them. With the first detection of GWs by LIGO and the matching of predictions followed by subsequent processes mentioned above, one can certainly say that the predictions made by Einstein a hundred years ago in 1916 were correct and very robust, to say the least. While the inspiral and merger phases are described by post-Newtonian and full numerical simulations respectively, the study that deals with the ringdown phase of a binary merger is solely based on perturbation theory, which will be the focus of a couple of chapters in this thesis.

The second experimental/observational milestone towards understanding the strong gravity regime came from the Event Horizon Telescope [27]. They relied upon the technique of Very Long Baseline Interferometry (VLBI) to construct an "Earth-sized" radio telescope capable of resolving horizon scale structure. Towards this goal, the observational targets of the EHT collaboration included the two BHs with the largest angular diameter as observed from Earth, viz. the BH at the center of the supergiant elliptical galaxy Messier 87 ($M87$), and Sagittarius A^*, at the center of our galaxy Milky Way. The physical principle behind the imaging of BHs lies in the idea of the bending of light due to the spacetime curvature, which is one of the extraordinary predictions of GR. The status of GR was further strengthened by other complementary activities like the detailed high-precision tracking of the $S2$ star orbiting the supermassive BH Sgr A^* by the GRAVITY Collaboration [42, 43], increasingly precise radio measurements of binary pulsar systems [44] and X-ray spectroscopy of compact binaries [45], just to name a few of them.

It is to be noted that, most of the astrophysical and cosmological observations have been consistent with the predictions of GR [28, 46, 47]. Even if modifications are required, the deviation from GR in such cases is little [25, 48, 49]. To figure out an appreciable divergence from GR, one has to rely on strong gravity regime with quantifiable effects. Such data from the strong regime of gravity provides chances to better test GR and observe variations from it, if any. Asymptotically, almost all the theories of gravity produce similar result [48, 50], it is only in the strong gravity regime, that the differences or deviations are more pronounced. Hence, one needs to probe spacetimes near extreme compact objects like BHs, wormholes, naked singularities (NS), etc., which serve as the best platforms to check the credibility of a particular theory of gravity. Also, as far as the recent advances in observational technologies are concerned, one has the nice opportunity to make the best use of them to

compare the observational data with the theoretical predictions and check, if some deviations from GR are detected. In this sense, it is always important to explore alternative theories of gravity rather than relying solely on one. Several alternative theories of gravity exist in the literature [51–60] which attempts to overcome the problems faced in GR. Research into all these theories is necessary to explore their implications for our understanding of the universe.

The present thesis explores the effect of different parameters of two theories, namely the recently proposed novel $4D$-Einstein-Gauss-Bonnet ($4D$-EGB) theory of gravity and Loop Quantum Gravity (LQG), on some astrophysical processes around the BH and NS solutions of these theories. We have studied how these parameters affect the QNMs, greybody factors, stability of the background spacetime, shadow contours, and super-radiance amplification factors in the above-mentioned solutions of the theories. There are various ways to study these effects. To study QNMs, one can employ perturbation techniques, where test fields and metric perturbation are used for the investigation of astrophysical problems, such as GW emission from gravitational collapses, checking the stability of BHs under small perturbations, and many more. This technique further finds its use in checking the stability of the spacetime around a compact object via time evolution of initial state of perturbing fields. The greybody factors can be computed by a classical scattering computation of scalar, EM and Dirac wave off the compact object. The shadow contours can be obtained by studying the trajectories traced out by photons in the spacetime.To study the super-radiance effect, one can consider the scattering of test fields off the rotating background spacetime.

One of the most well-studied examples of alternative theories of gravity are the Lovelock theories [60, 61]. The Lovelock theories of gravity are of particular interest because they are the only Lagrangian-based theories of gravity that give covariant, conserved, second-order field equations in terms of the metric tensor in arbitrary spacetime dimensions (see Ref. [61] for an excellent review). They are, therefore, considered as the most natural possible generalizations of Einstein's theory. Accordingly, we have worked on the theory where Einstein's equations are subject to next-to-leading-order corrections that are typically described by higher-order curvature terms (the first correction term which is quadratic in nature) in the action known as the EGB theory in the four spacetime dimensions (termed as novel $4D$-EGB theory [10]). We have carried out two works in this theory related to quasinormal modes (QNMs) and echoes in the BH and NS background of the theory. Some words about the naked singularity solutions are in order here. Even after five decades of serious efforts, there still does not exist any well-accepted proof or definite mathematical formulation of the well-known cosmic censorship conjecture [30] as per which every spacetime singularity must remain cloaked by an event horizon or in other words, there cannot be an NS as the end state of a gravitational collapse. However, in the recent works presented in [62, 63], it has been seen theoretically that if one starts from a regular initial condition, then an NS may form as the end state of a gravitational collapse. Hence, studies are not just confined to BHs, but NS also plays an important role in throwing light on physics taking place in strong gravity regimes.

As a second example of a theory of gravity other than GR, we have chosen LQG. It is well known that in the vicinity of BHs, where the effect of gravity is strong, quantum fluctuations of spacetime are expected to play an important role [5, 64]. On a more theoretical level, there are problems associated with a BH which hint that GR

might not be complete when explaining all aspects of a BH, particularly regarding its central singularity. The region around a singularity is characterized by extremely strong gravitational fields, where quantum effects cannot be ignored. However, GR fails to explain the quantum effects taking place at singularities and how they link up with quantum mechanics. To describe the behavior of matter and spacetime under such extreme conditions, a theory of quantum gravity is needed. Such a theory should allow the description to be extended closer to the center of the BH so as to provide a better understanding of physics at the singularity. Towards this direction, LQG turned out to be one of the few successful attempts to understand the quantum nature of gravity. There are a few LQG-inspired BH solutions [65–69] in literature and the characteristics of their shadows have been studied both for non-rotating [70] as well as rotating [71] cases. One of our investigations shows the presence of quantum effects on the shadow of the quantum-corrected non-rotating and rotating BHs. We also quantify the deviation introduced in the modified shadows due to the presence of quantum corrections in comparison to that of their classical counterpart. At the same time, we have made an attempt to look into the modification introduced in the super-radiance effect in the rotating BH background due to the quantum corrections.

Before outlining the motivation and going into more details of our work, we first try to give a brief overview of the two different theories of gravity, viz. novel $4D$-EGB gravity and LQG in the next subsection. We then discuss different astrophysical processes around the solutions of these theories as well as the methodologies to study them.

1.1 Different gravity theories discussed in the thesis

As already mentioned, this thesis discusses astrophysical processes around extreme compact objects in two different types of theories of gravity. Below we provide a brief description of both.

1.1.1 The novel $4D$-Einstein-Gauss-Bonnet Gravity

GR can be treated as an effective theory of some more fundamental theory, valid up to some finite energy scale [72, 73]. Interestingly, Lovelock [60] proved that in four dimensions, GR is the only metric theory of gravity that gives symmetric, covariant second-order field equations in terms of the metric tensor. In arbitrary spacetime dimensions, Lovelock theories (see Ref. [61] for an excellent review) are the most general class of theories that have the same above-mentioned behaviour of the field equations. The Lovelock lagrangian in D dimension is given by,

$$\mathcal{L} = \sqrt{-g}\left(-2\Lambda + R + \alpha\mathcal{G} + \cdots\right) \ , \tag{1.1}$$

where $\mathcal{G} \equiv R^2 - 4R_{\mu\nu}R^{\mu\nu} + R_{\alpha\beta\mu\nu}R^{\alpha\beta\mu\nu}$ is known as the Gauss-Bonnet combination and gives the leading order correction to the Einstein-Hilbert action with a cosmological constant Λ. Here, R is the well-known Ricci scalar, $R_{\mu\nu}$ are the components of the Ricci tensor, $R_{\alpha\beta\mu\nu}$ are the components of the Riemann tensor and α is the Gauss-Bonnet coupling constant.

1.1.1.1 The Einstein-Gauss-Bonnet Gravity

For the EGB gravity, the Lagrangian density from the Lovelock lagrangian in (1.1) by neglecting cubic and higher powers of curvature tensors, is given by

$$\mathcal{L}_{EGB} = \sqrt{-g}\,(-2\Lambda + R + \alpha\mathcal{G})\ . \tag{1.2}$$

Extremization of the action associated with this Lagrangian gives the Lanczos tensor [74]:

$$\begin{aligned} A_{\mu\nu} = &-\frac{1}{2}\alpha_0 g_{\mu\nu} + \alpha_1\left(R_{\mu\nu} - \frac{1}{2}g_{\mu\nu}R\right) \\ &+ \alpha_2\left(2R_{\mu\alpha\rho\sigma}R_{\nu}{}^{\alpha\rho\sigma} - 4R^{\rho\sigma}R_{\mu\rho\nu\sigma} - 4R_{\mu\rho}R_{\nu}{}^{\rho} + 2RR_{\mu\nu} - \frac{1}{2}g_{\mu\nu}\mathcal{G}\right)\ , \end{aligned} \tag{1.3}$$

where $\alpha_0 = -2\Lambda$, $\alpha_1 = 1$ and $\alpha_2 = \alpha$. This tensor provides an alternative set of field equations from those of Einstein, which has no higher than second derivatives of the metric, and which obeys the required symmetry and conservation properties. In $4D$ and lower, the coefficient of α_2 vanishes identically. The integral of the Gauss-Bonnet term over a four-dimensional spacetime $\mathcal{M}_4$ (properly compactified) is equal to a constant whose value depends upon the Euler characteristic of the manifold. Upon extremization, this term contributes precisely zero to $A_{\mu\nu}$. Thus the action from the GB term is invariant under the variation of the metric field whose boundary values are fixed. It is for this reason that the Gauss-Bonnet term in $4D$ is often referred to as a "topological term" and neglected as it does not contribute to local dynamics while it becomes local only in higher-dimensional spacetime. This is despite the fact that generically $\mathcal{G} \neq 0$ in $4D$.

This combination of Einstein-Hilbert and Gauss-Bonnet terms in the gravitational action results in theories that are known as EGB gravity. The Gauss-Bonnet term is the unique term that is quadratic in the curvature and results in second-order field equations. In D dimension, the action is of the form

$$S[g_{\mu\nu}] = \int_{\mathcal{M}} d^D x\sqrt{-g}(-2\Lambda + R + \alpha\mathcal{G})\,, \tag{1.4}$$

It needs to be mentioned here that this class of theories has been widely studied and an increased interest in this particular theory of gravity is due to the new developments in string theory side also [75–77]. It is well known that effective models of gravity in higher dimensions can be obtained from low energy limits of string theories. These effective models involve higher powers of the Riemann curvature tensor in the action in addition to the usual Einstein-Hilbert term [75]. The Gauss-Bonnet combination is of most interest among these higher powers of the Riemann tensor. Interestingly, the theory admits BH solutions [78–80]. Not only in string-generated gravity models, the Gauss-Bonnet BHs have gained interest in the context of brane world models [81], as well as in the context of possible production at the LHC [82]. Einstein-Gauss-Bonnet theories have also been extensively studied in the inflationary framework [83–85].

1.1.1.2 Glavan and Lin's approach

It is thus seen that in four dimensions and lower, the Gauss-Bonnet term does not seem to have a direct effect in the $4D$ theory of gravity. Recently, however,

a novel theory of gravity has been put forward by Glavan and Lin that claims to bypass these difficulties [10]. This theory has been dubbed *novel 4D-Einstein-Gauss-Bonnet* gravity and for a general D-dimensional theory, is based on the action as:

$$S_{EGB}[g_{\mu\nu}] = S_{EH}[g_{\mu\nu}] + S_{GB}[g_{\mu\nu}] + S_{matter}, \tag{1.5}$$

where S_{matter} represents action corresponding to any matter fields in the theory. The reader will note that the number of spacetime dimensions D is not yet specified. The Einstein-Hilbert action is

$$S_{EH}[g_{\mu\nu}] = \frac{1}{16\pi G_N}\int d^D x\sqrt{-g}\,[R - 2\Lambda]\,, \tag{1.6}$$

In Eq. (1.6) and in the rest of the chapter (2), we have chosen $G_N = 1/8\pi M_{\rm Pl}^2$, the D-dimensional Newton's constant to be unity, where $M_{\rm Pl}$ is the Planck mass that characterizes the strength of the gravitational interaction. The Gauss-Bonnet term action looks like

$$S_{GB}[g_{\mu\nu}] = \frac{1}{16\pi}\int d^D x\sqrt{-g}\alpha\mathcal{G}, \tag{1.7}$$

It is to be noted that in four spacetime dimensions, the Gauss-Bonnet term turns out to be a total divergence (i.e., it is a topological term in $4D$). Hence, it does not contribute to any gravitational dynamics. However, Glavan and Lin in [10] showed that by a proper re-scaling of the Gauss-Bonnet coupling constant $\alpha \to \alpha/(D-4)$ and then taking the limit $D \to 4$ at the level of equations of motion, one can obtain the novel four dimensional EGB gravity theory. Therefore, following Eq. (1.5), the action for novel four-dimensional EGB gravity with the scaled coupling constant $\alpha/(D-4)$ can be written as

$$S_{EGB}[g_{\mu\nu}] \quad = \frac{1}{16\pi}\int d^D x\sqrt{-g}\Big[R - 2\Lambda + \frac{\alpha}{D-4}\mathcal{G}\Big] + S_{\rm matter}\,, \tag{1.8}$$

The action can then be varied with respect to the metric and setting the variation to be equal to zero: $\delta S_{EGB}/\delta g^{\mu\nu} = 0$, one arrives at the following equations of motion

$$8\pi T_{\mu\nu} = G^{(\Lambda)}_{\mu\nu} + G^{(EH)}_{\mu\nu} + G^{(LL)}_{\mu\nu}, \tag{1.9}$$

where, $G^{(\Lambda)}_{\mu\nu} = \Lambda g_{\mu\nu}$, the Einstein tensor $G^{(EH)}_{\mu\nu} = R_{\mu\nu} - \frac{1}{2}Rg_{\mu\nu}$ and the Lanczos-Lovelock tensor

$$\begin{aligned} G^{(LL)}_{\mu\nu} = -\frac{\alpha}{D-4}\Big[&\frac{1}{2}g_{\mu\nu}(R_{\alpha\beta\sigma\rho}R^{\alpha\beta\sigma\rho} - 4R_{\alpha\beta}R^{\alpha\beta} + R^2) \\ &-2RR_{\mu\nu} + 4R_{\mu\alpha}R^{\alpha}_{\ \nu} + 4R_{\mu\alpha\nu\beta}R^{\alpha\beta} - 2R_{\mu\alpha\beta\sigma}R_{\nu}^{\ \alpha\beta\sigma}\Big]. \end{aligned} \tag{1.10}$$

The four-dimensional novel EGB theory, at the level of equations of motion, can be obtained as a limit $D \to 4$ [10], circumventing Lovelock's theorem. Such a theory admits BH solutions (it admits both dS as well as AdS branches, see [10, 86, 87] for details):

$$ds^2 = -f(r)dt^2 + f^{-1}(r)dr^2 + r^2(d\theta^2 + \sin^2\theta d\phi^2), \tag{1.11}$$

with

$$f(r) = 1 + \frac{r^2}{32\pi\alpha}\left[1 - \sqrt{1 + \frac{128\pi\alpha M}{r^3} + \frac{64\pi\alpha\Lambda}{3}}\right]. \tag{1.12}$$

where M is related to the gravitational mass of the BH.

This method is conceptually similar to the dimensional regularization procedure used in QFTs. The goal of this is to produce a new classical gravity theory in four dimensions that includes a non-vanishing contribution from the Gauss-Bonnet term to the field equations. It has subsequently attracted a great deal of attention in recent times. The re-scaling of α as $\alpha \to \alpha/(D-4)$ entirely removes the factor that usually leads to vanishing contribution from the Gauss-Bonnet term, and leaves a term that can, in general, be non-zero in the limit $D \to 4$.

Glavan and Lin in their paper [10] have shown that if they take D-dimensional Robertson-Walker geometries, with maximally symmetric spatial surfaces of dimension $D-1$, then the D-dimensional Friedmann equations remain well-behaved in the limit $D \to 4$. Similarly, the D-dimensional spherically symmetric vacuum solutions of the theory given by Eq. (1.4) with the vanishing bare cosmological constant, along with $(D-2)$-dimensional spherically-symmetric subspaces, were also found to be well behaved in the appropriate limit. It was shown that the $D \to 4$ singular limit of the Gauss-Bonnet term produces some non-trivial contributions to the gravitational dynamics, but preserves the number of graviton degrees of freedom. This novel EGB theory can be shown to be free from Ostrogradsky instability [10] and does not require coupling to any matter field. Moreover, such a theory bypasses all conditions imposed by Lovelock's theorem [60, 88, 89] according to which, Einstein's GR with the cosmological constant is the unique theory of gravity if we assume (i) the spacetime is $3+1$ dimensional, (ii) diffeomorphism invariance, (iii) metricity, and (iv) second order equations of motion. The problem of BH singularity is also found to be resolved in this theory. These results are suggestive that the theory may be well-behaved in general in the four-dimensional limit.

Different solutions and different aspects of $4D$-EGB gravity were studied so as to find new differences from GR as well as standard EGB theory. Since the proposal of the novel $4D$-EGB theory, a flurry of works have been done in this theory which includes the formulation of cosmological solutions [90, 91], spherical BH solutions [86, 87, 92, 93], solutions of star-like objects [94], radiating and collapsing solutions [95, 96], extending to four-dimensional Einstein-Lovelock theories [97], thermodynamic behaviour of BHs in such theories [98–101] and the gravitational and physical properties of BHs [8, 17, 19, 102–110]. Lot of works has been done on QNMs and stability of BHs arising out of EGB gravity in spacetime dimensions $D > 4$ [111–127]. The stability and QNMs of the asymptotically flat $4D$-EGB BH against perturbation by scalar, electromagnetic, Dirac fields have been studied in [17]. Following the $D \to 4$ regularization of the scalar and vector type gravitational perturbation of the higher dimensional EGB BH [128, 129], Konoplya *et.al* showed that the asymptotically flat, de Sitter (dS) and anti-de Sitter (AdS) BHs are unstable in the eikonal limit (large l) for large positive values of the Gauss-Bonnet coupling parameter [17, 130]. The QNMs of the $4D$-EGB BH in the asymptotically dS and AdS spacetime due to scalar, electromagnetic and Dirac perturbations have been studied in [110]. The quasibound states of massless scalar, electromagnetic and Dirac fields in the asymptotically flat $4D$-EGB BH and the associated stability problem has been studied

recently in [131]. In this regard, we have studied the QNMs and greybody factors of the novel four dimensional Einstein-Gauss–Bonnet BHs in asymptotically dS spacetime using scalar, electromagnetic and Dirac perturbations.

1.1.1.3 Limitations of the theory

Despite all the above-mentioned studies, the regularization scheme used in this novel $4D$-EGB theory [10] was found to be inconsistent on several grounds [132–140], which led to the development of different versions of regularized (consistent) $4D$-EGB theories [141–145]. There are several reasons why the method proposed in [10] does not work. It is well known that the Gauss-Bonnet term in four spacetime dimensions turns out to be a total divergence i.e., it is a topological term and hence it does not contribute to any gravitational dynamics. The field equations of EGB theory defined in its most general form in $D > 4$ dimensions can be split into two different parts. One of the parts of these field equations always remains higher dimensional, making the limiting procedure of $D \to 4$ non-trivial [132–135, 138]. Tree-level graviton scattering amplitudes were studied in this regard, independently of the Lagrangian, and it was shown that the dimensional continuation and $D \to 4$ limiting procedure applied to Gauss-Bonnet amplitudes does not produce any purely new four-dimensional Gauss-Bonnet gravitational amplitudes [136]. All these imply that the existence of $D \to 4$ limiting solutions does not mean the existence of a four-dimensional theory as proposed in [10]. Hence, several works appeared in the literature exploring different consistent versions of the $4D$-EGB theory to discuss the subtleties of the $D \to 4$ limit of the EGB gravity [10]. Interestingly enough, it has been found that the field equations of the different consistent versions of the $4D$-EGB gravity [91, 141–144] admit the same static spherically symmetric BH solution as was first proposed in [10] and from here onwards we will refer to it as $4D$-EGB BH. It needs to be mentioned that our analysis does not give preference to any particular version of the $4D$-EGB theory.

1.1.2 Loop Quantum gravity (LQG)

Although a great accomplishment in explaining the universe's large-scale structure, GR fails at the quantum level. Such loopholes have led to conceptual, mathematical and technical obstacles that have bedevilled physicists for a long time. It is believed that a viable effort to reconcile GR and quantum mechanics — two foundational theories of contemporary physics can provide a coherent quantum theory of gravity that might provide suitable solutions to such obstacles. LQG is one such non-perturbative and background-independent approach to quantum gravity theory. This theory is primarily driven by the necessity of creating a cogent theory by unifying GR with QFT, that seeks to address the shortcomings of GR at the quantum level by quantizing spacetime itself. It primarily focuses on extreme gravity regions like the Big Bang proximity and the interior of BHs where the continuous nature of spacetime as described by GR breaks down as it is expected that in such regions of strong gravitational fields, the classical trajectories might get altered by quantum effects and hence new effects will show up. The fundamental idea behind LQG is that time and space are not continuous but consists of distinct, indivisible components called "loops" or "spin networks". The discrete nature of the theory is manifested in the form of the lowest non-zero eigenvalue of the area operator that

is allowed in the theory – the area gap Δ, that dictates the quantum corrections to Einstein's equations. It originally started as a canonical quantization scheme towards GR, [146–148]. Here the phase space of GR is parametrized by the connection variables e.g. the Ashtekar-Barbero variables [149] which is based on the gauge group SU(2). These variables define a Hilbert space and further quantize the Hamiltonian constraint. One of the areas where LQG can be connected to observation is via its technical and conceptual application to the subfield of loop quantum cosmology (LQC) [150], where the problem of big bang singularity is resolved by offering finite-dimensional models of quantum cosmology [151]. However, it is difficult to obtain a smooth classical spacetime from fundamental quantum geometry present in LQG. This gives way for the development of spin foams [152], a path integral approach as well as the group field theory approach [153] to cope with these issues.

In our present thesis we have considered a macroscopic Kruskal extended Schwarzschild BH [16, 21, 22] encompassing both the "interior" region that contains classical singularity and the "exterior" asymptotic region that incorporates corrections due to quantum geometry effects of LQG and is rendered free from a singularity. It is well known that the Schwarzschild interior is isometric to the (vacuum) Kantowski-Sachs cosmological model and hence is naturally foliated by a family of homogeneous space-like 3-manifolds [66, 154–156]. Hence techniques from loop quantum cosmology (LQC) based on LQG can be used to construct a Hamiltonian framework based on connection and triad variables which help to pass to the quantum theory using the same methods that are used in full LQG. The phase space variables are the gravitational SU(2) connections A_a^i and their canonical conjugate momenta E_i^a (that represent (densitized) orthonormal triads). Using a step-by-step procedure based on a geometrical formulation of quantum mechanics, one can then extract an effective description from the resulting quantum theory. It is to be noted that so far, there is no systematic procedure for deriving the effective equations starting from (a symmetry-reduced version of) LQG, rather, these equations are inspired from LQC. This technique might be helpful in constructing a more complete quantum description of the singularity resolution for BHs and is considered as a powerful tool to construct the full quantum theory beyond the FLRW models. Such a theory is studied extensively as it gives rise to new physics from the underlying quantum Riemannian geometry.

In chapter (4) we have studied the shadows and super-radiance of a quantum-corrected BH and discussed the modifications introduced in shadow contours and super-radiance amplification factors due to the presence of quantum parameters.

In what follows, we will briefly describe the astrophysical processes which are the main focus of this thesis in the next subsection.

1.2 Astrophysical processes studied in the thesis

1.2.1 Quasinormal modes (QNMs)

QNMs are eigenmodes of dissipative systems. They are the proper modes at which a BH, a star, or any compact object oscillates when excited by a non-radial perturbation and the frequencies associated with these characteristic oscillations are termed as quasinormal frequencies (QNFs). QNMs are a fundamental feature of the gravitational signal emitted by compact objects in many astrophysical processes.

When a binary BH merger produces a GW signal, the ringdown phase is especially interesting because it can be explained by linear perturbations around a stationary BH and primarily corresponds to a superposition of QNMs. When a BH is perturbed, it responds to perturbations by emitting GWs whose evolution in time can be divided into three stages: 1) the first stage consists of an initial outburst of radiation for a relatively short period of time , 2) the second stage is usually a long period of damping proper oscillations, dominated by the so-called QNMs and 3) the third stage occurs at very large time where the QNMs are suppressed by power-law or exponential late-time tails. These QNMs, associated with the second stage of the evolution of perturbations have discrete frequencies and its detailed analysis via so-called "BH spectroscopy" [157], is a priceless tool for testing GR and searching for distinctive indicators of modified gravity. The spectrum acts as a fingerprint of the system and via the no-hair theorem only depends on the mass and spin as the two unknown parameters and are independent of the particular initial perturbation that excited them. To understand these QNMs theoretically, one can study them via the perturbation theory where the backgrounds are perturbed in a variety of ways, by adding dynamical non-vacuum test fields to the BH spacetime, such as scalar fields, neutrino fields, electromagnetic fields, Dirac fields etc., or by perturbing the spacetime directly with gravitational perturbations known as metric perturbation of the spacetime. It is seen that these perturbations follow linear second-order differential equations, the symmetry characteristics of which are determined by the background's symmetries. With the right choice of coordinates, these symmetries typically enable one to separate variables, which reduces the system to a collection of linear ordinary differential equations (ODEs) or a single ODE termed in the literature as master equation having the form

$$\frac{d^2\psi}{dr_*^2} + (\omega^2 - V(r))\psi = 0\,, \tag{1.13}$$

where ψ is the radial part of the perturbing field and $V(r)$ is the potential containing information about the background and the type of perturbation and r_* is the tortoise coordinate defined as

$$dr_* = \frac{dr}{f(r)}\,. \tag{1.14}$$

with $f(r)$ given by Eq. (1.11). QNMs are then defined as the eigen modes of this system of equations (1.13) with the precise choice of physically motivated boundary conditions of outgoing waves at spatial infinity (1.15) and ingoing waves at the horizon (1.16).

$$\psi \sim e^{i\omega r_*} \quad as \quad r_* \to +\infty\,, \tag{1.15}$$

$$\psi \sim e^{-i\omega r_*} \quad as \quad r_* \to -\infty\,. \tag{1.16}$$

These boundary conditions are chosen to make sure that no gravitational radiation unrelated to the initial perturbation disturbs the system at late times. The presence of the horizon, acting as a one-sided membrane serves the purpose of a sink and makes the system dissipative. The BH now behaves as an open system (with the

boundary conditions 1.15 and 1.16) and loses energy. Hence, the associated eigenvalues are complex, the real part of which is equal to the system's oscillation frequency and the imaginary part corresponds to the mode's damping time accounting for the energy loss. They differ from a normal-mode system in the sense that they are not truly stationary since they are damped quite rapidly. Also unlike normal modes, they seem to appear only over a limited time interval, rather than extending from arbitrary early to arbitrary late times. The 'normal' part in the term QNM points out to the fact that these modes are closely analogous to normal modes in the way they are determined. The 'quasi' part points out to the fact that they have several differences from the normal modes and are not quite the same. The most important difference is that they are not really stationary in time due to their strong damping. It needs to be mentioned that the QNMs generally do not form a complete set, in the sense that the time evolution of any initial perturbation could be described as a superposition of such QNMs. Also, they are excited only at a particular instant in time and decay exponentially with time. This implies that they cannot have existed for all times. It is limited in the beginning by the initial pulse, and towards late times by the power-law tail. QNMs were first detected in 1970s in numerical simulations of scattering of Gaussian wavepackets by Schwarzschild BHs. Regge-Wheeler [158] and Zerilli [159] gave a full mathematical treatment of the gravitational perturbation in a static spherically symmetric background. Later on Vishveshwara [160] noticed that at late times, these waveform consists of a damped sinusoid, having ringing frequency almost independent of the Gaussian parameters.

Admittedly, while some theories of alternative gravity may be well constrained by cosmological observations, solar system tests, and gravitational wave observations, others are just too complicated to work with. As a specific example, the lack of numerical relativity simulations or a perturbation theory for rotating BHs in alternative theories implies that we are not able to make an actual prediction for what will occur deep into the non-linear dynamical regime of gravity. Therefore, one already intriguing avenue of starting to test GR within or beyond its predicted limit is in the GW emission accompanying binary BH mergers. These occurrences explore the most extreme features of gravity, and ongoing advancements in both current and upcoming detectors promise high-accuracy observations that will require thorough explanations which may provide a window to look beyond GR. This will then pose a challenge to the current methods of treating GR since more accurate data necessitates more accurate modelling. It is expected that the upcoming observation cycles will yield intriguing results in BH spectroscopy with more accurate measurements.

Different methods are available in the literature (see [2, 3, 161–163]) to compute QNMs. One chooses the best methods amongst them pertaining to the context of the problem they are dealing with. Also, QNFs are only slightly affected (its value changes just by only a few percent) by considerable change in the BH parameters, so practically, it is important that QNMs should be calculated with high accuracy. Hence, both numerical and analytical approaches have appeared in the literature that makes attempt to calculate QNFs more accurately.

In general, it is difficult to find exact solutions to the wave Eq. (1.13) and hence one must resort to numerical methods. However, there are a few noteworthy exceptional spacetimes viz: near-extreme Schwarzschild-de Sitter [164], Nariai spacetime [165] where analytical methods can be exploited to compute the QNMs by replacing the true potential in the given spacetime by the Pöschl-Teller potential [166]. Such

analytical solutions concerning the QNM calculation are also possible for pure AdS spacetimes [167], dS spacetimes[168], BTZ BHs [169], massless topological BHs [170, 171].

On a broader perspective, QNMs can be calculated by sticking to some approximations, semi-analytical methods or numerical techniques viz: WKB approximation [172–176], phase integral method [177–180], monodromy technique [168, 181–184], series solution [185–187], resonance method [188], continued fraction method [189–191], geometric optics or eikonal limit [192–205], asymptotic iteration method [206–213], shooting method [214], time evolution [160, 162, 215–218], full numerical relativity [219–226], Prony's method [3, 227] and many more.

We shall now discuss the methods that we have adopted in our thesis to compute the QNFs in case of $4D$-EGB BH and NS.

1.2.1.1 Methodology used to compute quasinormal frequencies (QNFs)

(1) **WKB approximation and Padé approximation to compute the QNFs in novel $4D$-EGB BH**

In order to obtain the QNFs, we have used the 3rd order WKB approximation. Also to get better results, we have used 3rd order Padé approximation on the usual WKB formula.

As is well-known, the most important and recognizable usage of the WKB method is to solve the time-independent Schrödinger equation

$$-\frac{\hbar^2}{2m}\frac{d^2\psi(x)}{dx^2}+(V(x)-E)\psi(x)=0\,. \tag{1.17}$$

Due to the resemblance of Eq. (1.17) with the master equation (1.13), the idea to employ the WKB method for BH perturbation theory can be justified. The differential equation (1.13) to be analysed takes the general form

$$\frac{d^2\psi(r)}{dr_*^2}+Q(r_*)\psi(r)=0\,, \tag{1.18}$$

with $Q(r_*)=\omega^2-V(r_*)$. The function $-Q(r_*)$ is such that it is constant but not necessarily the same in both limits at $r_*\longrightarrow\pm\infty$ and it rises to a maximum near $r_*=r_{*0}$. $Q(r_*)$ can be split into three regions as shown in Fig. (1.1) and r_{*1} , r_{*2} are the two turning points i.e., $Q(r_{*1})=0$ and $Q(r_{*2})=0$. Region 2 is known as the matching region with $r_{*1}<r_{*0}<r_{*2}$. Now the basic approach in this technique is to match the WKB solutions in region 1 and 3 across region 2. For this, the turning point r_{*1} and r_{*2} must lie close to each other(which implies that $[-Q(r_*)]_{max}\ll|Q(\pm\infty)|$). At the classical turning points r_{*1} and r_{*2} , $\omega^2=V(r_*)$ and when the condition that r_{*1} and r_{*2} must lie close to each other is satisfied, we have $\omega^2\sim V_0$ (V_0 is the height of the potential maximum at r_{*0} as can be seen from Fig. (1.1). $Q(r_*)$ can be expanded in region 2 with the help of Taylor series expansion around the point $r_*=r_{*0}$ keeping terms including and upto the order $(r_*-r_{*0})^2$. Upon matching the solutions and applying the boundary conditions one finds the following "Bohr-Sommerfield quantization rule" defining the QNM frequencies:

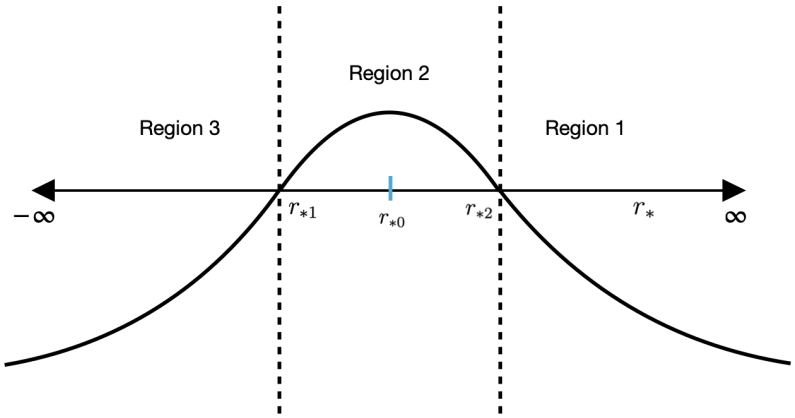

Figure 1.1: The figure (motivated from Fig. 1 of [172]) shows the function $-Q(r_*)$ with the two turning points r_{*1} and r_{*2} and the position r_{*0} where $-Q(r_*)$ attains its maximum value.

$$i\frac{Q_0}{\sqrt{2Q_0''}} = \left(n+\frac{1}{2}\right), \tag{1.19}$$

The factor n is known as the overtone number, which is a discrete quantity, and the fundamental oscillation mode is given by $n = 0$. Hence, the first order WKB approximation formula to find the QNFs is then given by

$$\omega^2 = V_0 - i\left(n+\frac{1}{2}\right)(-2V_0'')^{1/2}, \tag{1.20}$$

where a prime means derivative with respect to r_*. Here, V_0 is the height of the potential maximum and $V_0^{(n)}$ is the n-th derivative of the effective potential V with respect to r_*, calculated at the maximum of the potential that occurs at $r_* = r_{*0}$. The simplicity of the WKB method is well stated in Eq. (1.20): instead of solving a rather difficult differential equation (1.18) numerically, the frequencies are obtained by solving a much simpler one (1.20). Furthermore, it can easily be expanded to higher orders of approximation by directly adding more terms to the equation (1.19) which is obtained by considering the higher order terms in the Taylor series expansion of $Q(r_*)$ about $r_* = r_{*0}$. For example, to study the 1st, 2nd and 3rd order WKB approximation, the potential in the interior region is expanded upto second, fourth and sixth order respectively, using the Taylor series expansion. Thus, the formula for QNFs using third order WKB approach is given by [173]

$$\omega^2 = [V_0 + (-2V_0'')^{1/2}\tilde{\Xi}(n)] - i\left(n+\frac{1}{2}\right)(-2V_0'')^{1/2}[1+\tilde{\zeta}(n)], \tag{1.21}$$

where $\tilde{\Xi}(n)$ and $\tilde{\zeta}(n)$ contains terms upto fourth and sixth order derivatives of the potential evaluated at $r_* = r_{*0}$ respectively. Here, $\tilde{\Xi} = \Xi/i$, $\tilde{\zeta} = \zeta/(n+\frac{1}{2})$ with Ξ and ζ given by

$$\Xi(n) = \frac{i}{(-2V_0'')^{1/2}}\left[\frac{1}{8}\left(\frac{V_0^{(4)}}{V_0''}\right)\left(\frac{1}{4}+\nu^2\right) - \frac{1}{288}\left(\frac{V_0^{(3)}}{V_0''}\right)^2(7+60\nu^2)\right], \tag{1.22}$$

$$\zeta(n) = \frac{(n+\frac{1}{2})}{(-2V_0'')^{1/2}}\left[\frac{5}{6912}\left(\frac{V_0^{(3)}}{V_0''}\right)^4(77+188\nu^2) - \frac{1}{384}\left(\frac{V_0^{(3)^2}V_0^{(4)}}{V_0''^3}\right)\right.$$
$$\times(51+100\nu^2) + \frac{1}{2304}\times\left(\frac{V_0^{(4)}}{V_0''}\right)^2(67+68\nu^2) + \frac{1}{288}\left(\frac{V_0^{(3)}V_0^{(5)}}{V_0''^2}\right)$$
$$\left.\times(19+28\nu^2) - \frac{1}{288}\left(\frac{V_0^{(6)}}{V_0''}\right)(5+4\nu^2)\right], \tag{1.23}$$

where $\nu = n + 1/2$, where n is a positive integer.

It should be noted that the multipole number l and the overtone number n are the important factors that determine the accuracy of the WKB method. It has been shown in [228] that, when the multipole number is larger compared to the overtone: $l \gg n$, the WKB approach works extremely well. Under such conditions, WKB is such a good approximation that its results are in very good agreement with the results from numerical integration of the wave equation. However, the WKB approach does not yield satisfactory results if $l = n$ and is not applicable for $l < n$. On the other hand, as l increases, the results given by WKB method are progressively better.

Padé approximation:

Recently, it has been proposed in [176, 229] that, if one needs to increase the accuracy of the higher order WKB approach, then, one can use Padé approximation on the usual WKB formula. These works show that Padé approximation can be often found to give desirable results even beyond the range of applicability of WKB approximation. It was found that by extending the order of the WKB terms i.e., increasing the order of the Taylor series expansion of the potential and constructing the well known Padé approximants of the formal series for ω^2, the Padé transforms always yield results that are in good agreement with the exact numerically obtained QNMs. In this thesis, in our first work, we have used 3rd-order Padé approximations over the 3rd-order WKB methods to get more accurate results while computing the QNFs of the $4D$-EGB dS BH.

Under the Padé approximation, a function of the form $f(x)$ is approximated using rational polynomials:

$$f(x) \approx \frac{A_0 + A_1 x + A_2 x^2 + ... + A_N x^N}{B_0 + B_1 x + B_2 x^2 + ... + B_M x^M}, \tag{1.24}$$

where $A_i s$ and $B_j s$ are constants. An $[N/M]$ Padé approximant is formed of a N-th degree polynomial in the numerator and M-th degree polynomial in the denominator.

$$P_M^N(x) = \frac{\sum_{i=0}^{N} A_i x^i}{\sum_{j=0}^{M} B_j x^j}. \tag{1.25}$$

An $[N/M]$ Padé approximant is always constructed to agree with $(N+M)$th order of the Taylor series. We have seen that WKB method makes use of the

Taylor series expansion. The problem with Taylor series expansion is that it uses repeated differentiation to produce a series expansion of a function $f(x)$ about a particular point $x = a$ and is expressed as:

$$\begin{aligned} f(x) \quad &= f(a) + f^{'}(a)(x-a) + \tfrac{(x-a)^2}{2!} f^{''}(a) + \tfrac{(x-a)^3}{3!} f^{(3)}(a) \\ &\quad + \ldots\ldots + \tfrac{(x-a)^n}{n!} f^{(n)}(a) + \cdots \end{aligned} \tag{1.26}$$

The Taylor series expansion follows the original function quite well only up to a short range and hence cannot extrapolate the function for very long before rapidly diverging to positive or negative infinity whereas Padé approximants often follow the original function more closely for longer. Dividing one polynomial by other polynomial in Padé approximations cancels out the tendency to shoot towards plus or minus infinity. Padé approximants can converge faster than other approximation methods. This rapid convergence makes Padé approximation a valuable tool for numerical calculations and simulations. Such approximations are generally numerically stable, meaning that they produce reliable results even in the presence of rounding errors or computational limitations. This stability makes Padé approximation suitable for use in numerical simulations and computations. It is in this sense that we have used Padé approximations in our case in calculating the QNMs as an improvement over WKB where only the Taylor series expansion of the potential function is used. It is believed that the development of a mathematically strict and universal method of calculation of QNMs based on the Padé approximation would give a very powerful tool to study BH spectroscopy [176, 229, 230].

(2) **Prony's method to extract the QNFs in novel $4D$-EGB naked singularity from time evolution data**

In our second work in this thesis, while studying the stability of the $4D$-EGB NS, we have extracted the mode frequencies from the time profile of perturbing fields by using Prony's method [3, 227] of fitting the time-domain data with a series of damped exponentials with some excitation factors $C_j s$ given by

$$\Psi(t) \simeq \sum_{j=1}^{p} C_j e^{-i\omega_j t}, \tag{1.27}$$

where $\Psi(t)$ denotes the time evolution of the field in context.

We suppose that the quasinormal ringing epoch starts at $t = t_0 = 0$ and ends at $t = Nh$, where N is an integer and $N \geq 2p - 1$ with p being the total number of terms that appear in Eq. (1.27) for fitting the time-domain data within $t = t_0 = 0$ and $t = Nh$. Here, h is the step size of the integration grid as shown in Fig. (1.2), used for obtaining the value of the perturbing field at different times. Then the formula (1.27) is valid for each value from the profile data such that for each $n \in (0, N)$

$$x_n \equiv \Psi(nh) = \sum_{j=1}^{p} C_j e^{-i\omega_j nh} = \sum_{j=1}^{p} C_j z_j^n . \tag{1.28}$$

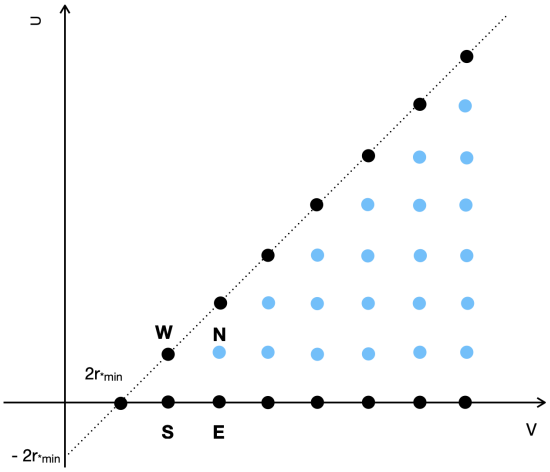

Figure 1.2: The figure (motivated from Fig. 5 of [231]) shows the numerical grid used for integration in the (u, v) plane to find the value of the perturbing fields at different times. The black points represent the grid points where the value of the solution (field) is known. The blue points represent the grid points where the solution needs to be calculated.

where $z_j = e^{-i\omega_j h}$. The Prony method thus helps in finding z_j in terms of x_n, which are known from the profile data and hence helps to calculate the QNFs ω_j since the step size h is also known. In order to do this, a polynomial function $A(z)$ is defined as

$$A(z) = \prod_{j=1}^{p}(z - z_j) = \sum_{m=0}^{p} \alpha_m z^{p-m}, \qquad \alpha_0 = 1\,. \tag{1.29}$$

Consider the following sum:

$$\begin{aligned} \sum_{m=0}^{p} \alpha_m x_{n-m} &= \sum_{m=0}^{p} \alpha_m \sum_{j=1}^{p} C_j z_j^{n-m} \\ &= \sum_{j=1}^{p} C_j z_j^{n-p} \sum_{m=0}^{p} \alpha_m z_j^{p-m} \\ &= \sum_{j=1}^{p} C_j z_j^{n-p} A(z_j) = 0\,. \end{aligned} \tag{1.30}$$

Since $\alpha_0 = 1$ we find

$$\sum_{m=1}^{p} \alpha_m x_{n-m} = -x_n\,. \tag{1.31}$$

Substituting $n = p, ..., N$ into Eq. (1.31) we obtain $N - p + 1 \geq p$ linear equations for p unknown coefficients α_m.

We rewrite these equations in the matrix form

$$\begin{pmatrix} x_{p-1} & x_{p-2} & \dots & x_0 \\ x_p & x_{p-1} & \dots & x_1 \\ \vdots & \vdots & \ddots & \vdots \\ x_{N-1} & x_{N-2} & \dots & x_{N-p} \end{pmatrix} \begin{pmatrix} \alpha_1 \\ \alpha_2 \\ \vdots \\ \alpha_p \end{pmatrix} = - \begin{pmatrix} x_p \\ x_{p+1} \\ \vdots \\ x_N \end{pmatrix}.$$

Such a matrix equation

$$X\alpha = -x\,, \tag{1.32}$$

can be solved in the least-squares sense

$$\alpha = -(X^\dagger X)^{-1} X^\dagger x\,, \tag{1.33}$$

where $X^\dagger$ denotes the Hermitian transposition of the matrix X.

Since the coefficients α_m of the polynomial function $A(z)$ are found, we can calculate numerically the roots z_j of the polynomial and the QNFs ω_j of the j-th mode as:

$$\omega_j = \frac{i}{h}\ln(z_j)\,.$$

1.2.2 Greybody factors

Studying the absorption and scattering cross sections of waves by BHs has been done since the 1970's. Suppose a wave is impinging on the BH, then the greybody factor $\gamma_l(\omega)$ can be defined as the probability of the wave to be absorbed by the BH. The greybody factors can be computed by a classical scattering computation of a wave packet off the BH. While calculating the greybody factors, one relaxes the boundary condition of no-incoming wave from infinity. Hence this case is different from that in QNMs. The BH geometry outside the event horizon acts as a potential and the waves will be filtered by this potential: part of it will tunnel through the potential and the rest will be reflected. It is known, in general, that the explicit form of the potential depends on the geometry of the spacetime and the properties of the perturbation under study. Since the greybody factor is defined in terms of transmission and reflection coefficients corresponding to the potential barrier, so it is straightforward that the greybody factor will also depend on some parameters related to the potential barrier.

Let us assume a wave is coming from the past cosmological horizon r_c corresponding to $r_* \to \infty$ ($r \to r_c$). When the wave reaches the BH, some of it will be reflected due to the gravitational potential and some of them will be transmitted. After scattering off the effective potential, the asymptotic behaviour of the wave could be written in tortoise coordinate as

$$\psi(r_*) = T(\omega)e^{-i\omega r_*};\;\; r_* \to -\infty\,, \tag{1.34}$$

$$\psi(r_*) = e^{-i\omega r_*} + R(\omega)e^{i\omega r_*};\;\; r_* \to \infty\,. \tag{1.35}$$

The greybody factor $\gamma_l(\omega)$ for a given frequency ω and l is given by,

$$\gamma_l(\omega) = |T(\omega)|^2\,.$$

In the WKB approximation, the reflection coefficient is given by [232]

$$R(\omega) = (1 + e^{-2\pi i\beta})^{-\frac{1}{2}}\,, \tag{1.36}$$

where β, under the third order WKB approximation, is given by

$$\frac{i(\omega^2 - V_0)}{\sqrt{-2V_0''}} - V_2 - V_3\,, \tag{1.37}$$

where V_2 and V_3 is given by

$$V_2 = -i\,\Xi(n), \tag{1.38}$$

$$V_3 = \frac{-1}{\sqrt{-2V_0''}}\,\zeta(n)\,, \tag{1.39}$$

where Ξ and ζ are same as in Eqs. (1.22) and (1.23) respectively. Conserving probability we get

$$\gamma_l(\omega) = |T(\omega)|^2 = 1 - |R(\omega)|^2\,. \tag{1.40}$$

The above-mentioned procedure of finding the reflection coefficient has been extensively used in past literature [233–235].

1.2.3 Echoes

The quantum parameters of a theory are believed to show their prominence in extreme gravity regimes, but if one tries to get a signature of them from an observational viewpoint then one faces the question of whether their effects survive in weak gravity regions also, i.e., well outside the horizons. It was found while studying the radial plunge of a test particle into a thin-shell wormhole that any correction at the horizon scale due to a surface [236] or to quantum effects [237–240] will reveal itself in secondary pulses that appear in the late-time ringdown waveform known as echoes. The presence of a photon sphere in spacetime as well as a sufficiently large "cavity" serves the purpose of a crucial ingredient for the appearance of echoes in the GW signal. In absence of these ingredients, there will be no trapped states in the spectrum, and the late-time ringdown in these cases will be simply characterized by a damped sinusoid, without the echo structure. It then follows that one can rely on the signal detected by GW detectors to find signatures of quantum imprints in the form of echoes even at regions very very far away from those where its effects are pronounced strongly. Echoes are universally characterized by a modulated and distorted train of signals of the modes of vibration associated with the photon sphere that shows up in the late-time ringdown phase, whose amplitude gets smaller and frequency content also goes down. Thus the presence of echoes is expected if the BH is surrounded by a mirror or any membrane-like structure near the horizon [241, 242], that reflects GWs. Thus echoes are produced when GWs that get trapped between the angular momentum barrier and a "nontrivial structure" at or near the BH horizon (a reflective barrier) slowly leak out in each interaction with the angular momentum barrier after getting reflected from the reflective barrier (see Fig. (1.3)). Thus echoes act as a smoking gun for new physics, potentially reaching microscopic or even Planckian corrections at the horizon scale [241, 242].

In general, echoes highlight the existence of horizonless compact objects and have been predicted to be present in the ringdown signals of wormholes, fuzzballs, and other ECOs [242–249]. The presence of echoes has also been associated with modified theories of gravity [250] and the existence of higher dimensions [251, 252]. Echoes in GWs are also expected to bear signatures of quantum gravity via quantization of the BH area [253, 254], although, Coates *et al.* [255] have argued differently. For a detailed review on echoes in GW, we refer the reader to the excellent review by Cardoso and Pani [7]. Tentative evidence of echoes in GW observations has been claimed by several authors [256–262], but such findings were disputed by others [263–

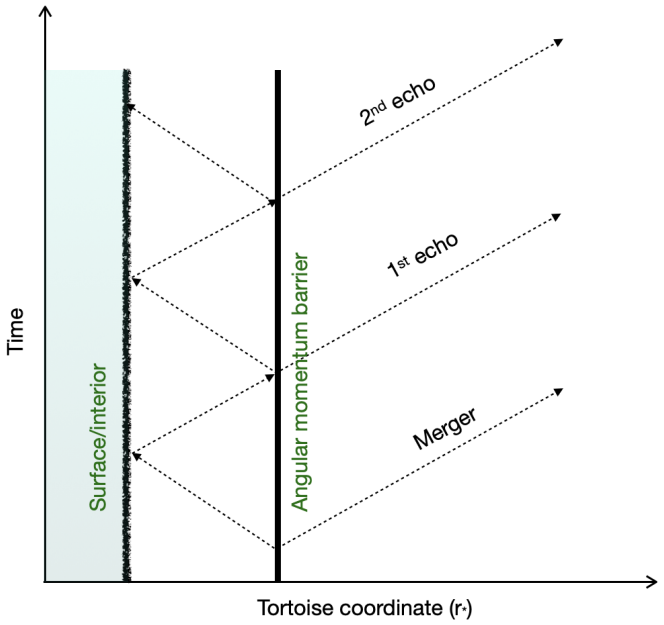

Figure 1.3: The figure (motivated from Fig. 10 of [7]) shows the spacetime depiction of GW echoes reflected from a nontrivial structure at or near the BH horizon (a reflective barrier), following a collapse from binary compact object merger event.

266]. Also studies of the LIGO-Virgo-KAGRA Collaboration did not find evidence for echoes, but rather put constraints on deviations from GR [40, 41].

The GW detectors thus provide a unique opportunity to test GR, as well as the nature of the merger remnant, by searching for GW echoes. In general, it is very challenging to search for non-GR effects in existing observations for several reasons. A key limitation is the sensitivity of the present-day detectors, which require a very careful treatment of the noise and implies that only the loudest part of the signal around the merger can be clearly identified. Nonetheless, these echoes are studied widely in various spacetimes to check for any deviations from GR and to understand the nature of these compact objects.

In the chapter 3 of this thesis, these echoes can be seen in the time domain evolution of the perturbing test fields: scalar, electromagnetic and Dirac.

1.2.4 Shadows

The most common definition of shadow is the dark area that is created on a surface (such as a screen or the ground) when light falling on it encounters an obstacle in its path. In addition, the word 'shadow' can also refer to a body's dark silhouette that is seen against a bright background. In this case, the only thing visible is the outline of the body. In the context of astrophysical objects, like BHs, shadow refers to a dark region seen in the image of BHs, surrounded by a bright emission ring. This phenomenon is strongly influenced by the bending of light in the strong gravitational field near the BHs, as well as the event horizon's ability to trap light. The initial idea about the shadow of a BH was given by Synge [267] (where he studied the 'escape cone' of light which is the complement of the shadow cone) and Luminet [268], for a Schwarzschild BH and later Bardeen [269] extended

the idea for the Kerr BH.

A cartoon diagram is shown in Fig. (1.4) to give an overview of how the shadow contour is formed. Photons approaching the BH via path labelled as 1 plunge into the BH and hence will never come out of it. These are the ones responsible for the dark part of the shadow whereas those following path 3 will simply undergo gravitational lensing and will fly away to infinity. For obtaining shadows, the path labeled as 2 having critical impact parameter b_c, is important. All those photons approaching the BH along this path will go in loops around the BH in unstable circular null geodesics and will either plunge into the BH or get scattered owing to even a slight perturbation. Hence it is these photons that determine the outer contour of the shadow. One might naively think of the event horizon to determine the boundary of the shadow since event horizon is the last region of escape for photons. However, in reality, this is not true. As a matter of fact, for Schwarzschild spacetime, the BH shadow is about two and a half times larger than the event horizon in angular size than the naive Euclidean estimate suggests [27]. There are two reasons behind this. Firstly, it is the photon sphere (or the photon region if

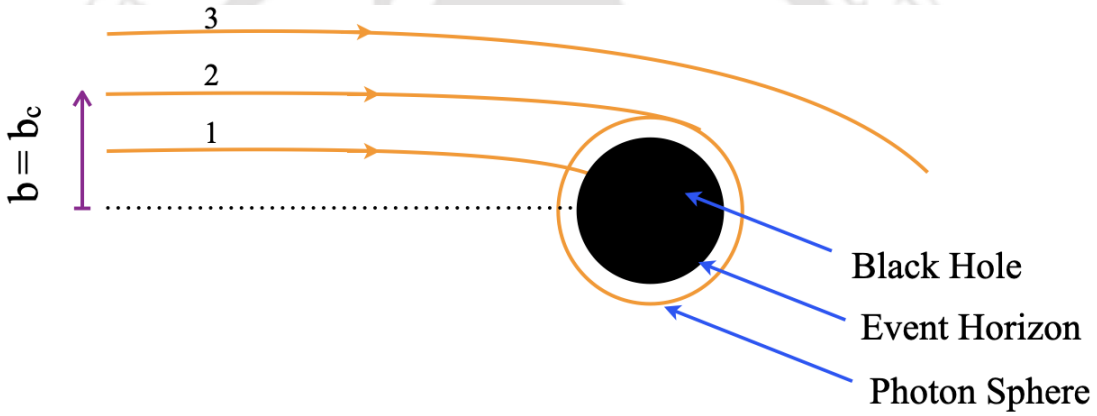

Figure 1.4: The figure (motivated from Fig. 3 of [270]) shows the photon path corresponding to the critical impact parameter b_c responsible for forming the shadow contour.

one incorporates rotation) outside the event horizon, composed of unstable photon circular orbits (the photon sphere radius $r_{ps} = 3M$ in the Schwarzschild case, M is the BH mass) that determines the boundary of shadow. The second reason is gravitational lensing. The bending of light around the compact object will make the photon sphere look bigger for the observer and hence the shadow contour will appear greater than the boundary of the event horizon. It is in fact greater than the photon sphere radius. For the case of a Schwarzschild BH, the event horizon radius is at $2M$, the photon sphere radius is at $3M$ whereas the shadow radius is at $3\sqrt{3}M$. In fact, the boundary of the shadow corresponds to light rays that spiral towards the photon sphere and not towards the horizon. Thus the shadow contour is the gravitationally lensed image of the photon sphere and it has been found that the impact parameter of the photon sphere approximately equals the radius of the BH shadow. Apart from BHs, some spherically symmetric NS models viz: Janis-Newman-Winicour [271] and Joshi-Malafarina-Narayan NSs [63], for some particular values of theory parameters, possess photon spheres and can cast shadows much similar to Schwarzschild BHs. Shadow is not only the property of a BH, but it can also be cast by various compact

objects like naked singularities, gravastars, boson stars, wormholes etc. [272–276] . Depending on whether a spacetime allows integrability of the photon equations or not, one adopts either an analytical or numerical approach to compute the shadows. Below we give a very concise overview of these approaches.

1.2.4.1 Analytical calculation for BH shadows

In order to construct the shadow contour analytically, the important thing is the existence of constants of motion that allow to reduce the differential equations for lightlike geodesics, which are originally of second order, to a system of first-order equations. It is thus convenient to calculate shadows analytically in systems where the photon motion in the spacetime around the compact object in question is integrable. However, one is supposed to make some idealized assumptions while following this approach such as: (i) one has to consider a situation where an observer sees a BH against a backdrop of light sources, with no light sources between the observer and the BH and (ii) light travels unperturbed via any medium along lightlike geodesics of the spacetime metric [12]. This setting, no doubt, helps one to analytically calculate the shape and the size of the shadow, for an observer anywhere outside the BH, for a large class of BH models. Although, one cannot expect realistic image of the shadow from this approach. This is because, unlike the unrealistic assumption, there will always be light sources between the observer and the BH and the light rays on its journey from the BH to the observer will deviate from lightlike geodesics of the spacetime metric because their propagation will be partly influenced by a medium resulting in refraction, scattering or absorption. However one still studies the analytical approach as it helps in analyzing some important aspects: (i) how the results are affected by certain parameters of the model and (ii) how good is the validity of numerical codes by providing a test-bed for checking the codes with simple examples that has already been studied via the analytical approach. Thus it lays out the basic theoretical foundation to study and analyse the shadows for the more complicated cases.

To calculate the BH shadows, one investigates the geodesic equations for photons. In most of the cases, it is found that these equations undergo a separation of variables and the number of integration constants is equal to the degrees of freedom of the photon motion system. Therefore the system is integrable. In the case of Schwarzschild, owing to the spherical symmetry of the background we have two constants of motion, namely the energy E and the z-component of the angular momentum L. For the Kerr case, since, it is not spherically symmetric, at first it might seem that the spacetime might not allow integrable lightlike geodesic equations. However, admirably, it is seen that besides the constants of motion E, L (associated with the Killing vectors connected respectively to stationarity and axial-symmetry of the spacetime) and the photon's rest mass (which is zero), one has an additional constant: the Carter constant $\mathcal{Q}$, due to the presence of a hidden symmetry because of the existence of a Killing tensor. This constant results from the separability of the Hamilton–Jacobi equation for geodesics [277]. Thus the null geodesics are fully separable in the Kerr spacetime also, leading to four constants of motion which further allows one to write all four geodesic equations as first-order equations. This separability further helps in simplifying the expression of motion dynamics for null geodesics with just two independent critical impact parameters also termed in the

literature as Chandrasekhar's constant [278] given by

$$\xi = \frac{L}{E} \quad and \quad \eta = \frac{\mathcal{Q}}{E^2}\,, \tag{1.41}$$

which is necessary to obtain the contour of the shadow. On the other hand in the case of Schwarzschild one needs just one critical impact parameter for the case. It is thus seen that in special cases for which the geodesic motion is integrable (e.g. Kerr), it is possible to have an analytical closed form for the shadow edge. In fact, a striking correspondence between the existence of spherical lightlike geodesics and the separability condition was found by Glampedakis and Pappas in [279], that if an axisymmetric and stationary metric admits no non-equatorial spherical lightlike geodesics, in no coordinate system, then the separability condition cannot be satisfied. The next questions that follows this is whether circular lightlike geodesics can be expected in all classes of BHs. The answer to this query was provided by Cunha and Herdeiro in [280] where they have shown that as long as one is interested in the domain of outer communication of an axisymmetric, stationary and asymptotically flat BH with a topologically spherical and non-degenerate horizon, one will always have the circular lightlike geodesic. However, there are some classes of BHs where these features are not available generically and hence the null geodesic equations have to be solved numerically.

1.2.4.2 Numerical calculation for BH shadows

In the real world, we come across very few systems which are completely integrable. For systems which are not completely integrable, one must resort to numerical methods to calculate the shadows. Here instead of evolving the light rays coming directly from a light source and detecting the ones that reach the observer, backward ray-tracing method [281–285] is employed. In this numerical method, the light rays are traced back from the observer in time and the information carried by each ray is respectively assigned to a pixel to obtain a final image in the observer's sky. Then those light rays which fall down into the event horizon of BH corresponds to black pixels composing the BH shadow. For further studies related to the numerical calculation of BH shadows, which are not the subject of the present thesis, one can refer to [286].

The study of shadows is motivated by the fact that the BH shadows obtained by theoretical calculation can be used to produce some theoretical templates for the future astronomical observations announced by the upgraded Event Horizon Telescope [287] and BH Cam [288]. Further analysis of such templates serves as a tool to promote the development of BH physics and verify various gravity theories. An important thing that needs to be pointed out while discussing shadows is that theoretically, it has been found in some works that neither the presence of the event horizon nor the photon sphere is the necessary condition for compact object to cast the shadow, rather what is important is that the central object must be compact enough having strong gravitational effects to bend light to cast a shadow. This has triggered the studies of shadow in such ultra-compact objects like wormholes, NSs, etc. Such spacetimes have been studied in great details in the literatures [274, 289, 290] and some of them are important in the sense that they tend to mimic the shadow of a BH and hence provide us with a lucky chance to check for alternatives to BHs. Thus, shadows serve as an important tool to distinguish BHs from other

ultracompact objects which are sometimes called BH mimickers or BH impostors like wormholes, NSs, boson stars, Proca stars or Fermion stars etc. Although there is no observational evidence of these objects to date, yet their existence cannot be ruled out and hence continuing their theoretical studies as well as investigating the observational consequences of their existence is certainly an important line of research. Their studies have received a tremendous boost with the introduction of the EHT and studies are carried out in different compact objects in different theories of gravity so as to keep in hand as much theoretical data and information as possible so as to compare with the observational one.

In the present thesis in chapter (4) we have obtained the shadow contours for a quantum corrected BH for the rotating and non-rotating cases and have found that for both cases, there exist sufficient constants of motion so as to render the underlying system integrable which further reduces our task since the shadows can be computed analytically.

1.2.5 Super-radiance

Super-radiance is a radiation amplification phenomenon that is observed in many different contexts and in many areas of physics. One of the early examples of super-radiance in high energy physics was Klein's paradox [291], in the context of relativistic particle mechanics which tried to explain the occasional amplification of reflected number density of particles in comparison to the incident density during scattering processes. Super-radiance generally comes hand in hand with the existence of a dissipative process. BHs are characterized by an event horizon that functions as a one-way membrane. The event horizon in the context of BHs serves the purpose of a dissipative surface. Another example of a process close to that of super-radiance is the Penrose process [292]. Penrose showed that the ergoregion of Kerr BHs can aid in a special scattering process through which energy can be extracted out of the BH. He showed that if a particle upon entering the ergoregion from outside can disintegrate into two particles, then, it can be arranged in a way such that, one of them has negative energy and can be engulfed by the BH. However, energy conservation dictates that the other one must have a positive energy greater than that of the incident particle. This is a characteristic feature of super-radiance. Zeldovich in [293, 294] showed that classical multipole waves that are incident on any rotating body with some kind of dissipation will be amplified upon being reflected by the rotating body. In [295], the analytical formulas for the amplification factor of scalar waves upon reflection from a rotating BH has been obtained. Later on in [296], Press and Teukolsky numerically computed the amplification factor of scalar waves for the particular case $a = M$ and found that the amplification effect is extremely small: the energy flux in the wave increases, upon reflection of the wave, by not more than 0.4%.

While the Penrose process looks at particle scattering against BHs, one can easily consider fields in a similar setting. Various spin fields scattering against BH spacetimes can also give rise to super-radiance (although Dirac fields do not exhibit super-radiance in the classical Kerr geometry). Accordingly, we have studied the scattering of scalar field against a quantum-corrected rotating BH in chapter (4) and determined the conditions under which the fields undergo super-radiance scattering. We have used the Teukolsky formalism to obtain the condition for super-radiance

to occur and the expression for super-radiant amplification factor. The approach has been discussed in 4.4.2. A detailed method to compute the super-radiance amplification factors in the context of the LQG-inspired rotating AOS BH has been provided in Appendix (B.1.2). For further reference and contemporary work on BH super-radiance, one can refer to [14, 297].

1.3 Motivation behind our work

Asymptotically, BHs in a number of alternative theories of gravity may give rise to the same observational signature as that in GR [298]. However, the same behaviour is not expected for strong gravity regimes. BHs in different theories can lead to qualitatively different features near the event horizon. Hence, exploring various alternative theories of gravity in the strong field regime still remains a thriving and fascinating field of study in the context of GW signatures of BHs.

The recent detection of GW has opened a new window to gravitational physics by giving unprecedented access to the regime of strong gravity. So far, the GW measurements are in good agreement with the predictions of GR, but the rapidly increasing number of events and the improved sensitivity of the detectors expected in the near future will enable one to verify GR to a high degree of precision or, alternatively, to detect some deviations from GR. In this perspective, it is important to consider alternative theories of gravity or extensions of GR, and study how their predictions deviate from GR, so that future analyses can extract the most relevant information from upcoming GW data. The most straightforward extension are scalar-tensor theories which involve, directly or in disguise, a scalar field in addition to the usual metric tensor.

The study of alternatives to standard BHs is further motivated by the information loss problem that might give rise to firewalls and quantum effects on the horizon scale. One of the methods to study the modifications arising out of such effects at the horizon is to replace the fully absorbing boundary condition at the horizon with some reflection very close to the would-be horizon, e.g., via membrane paradigm inspired models [245, 299–301]. We want to emphasize that knowledge of spectra of rotating BHs in specific theories is necessary if we want to be able to set constraints on such theories with ringdown observations, as well as performing a Bayesian comparison with GR.

Thus taking into account the present rate of advancement of technologies in the field of observations, we now have at hand not just the theoretical output but also the advantage of checking the theoretical predictions or models with the observational results which can further help in strengthening the idea of accepting or giving away some theories, making strong comments on the existence of some objects whose existence have been questioned since a long time due to the absence of any proper technology to observe or detect them either directly or indirectly. Accordingly, we have explored different solutions (BHs and NSs) in two different theories of gravity and have studied aspects of different physical processes around them.

Out of the different theories of gravity we have explored the following two theories with the concerned underlying motivation as explained below:

- $4D$**-Einstein-Gauss-Bonnet gravity**

This theory, first proposed in [10] as a $D \to 4$ limit of D dimensional Einstein-Gauss-Bonnet theory directly challenges Einstein's GR in $4D$ as it bypasses all the Lovelock's theorem. It is worth to mention that the higher curvature terms can modify the structure of the BH solutions, showing different properties with respect to the solutions in GR. Thus the study of such BH solutions with the presence of higher curvature terms is undoubtedly interesting from the physical point of view. Also, studying different astrophysical processes around it gives one the opportunity to not only understand the distinctive features of this theory but also to test its credibility.

While there were many works on constructing different BH solutions in this theory, such as static spherically symmetric BHs [10], BHs in AdS spaces [86], rotating BHs and their shadows [93, 302], generalised four dimensional BHs in Einstein-Lovelock gravity [97], radiating Vaidya like BHs [87], regular BHs [92, 303]; not much effort has gone into figuring out the QNMs of spherically symmetric BHs, particularly in non-asymptotically flat spacetimes, with the exceptions of [17–20]. Our aim is to fill up this gap in the literature by studying the QNMs of spherically symmetric BH in novel four-dimensional EGB gravity in asymptotically dS spacetime since our universe asymptotes to a dS spacetime in the infinite future, a fact that is strengthened by the existence of a nonzero cosmological constant.

The QNMs as we know serve as a characteristic fingerprint as it helps in commenting directly on the parameters of the source whose QNMs are being studied. Also with GW detection imminent on the horizon, possible strong-field deviations from GR is a topic that has received much attention recently. Henceforth it has strengthened the use of QNMs to help probe the BHs. In this direction, it is always good to have in hand the QNMs of a number of spacetime solutions since with every new detections, they can be crosschecked to see if theoretical calculations are matching with the observational ones. It has been seen that in the eikonal limit, the characteristic ring feature as obtained in the existing EHT images, which depends upon the impact parameter of the photon ring is directly related to the QNMs. QNMs can also be interpreted as waves trapped at the unstable circular null geodesic (also known as the light-ring) and slowly leaking out. The instability timescale of the geodesic is equal to the decay timescale of the QNM, and the oscillation frequency is given by $\omega \sim \frac{c}{r_{LR}}$, with c the speed of light and r_{LR} being the radius of the light-ring [198]. Thus, constraints on QNMs can in principle provide complementary information on the BH metric at the photon ring.

The development of new tools to study QNMs has received a tremendous boost with the possibility that classical BH oscillations could yield insights into their quantum behavior. This idea was first suggested by York [304] and Hod [4] and further explored by Dreyer [305] in the context of LQG. Subsequently the idea was revisited by many authors (see e.g. [306–311]). Although the relation between QNMs and area quantization stumbled in cases like charged and rotating four-dimensional geometries, yet Hod's suggestion was at the very least an important thrust to complete our understanding of classical BH oscillation spectra. Not only this but some literatures have highlighted striking relations between classical and thermodynamical properties of black objects

which indicates that the thermodynamical phase transitions correspond to changes in the QNM spectrum [312–317].

From the QNMs, one can learn a lot about stability. The QNM spectrum contains all the information about stability. In case of the Schwarzschild BH, stability is demonstrated by Kay and Wald [318] who showed the boundedness of all solutions with data of compact support. Whiting [319] has proven that there are no exponentially growing modes for the case of a Kerr BH, and in his proof, he showed that the growth of the modes is at most linear. Recent numerical evolution calculations [217, 218] for slowly and fast rotating Kerr BHs pick up all the expected features (QNM ringing, tails) and show no sign of exponential growth.

Along with QNMs, greybody factors [5, 114, 320, 321] have also been widely studied in the literature. They serve as an important parameter that throws light on how the spacetime around the compact object determines the reflection and transmission coefficients and are fundamental in understanding the quantum nature of BHs and their thermodynamic properties. Such studies can help in gaining insights into the properties of the BH and its surrounding environment which can further help astrophysicists interpret observational data from BHs.

So working along this line in our first work [8], we have studied the QNMs and greybody factors of the novel four dimensional Einstein-Gauss–Bonnet BHs in asymptotically dS spacetime for scalar, electromagnetic and Dirac perturbations and observed how the presence of the Gauss-Bonnet coupling constant α modifies the QNMs of these spacetimes.

Apart from expecting the QNMs in the ringdown stage of compact binary mergers, one also has the probability to detect what is known as echo signals in GW data. These echoes are expected to be present in the GW signal by Wormholes, NS and other ECOs. Recent detections of merging BHs allow observational tests of the nature of these compact objects. The work by Abedi-Dykaar-Afshordi (ADA) in [256] claimed tentative evidence for repeating damped echo signals following the gravitational-wave signals of the binary BH merger events recorded in the first observational period of the Advanced LIGO interferometers hinting at some Planck-scale structure near BH horizons at false detection probability of 1 % (corresponding to 25 σ significance level). However, just after this work, the authors in [263] reanalyzed the same data and falsified their claim.

It is only with future observations from interferometric detectors at higher sensitivity along with more physical echo templates that one will be able to confirm their existence. Thus the presence of echoes serves as an important tool that provides possible empirical evidence for confirming the nature of the compact object and might shed light on the existence of ECOs and alternatives to classical BHs, such as in firewall or fuzzball paradigms.

It is worth mentioning that apart from BHs, NSs are also one platforms where such echoes have been studied theoretically before as in the ringdown signal due to perturbing fields in the case of Janis-Newman-Winicour naked spacetime, which has a surface like NS at a finite radial distance [322]. So

taking into account these motivations, in our thesis, we have studied the $4D$-EGB NS to check if there exists some distinctive features from BH and we have found that the distinction is elucidated by the presence of echoes. However for any astrophysical system to be observationally relevant it has to be sufficiently stable. We have further checked this stability of a $4D$-EGB NS by studying the response of the spacetime towards the perturbation by test fields-scalar, electromagnetic and Dirac fields.

Even though the four-dimensional Gauss-Bonnet theory was formulated at the level of field equations, nonetheless, it is instructive and important to probe different aspects of this theory, particularly to those which are not restricted to the field equation alone. This will not only add other important directions in the discussion of four-dimensional Gauss-Bonnet theory but also help to find further flaws or strengths of this theory at a more fundamental level. Such theories are of interest partly because string theory predicts that at the classical level, Einstein's equations are subject to next-to-leading-order corrections that are typically described by higher-order curvature terms in the action.

- **Loop Quantum Gravity**

By quantizing gravity, LQG offers a framework for examining the universe's behaviour at the tiniest scales, when quantum mechanics' effects become more pronounced. The implications of LQG for comprehending BHs and their quantum behaviour will help us gain a deeper grasp of these mysterious celestial objects. This theoretical framework is essential for advancing our knowledge of the fundamental nature of the universe. LQG, thus has the potential to revolutionise our knowledge of the universe and its rules by resolving the drawbacks of current theories and offering a fresh viewpoint on the quantum nature of spacetime.

We have thus explored rotating and non-rotating BH solutions in this theory. The BH solution that we have chosen has been already derived by Ashtekar, Olmedo and Singh in [16, 21, 22] (known as AOS BH) by solving the effective equations incorporating quantum corrections. We have investigated the presence of quantum effects on the shadow of both non-rotating and rotating quantum-corrected BHs (LQG-inspired BH solutions) and how much deviation is introduced in the modified shadows due to the presence of quantum corrections in comparison to that of Schwarzschild and Kerr case. Also, we have made an attempt to look into the super-radiance effect in such background.

There are several compelling reasons why scientists are drawn to studying the shadows of BHs and other compact objects. Recent observation of the BH $M87$ and Sagittarius A^* has geared up the interest in the study of shadows. The analysis of the shape and size of these shadows provides insights into the properties of the BH, such as its mass and spin. Not only this, it also provides a direct test of Einstein's theory of GR, which predicts the existence of BHs and the distortion of spacetime around them. By comparing the observed BH shadows with the theoretical predictions, we can validate or refine our

understanding of the fundamental laws of gravity. Thus shadow holds within it a number of opportunities that have made it a captivating area of research in astrophysics and also offers a unique window into the extreme gravitational effects that occur near these enigmatic celestial objects.

Apart from shadows, we have also explored the super-radiance effect of a scalar wave from rotating AOS BHs in our thesis. The study of super-radiance sheds light on BH behaviour in quantum mechanics from a theoretical standpoint. It provides insight into the interplay between quantum mechanics, gravity, and the behaviour of matter in extreme gravitational fields by comprehending how BHs can transfer energy from rotating motion to external waves or particles. Moreover, the observation and analysis of superradiant phenomena around BHs can serve as a powerful tool for probing the nature of dark matter which is predicted to exhibit superradiant amplification around spinning BHs [323]. Furthermore, super-radiance research has consequences for GW detection. GW signals picked up by LIGO and Virgo detectors may exhibit unique characteristics as a result of the waves surrounding BHs being amplified. Researchers can gain a better understanding of BH properties and the dynamics of their interactions with the surrounding environment by analyzing these signals.

Also, it is well known that the primordial BHs (PBHs) are microscopic in size and therefore the quantum effects at this scale are not going to be negligible. Since AOS BH shows significant quantum effects at the Planck scale it may model these PBHs. Therefore investigation of these quantum induced spacetime can be useful to understand the nature of PBHs. It is our belief that such studies will help illuminate the properties of Planck-scale physics.

We shall now discuss our work on $4D$-EGB BH in asymptotically dS spacetime in the next chapter.

Chapter 2

Quasinormal modes and greybody factors of the novel four dimensional Einstein-Gauss–Bonnet black holes in asymptotically de Sitter spacetime: scalar, electromagnetic and Dirac perturbations

2.1 Introduction

Black Holes (BH) are one of the most intriguing objects in the theory of General Relativity (GR). They are the simplest objects that one can come across in the study of GR, simply because they are parametrised by only three parameters: the mass, the charge and the spin. It is one of the reasons why BHs have attracted so much attention apart from the fact that they are mathematically beautiful as well as strange objects by their own merit at the same time.

Among many other interesting areas of studies, quasinormal modes (QNM) have gained attention for the last few decades in discussing the perturbations of BHs [2, 3, 161, 162]. quasinormal frequencies (QNF) carry unique information about BH parameters and despite their classical origin, it was found that QNMs might provide a hint into the quantum nature of BHs [305, 324, 325]. In addition, QNMs in anti-de Sitter (AdS) spacetime have been shown to appear naturally in the description of the dual conformal field theories (CFT) living on the boundary (see [2] for a detailed list of references). QNMs of BHs have already been observed in the ground based experiments [28, 326] and they already present a plethora of information about BHs. However, research areas still remain open towards interpreting those results which require the exploration of alternative theories of gravity[327, 328] towards understanding fundamental problems like singularity resolution or a quantum nature of gravity. One such alternative theory is the Einstein-Gauss-Bonnet (EGB) theory of gravity which consists of higher curvature corrections to the Einstein-Hilbert term in the gravitational action. There had been a lot of interests in BHs arising from higher curvature corrections to Einstein-Hilbert action as mentioned in chapter (1). However, it is imperative to note that the Gauss–Bonnet

action in D-spacetime dimensions, having the following form $\int d^D x\sqrt{-g}\alpha\mathcal{G}$, with $\mathcal{G} \equiv R^2 - 4R_{\mu\nu}R^{\mu\nu} + R_{\alpha\beta\mu\nu}R^{\alpha\beta\mu\nu}$ and α being the Gauss-Bonnet coupling constant, gives non-trivial equations of motion only in $4+1$ dimensions or higher, while in $3+1$ dimensions, the Gauss–Bonnet term reduces to a topological surface term (see [60, 88] for details). Thus, in four spacetime dimensions, the Gauss–Bonnet term does not contribute to the gravitational dynamics since it becomes a surface term. Although, the role played by the Gauss–Bonnet term in four dimensional gravity theories has been intriguing for a long time and few studies towards that direction could be found in [329, 330].

Very recently, Glavan and Lin [10] have shown by constructing a model of the novel four dimensional Einstein-Gauss–Bonnet ($4D$-EGB) gravity that the four important criteria, dictated by Lovelock's theorem for Einstein's GR with the cosmological constant Λ to be a unique theory of gravity (viz. existence of $3+1$ dimensional spacetime, general coordinate invariance, metricity and existence of second order equations of motion), can be overridden and the model can exhibit modified dynamics. This theory has been defined in four spacetime dimensions as $D \to 4$ limit of the higher dimensional Gauss–Bonnet theory. It has been shown that the EGB gravity theory can be reconstructed in a particular way where the Gauss–Bonnet coupling constant α, can be re-scaled as $\frac{\alpha}{D-4}$. This theory in four spacetime dimensions was soon termed as the novel $4D$-EGB theory, which is defined as a $D \to 4$ limit at the level of equations of motion. In this limit, the theory produces some non-trivial contributions to gravitational dynamics and some solutions as well. The discovery of such a theory in $D = 4$ dimensions, therefore, has generated tremendous interest in the area of higher curvature theories which has been reflected in the large volume of works as mentioned in chapter (1) being done in a short span of time. However, it should be noted that, since the proposal of the solution by Glavan and Lin in their original work, there have been several studies which questions the existence of this particular solution [132, 137, 143]. These studies argue that there is no consistent way of taking the $D \to 4$ limit of a D dimensional theory, as was suggested by Glavan and Lin. It was also shown in [331], by considering a semi-classical quantum tunnelling of the vacuum of the solution, that the vacuum decay rate would exhibit diverging behaviour or complex behaviour, leading to an unstable or non-physical vacuum of the $4D$-EGB solution. Since then, several regularization schemes have been proposed in order to overcome these shortcomings [91, 141, 142]. This subsequently led to the development of different versions of regularized (consistent) $4D$-EGB theories. An explicit formulation of the $4D$-EGB theory based on the idea of an extra dimension of zero proper length has also been proposed [332], that does not require any singular rescaling of couplings followed by a classical regularization of divergent actions. For a comprehensive discussion on the recent developments in 4D-EGB theories, we refer to the excellent review article [74].

All these theories were seen to admit the same static spherically symmetric BH solution as was found in the original work. Hence, several works were done in the literature in the $4D$-EGB theory. However, very little attention has been paid to the dS sector of the solution proposed by Glavan and Lin. Observations suggest that the present-day universe is undergoing an accelerated expansion, consistent with a positive cosmological constant ($\Lambda > 0$)) leading to a de Sitter-like geometry at large scales [333–335]. The early universe's inflationary era is also modeled using

near-de Sitter geometries. Hence studying QNMs in de Sitter spacetime might provide insights into the decay of perturbations and stability of the inflationary phase. QNMs in dS spacetime can reveal the stability and decay of perturbations in the late-time accelerated expansion phase of the universe. Also the QNM spectrum of black holes in dS spacetime can carry imprints of the cosmological constant, which may be detectable in gravitational wave observations. Thus the study of QNMs in asymptotically de Sitter spacetime, can help understand both fundamental cosmological questions and thermodynamical aspects all while linking theory to observable phenomena like gravitational waves. So, in this work [1] we have aimed at studying the QNMs of spherically symmetric BHs in four dimensional novel EGB gravity in asymptotically dS spacetime by analysing the BH's response to the scalar, electromagnetic and Dirac perturbation and studied its behaviour with change in the parameter of the theory - the Gauss-Bonnet coupling constant α. We have also studied the behaviour of greybody factors in presence of α and have explored the eikonal modes for all the three types of perturbation which has been discussed in this part of the thesis. Note that in this work, we would proceed by considering the solution as proposed by Glavan and Lin. We have worked in units where $G = c = 1$.

2.2 Background spacetime

It is well known that Einstein's General theory of Relativity is a perturbatively non-renormalizable theory, and it can be made sensible by adding higher curvature corrections to the Einstein-Hilbert action in strong gravity regimes. Among different choices of higher curvature terms, the Lovelock corrections play a crucial role in the sense that the field equations contain terms only up to the second derivative of the metric and secondly, the gravitational dynamics remain free of the Ostrogradsky instabilities. Of particular interest is the third order Lovelock correction, known as the Gauss-Bonnet term whose corresponding action looks like

$$S_{GB}[g_{\mu\nu}] = \frac{1}{16\pi}\int d^D x\sqrt{-g}\alpha\mathcal{G}, \tag{2.1}$$

where, α is the Gauss-Bonnet coupling constant and $\mathcal{G}$ is the Gauss-Bonnet term having the form $\mathcal{G} = R_{\alpha\beta\mu\nu}R^{\alpha\beta\mu\nu} - 4R_{\mu\nu}R^{\mu\nu} + R^2$. Incorporating such terms in the Einstein-Hilbert action had already generated many interesting scenarios, a few of which was mentioned in the introduction of this thesis. It was found that such a theory admits BH solutions (it admits both dS as well as AdS branches, see

$$ds^2 = -f(r)dt^2 + f^{-1}(r)dr^2 + r^2(d\theta^2 + \sin^2\theta d\phi^2), \tag{2.2}$$

with

$$f(r) = 1 + \frac{r^2}{32\pi\alpha}\left[1 - \sqrt{1 + \frac{128\pi\alpha M}{r^3} + \frac{64\pi\alpha\Lambda}{3}}\right]. \tag{2.3}$$

In the above M is related to the BH mass. In the limit $\alpha \to 0$, the above solution reduces to the Schwarzschild-dS solution and as $r \to \infty$, $f(r)$ reduces to

[1] The work presented in this chapter is based on [8]

the asymptotically dS spacetime with positive cosmological constant. The Gauss-Bonnet coupling constant α can in principle be either positive or negative. In fact, it can be shown that in appropriate parameter region, the solution has two horizons: the event horizon r_H and the cosmological horizon r_c. However, in the $\alpha < 0$ regime, the metric function does not remain real for small values of the radial coordinate. However, we are not interested in very small values of r, rather our interest lies in the region $r_H < r < r_c$, therefore, we can, in principle allow α to take negative values.

2.3 Probing the background with test fields: scalar, electromagnetic and Dirac perturbations

It is well known that the merger event of two compact objects consists of three basic stages - (i) the inspiral stage which can be well computed by post-Newtonian theory, (ii) the merger stage which can only be analyzed via numerical techniques and (iii) the ringdown stage - the final stage, which can be studied by the technique of perturbation theory. After the merger event, the final product is not stable, rather, it is in a perturbed state and gives off the perturbation in the form of GW signal which in general can be divided in three parts: (i) a prompt response at early times that depends strongly on the initial conditions; (ii) an exponentially decaying 'ringdown' phase at intermediate times, where QNMs dominate the signal, which depends entirely on the final product's parameters; (iii) a late-time tail (tails are due to backscattering off the background curvature), usually a power-law fall-off of the signal.

At the theoretical level, the QNM spectrum is of great relevance for BH physics as it serves as one way of checking and proving whether BHs are stable or not against small perturbations. If they are stable, then, there should not exist any unstable modes and they can be accepted as real astrophysical entities. Also QNMs serve as characteristic fingerprint of the compact objects as they help in determining their parameters. The theory of perturbations of different compact objects have been one of the main topics of relativistic astrophysics for the last few decades that helps one to delve into the depths of information about these objects. They are of particular importance today, because of their relevance to GW astronomy and forms the basis for calculating such QNMs and frequencies. In this chapter we have studied the QNMs of the metric (2.2) with $f(r)$ given by (2.3) using test fields: scalar, electromagnetic and Dirac perturbations to see how they get modified in presence of the Gauss-Bonnet coupling constant α. In our perturbative approach we assume that the test fields contribute very little to the energy density (i.e., the quadratic terms in these fields have been dropped throughout, assuming that the energy-momentum tensors of these test fields are negligible). The problem then reduces to that of the test fields evolving in a fixed background.

For convenience, we have taken a rescaling of the Gauss-Bonnet coupling constant $32\pi\alpha \to \alpha$, and used this as the new Gauss-Bonnet coupling constant. So the expression (2.3) simply reduces to

$$f(r) = 1 + \frac{r^2}{\alpha}\left[1 - \sqrt{1 + \frac{4\alpha M}{r^3} + \frac{2\alpha\Lambda}{3}}\right]. \tag{2.4}$$

We shall now discuss the dynamics of the scalar, electromagnetic and Dirac fields on the $4D$-EGB BH background.

2.3.1 Scalar field

A massless scalar field Φ in a BH background (curved spacetime) is governed by the Klein-Gordon equation

$$\frac{1}{\sqrt{-g}}\partial_\mu\left(\sqrt{-g}g^{\mu\nu}\partial_\nu\Phi\right)=0\,. \tag{2.5}$$

The spherical symmetry of the background spacetime allows us to separate out the angular dependence of the scalar field Φ as,

$$\Phi(t,r,\theta,\phi)=\sum_{l,m}\frac{1}{r}\Psi_{scalar}(t,r)Y_{lm}\left(\theta,\phi\right)\,, \tag{2.6}$$

where $Y_{lm}\left(\theta,\phi\right)$ are the spherical harmonics of degree l and order m. Substituting (2.6) in (2.5), it is found that the angular and radial parts are separable. This has been possible only because of the symmetry of the background which has admitted the field evolution to be independent of rotations. This suggests that the angular variables θ and ϕ should factor out of the problem which further admits separation of variables. Hence, Eq. (2.5) takes the form

$$\frac{\partial^2\Psi_{scalar}(t,r)}{\partial t^2}-\frac{\partial^2\Psi_{scalar}(t,r)}{\partial r_*^2}+V_{scalar}(r)\Psi_{scalar}(t,r)=0\,. \tag{2.7}$$

Further considering the time dependence to be of the form $e^{-i\omega t}$ we have

$$\Phi(t,r,\theta,\phi)=\frac{1}{r}\psi_{scalar}(r)e^{-i\omega t}Y_{lm}\left(\theta,\phi\right)\,.$$

Hence Eq. (2.7) takes the form of a Schrödinger like wave equation for a particle encountering a potential barrier on the infinite line and is termed as the master wave equation in the context of perturbation theory as

$$\frac{d^2\psi_{scalar}(r)}{dr_*^2}+(\omega^2-V_{scalar}(r))\psi_{scalar}(r)=0\,, \tag{2.8}$$

where,

$$V_{scalar}(r)=f(r)\left(\frac{l(l+1)}{r^2}+\frac{1}{r}\frac{df(r)}{dr}\right), \tag{2.9}$$

is the effective potential for scalar field perturbation and the coordinate r_* is defined analogous to the tortoise coordinate of BHs as

$$dr_*=\frac{dr}{f(r)}\,. \tag{2.10}$$

2.3.2 Electromagnetic field

The motion of a test electromagnetic field in a curved background is given by the equation

$$\frac{1}{\sqrt{-g}}\partial_\mu\left(\sqrt{-g}F_{\gamma\sigma}g^{\gamma\nu}g^{\sigma\mu}\right)=0, \tag{2.11}$$

where $F_{\gamma\sigma}=\partial_\gamma A_\sigma-\partial_\sigma A_\gamma$ and A_μ is the four-vector potential. The spherical symmetry of the background spacetime allows us to decompose the angular part of A_μ in terms of the vector spherical harmonics,

$$\begin{aligned}&A_\mu(t,r,\theta,\phi)\\&=\sum_{l,m}\left(\begin{bmatrix}0\\0\\\frac{a^{lm}(t,r)}{\sin\theta}\partial_\phi Y_{lm}\\-a^{lm}(t,r)\sin\theta\partial_\theta Y_{lm}\end{bmatrix}+\begin{bmatrix}f^{lm}(t,r)Y_{lm}\\h^{lm}(t,r)Y_{lm}\\k^{lm}(t,r)\partial_\theta Y_{lm}\\k^{lm}(t,r)\partial_\phi Y_{lm}\end{bmatrix}\right),\end{aligned} \tag{2.12}$$

where the first term inside the summation is of odd parity, $(-1)^{l+1}$, while the second term is of even parity $(-1)^l$. Plugging Eq. (2.12) back into Eq. (2.11) one can arrive at the equation,

$$\frac{\partial^2\Psi_{em}}{\partial t^2}-\frac{\partial^2\Psi_{em}}{\partial r_*^2}+V_{em}(r)\Psi_{em}=0, \tag{2.13}$$

where $\Psi_{em}=a^{lm}$ for odd parity and $\Psi_{em}=\frac{r^2}{l(l+1)}\left(\partial_t h^{lm}-\partial_r f^{lm}\right)$ for even parity and

$$V_{em}(r)=f(r)\frac{l(l+1)}{r^2}, \tag{2.14}$$

is the effective potential for electromagnetic perturbation.

2.3.3 Dirac field

The dynamics of a massless fermionic field Υ in a curved background is determined by the Dirac equation,

$$\gamma^\mu\left(\partial_\mu-\Gamma_\mu\right)\Upsilon=0, \tag{2.15}$$

where γ^μ are the coordinate dependent Dirac four-matrices and Γ_μ are the spin connections in the tetrad formalism. Following [336], we separate out the angular dependence and rewrite the covariant equations of motion given by Eq. (2.15) as

$$\frac{\partial^2\Psi^\pm_{dirac}}{\partial t^2}-\frac{\partial^2\Psi^\pm_{dirac}}{\partial r_*^2}+V^\pm_{dirac}(r)\Psi^\pm_{dirac}=0, \tag{2.16}$$

where

$$V^\pm_{dirac}(r)=\frac{l+1}{r}f(r)\left(\frac{l+1}{r}\mp\frac{\sqrt{f(r)}}{r}\pm\frac{d\sqrt{f(r)}}{dr}\right), \tag{2.17}$$

are the effective potential corresponding to the two chiralities labelled as '+' and '−'. It is to be noted that for the background spacetime of the form (2.2), the potentials $V_+^{dirac}(r)$ and $V_-^{\text{dirac}}(r)$ can be transformed into one another following a Darboux transformation (DT) implying that the QNMs obtained from these two seemingly different potentials are isospectral. The DT is a method for relating second-order

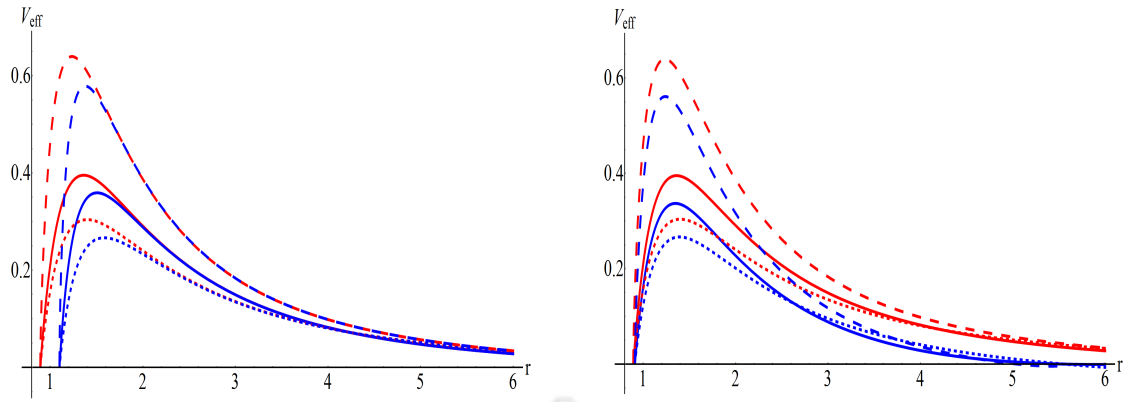

(a) $\alpha = 0.2$ (red) and $\alpha = -0.2$ (blue) (b) $\Lambda = 0.02$ (red) and $\Lambda = 0.08$ (blue)

Figure 2.1: The figure plots the effective potential V_{eff} with the radial coordinate r for the scalar (solid), electromagnetic (dotted) and Dirac (dashed) perturbation.

ordinary differential equations (ODE) written in a form without involving first-order derivative terms [337, 338]. Such forms of an ODE are generally known as the canonical form. For the case of BH perturbation theory, it was observed that the equations governing the BH perturbations of different parity are related. The Regge-Wheeler equation governing the odd parity perturbations [158] and the Zerilli equation governing the even parity [159] one are isospectral. Chandrasekhar [278] showed that the solutions of the two different parity perturbation equations are related to each other. The transformation proposed by Chandrasekhar to relate the odd and even parity perturbations is one example of the DT. The fact that the solutions to BH perturbation equations corresponding to different parity can be transformed among each other using the DT can be seen from the simple fact that such equations can be written as Schrödinger like second-order ODEs. In the case of the Dirac equation in curved space-time, Ψ^{+}_{dirac} and Ψ^{-}_{dirac} are related by the DT as

$$\Psi^{+}_{dirac} = c\left(\sqrt{f(r)} + \frac{d}{dr_*}\right)\Psi^{-}_{dirac},\ c = constant. \tag{2.18}$$

Therefore one can use either of the two potentials given in Eq. (2.17) for calculation of QNMs. In our case we have used $V^{\text{dirac}}_{+}(r)$ for calculations both in this and the following chapter.

It is worth mentioning here that the stability of the scalar and electromagnetic perturbations in a general BH background can be confirmed from the positive definiteness of the effective potential [17, 339]. However, it was shown very recently that the situation with the Dirac field is a little bit different, particularly if one considers higher curvature corrected BHs as well as study them in asymptotically dS spacetimes. Firstly, it was shown that even if the effective potential for one of the chiralities consists of a negative gap, the Dirac field perturbation can keep the BH stable [340]. However, the positive definiteness of any one of the potentials, for any one of the chiralities does not help in asymptotically dS BH backgrounds because the potential for both chiralities, in general, may have negative gaps [341]. Keeping these features in mind, we plan to study the QNMs of the novel Gauss-Bonnet dS BH in four spacetime dimensions. We plot the effective potential of all the three kinds of perturbations in Fig. (2.1). In the next section we will look into

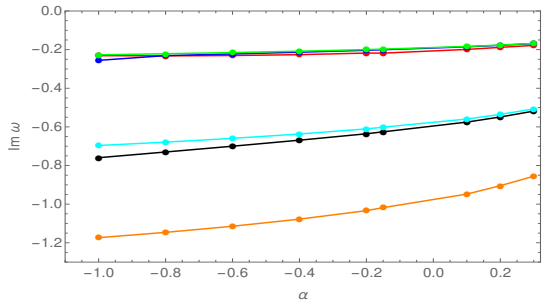

(a) Scalar perturbation

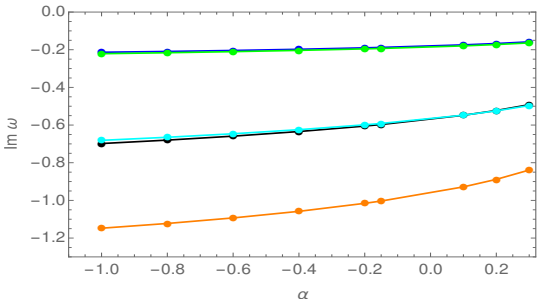

(b) Electromagnetic perturbation

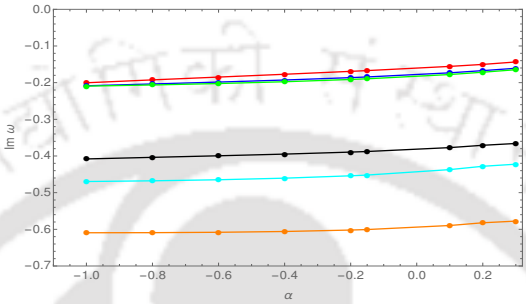

(c) Dirac perturbation

Figure 2.2: The figure plots the imaginary parts of the QNFs vs α of the $4D$-EGB dS spacetime, for different types of perturbations, for a fixed mass of $M = 0.5, \Lambda = 0.02$. The different colors denote the different modes for different values of (l, n): red $(0, 0)$; blue $(1, 0)$; black $(1, 1)$; green $(2, 0)$; cyan $(2, 1)$ and orange $(2, 2)$

the computation of the QNFs for the above three types of perturbations.

2.3.4 Computing the QNFs

As already mentioned in the introduction (1.2.1.1), we have generated the QNFs for the scalar, electromagnetic and Dirac perturbations of the $4D$-EGB dS BH using the 3rd order WKB approximation using the formula (1.21). Also, for better results, we have used Padé approximation as an improvement over the WKB method. The results of both these approximations have been quoted in order to look for the improvements that the Padé approximation induces.

After separation of variables, the radial parts of the equations (2.5), (2.11) and (2.15) take the form

$$\frac{d^2\psi_i(r)}{dr_*^2} + (\omega^2 - V_i(r))\psi_i(r) = 0 \;\; (i \in scalar,\; em,\; dirac), \tag{2.19}$$

The QNMs 'ω' are then, the solutions of this equation satisfying the conditions of purely outgoing waves at cosmological horizon and pure ingoing waves at the event horizon. The frequencies have been obtained for a wide range of parameter values, by individually varying l, α and Λ.

2.3.4.1 Results

The results for all the three types of perturbations are presented in Table (2.1) and Table (2.2). Our findings are summarised in figures (2.2), (2.3), (2.4), (2.5) and

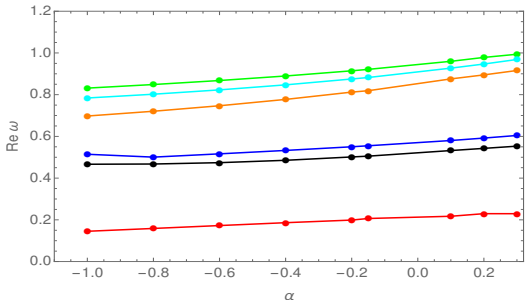

(a) Scalar perturbation

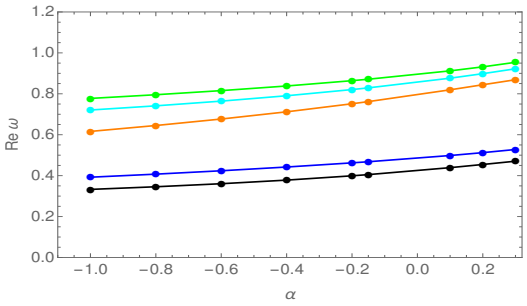

(b) Electromagnetic perturbation

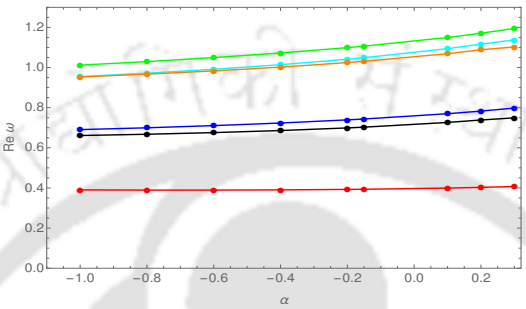

(c) Dirac perturbation

Figure 2.3: The figure plots the real parts of the QNFs vs α of the $4D$-EGB dS spacetime, for different types of perturbations, for a fixed mass of $M = 0.5, \Lambda = 0.02$. The different colors denote the different modes for different values of (l, n): red $(0, 0)$; blue $(1, 0)$; black $(1, 1)$; green $(2, 0)$; cyan $(2, 1)$ and orange $(2, 2)$

(2.6).

(1) **Scalar perturbation**

The inference that can be made from figures (2.2), (2.3), (2.4), (2.5) and (2.6) is that both the oscillation frequency (real part of the QNF) and the damping rate (imaginary part of the QNF) decreases with increasing values of Λ. Also as α decreases and eventually becomes negative, the real part of the frequency decreases whereas the imaginary part becomes more negative implying that the damping increases. For positive increasing values of α, the real part of the frequency increases, except for the $l = 0$ mode where the real part was found to be decreasing with increasing α, whereas the imaginary part increases.

(2) **Electromagnetic perturbation**

We observed similar behaviour to the case of scalar perturbation in case of the electromagnetic perturbation i.e., both the oscillation frequency and the damping rate decreases with increasing values of Λ. As α becomes more negative, the real part of the frequency decreases, whereas the imaginary part becomes increasingly more negative implying that the decay of the modes is faster. For increasing values of α, both the real part and the imaginary part increases, implying increasing oscillation and a decrease in the damping rate.

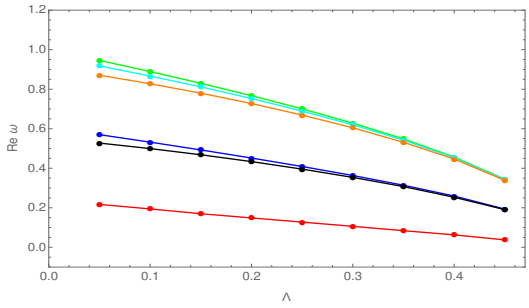

(a) Scalar perturbation

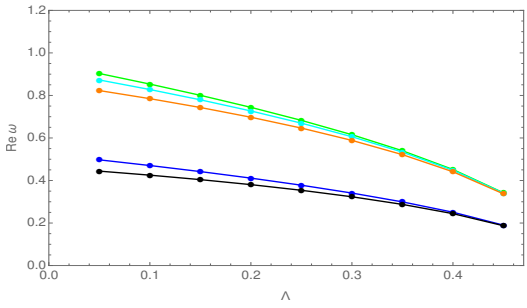

(b) Electromagnetic perturbation

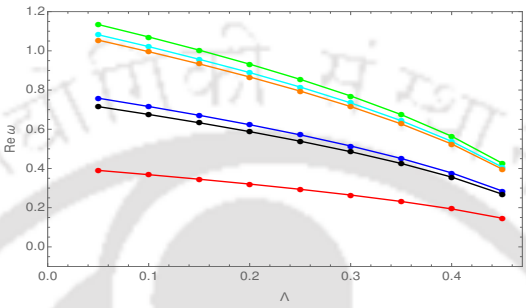

(c) Dirac perturbation

Figure 2.4: The figure plots the real parts of the QNFs vs Λ of the $4D$-EGB dS spacetime, for different types of perturbations, for a fixed mass of $M = 0.5, \alpha = 0.2$. The different colors denote the different modes for different values of (l, n): red $(0, 0)$; blue $(1, 0)$; black $(1, 1)$; green $(2, 0)$; cyan $(2, 1)$ and orange $(2, 2)$

(3) **Dirac perturbation**

The qualitative behaviour of the Dirac case is also pretty similar to the above two cases. The oscillation frequency and the damping rate decreases with increasing values of Λ. With decreasing values of α, the real part of the frequency decreases, whereas the imaginary part becomes more negative implying increase in the damping rate and vice-versa.

(4) **Common behaviour exhibited by all the three types of perturbations**

One common nature observed in all the three cases is that for a fixed value of l, as n increases, the real part of the frequency decreases, whereas the imaginary part becomes more negative implying that as the overtone increases for a fixed l, the damping rate increases. We also observe that for all the three types of perturbations, as α decreases, the oscillation frequency decreases with increasing damping rates, whereas as Λ decreases, the oscillation frequency increases with increasing damping rates. The results are summarised in figures (2.2), (2.3), (2.4), (2.5) and (2.6), where we have plotted the real and imaginary part of the QNF for different sets of parameter values. In particular, the plot of real vs. imaginary part of the frequencies tell us the same story as we have observed above: for all three types of perturbations studied in this work, the behaviours are quite similar for the real vs. imaginary parts of ω when we (i) varied α, keeping Λ fixed and (ii) varied Λ, keeping α fixed. In the case (i),

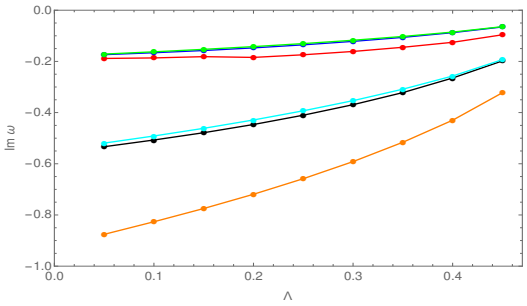

(a) Scalar perturbation

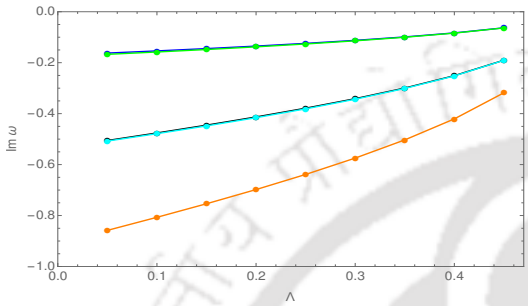

(b) Electromagnetic perturbation

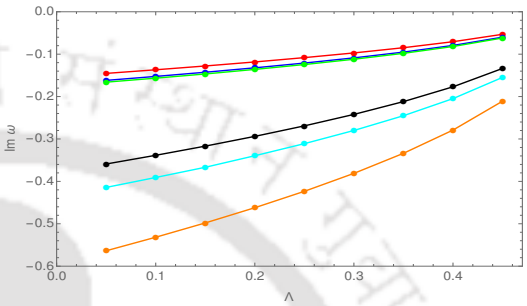

(c) Dirac perturbation

Figure 2.5: The figure plots the imaginary parts of the QNFs vs Λ of the $4D$-EGB dS spacetime, for different types of perturbations, for a fixed mass of $M = 0.5, \alpha = 0.2$. The different colors denote the different modes for different values of (l, n): red $(0, 0)$; blue $(1, 0)$; black $(1, 1)$; green $(2, 0)$; cyan $(2, 1)$ and orange $(2, 2)$

the Re(ω) grows as $-$Im(ω) decreases while for the case (ii), Re(ω) decreases as $-$Im(ω) decreases.

2.3.5 Eikonal QNMs, Lyapunov exponents and null geodesics

In the previous section we studied the QNFs for the $4D$-EGB dS BH solution employing third order WKB and Padé approximants. In this section, we would be interested in looking at the QNFs in the eikonal limit i.e., for very very large l values.

It has been well known that for static spacetimes, the scalar, electromagnetic and Dirac perturbations have similar behaviour in the eikonal limit [342] and their effective potential in this limit could be simultaneously given by

$$V_{eikonal} = l(l+1)\frac{f(r)}{r^2}\,. \tag{2.20}$$

Exploiting this simple observation and the fact that the location (r_{*0}) of the peak of the effective potentials in the eikonal limit, coincides with the radius (r_{ps}) of the unstable null geodesics, Cardoso *et.al.* [198] showed that the QNFs of a spherically symmetric, asymptotically non-AdS BH, in the eikonal limit, could be expressed by a very simple formula, which only depends on the metric function $f(r)$ and the position of the unstable null geodesic r_{ps}, given by

$$\omega_{QNM} = \Omega_{ps} l - i(n + 1/2)|\wp|\,, \tag{2.21}$$

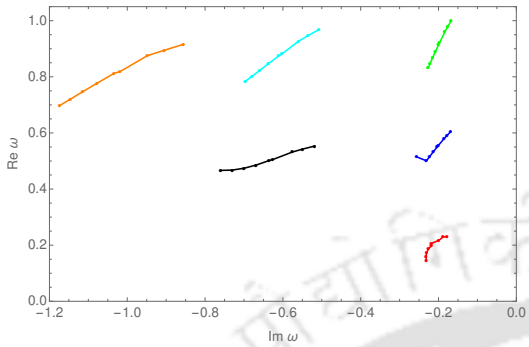

(a) Scalar perturbation(α is varied)

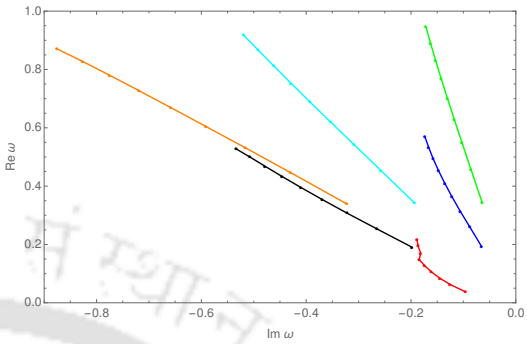

(b) Scalar perturbation(Λ is varied)

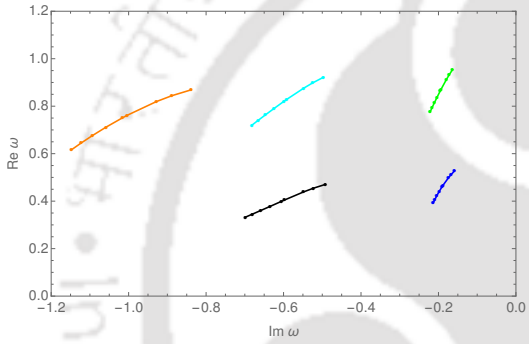

(c) Electromagnetic perturbation(α is varied)

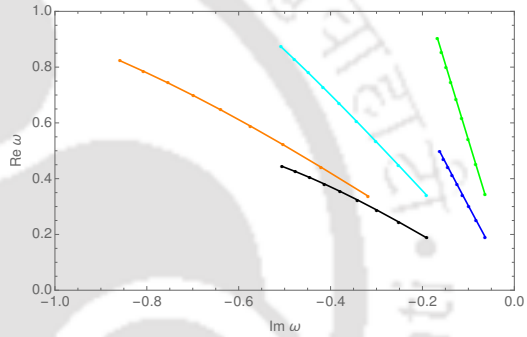

(d) Electromagnetic perturbation(Λ is varied)

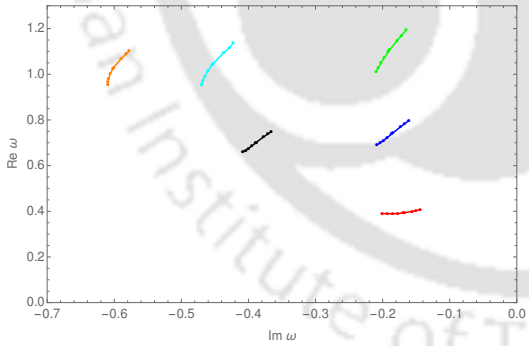

(e) Dirac perturbation(α is varied)

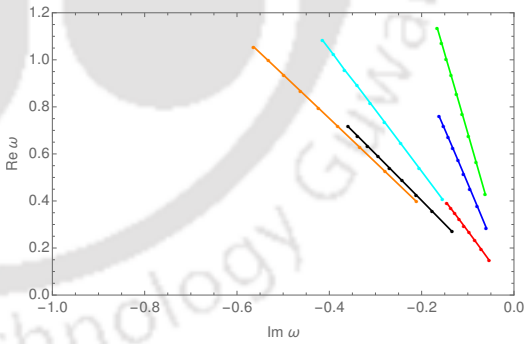

(f) Dirac perturbation(Λ is varied)

Figure 2.6: The figure plots the real part of the QNFs vs the imaginary part for different parameters (α, Λ) of the four dimensional Einstein-Gauss-Bonnet dS spacetime, for different types of perturbations, for a fixed mass of $M = 0.5$. The different colors denote the different modes for different values of (l, n): red $(0, 0)$; blue $(1, 0)$; black $(1, 1)$; green $(2, 0)$; cyan $(2, 1)$ and orange $(2, 2)$

Λ	*Scalar frequencies*		*EM frequencies*		*Dirac frequencies*	
	WKB	Padé	WKB	Padé	WKB	Padé
$l = 0,\ n = 0$						
0.05	0.191851 - 0.203018 i	0.217115 - 0.188491 i	-	-	0.35688 - 0.173238 i	0.39021 - 0.14534 i
0.1	0.176822 - 0.200981 i	0.194184-0.186394 i	-	-	0.338482 - 0.162822 i	0.368328-0.13681 i
0.15	0.160047 - 0.196268i	0.169978-0.181467 i	-	-	0.318778 - 0.151993 i	0.34516-0.127841 i
0.2	0.141785 - 0.18859 i	0.148664-0.184423 i	-	-	0.297486 - 0.140628 i	0.320425-0.118332 i
0.25	0.122442 - 0.17803 i	0.127506-0.174134 i	-	-	0.274207 - 0.12855 i	0.293732-0.108145 i
$l = 1,\ n = 0$						
0.05	0.565756 - 0.17396 i	0.569998 - 0.173652 i	0.491597 - 0.162554 i	0.497129 - 0.162263 i	0.745408 - 0.169465 i	0.758533 - 0.16181 i
0.1	0.528726 - 0.166532 i	0.532142-0.166151 i	0.46572 - 0.154036 i	0.470431-0.153756 i	0.704743 - 0.159868 i	0.71612-0.152461 i
0.15	0.490219 - 0.157751 i	0.492718-0.157472 i	0.438005 - 0.144944 i	0.441911-0.14467 i	0.661493 - 0.149753 i	0.671201-0.142623 i
0.2	0.450008 - 0.147533 i	0.451764-0.147167 i	0.408084 - 0.135147 i	0.411209-0.134873 i	0.615113 - 0.138992 i	0.623236-0.132176 i
0.25	0.407704 - 0.135771 i	0.408856-0.135299 i	0.375435 - 0.124459 i	0.377818-0.124186 i	0.564831 - 0.127412 i	0.571455-0.120958 i
$l = 1,\ n = 1$						
0.05	0.52127 - 0.53719 i	0.527453 - 0.533341 i	0.435811 - 0.510813 i	0.444061 - 0.505422 i	0.708779 - 0.51868 i	0.715535 - 0.359014 i
0.1	0.494656 - 0.510235 i	0.49951-0.50712 i	0.418053 - 0.480494 i	0.425114-0.47587 i	0.673411 - 0.487725 i	0.675567-0.338491 i
0.15	0.464595 - 0.480984 i	0.46831-0.478612 i	0.398227 - 0.449089 i	0.404096-0.445216 i	0.635276 - 0.455507 i	0.633195-0.316863 i
0.2	0.431015 - 0.448461 i	0.433718-0.446559 i	0.375867 - 0.416157 i	0.380581-0.413006 i	0.593788 - 0.421635 i	0.587946-0.293851 i
0.25	0.393812 - 0.411944 i	0.395598-0.41023 i	0.350355 - 0.381107 i	0.353984-0.378636 i	0.54813 - 0.385565 i	0.539103-0.269094 i
$l = 2,\ n = 0$						
0.05	0.944699 - 0.1714 i	0.945696 - 0.171379 i	0.902054 - 0.167263 i	0.903127 - 0.167234 i	1.12689 - 0.169579 i	1.13428 - 0.166011 i
0.1	0.888283 - 0.16259 i	0.889111-0.162562 i	0.852451 - 0.158068 i	0.853368-0.15804 i	1.06456 - 0.160023 i	1.07089-0.15655 i
0.15	0.829162 - 0.152897 i	0.829823-0.152864 i	0.799758 - 0.148314 i	0.80052-0.148286 i	0.998434 - 0.149928 i	1.00374-0.146701 i
0.2	0.766736 - 0.142233 i	0.767245-0.142194 i	0.743323 - 0.137876 i	0.743934-0.137848 i	0.927684 - 0.13917 i	0.932051-0.135917 i
0.25	0.700131 - 0.130461 i	0.700513-0.130413 i	0.68222 - 0.126579 i	0.682688-0.126551 i	0.851162 - 0.127577 i	0.854649-0.124474 i
$l = 2,\ n = 1$						
0.05	0.915765 - 0.519938 i	0.917682 - 0.519229 i	0.870677 - 0.508523 i	0.87277 - 0.507717 i	1.10179 - 0.513102 i	1.08211 - 0.414238 i
0.1	0.864759 - 0.492051 i	0.866335-0.491433 i	0.825968 - 0.479385 i	0.827758-0.478689 i	1.04337 - 0.483418 i	1.02162-0.390803 i
0.15	0.810215 - 0.461984 i	0.811479-0.461475 i	0.777896 - 0.448823 i	0.779385-0.448236 i	0.980924 - 0.452281 i	0.95681-0.366767 i
0.2	0.751675 - 0.429274 i	0.752663-0.428857 i	0.779385-0.448236 i	0.726982-0.415958 i	0.913617 - 0.419307 i	0.88925-0.339532 i
0.25	0.688381 - 0.393375 i	0.689123-0.392995 i	0.668676 - 0.381683 i	0.669603-0.381303 i	0.84028 - 0.383964 i	0.815449-0.311051 i
$l = 2,\ n = 2$						
0.05	0.866557 - 0.878753 i	0.870839 - 0.875728 i	0.818191 - 0.861649 i	0.822857 - 0.858214 i	1.05787 - 0.865609 i	1.05469 - 0.563642 i
0.1	0.824142 - 0.829065 i	0.827575-0.826545 i	0.780821 - 0.809826 i	0.784814-0.806893 i	1.00575 - 0.813699 i	0.995787-0.531736 i
0.15	0.777282 - 0.77677 i	0.779939-0.774784 i	0.739979 - 0.756148 i	0.743273-0.753722 i	0.949425 - 0.759757 i	0.933381-0.49803 i
0.2	0.725457 - 0.720678 i	0.727435-0.719142 i	0.69488 - 0.699911 i	0.697483-0.697981 i	0.888002 - 0.703117 i	0.866721-0.462122 i
0.25	0.667922 - 0.659599 i	0.669273-0.658321 i	0.644467 - 0.640159 i	0.646417-0.638696 i	0.82024 - 0.642859 i	0.794751-0.423441 i

Table 2.1: The table shows the QNFs for scalar, electromagnetic and Dirac perturbation calculated using 3rd order WKB and 3rd order Padé approximation for different modes and for different values of the cosmological constant Λ with a fixed value of $\alpha = 0.2$

α	*Scalar frequencies*		*EM frequencies*		*Dirac frequencies*	
	WKB	Padé	WKB	Padé	WKB	Padé
$l = 0,\ n = 0$						
-0.4	0.180832 - 0.27735 i	0.186337-0.225981 i	-	-	0.296146 - 0.219785 i	0.390391-0.177111 i
-0.2	0.195772 - 0.253448 i	0.198904-0.217768 i	-	-	0.322481 - 0.208132 i	0.392702-0.169171 i
0.1	0.201651 - 0.214774 i	0.217165-0.198971 i	-	-	0.35669 - 0.187761 i	0.399369-0.155677 i
0.2	0.199762 - 0.203244 i	0.229576-0.188228 i	-	-	0.367382 - 0.179329 i	0.402809-0.150239 i
0.3	0.193427 - 0.190947 i	0.229452-0.178089 i	-	-	0.377815 - 0.169283 i	0.40716-0.143584 i
$l = 1,\ n = 0$						
-0.4	0.536686 - 0.218129 i	0.532734-0.213291 i	0.446086 - 0.205134 i	0.442128-0.197707 i	0.699842 - 0.209979 i	0.72356-0.192807 i
-0.2	0.549937 - 0.206004 i	0.550216-0.203365 i	0.461665 - 0.194293 i	0.462492-0.189986 i	0.717943 - 0.1996 i	0.739206-0.186294 i
0.1	0.57638 - 0.185835 i	0.580238-0.185338 i	0.493014 - 0.175219 i	0.498365-0.174221 i	0.753786 - 0.182295 i	0.769883-0.173194 i
0.2	0.587311 - 0.177812 i	0.591926-0.177599 i	0.506358 - 0.167434 i	0.512385-0.167129 i	0.768739 - 0.175014 i	0.782949-0.167197 i
0.3	0.599501 - 0.168454 i	0.604401-0.16845 i	0.521617 - 0.1582 i	0.527825-0.158251 i	0.78572 - 0.166146 i	0.798141-0.160778 i
$l = 1,\ n = 1$						
-0.4	0.47996 - 0.673781 i	0.485412-0.668869 i	0.36924 - 0.643044 i	0.378135-0.634388 i	0.63944 - 0.652996 i	0.686091-0.394849 i
-0.2	0.495205 - 0.640069 i	0.501489-0.635617 i	0.39027 - 0.613196 i	0.399185-0.605314 i	0.662923 - 0.619354 i	0.699135-0.389366 i
0.1	0.524966 - 0.578625 i	0.532149-0.575213 i	0.430211 - 0.554447 i	0.439029-0.548075 i	0.710442 - 0.561208 i	0.726343-0.377132 i
0.2	0.535675 - 0.552912 i	0.542598-0.548649 i	0.44563 - 0.528629 i	0.454575-0.522776 i	0.72886 - 0.536773 i	0.738618-0.370809 i
0.3	0.545344 - 0.522544 i	0.553166-0.518376 i	0.461115 - 0.49729 i	0.470598-0.491876 i	0.747842 - 0.507336 i	0.749214-0.365865 i
$l = 2,\ n = 0$						
-0.4	0.890563 - 0.20879 i	0.889549-0.208055 i	0.839297 - 0.20436 i	0.838182-0.203475 i	1.06099 - 0.206307 i	1.07246-0.19753 i
-0.2	0.914376 - 0.200167 i	0.914363-0.19977 i	0.864146 - 0.196003 i	0.864129-0.195497 i	1.08844 - 0.198134 i	1.09919-0.191307 i
0.1	0.959097 - 0.183588 i	0.959925-0.183664 i	0.911108 - 0.179739 i	0.912119-0.179628 i	1.14091 - 0.182208 i	1.14975-0.177852 i
0.2	0.977433 - 0.17629 i	0.978527-0.176265 i	0.930539 - 0.172552 i	0.931706-0.172521 i	1.16271 - 0.175093 i	1.17078-0.171533 i
0.3	0.99823 - 0.167449 i	0.999374-0.167457 i	0.952729 - 0.163741 i	0.953937-0.163749 i	1.18763 - 0.166321 i	1.19494-0.164708 i
$l = 2,\ n = 1$						
-0.4	0.844874 - 0.637983 i	0.847039-0.636781 i	0.787721 - 0.626041 i	0.790421-0.624512 i	1.01882 - 0.629338 i	1.01416-0.460468 i
-0.2	0.872879 - 0.611238 i	0.875131-0.610292 i	0.818125 - 0.600068 i	0.820701-0.598741 i	1.05027 - 0.603375 i	1.04124-0.454037 i
0.1	0.924658 - 0.559073 i	0.927215-0.559376 i	0.874034 - 0.548465 i	0.876359-0.547481 i	1.11083 - 0.552839 i	1.0941-0.437141 i
0.2	0.944793 - 0.535835 i	0.946892-0.535036 i	0.896104 - 0.525452 i	0.898376-0.52458 i	1.13518 - 0.530337 i	1.11664-0.428069 i
0.3	0.966438 - 0.507735 i	0.968645-0.507014 i	0.920002 - 0.497242 i	0.922308-0.496468 i	1.16186 - 0.502703 i	1.13789-0.422383 i
$l = 2,\ n = 2$						
-0.4	0.771374 - 1.08336 i	0.777263-1.07762 i	0.704299 - 1.06566 i	0.711909-1.05811 i	0.950708 - 1.06974 i	1.00201-0.605908 i
-0.2	0.806628 - 1.03816 i	0.812274-1.03368 i	0.744812 - 1.0216 i	0.751293-1.01558 i	0.987769 - 1.02449 i	1.0245-0.601971 i
0.1	0.868698 - 0.94851 i	0.875572-0.947909 i	0.814313 - 0.932399 i	0.819472-0.928275 i	1.05991 - 0.935659 i	1.06913-0.58956 i
0.2	0.890101 - 0.907925 i	0.894772-0.904524 i	0.839203 - 0.892084 i	0.844248-0.888357 i	1.08741 - 0.895997 i	1.08845-0.582131 i
0.3	0.910593 - 0.858723 i	0.915856-0.85535 i	0.863356 - 0.842427 i	0.868766-0.838855 i	1.11535 - 0.847334 i	1.10249-0.577596 i

Table 2.2: The table shows the QNFs for scalar, electromagnetic and Dirac perturbation calculated using 3rd order WKB and 3rd order Padé approximation for different modes and for different values of the coupling constant α with a fixed value of $\Lambda = 0.02$

l	*Scalar*	*EM*	*Dirac*	*Approximate frequency from Eq. (2.21)*
3500	1321.97 - 0.169845 i	1321.97 - 0.169845 i	1322.16 - 0.169845 i	1321.778513516667 - 0.169844849949930 i
4000	1510.79 - 0.169845 i	1510.79 - 0.169845 i	1510.98 - 0.169845 i	1510.604015447620 - 0.169844849781841 i
4500	1699.62 - 0.169845 i	1699.62 - 0.169845 i	1699.81 - 0.169845 i	1699.429517378572 - 0.169844849666595 i
5000	1888.44 - 0.169845 i	1888.44 - 0.169845 i	1888.63 - 0.169845 i	1888.255019309525 - 0.169844849584157 i
5500	2077.27 - 0.169845 i	2077.27 - 0.169845 i	2077.46 - 0.169845 i	2077.080521240477 - 0.169844849523160 i

Table 2.3: The table shows the QNFs for the $n = 0$ mode and for very large multipole numbers l for a four dimensional Einstein-Gauss-Bonnet dS BH with $M = 0.5$, $\alpha = 0.2$ and $\Lambda = 0.05$

where, $\Omega_{ps} = \sqrt{\frac{f_{ps}}{r_{ps}^2}}$ and

$$\wp = \frac{1}{\sqrt{2}}\sqrt{\frac{-r_{ps}^2}{f_{ps}}\left(\frac{d^2}{dr_*^2}\frac{f}{r^2}\right)_{r=r_{ps}}}, \tag{2.22}$$

where the subscript 'ps' denotes that the corresponding quantity has been calculated at the unstable null radius r_{ps} and r_* is the tortoise coordinate. Physically, Ω_{ps} denotes the angular frequency of the unstable orbiting photons and $\wp$ denotes the principle Lyapunov exponent at the unstable null geodesics. Thus in the eikonal limit, the real part of the QNMs can be related to the orbital frequency Ω_{ps} of null rays at the unstable photon orbit and the imaginary part can be related to the Lyapunov exponent $\wp$ of the unstable photon orbit. We find the eikonal frequencies for all the three types of perturbation using the third order WKB approximation and also from the approximate formula given by Eq. (2.21) and report the numbers in Table (2.3). The convergence of the frequencies with each other and with the approximate formula with increasing value of l is evident from the table.

2.4 Greybody Factor

In this section we discuss the frequency dependent reflection and transmission coefficient, $R(\omega)$ and $T(\omega)$ respectively, for a scattering process of the scalar, electromagnetic and Dirac wave from the novel $4D$-EGB dS BH. This case is different from the QNF calculation since the boundary condition: there should be no incoming wave from infinity, is no longer imposed now as we need an incoming wave from infinity to calculate the greybody factors.

We have plotted the behaviour of the reflection and transmission coefficient with the frequency of the wave, for a wide range of parameter values in Fig. (2.7). It is seen that the general nature of the greybody factors for all the three types of waves: scalar, electromagnetic and Dirac is essentially similar. The greybody factors decrease with an increasing l and increasing Gauss-Bonnet coupling constant α. This also implies that the greybody factors for negative α would be greater than positive ones. The greybody factors tend to increase with an increase in the cosmological constant. We have summarised the behaviour of the greybody factors for all the three cases in Table (2.4) for different sets of parameters α, Λ and l.

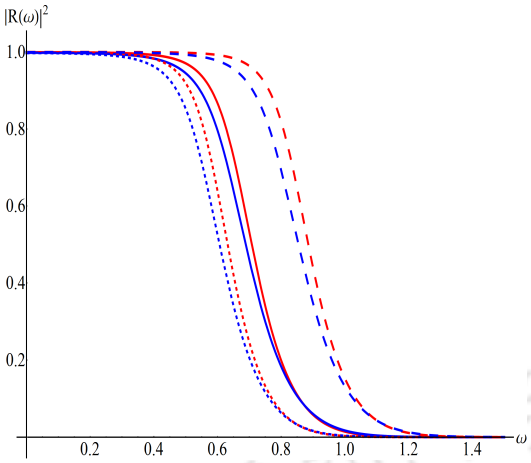

(a) $\alpha = 0.4$ (red) and $\alpha = 0.1$ (blue) for $\Lambda = 0.02$ and $l = 1$

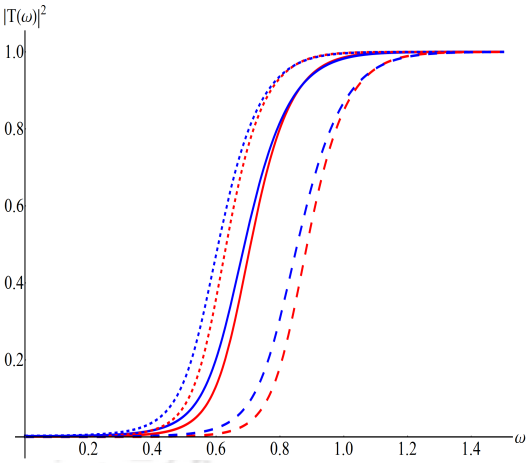

(b) $\alpha = 0.4$ (red) and $\alpha = 0.1$ (blue) for $\Lambda = 0.02$ and $l = 1$

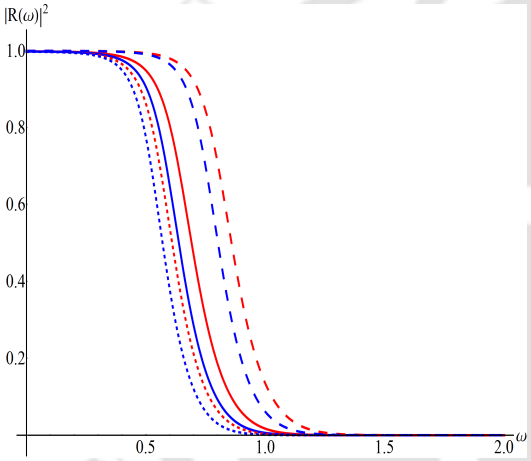

(c) $\Lambda = 0.02$ (red) and $\Lambda = 0.08$ (blue) for $\alpha = 0.15$ and $l = 1$

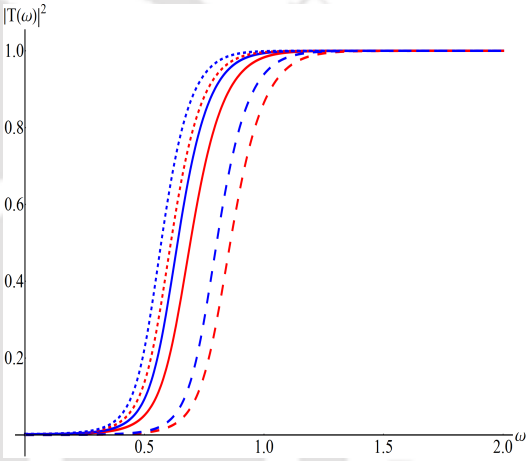

(d) $\Lambda = 0.02$ (red) and $\Lambda = 0.08$ (blue) for $\alpha = 0.15$ and $l = 1$

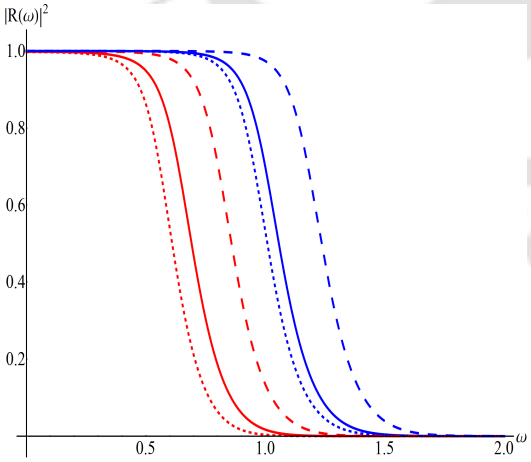

(e) $l = 1$ (red) and $l = 2$ (blue) for $\Lambda = 0.02$ and $\alpha = 0.15$

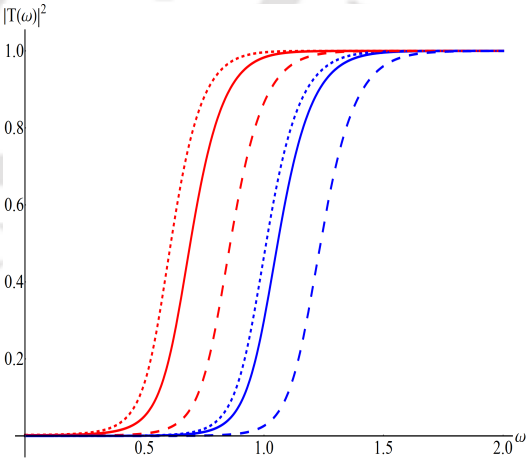

(f) $l = 1$ (red) and $l = 2$ (blue) for $\Lambda = 0.02$ and $\alpha = 0.15$

Figure 2.7: The figure plots the reflection and transmission coefficient of the scattered scalar (solid), electromagnetic (dotted) and Dirac (dashed) wave for $M = 0.5$ and different parameter values.

ω	*Scalar case* $\lvert T(\omega)\rvert^2$	*EM case* $\lvert T(\omega)\rvert^2$	*Dirac case* $\lvert T(\omega)\rvert^2$
$l=1, \quad n=0, \quad \alpha=0.4, \quad \Lambda=0.02$			
0	0.000773933	0.00108008	0.000104834
0.4	0.00804935	0.0176695	0.000716339
0.8	0.80129	0.932633	0.181766
1.0	0.985614	0.99713	0.847873
1.2	0.99943	0.999939	0.989076
$l=1, \quad n=0, \quad \alpha=0.1, \quad \Lambda=0.02$			
0	0.0020804	0.00297354	0.000500328
0.4	0.0171343	0.0377988	0.00275507
0.8	0.817021	0.937127	0.307556
1.0	0.982834	0.996419	0.868466
1.2	0.999061	0.999892	0.987348
$l=1, \quad n=0, \quad \alpha=0.15, \quad \Lambda=0.02$			
0	0.00186814	0.0028915	0.000138091
0.4	0.0157618	0.0361107	0.000928069
0.8	0.814444	0.933686	0.300518
1.0	0.983062	0.996153	0.902012
1.2	0.999105	0.999882	0.992818
$l=1, \quad n=0, \quad \alpha=0.15, \quad \Lambda=0.08$			
0	0.00221037	0.00275257	0.000266319
0.4	0.0251606	0.0502415	0.00216865
0.8	0.906484	0.968742	0.52664
1.0	0.993986	0.998805	0.951385
1.2	0.999791	0.999978	0.997278
$l=1, \quad n=0, \quad \alpha=0.15, \quad \Lambda=0.02$			
0	0.00186903	0.00268915	0.000421534
0.4	0.0157688	0.0348879	0.00237434
0.8	0.814445	0.936004	0.290641
1.0	0.983062	0.99645	0.865661
1.2	0.999105	0.999897	0.987467
$l=2, \quad n=0, \quad \alpha=0.15, \quad \Lambda=0.02$			
0	0.0000821326	0.000103032	0.0000164771
0.4	0.000328439	0.000454599	0.000053879
0.8	0.0205558	0.0375335	0.00187998
1.0	0.301218	0.468458	0.0262424
1.2	0.861667	0.920698	0.371926

Table 2.4: The table shows the greybody factor of the scattered scalar, electromagnetic and Dirac wave for different parameter values.

2.5 Conclusion and discussions

Very recently, it has been shown [10] that the EGB gravity theory in 4 dimensions can be reconstructed in a particular way where the Gauss-Bonnet coupling constant can be re-scaled as $\alpha/(D-4)$. This theory in four spacetime dimensions, defined as a $D \to 4$ limit at the level of equations of motion, admits BH solutions in asymptotically flat and AdS spaces. The QNMs of the scalar, gravitational and Fermionic fields for the asymptotically flat BHs in this background were already studied in [17, 110]. Motivated by this, in this chapter, we have extended the calculations to asymptotically dS spacetime and evaluated the QNMs of massless scalar, electromagnetic and Dirac field respectively. The method to compute the QNFs have already been discussed in the 1st chapter (1.2.1.1). As an addition, we have also computed the greybody factors in this background using the 3rd order WKB method as discussed in (2.4). We summarise the results of our study in Table (2.5). We find that both the oscillation frequency and the damping time decreases with

Parameter changes	*Greybody factor* $\lvert T(\omega)\rvert^2$	*QNF*(ω)	
		Re (ω)	*Im* (ω)
Scalar case			
$\alpha \uparrow$	$\downarrow$	$\uparrow$	$\uparrow$
$\Lambda \uparrow$	$\uparrow$	$\downarrow$	$\uparrow$
$l \uparrow$	$\downarrow$	$\uparrow$	$\uparrow$
Electromagnetic case			
$\alpha \uparrow$	$\downarrow$	$\uparrow$	$\uparrow$
$\Lambda \uparrow$	$\uparrow$	$\downarrow$	$\uparrow$
$l \uparrow$	$\downarrow$	$\uparrow$	$\downarrow$
Dirac case			
$\alpha \uparrow$	$\downarrow$	$\uparrow$	$\uparrow$
$\Lambda \uparrow$	$\uparrow$	$\downarrow$	$\uparrow$
$l \uparrow$	$\downarrow$	$\uparrow$	$\downarrow$

Table 2.5: Qualitative changes in the greybody factor and the QNF for all the three cases i.e. scalar, electromagnetic and Dirac cases with increasing values of α, Λ and l. An increase/decrease in a particular quantity has been shown by an up/down arrow.

increasing values of the cosmological constant Λ. On the other hand, we observe that as the Gauss-Bonnet coupling α decrease and eventually crosses over to negative values, the real part of the frequency starts decreasing whereas the imaginary part also starts to become more negative, implying that the damping increases. For positive increasing values of α, the real part of the frequency increases. This remains the qualitative feature of all the three different types of perturbations that we have

considered in this chapter. Although the stability of the scalar and electromagnetic perturbations can be confirmed from the positive definiteness of the potential, but the same cannot be concluded for the Dirac case. Thus, one may require to perform a full time domain analysis in order to understand the stability feature of the spacetime under Dirac perturbation. The present study therefore, can only give the qualitative nature of variations of the QNFs with the Gauss-Bonnet coupling constant α and cosmological constant as far as fermionic perturbation is concerned.

It needs to be mentioned here that the WKB approach limits the spectral analysis of dS BHs, as this method does not capture the dS modes associated with the cosmological horizon. It is known that WKB method can be used for effective potentials which have the form of potential barriers that approach to a constant value at the horizon and spatial infinity [3], so, it does apply in our study to determine the QNFs of 4D-EGB BH in asymptotically dS spacetime, however only the photon sphere modes can be obtained with this method and not the dS modes. WKB fails for dS modes mainly because the effective potential doesn't form a proper barrier with two turning points.Also QNMs in dS spacetimes, especially those linked to the cosmological horizon, are often purely damped (purely imaginary)[343–345]. This means that there is no oscillation and the wavefunction is exponentially decaying everywhere. However the use of WKB depends on matching oscillatory solutions between turning points. Since there is no oscillation in case of purely damped modes, so there exists no region where WKB's oscillatory approximation is valid. To capture de Sitter modes effectively, alternative methods such as pseudospectral methods - which is a discretization method, can be employed [343]. Such methods are adept at capturing the full spectrum of modes, including those associated with the cosmological horizon.

Along with the QNMs, we have also performed the calculation of the greybody factor for all the three different types of perturbations. We have figured out that the general feature of the greybody factors for the three different types of perturbation fields is essentially similar. The greybody factor decreases with an increasing l and an increase in the Gauss-Bonnet coupling constant α. Finally, the greybody factors tend to increase with an increase in the cosmological constant. This behaviour could be easily explained by looking at Fig. (2.1). The fraction of the wave transmitted upon scattering depends inversely on the height of the effective potential. With an increase in α, the effective potential increases, for all three cases, and hence the transmission coefficient decreases. On the other hand, with an increase in Λ, the effective potential decreases and hence the transmission coefficient increases. The dependence on l could similarly be seen from Eq. (2.9), Eq. (2.14) and Eq. (2.17). The effective potential for all the three cases increases with an increase in l and hence the transmission coefficient decreases.

Novel $4D$-EGB gravity has created a lot of uproar ever since it was proposed. The importance of the theory lies in the fact that, so far, which was a higher dimensional theory (the Gauss-Bonnet term was only a topological term in four dimensions), can now be applied in the context of four dimensional spacetime in which we live in. This can open up many interesting windows to the study of alternative theories of gravity. Moreover, having a look at the AdS branch will also be interesting in its own right. Calculations of the perturbations and the stability study of the novel $4D$-EGB BH in AdS background will be an important future extension of the present work. This may also be important to understand the AdS/CFT (Conformal Field Theory)

conjecture, since QNMs describe the approach to equilibrium in the conformal field theory side.

In the next section we have explored the NS solution in the novel $4D$-EGB theory which is obtained by considering large enough values of the Gauss-Bonnet coupling constant α. We have made an attempt to check whether such a spacetime is astrophysically viable or not and if it actually exists, how can one distinguish such a spacetime from BH background from the technique of perturbation viewpoint.

Chapter 3

Naked singularity in novel $4D$ Einstein-Gauss-Bonnet gravity: Echoes and Instability

3.1 Introduction

The first dynamical collapse solution of a spherically symmetric and homogeneous dust cloud was derived by Datt in 1937 [346] and Oppenheimer and Snyder in 1939 [347], where it was shown that the final end state of such a collapse will always be a Schwarzschild black hole (BH). However, since the model was based on the ideal assumption of homogeneity which, in general, is not a realistic scenario, one is motivated to consider more physical situations for the collapsing body. Also what will be produced as a final product of the collapsing matter depends on the initial data. General Relativity (GR) predicts that when large enough masses collapse under their own gravity, a spacetime singularity forms necessarily. Nevertheless, this does not simultaneously imply that along with the singularity, an event horizon will also be formed necessarily. In cases where a singularity is formed without an event horizon, one gets a naked or visible singularity [348, 349]. According to cosmic censorship conjecture [30], all singularities arising out of gravitational collapse are shielded by an event horizon, and that no "naked singularities" visible to a distant observer can exist in nature. This implies that one cannot expect the formation of an NS as the end state of a gravitational collapse. However, works like [62, 63] have shown theoretically that if one starts from a regular initial condition, then an NS may form as the end state of a gravitational collapse.

The four dimension Einstein-Gauss-Bonnet ($4D$-EGB) BH for large enough values of the coupling constant ($\alpha > M^2$) leads to a Naked Singularity (NS) [350], violating the Cosmic Censorship Conjecture. A brief overview of the different aspects of the $4D$-EGB theory of gravity has already been explained in chapter (1). Gyulchev *et al.* [350] studied the image of thin accretion disk around the weakly naked (with a photon sphere) $4D$-EGB singularity and observed a series of distinctive bright rings in the central part of the image which are otherwise absent for $4D$-EGB BHs. However, for any astrophysical system to be observationally relevant, it has to be sufficiently stable. This means that such systems must be stable or exist over timescales comparable to or longer than the duration of the observations. If they are unstable, they might radiate energy or change structure so rapidly

that they go undetected, or cannot be studied in detail. Stability ensures that the observable properties (such as emitted radiation, gravitational waves, or shadows) remain steady or evolve predictably during and across observation windows. Hence, while encountering a spacetime with a central NS, one naturally seeks answer to the question "Whether such a spacetime with a central NS is at all stable under perturbation? If so, how its response will be different from that of a standard $4D$-EGB BH [17, 130]? There are various compact objects that can mimick BHs so it is always good to look out for various ways that can help check for the differences between a BH and its mimickers. Such studies are important as they help in testing theories of gravity and also to comment on the status of compact objects other than BHs.

In chapter (2) we studied the asymptotically de Sitter $4D$-EGB BH solutions and their QNMs and greybody factors. In the present work [1], we have considered the NS solution of the novel $4D$-EGB theory and made an attempt to search for any distinctive feature exhibited by the NS solution as compared to the BH solution in the $4D$-EGB theory of gravity. We have done this from perturbation viewpoint by studying the nature of the time-evolution of test fields on the background. For stability purpose, we have studied the response of the $4D$-EGB NS-spacetime towards perturbation by test fields. Accordingly, we probe the spacetime by test scalar, electromagnetic and Dirac fields. Once again we note that such an analysis does not give preference to any particular version of the (consistent) $4D$-EGB theory and hence can be considered to hold equally in all the different consistent versions of $4D$-EGB theory that gives rise to the same solution (1.11).

It should be noted that since now, in case of an NS, there is no event horizon, so the boundary conditions as compared to BH will change. Near the singularity one needs to choose a proper boundary condition so that the dynamics of the perturbing field in an NS background can be determined. In course of our study we find that in case of NS, the time-domain profile shows the presence of echoes. Such echoes are found to be absent in case of BHs and hence they serve to distinguish the NS background from BHs. Hunting for them in the signals detected by gravitational wave (GW) detectors is very crucial as their presence, as already mentioned in chapter (1), might throw light on not only the existence of objects alternative to BHs like worm holes, fuzzballs and other exotic compact objects but also on the quantum nature of gravity to some extent. Throughout this chapter, we employ units in which $G = c = 1$.

3.2 Background Spacetime

The background is the same asymptotically flat, static, spherically symmetric metric in $4D$-EGB theory as discussed in chapter (2) and is given by

$$ds^2 = -f(r)dt^2 + \frac{1}{f(r)}dr^2 + r^2\left(d\theta^2 + \sin^2\theta d\phi^2\right) . \tag{3.1}$$

For convenience we have taken a rescaling of the Gauss-Bonnet coupling constant $16\pi\alpha \to \alpha$, and used this as the new Gauss-Bonnet coupling constant. So the metric

[1] The work presented in this chapter is based on [9]

(1.12) (without the cosmological constant Λ) simply reduces to

$$f(r) = 1 + \frac{r^2}{2\alpha}\left(1 - \sqrt{1 + \frac{8\alpha M}{r^3}}\right), \tag{3.2}$$

with α being a positive constant and M being the (Arnowitt–Deser–Misner) ADM mass. The spacetime (3.1) also appears as a solution to semi-classical Einstein's equation with Weyl anomaly and in the context of Einstein gravity with quantum corrections [351, 352]. The uniqueness of the BH solution (3.1) in the scalar-tensor formulation of the $4D$-EGB theories has been discussed in [353] along with another branch of solution that leads to an NS.

The nature of the solution (3.1) depends on the values of the dimensionless constant parameter $\gamma = \alpha/M^2$.

(1) For γ in the range $[0, 1]$, the spacetime defined by Eq.(3.1) represents a BH of mass M, characterised by an outer event horizon at r_+ and an inner horizon at r_-, hiding a central curvature singularity at $r = 0$, where

$$r_\pm = M\left(1 \pm \sqrt{1-\gamma}\right). \tag{3.3}$$

(2) For $\gamma = 1$, the line element (3.1) corresponds to an extremal BH characterised by a single horizon at $r_+ = r_- = M$.

(3) However, for $\gamma > 1$, the horizons cloaking the singularity cease to exist and the singularity at $r = 0$ becomes globally naked [350]. It is this range of γ that we are interested in this chapter.

It was shown that the Kretschmann scalar diverges at the location of the singularity at $r = 0$, however it does so in a slower rate than the Schwarzschild one. Also from Fig. (3.1) one can see that the angular momentum barrier (peak of the potential) remains only for γ in the range $(1, 3\sqrt{3}/4)$ which means that the spacetime is surrounded by a photon sphere of radius r_{ps} only for this range of γ and the singularity in this case is classified as being "Weakly naked", whereas for $\gamma > 3\sqrt{3}/4 (= 1.29904)$, this peak in the potential vanishes and the potential is characterized by infinite wall near the singularity. Hence for this range of γ no such photon rings are present and the singularity is classified as "strongly naked" [354].

We shall now discuss the response of the NS background to the scalar, electromagnetic and Dirac perturbations.

3.3 Perturbation by test fields

To analyse the stability and ringdown signatures of the spacetime (3.1) with a central NS, we study the perturbation of the spacetime against test scalar, electromagnetic and Dirac fields.

The dynamics of these test fields along with their effective potentials in a curved background have already been discussed in (2.3.1), (2.3.2) and (2.3.3). In all the three cases it has been found that the perturbation equation takes the form of a Schrödinger like equation given by

$$\frac{\partial^2\Psi_i}{\partial t^2} - \frac{\partial^2\Psi_i}{\partial r_*^2} + V_i(r)\Psi_i = 0\,. \tag{3.4}$$

where, i = *"scalar"* refers to scalar field, i = *"em"* refers to electromagnetic field and i = *"Dirac"* refers to Dirac field. However in case of Dirac field, as already stated, we will have two equations of the form (2.17) corresponding to the two chiralities labelled as '+' and '−'. An interesting feature is that both these equations corresponding to two different potentials yield the same set of QNFs and are hence termed as isospectral as the corresponding potentials can be related to each other via Darboux transformation. Thus, we will only consider the potential V^+_{dirac} for our calculation. Here r_* is the tortoise coordinate defined as

$$dr_* = \frac{dr}{f(r)}\,. \tag{3.5}$$

Close to the singularity, the coordinate r_* varies linearly with r, such that the singularity is by definition at $r_* = 0$. [2]

Having set up the perturbation equations and knowing the potentials, we are now in a state to comment on the viability of this solution and seek for some distinctive features in the ringdown part of the signal. However, before answering this question, we stumble upon another question - "Can one actually have sensible dynamics in NS spacetime, since, it violates the well known Cosmic Censorship Conjecture?"

A stronger version of the Cosmic Censor hypothesis asserts that any physically reasonable spacetime must be globally hyperbolic which by definition implies that in such spacetimes, there exist an initial data surface (Cauchy surface) whose domain of dependence is the entire spacetime. This makes it possible to determine or predict the dynamical equations in certain regions of the spacetime from initial conditions on such a surface. However, the same is not true for non-globally hyperbolic spacetimes, as in case of NS, due to the presence of the singularity, the dynamical equations say nothing about what can (or cannot) come out of a singularity. Unless some additional type of boundary conditions can be imposed upon the singularity, a complete breakdown of predictability occurs in any region of the spacetime where the singularity can be seen. It is seen that the problem of defining the dynamics in such a background can be loosely translated into the problem of finding self-adjoint extensions of the spatial part of the wave operator given by

$$A_i \equiv -\frac{d^2}{dr_*^2} + V_i\,. \tag{3.6}$$

In our present study we get an NS with $\gamma > 1$ that renders the spacetime globally non-hyperbolic. So, even before checking the stability and analysing the time evolution of test fields in this background, the very question that comes to our mind is whether it is possible to define dynamics in such a spacetime, meaning, "Is sensible dynamics allowed or not?" It has been found in one of the seminal papers by Wald [355] and also in a number of literatures (see Refs.[356–359]) that,

[2]For numerical computations, we shifted the origin of the tortoise coordinate from $r = 0$ to $r = 0 + \epsilon$, $\epsilon << 1$. Thus, the exact position of the singularity is excluded from the domain of numerical study but the effect of the singularity in terms of the divergence of the effective potential drives the dynamics of the test fields.

it is possible to uniquely define dynamics of test fields even in such a spacetime, provided there exists a unique self-adjoint extension of the operator A_i . This operator acts on the Hilbert space of square integrable functions, $\mathcal{H} = L^2(r_*, dr_*)$ on a static hypersurface orthogonal to a unit time-like Killing vector ∂_t. To analyse the existence of a unique self-adjoint extension of the operator A_i, one studies the eigenfunction of the equation,

$$A_i\psi_i = \pm i\ \psi_i\ . \tag{3.7}$$

The operator A_i is said to be essentially self-adjoint (existence of a unique self-adjoint extension) if atleast one of the eigenfunctions of A_i (for each sign of i) fails to be square integrable near the singularity. Close to the singularity, one can approximate

$$f(r) \approx 1 - \sqrt{\frac{2}{\gamma M}}\ r^{1/2} + O\left(r^{3/2}\right), \tag{3.8}$$

$$r_* \approx r + O\left(r^{3/2}\right), \tag{3.9}$$

$$V_i(r) \approx \frac{l(l+1)+2C_i}{2\gamma M^2} + \frac{l(l+1)}{r^2} + O\left(r^{-3/2}\right), \tag{3.10}$$

where $C_i = 1,\ 0,\ 3(8\gamma-1)(l+1)/(32\gamma)$ for scalar, electromagnetic and Dirac perturbations respectively. Thus, close to the singularity one can write Eq. (3.7) as

$$-\frac{d^2\psi_i(r_*)}{dr_*^2} + \left(\frac{l(l+1)}{r_*^2} + \cdots\right)\psi_i(r_*) = \pm i\ \psi_i(r_*)\ . \tag{3.11}$$

The general solution to Eq. (3.11) close to the singularity is of the form (for both signs of the eigenvalue $\pm i$)

$$\psi_i \sim \mathcal{C}_1\left(r_*^{-l} + \cdots\right) + \mathcal{C}_2\left(r_*^{l+1} + \cdots\right) \text{ as } r_* \to 0. \tag{3.12}$$

The first solution fails to be square integrable near the singularity and hence, A_i is essentially self adjoint. Thus we have seen that following Wald's prescription, we have found that a unique self-adjoint extension exists in this case which implies that we can now carry out our further study of stability analysis and signatures of ringdown in this non-globally hyperbolic spacetime.

It is important to note that addition of positive terms to the effective potential in Eq. (3.11) (including mass of the test field) does not alter the essential self adjointness of the operator A_i. Such terms effectively act as repulsive terms, increasing the rate of divergence of the larger solution and the convergence of the smaller solution close to the singularity [360, 361].

3.3.1 Potential profile

We plot the effective potential for scalar, electromagnetic and Dirac perturbation as a function of the coordinate r_* for different values of the dimensionless parameter γ in the NS regime in Fig. (3.1).

We observe that in the regime of weakly NS $\left(1 < \gamma < 3\sqrt{3}/4\right)$, the potential profile for all the three types of perturbations are characterised by a peak at $r_* > 0$ which rises to an infinite wall close to the singularity $[V(r \to 0) \to \infty]$, except for the $l = 0$

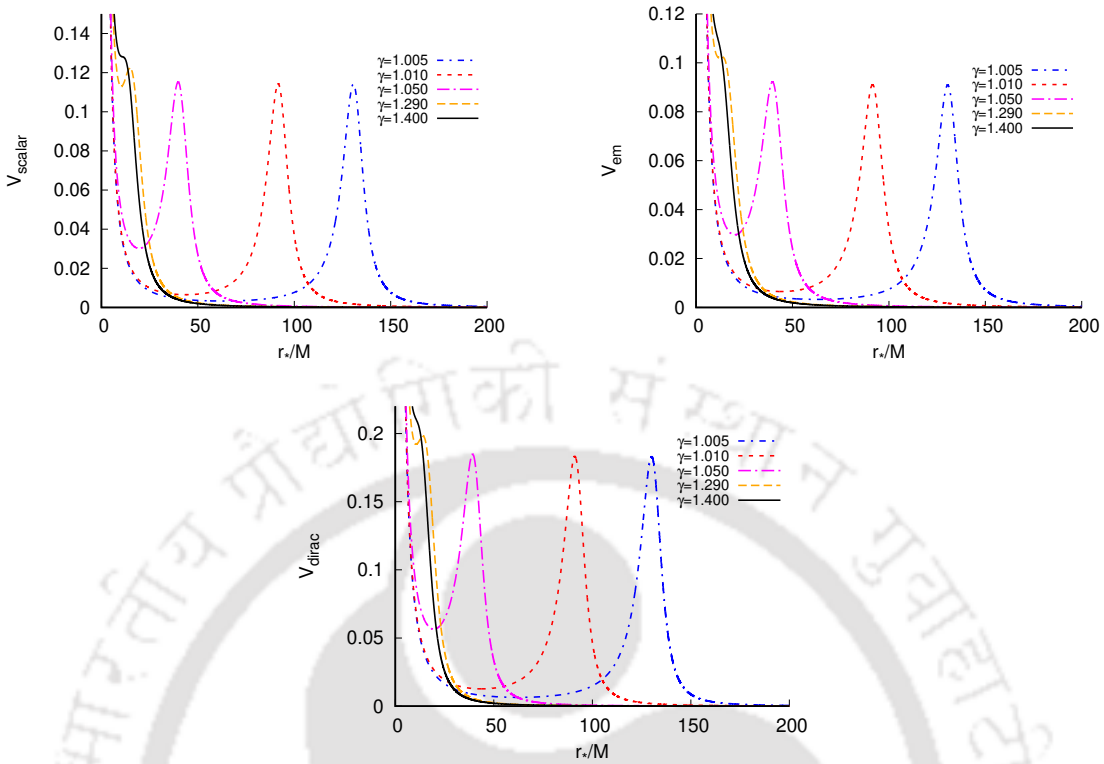

Figure 3.1: Plots of the effective potential for massless scalar (top left panel), electromagnetic (top right panel) and Dirac (bottom panel) perturbations with respect to the coordinate r_* for $l = 1$ and different values of γ in the NS regime.

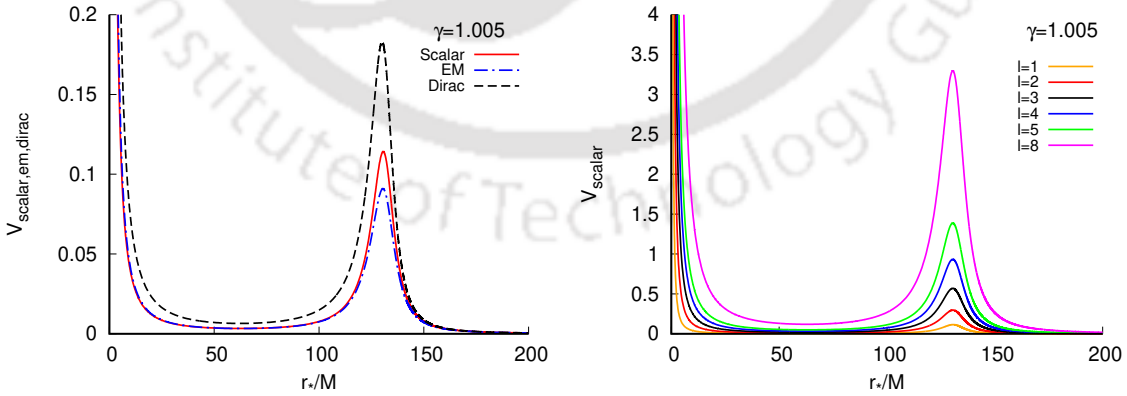

Figure 3.2: The left panel shows the difference in the effective potential for the scalar, electromagnetic and Dirac perturbations for $\gamma = 1.005$ and $l = 1$. The right panel shows the effective potential for massless scalar perturbation for $\gamma = 1.005$ for different values of l.

mode of scalar perturbation. The effective potential for the $l = 0$ mode of scalar perturbation diverges to $-\infty$ close to the singularity, $\left[V^{l=0}_{scalar}\left(r \to 0\right) \longrightarrow -\infty\right]$, rendering the system unstable [3]. Henceforth, unless otherwise mentioned we will only consider $l > 0$ modes of scalar and electromagnetic perturbations and $l \geq 0$ modes of Dirac perturbation.

The divergence of the effective potential near the singularity distinguishes the spacetime (3.1) with an NS from the corresponding BH solution. In case of a BH, the effective potential is characterized by a single potential peak outside the event horizon, whereas in case of an NS, as can be seen from Figs. (3.1) and (3.2), for a particular range of γ values, we get a potential well between the peak of the potential and the divergence near the singularity. This nature of the potential is further responsible for producing distinctive features for an NS spacetime in the form of echoes that can help distinguish an NS from a BH. As γ is increased from $\gamma \approx 1$, the potential peak shifts towards smaller values of r_*, and the width of the potential well also decreases. The potential peak keeps on shifting until it changes to a plateau and finally merges with the potential wall at sufficiently large values of γ. In this case, the effective potential is characterised solely by the infinite wall near the singularity and the potential well vanishes. We also note from Fig. (3.2) that the height of the peak of the potential profile for a given value of the parameter γ changes with the type of perturbation considered. From Fig. (3.2) we note that for a given γ the height of the peak of the effective potential is maximum for the Fermionic (or Dirac) perturbation and minimum for electromagnetic perturbation. Also, for each type of perturbation the peak height and width increases with the multipole number. It is these behaviour of the potentials that will modify the signal accordingly that reaches an asymptotic observer and provide hints to some unique characteristics.

In the next section we will integrate the master equation numerically and obtain the time-domain profile of the test fields in the background to explore the stability and other features of the $4D$-EGB NS solution.

3.3.2 Time evolution of Perturbation

To study the time-evolution of the perturbation we rewrite the perturbation equations (2.7),(2.13) and (2.16) in terms of null coordinates, $u = t - r_*$ and $v = t + r_*$,

$$4\frac{\partial^2}{\partial u \partial v}\Psi_i\left(u,v\right) + V_i\left(u,v\right)\Psi_i\left(u,v\right) = 0 \;;\; i \in \left(scalar,\ em\ , dirac\right). \tag{3.13}$$

To numerically integrate Eq. (3.13), we follow the integration scheme, proposed by Chirenti and Rezolla [231],

$$\Psi_i(N) = \left(\Psi_i(W) + \Psi_i(E)\right)\frac{16 - \Delta^2 V_i(s)}{16 + \Delta^2 V_i(s)} - \Psi_i(S) + \mathcal{O}\left(\Delta^4\right), \tag{3.14}$$

where Δ is the step-size and $S = (u, v)$, $W = (u + \Delta, v)$, $E = (u, v + \Delta)$ and $N = (u + \Delta, v + \Delta)$ are the grid-points in the $u - v$ plane. Eq. (3.13) is then numerically integrated in the (u, v) plane with the algorithm (3.14) using a triangular grid as shown in Fig. (3.3). For an effective potential of the form, depicted in Figs. (3.1), (3.2), the above integration scheme is found to be more stable compared to

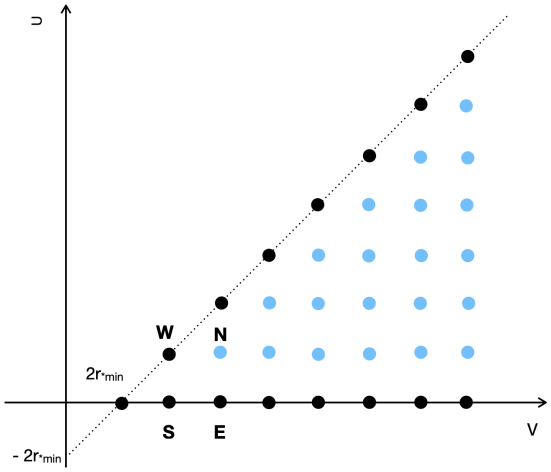

Figure 3.3: The figure (motivated from Fig. 5 of [231]) shows the numerical grid used for integration in the (u, v) plane and the domain of interest. The black points represent the grid points where the value of the solution (field) is known. The blue points represent the grid points where the solution needs to be calculated.

more popular integration scheme due to Gundlach, Price and Pullin [362], consistent with the observation in Ref. [231].

In general, in the linear regime the eigen frequencies are not sensitive to the choice of the initial conditions, hence, we model the initial perturbation by a Gaussian wave packet of width σ centered around $v = v_c$,

$$\Psi_i(u = 0, v) = e^{-\frac{(v-v_c)^2}{2\sigma^2}}. \tag{3.15}$$

We also assume that close to the singularity the perturbation is constant,

$$\Psi_i(r_* = 0, t) = \Psi_i(u = v - v_0, v) = 0, \ \forall t; \ \epsilon << 1. \tag{3.16}$$

The choice of the null boundary condition (3.16) deserve some attention as we will see soon that this guarantees that the perturbation field close to the singularity is normalizable.

If we now assume the time-dependence of the perturbation field as $\Psi_i(t, r_*) = e^{-i\omega t}\psi_i(r_*)$, we can write Eqs. (2.7),(2.13) and (2.16), near the singularity (upto leading order in r_*) as

$$-\frac{d^2\psi_i(r_*)}{dr_*^2} + \left(\frac{l(l+1)}{r_*^2} + \cdots\right)\psi_i(r_*) = \omega^2\psi_i(r_*) \ . \tag{3.17}$$

The general solution of the Eq. (3.17) is of the form as Eq. (3.12) and for ψ_i to be normalizable close to the singularity, $\mathcal{C}_1$ must vanish, which implies

$$r_*^l\psi_i\,|_{r_*=0} = 0. \tag{3.18}$$

Thus, boundary condition (3.16) guarantees that the perturbation field is normalizable close to the singularity and is also consistent with Ref. [355].

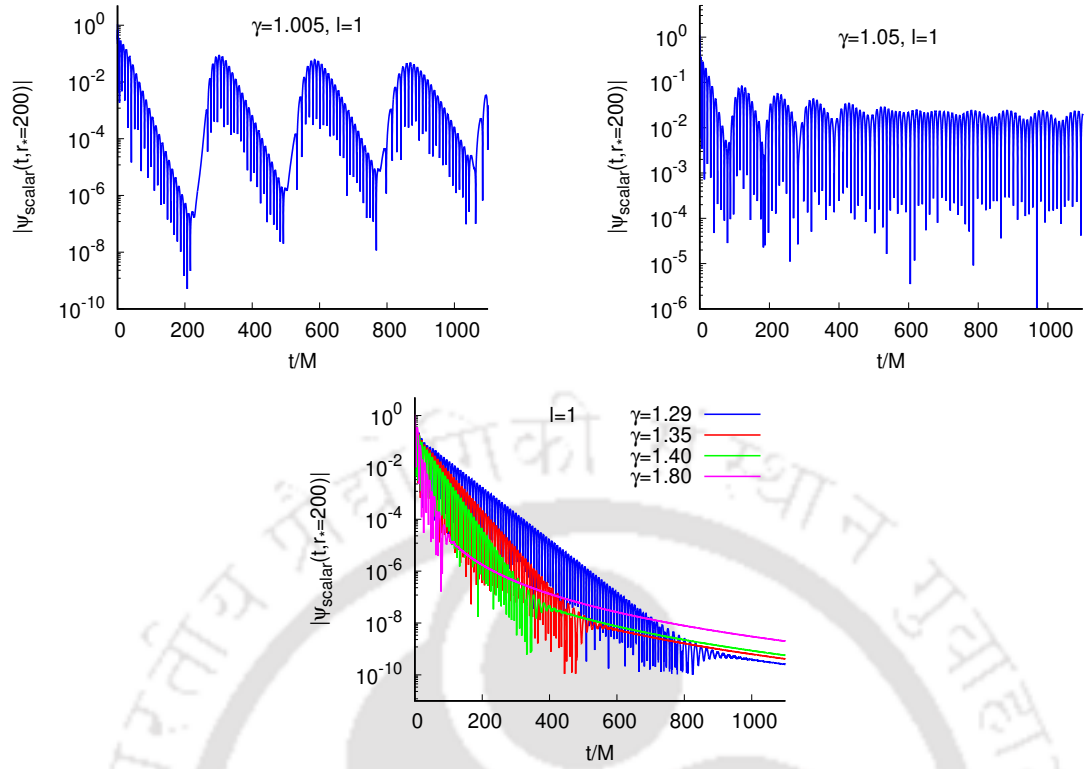

Figure 3.4: Semi-logarithmic plots of the time-evolution of massless scalar field perturbation for the $l = 1$ mode and different values of γ . The time-profile has been extracted at $r_* = 200$.

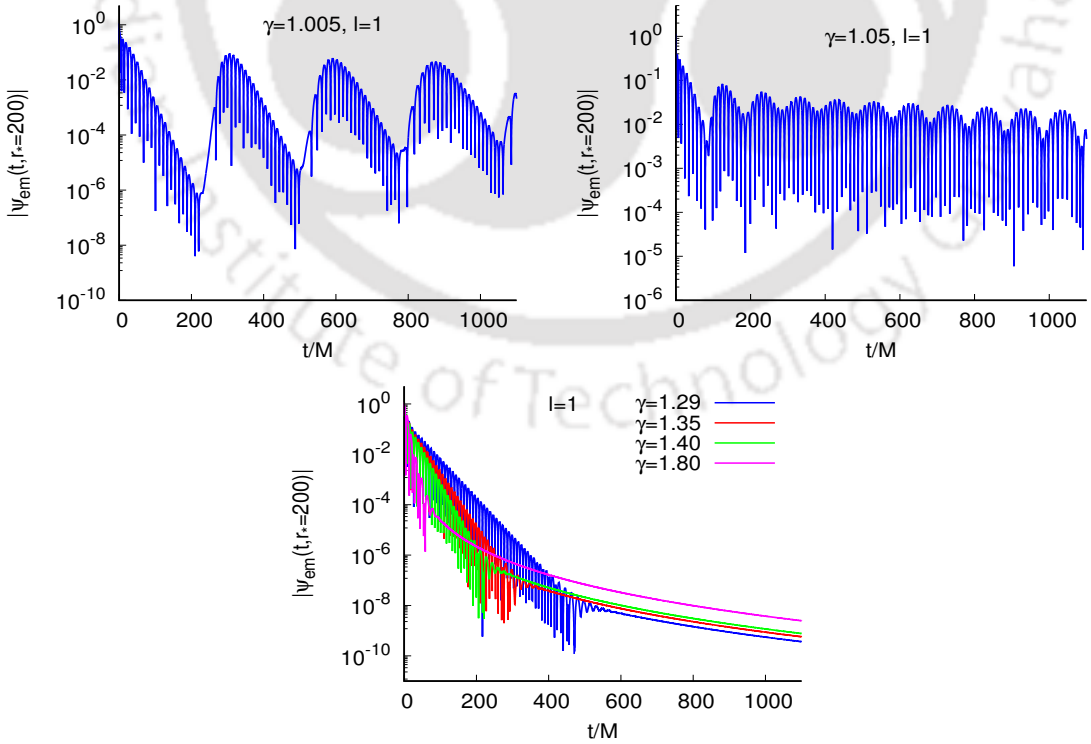

Figure 3.5: Semilogarithmic plots of the time-evolution of the $l = 1$ mode of electromagnetic perturbation. The time-profile has been extracted at $r_* = 200$.

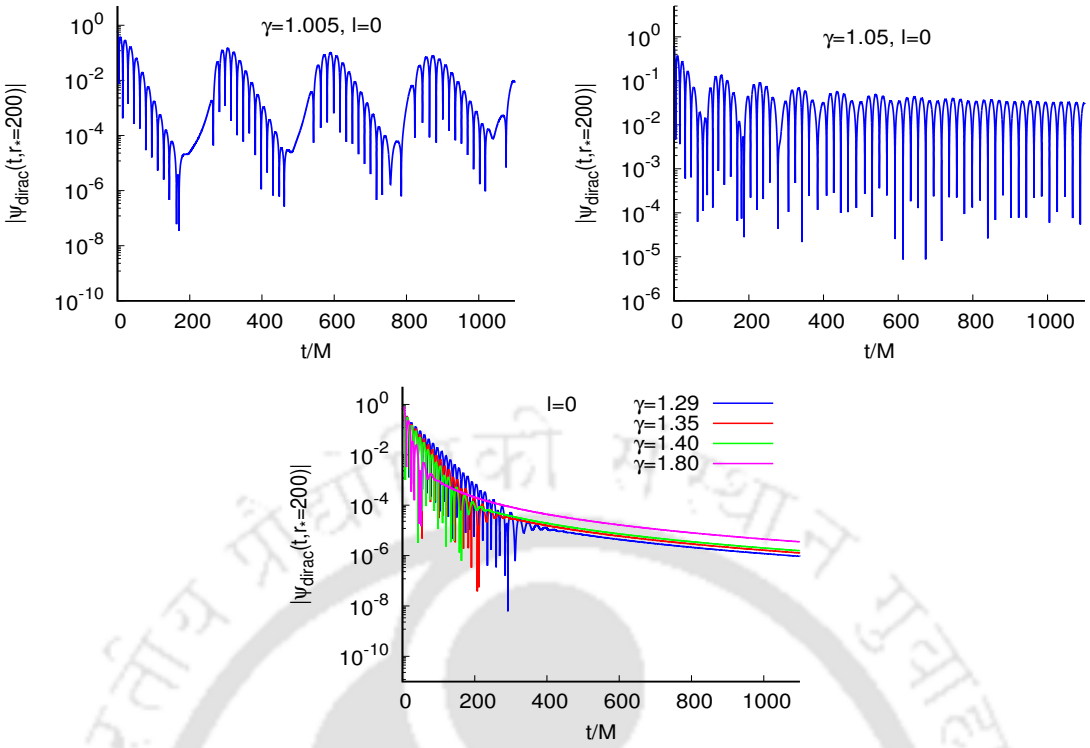

Figure 3.6: Semilogarithmic plots of the time-evolution of the $l = 0$ mode of Dirac perturbation. The time-profile has been extracted at $r_* = 200$.

3.3.3 Observations: Echoes and instability

The time evolution of the scalar perturbation for the $l = 1$ mode along a line of constant r_* has been shown in Figure (3.4). We observe that close to the BH limit ($\gamma = 1$) the time profile of the scalar perturbation is characterised by distinct echoes with diminishing amplitude and frequency. This is evident from the potential profile since one can see that for this range of gamma, the potential profile exhibits a well-shaped nature that serves the purpose of a trapping cavity to trap the signal that has transmitted through the angular momentum barrier, which then bounces off the barrier near the singularity and a portion of it leaks out to an asymptotic observer upon interaction with the peak of the potential again thereby giving rise to echoes whose amplitude and frequency goes on decreasing at each interaction with the barrier as shown in Fig. (1.3). The timescale between two such consecutive echoes will be proportional to two times the distance between infinite potential wall near the singularity and the peak of the potential barrier. As γ increases, the width of this well decreases, the time gap between two corresponding echoes decreases and hence they start overlapping eventually making these echoes less prominent. For sufficiently large values of γ, this well vanishes and there is no cavity left to trap these modes and so the enveloping oscillation of the echoes align to give rise to characteristic QNMs. Regarding the ringdown phase, it is difficult to exactly point out when this phase sets in. In our case, we have chosen the initial time value ($t_{initial} = t_o$) roughly from the time-domain profile, when the ringdown phase appears to set in and extracted the fundamental QNF using Prony's method. We have repeated this procedure by choosing $t_{initial} = t_o + \Delta t$, $t_{initial} = t_o - \Delta t$ and checked if the fundamental QNF remains stable for these cases. At sufficient late

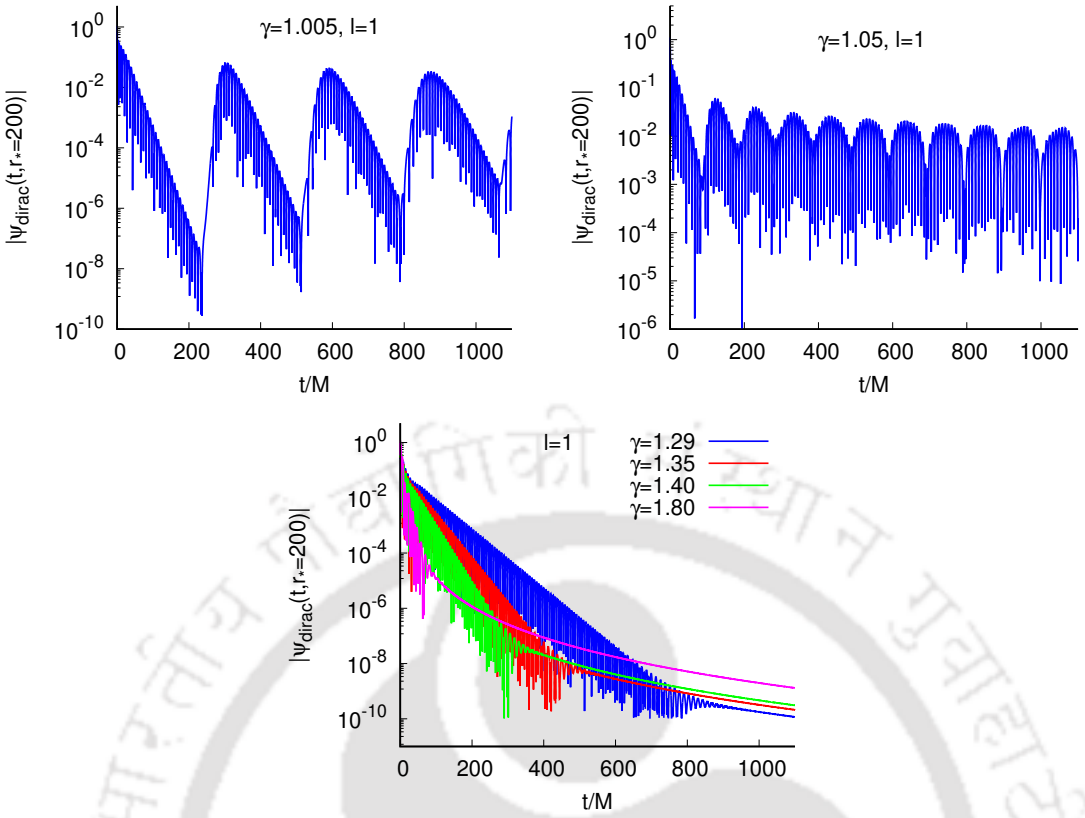

Figure 3.7: Semilogarithmic plots of the time-evolution of the $l = 1$ mode of Dirac perturbation. The time-profile has been extracted at $r_* = 200$.

times, the signal will decay to give late-time tails. A study on the time domain profiles for all the three different types of perturbations suggests that the tail falls off as $t^{-(2l+2+\gamma)}$.

It may be noted that although the existence of distinct echoes in the time evolution of massless scalar perturbations are indicative of the presence of weakly NS in the spacetime, the quasinormal ringing and late-time tails can also be observed in the time evolution of massless scalar field, when the singularity is strongly naked.

Time evolution of the $l = 1$ mode of electromagnetic and $l = 0, 1$ modes of Dirac fields also show similar characteristics (Figs. (3.5), (3.6) and (3.7)). However, for higher values of the multipole number, all the three types of perturbation (scalar, electromagnetic and Dirac) grows unboundedly with time suggesting an instability. This restricts the parameter space of α. For the scalar case, as already shown, the effective potential for the $l = 0$ mode diverges to $-\infty$ close to the singularity, $\left[V^{l=0}_{scalar}\,(r \to 0) \longrightarrow -\infty\right]$, rendering the system unstable. Figure (3.8) shows the time-evolution of the $l = 2, 3, 4, 8$ modes of the perturbations. To ascertain that the instability of the $4D$-EGB NS-spacetime is not a numerical artefact, we have also checked our results by slightly shifting the location of the inner boundary, ($r_{in} = r^0_{in} \pm \epsilon^2$, where $r^0_{in} \sim \epsilon$; $\epsilon << 1$). The consistency of our numerical analysis is further supported by testing the instability of the negative-mass Schwarzschild singularity against even parity metric perturbations [359, 363, 364].

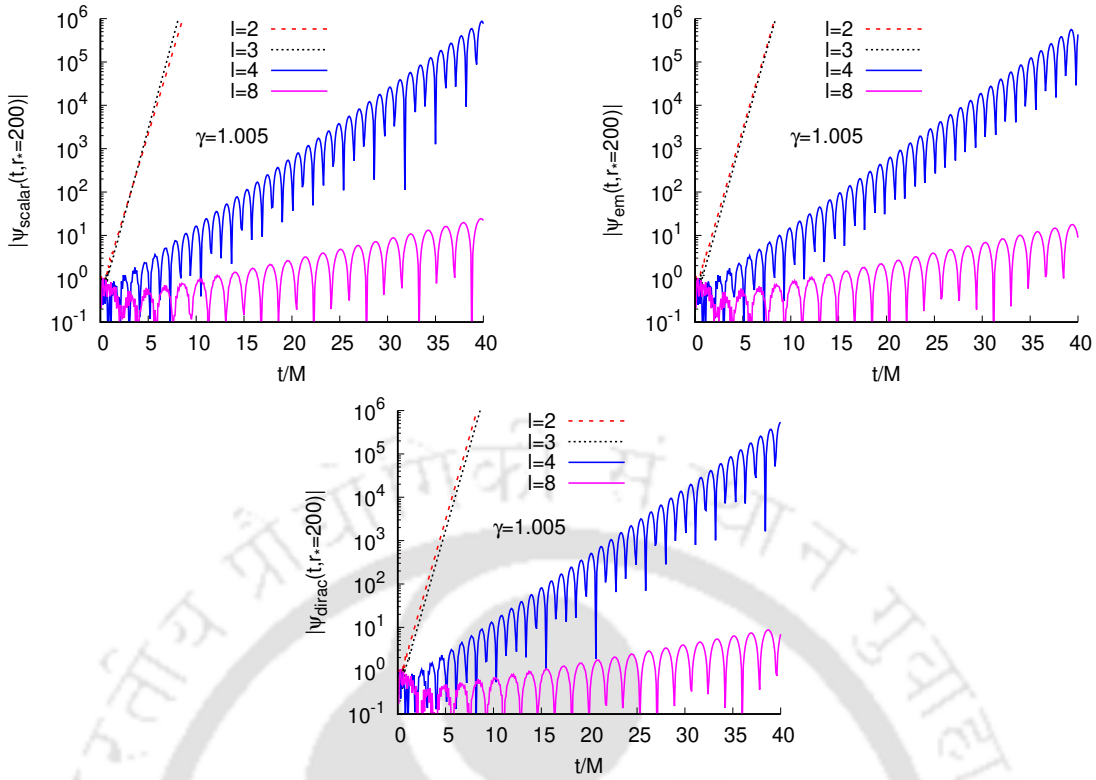

Figure 3.8: Semilogarithmic plots of the time-evolution of the $l = 2, 3, 4, 8$ modes of scalar (top left panel), electromagnetic (top right panel) and Dirac fields (bottom panel) for $\gamma = 1.005$.

3.3.4 Extracting the QNMs from time profile data: Prony's method

Now a natural question after observing these time profile data would be to which value of the QNF do they correspond. The answer can be found out with the help of Prony's method of fitting the time profile data by superposition of damped exponents with some excitation factors. This has already been described in chapter (1). Once the echoes align, mode frequencies can be extracted from the time profile by using Prony's method [3, 227].

$$\psi(t) \simeq \sum_{j=1}^{p} C_j e^{-i\omega_j t} , \tag{3.19}$$

where C_j denotes the excitation factors and ω_j is the complex QNF of the j-th mode. The real part of the QNF corresponds to the actual frequency of the wave motion while the imaginary part corresponds to the damping rate. The fundamental QNM frequency is characterised by the value of ω_j with the lowest damping rate i.e., with the smallest $Im(\omega)$. The timescale of decay of a mode can be roughly calculated from the imaginary part of the QNM frequency using:

$$\tau_{QNM} \approx \frac{1}{|Im(\omega_j)|} \tag{3.20}$$

Table (3.1) shows the characteristic fundamental QNFs for the $l = 1$ mode of scalar and electromagnetic perturbation and $l = 0, 1$ modes of Dirac perturbation. The

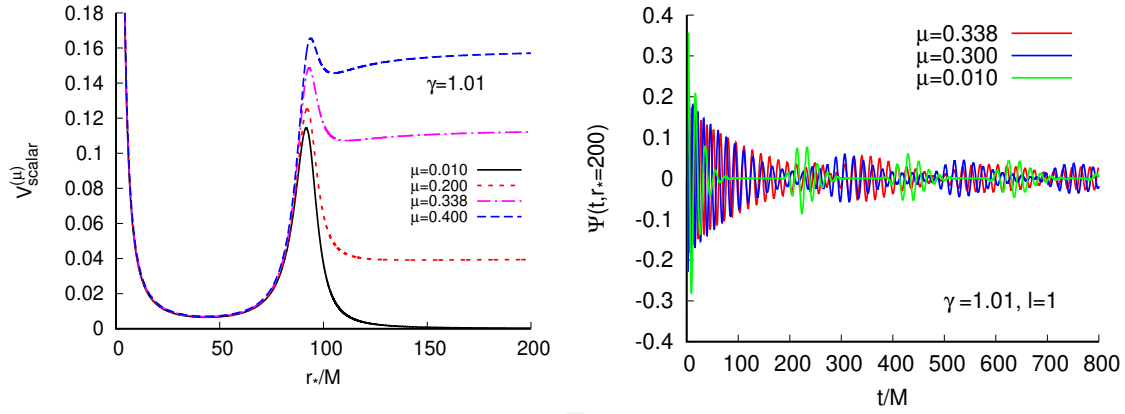

Figure 3.9: Plots of the effective potential for massive scalar field (left) and the corresponding time-domain profile (right) for the $l = 1$ mode with $\gamma = 1.005$.

QNFs has been extracted for values of the dimensionless parameter γ for which the echoes have aligned. We observe that the magnitude of both the real and imaginary parts of the QNFs increases with γ for each type of perturbation.
Another important feature that needs to be mentioned here is that echoes have modes linked to the potential well, representing stable light rings in the eikonal limit, which could potentially be analyzed using a WKB approach as done in [365]. In the eikonal limit ($l >> 1$), massless fields propagate as null particles. It has been well known that for static spacetimes, the scalar, electromagnetic and Dirac perturbations have similar behaviour in the eikonal limit and their effective potential in this limit could be simultaneously given by

$$V_{eikonal} = l(l+1)\frac{f(r)}{r^2}\,. \tag{3.21}$$

One can then see from Fig. (3.10) that, in the eikonal limit, there exists two light rings, one at $r = r_{LR1}$ which is a stable light ring and the other at $r = r_{LR2}$ which is an unstable light ring. The stable light ring effectively confines the field leading to long-lived modes which manifests themselves in the form of echoes in the time-domain evolution of perturbing fields. A WKB analysis of these trapped (long-lived) modes can then be done following [365]. In the eikonal limit, the frequency of a class of long-lived modes in four spacetime dimensions is given by WKB approach as

$$\omega \sim al - ibe^{cl} \qquad l >> 1 \tag{3.22}$$

Here a,b and c are positive constants. The constant 'a' is found to be associated with the angular velocity Ω_{LR1} of the stable null geodesic at the light-ring location $r = r_{LR1}$ given by

$$a \sim \Omega_{LR1} \equiv \frac{\sqrt{f(r_{LR1})}}{r_{LR1}} \tag{3.23}$$

Thus it can be seen that the modes of the echoes can be linked to the potential well, representing stable light rings.

Further, if we now consider the mass (μ) of the perturbing scalar field to be non zero then the effective potential in Eq. (2.9) gets modified to,

$$V^{(\mu)}_{scalar}(r) = f(r)\left(\frac{l(l+1)}{r^2} + \frac{1}{r}\frac{df(r)}{dr} + \mu^2\right)\,. \tag{3.24}$$

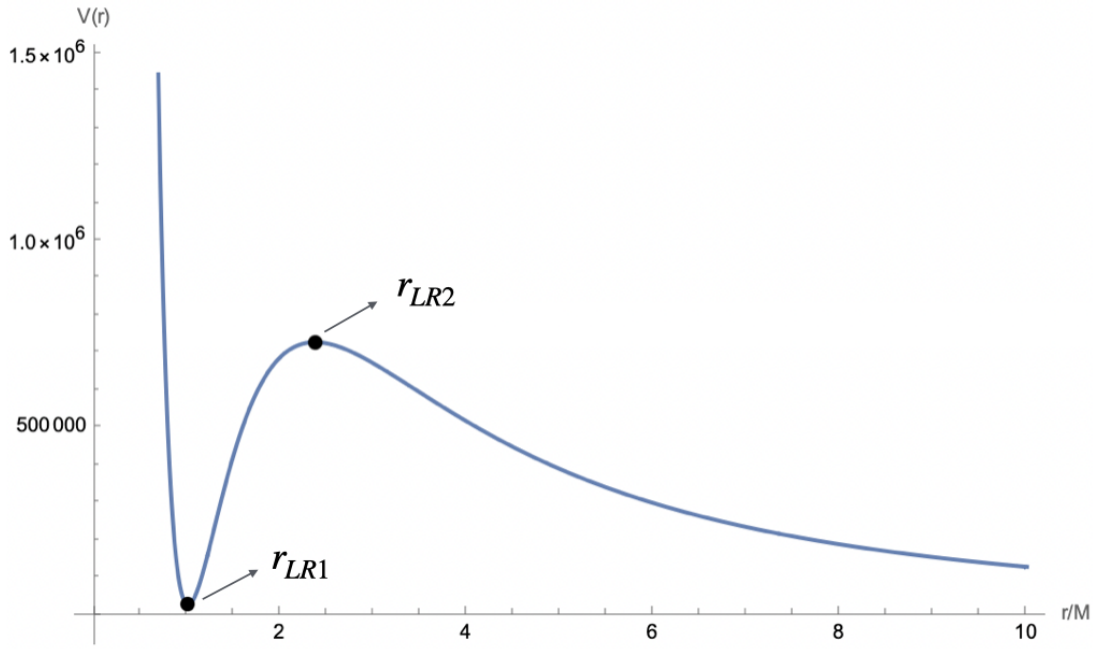

Figure 3.10: The figure shows the potential profile in the eikonal limit for M=1 and $\gamma = 1.005$

Table 3.1: Characteristic fundamental QNFs for $l = 1$ mode of massless scalar and electromagnetic perturbations and $l = 0, 1$ modes of massless Dirac perturbations.

γ	Scalar	Electromagnetic	Dirac	
	ω $(l = 1)$	ω $(l = 1)$	ω $(l = 0)$	ω $(l = 1)$
1.25	$0.3699 - 0.0082i$	$0.3528 - 0.0132i$	$0.2545 - 0.0131i$	$0.4676 - 0.0084i$
1.28	$0.3797 - 0.0107i$	$0.3613 - 0.0166i$	$0.2614 - 0.0149i$	$0.4787 - 0.0113i$
1.29	$0.3827 - 0.0116i$	$0.3638 - 0.0177i$	$0.2634 - 0.0155i$	$0.4820 - 0.0123i$
1.30	$0.3855 - 0.0125i$	$0.3662 - 0.0188i$	$0.2653 - 0.0161i$	$0.4852 - 0.0133i$
1.35	$0.3977 - 0.0170i$	$0.3766 - 0.0243i$	$0.2750 - 0.0207i$	$0.4985 - 0.0186i$
1.40	$0.4074 - 0.0215i$	$0.3842 - 0.0301i$	$0.2827 - 0.0248i$	$0.5097 - 0.0241i$
1.60	$0.4314 - 0.0390i$	$0.3943 - 0.0451i$	$0.2957 - 0.0392i$	$0.5375 - 0.0399i$

Thus the asymptotic value of the effective potential changes to $V^{(\mu)}_{scalar}\,(r \to \infty) \to \mu^2$ as can be seen in Fig. (3.9). In this case also a potential well exists that gives rise rise to echoes as in the massless case for values of γ close to unity, however for sufficiently large mass of the probing scalar field, it can be seen from the potential profile that there exists a trough in the effective potential outside the peak, resulting in quasi-bound states, which are manifested as elongation of the individual echoes (see Fig. (3.9)).

The QNFs evaluated using Prony's method depends on the choice of the starting point of the ringdown profile. To eliminate possible errors in the determination of the QNFs we have verified the QNM frequencies with time-profile date generated using different grid sizes (Δ). For each such time profile, we have checked the stability of the fundamental QNM frequencies by fitting with the series in Eq. (3.19) with different number of terms ($\sim 100 - 200$).

3.4 Conclusion and discussions

The Cosmic Censorship Conjecture [30] suggests that spacetime singularities must always be hidden by an event horizon, however, it has been argued that under suitable initial conditions of the collapsing matter, (if the collapse starts from a regular initial data) gravitational collapse may lead to an NS [62, 63]. In general for gravitational collapse, the quantum considerations are towards an avoidance of a singularity [366–368]. So, if for certain values of theory parameters, a gravity theory predicts the occurrence of an NS, then it is of paramount importance to check the stability of such a spacetime with NS against perturbation. If such a spacetime happens to be sufficiently stable, then one asks the associated question of how to observationally distinguish such an atypical spacetime.

In the present work, we considered an asymptotically flat, static, spherically symmetric spacetime (3.1) with a central singularity. We observed that the singularity becomes globally naked for $\gamma > 1$. It is important to emphasise that the metric (3.1) satisfies the field equations of all variants of the (consistent) $4D$-EGB theory [91, 141–144], hence, we studied the stability and response of such an NS-spacetime against perturbation by test fields without resorting to any particular version of the (consistent) $4D$-EGB theory.

We added test scalar, electromagnetic and Dirac fields in the background of the $4D$-EGB NS-spacetime and observed the time evolution of the perturbations numerically. The effective potential of all the three types of perturbation diverges to ∞ close to the singularity. So, we chose the null Dirichlet boundary condition consistent with [322, 369]. We observe that for the $l = 1$ mode of scalar and electromagnetic perturbations and for the $l = 0, 1$ modes of Dirac perturbation, when $\alpha \gtrsim M^2$ (γ is slightly greater than unity - weakly NS regime) , the signature of the difference between the spacetime due to a BH and the NS is quite distinctly elucidated by the existence of echoes in case of the $4D$-EGB NS spacetime. However, that is not the only interesting feature that we obtain. We also find that as the coupling constant is increased further, the timegap between the individual echoes decreases and finally for sufficiently large gamma values the echoes align,the QNM structure of the $4D$-EGB NS-spacetime ringdown becomes prominent and one can obtain the characteristic QNF of the spacetime from the time domain data using Prony's method. However, as l is increased from unity, the time-domain profile (Fig. (3.8)) suggests an instability. The scalar case exhibits instability for $l = 0$ itself due to the divergence of the potential to $-\infty$ close to the singularity. We have verified the instability of the spacetime for all the types of perturbations till $l = 10$.

Such studies not only help in pointing out the distinctive nature of such atypical spacetimes but also helps in putting constraint on the parameter theory which itself is interesting from observational viewpoint. So, we conclude that the $4D$-EGB spacetime with NS is unstable against test scalar, electromagnetic and Dirac perturbations which constraints the Gauss-Bonnet coupling constant $\alpha \leq M^2$.

भारतीय प्रौद्योगिकी संस्थान गुवाहाटी
Indian Institute of Technology Guwahati

Chapter 4

Shadow of quantum extended Kruskal black hole and its super-radiance property

4.1 Introduction

Black Hole (BH) solutions are ubiquitous in the theory of gravity. In fact it is believed that every galaxy contains one supermassive BH at its centre. Several observational evidences have confirmed this, including the one in our galaxy. From the very beginning of Einstein's general theory of relativity, vast attention has been given to these compact objects, starting from various observational to theoretical aspects and their analyses. While its existence is now unquestionable, its detection, since nothing can escape from it, still remains a very tough job. Recent detections of the Gravitational Wave (GW) signals from the merger events of compact objects by the GW detectors have shed light on their indirect detection. However for direct detection, one needs to actually rely on the photons coming from near the BH, reaching an asymptotic observer (detector) and check if these can be closely connected to an important observable. So one needs to actually track the escape of photons from such gravitationally intense compact objects and hence carry out observations and analysis in the electromagnetic channel. In this direction, the concept of "BH shadow" becomes very important. We know that in general shadow actually corresponds to a lack of radiation - the absence of photons, the same goes with when one talks in context of BHs and other compact objects. It is a region in the observer's sky from where there is no incoming radiation. Synge [267] and Luminet [268] gave the initial idea about the shadow of a BH which was later extended for Kerr case by Bardeen in [269]. Recently, the event horizon telescope has observed the shadow of the BH in the centre of the $M87^*$ galaxy [27] and the shadow of the Supermassive BH Sagittarius A^* in the Center of the Milky Way Galaxy [370]. This was a major breakthrough that was achieved exactly a century after the first observation of gravitational light deflection during a solar eclipse in 1919 which was the first experimental confirmation of a prediction from the general theory of relativity. Till the emergence of this concept, huge attention has been devoted to find the characteristics of shadows of different BHs (for a review and more references on the development of the subject, see [11, 12]), for various reasons. In general it was found out that for a wide range of rotating BHs, the shadow radius is dependent on

the BH spin parameter, the configuration of the light emission region near the BH and on the angle of inclination [371]. Studies along different avenues such as: shapes of BH shadows with various configurations and in various background geometries [285, 372–375], non-rotating and rotating BH spacetime shadows in several modified theories of gravity [376–381], constraining and measuring BH parameters from the study of shadows [382–386], BH shadows in dynamically evolving spacetimes [387], testing the general theory of relativity using BH shadows [388–390], proposing new methods of calculating BH shadows [391, 392], shadows of quantum corrected BHs [393–395], proposals to use shadows as standard rulers [396, 397] were already done in the literature. On another hand, it is to be mentioned that the shadow of an object in the sky does not always necessarily mean to be that of a BH, it may be of some exotic compact objects too [7, 13, 62, 398, 399] and all the above analyses can be done with such shadows which will further give us important information about these objects too. Thus shadow in itself holds a lot of opportunity for us to explore to infer important conclusions regarding not only these mysterious compact objects but also the alternatives to GR.

It is known that in strong gravitational regime, the quantum nature of spacetime cant be neglected and it is very important to construct a viable theoretical model of the dynamics of gravity. Furthermore, the singularity inside the BH has been a troubling and uncomfortable region. Non-singularly complete solutions, such as regular BHs are one of the suitable candidates to avoid such situations. There exists already many regular BH solutions in the literature [400–404]. However, in most of the cases, such BH spacetimes are not obtained as a solution of some underlying theory, neither are they connected to any quantum theory of gravity. On the other hand, it is well know that near the BH singularity the quantum effects are not negligible and must be incorporated within the solution itself. In this respect, Loop Quantum Gravity (LQG) has been one of the very few successful attempts to come up with a better understanding of quantum gravity.

There are few LQG inspired BH solutions [65–69] in literature and the characteristics of their shadows have been studied both for non-rotating as well as rotating [394] cases. Very recently, Ashtekar, Olmedo and Singh [16, 21, 22] found a complete regular static BH spacetime from an effective LQG motivated theory which is a quantum extended version of Kruskal geometry. The usual singular point $r = 0$ is hidden within a minimum area element. Throughout the rest of the chapter [1], we will denote this background as AOS BH, named after Ashtekar, Olmedo and Singh. Not many works have been done on this particular BH background except [405], where the authors have studied scalar perturbations of the AOS BH and found significant difference in the QNFs when compared with the Schwarzschild one. The purpose of the present chapter is to understand the quantum correction through its effect on the BH shadow. In the process, we also find the rotating counter part of the static AOS BH by employing the modified Newman-Janis Algorithm (NJA). It is important to note that the AOS BHs are not derived from an underlying physical theory. The effective equations are yet to be systematically derived from the quantum evolution in this model. Inspite of this, we have studied the rotating solution obtained via modified NJA as it simply serves the purpose of one possible model for capturing quantum corrections to the classical Kerr metric. We have then obtained the shadows for both non-rotating and rotating AOS BHs. Along with

[1] The work presented in this chapter is based on [15]

the shadows, in this chapter we have tried to analyse how the quantum parameters modify the super-radiance amplification and what information can they provide us with regarding the physics taking place at quantum length. In context of BHs, it is well known that super-radiance involves amplification in the radiation that has been scattered off a BH and has been observed in many different contexts and in many areas in physics. BH super-radiance and stability has been studied in detail in various contexts and similar works can be found in the literature [406–416]. Its study is important as it is greatly connected with the understanding of BH thermodynamics. Theoretically one can study this effect by scattering of fields from BH spacetime. In our work we have considered the scattering of a massless scalar field from rotating AOS BH and studided how the quantum parameters affect the condition for massless scalar field super-radiance,amplification factor and available window of energy for the scalar field to perform super-radiance.

We observe that the LQG inspired corrections can provide noticeable effect on the shadow and super-radiance amplification only when the BH is of the order of Planck size and for the rotating case, the effect is more pronounced for very fast rotating BHs. Thus if one needs to draw any sort of inference regarding the modifications pronounced by the quantum parameters, one must look for small mass and highly spinning quantum BHs solutions. However as we are working in the Planckian length, so these modifications are very very small and therefore at present, in all practical situations, the quantum effects should remain non-detectable. Nevertheless, new physics can appear at different length scales in the theory. Having said this, completely from the theoretical aspect, we investigate the shadows and super-radiance at the Planck scale. On the other hand the microscopic BHs are important at primordial level. Therefore understanding these LQG inspired BHs might be relevant to understand few important aspects of the inflationary era during the early stages of our universe. We use units where $G = c = \hbar = 1$ unless otherwise specified.

4.2 AOS black hole

AOS BH is a complete regular static solution of LQG motivated effective theory [16, 21, 22]. This does not contain the singular point $r = 0$ as it has been hidden by a minimum area element, determined by "some" underlying microscopic theory. The original solution is spherically symmetric and non-rotating. This solution was obtained as an effective theory and not from full dynamical equations. Here we first briefly review the original non-rotating AOS BH as obtained by the authors in [22] and then its rotating counter part that we have obtained for the very first time by using the NJA formalism.

4.2.1 Non-rotating AOS: a brief review

The effective solution was first obtained in a symmetry reduced phase space framework and then expressed as a quantum corrected spacetime metric as is done in LQC. The effective metric, exterior to trapping and anti-trapping horizons, is given by static, spherically symmetric form:

$$g_{\mu\nu}dx^{\mu}dx^{\nu} \equiv ds^2 = -\frac{p_b^2}{p_c\, L_o^2}dx^2 + \frac{\tilde{\gamma}^2 p_c\, \delta_b^2}{\sinh^2(\delta_b b)}dT^2 + p_c d\omega^2 \ , \tag{4.1}$$

where, x and T are the time and radial coordinates, respectively and $d\omega^2$ is the metric on a unit 2-sphere and $\tilde{\gamma}$ is the Barbero-Immirzi parameter[2]. The parameters appearing in metric coefficients are determined as

$$\begin{aligned}
&\tan\left(\frac{\delta_c c\,(T)}{2}\right) = \frac{\tilde{\gamma} L_0 \delta_c}{8m} e^{-2T}\ , \\
&p_c\,(T) = 4m^2\left(e^{2T} + \frac{\tilde{\gamma}^2 L_0^2 \delta_c^2}{64m^2} e^{-2T}\right)\ , \\
&\cosh\left(\delta_b\, b(T)\right) = b_o \tanh\left(\frac{1}{2}\left(b_o T + 2\tanh^{-1}\left(\frac{1}{b_o}\right)\right)\right), \\
&p_b(T) = -2m\tilde{\gamma} L_0 \frac{\sinh\left(\delta_b\, b(T)\right)}{\delta_b} \frac{1}{\tilde{\gamma}^2 - \frac{\sinh^2(\delta_b\, b(T))}{\delta_b^2}}\ ,
\end{aligned} \tag{4.2}$$

where $m = \frac{GM}{c^2} = M$ (in the units mentioned above) is the mass parameter, $b_o^2 = 1+\tilde{\gamma}^2\delta_b^2$ and $b(T), c(T), p_{b(T)}$ and $p_{c(T)}$ are the 4 dimensional phase space coordinates. Here δ_b and δ_c are the quantum parameters that encloses within itself the entire quantum corrections given by,

$$\delta_b = \left(\frac{\sqrt{\Delta}}{\sqrt{2\pi}\tilde{\gamma}^2 m}\right)^{1/3}\ ; \quad L_o\delta_c = \frac{1}{2}\left(\frac{\tilde{\gamma}\Delta^2}{4\pi^2 m}\right)^{1/3}\ . \tag{4.3}$$

It is these parameters that will modify the shadow and super-radiance that we will be studying. In the above, Δ is the minimum non-zero eigenvalue of the area operator in LQG, given by $\Delta \approx 5.17\ell_{Pl}^2$ and $\tilde{\gamma} \approx 0.2375$. L_o is an infrared regulator introduced to make the phase space description and hence the physical results well-defined. The location of horizon is determined by $T = 0$.

In order to express (4.1) in our familiar static, spherically symmetric form

$$ds^2 = -f(r)dt^2 + \frac{dr^2}{g(r)} + h(r)\left(d\theta^2 + \sin^2\theta d\phi^2\right)\ , \tag{4.4}$$

in Schwarzschild like coordinates the following change of notations has been considered in [21]:

$$t = x, \quad r_S = 2m, \quad r = r_S\, e^T, \quad b_0 \equiv (1+\tilde{\gamma}^2\delta_b^2)^{\frac{1}{2}} = 1+\epsilon\ . \tag{4.5}$$

In this case the metric coefficients are identified as:

$$-f(r) = -\left(\frac{r}{r_S}\right)^{2\epsilon} \frac{\left(1-\left(\frac{r_S}{r}\right)^{1+\epsilon}\right)\left(2+\epsilon+\epsilon\left(\frac{r_S}{r}\right)^{1+\epsilon}\right)^2}{16\left(1+\frac{\delta_c^2 L_0^2\tilde{\gamma}^2 r_S^2}{16r^4}\right)(1+\epsilon)^4}\left((2+\epsilon)^2 - \epsilon^2\left(\frac{r_S}{r}\right)^{1+\epsilon}\right)\ ; \tag{4.6}$$

$$\frac{1}{g(r)} = \left(1+\frac{\delta_c^2 L_0^2\tilde{\gamma}^2 r_S^2}{16r^4}\right)\frac{\left(\epsilon+\left(\frac{r}{r_S}\right)^{1+\epsilon}(2+\epsilon)\right)^2}{\left(\left(\frac{r}{r_S}\right)^{1+\epsilon}-1\right)\left(\left(\frac{r}{r_S}\right)^{1+\epsilon}(2+\epsilon)^2-\epsilon^2\right)}\ ; \tag{4.7}$$

[2]Note that we will be denoting the Barbero-Immirzi parameter of LQG [417] by $\tilde{\gamma}$ instead of γ as was done in our original work [15] to avoid any confusion with the dimensionless parameter $\gamma = \frac{\alpha}{M^2}$ introduced in chapter (3).

and

$$h(r) = 4m^2\left(e^{2T} + \frac{\tilde{\gamma}^2 L_0^2 \delta_c^2}{64m^2} e^{-2T}\right) = r^2\left(1 + \frac{\tilde{\gamma}^2 L_0^2 \delta_c^2 r_S^2}{16 r^4}\right) . \tag{4.8}$$

Henceforth the quantum parameters are δ_c and ϵ (since we switched from δ_b to ϵ). This form of the metric will be suitable for our main purpose.

Few important features of the form (4.4) are worth mentioning here. $f(r)$ diverges as one goes to $r \to \infty$. But still AOS can be shown to be asymptotically Minkowski. As mentioned in [21] while one generally checks asymptotic flatness by checking the $r \to \infty$ limit of the metric components, and comparing with $\eta_{\mu\nu}$, one can show that a given metric $g_{\mu\nu}$ can be taken to be asymptotically flat at spatial infinity if the components reduce at least as fast as $1/r$ as $r \to \infty$, to the components of some flat metric $\tilde{\eta}_{\mu\nu}$ which exists, while the coordinates (t, θ, ϕ) are kept constant. In [21], they show asymptotic flatness of the above metric using this idea and a time dependent coordinate change. Then, this time coordinate is no longer associated with a timelike Killing vector. For the detailed analysis see Sec IV.B. of [21]. Also since the effective equations of the theory have been obtained starting with a symmetry reduced theory, it is not known if there is a 4-dimensional covariant action whose symmetry reduction yields these equations.

4.2.2 Rotating spacetime through modified Newman-Janis Algorithm (NJA)

Although non-rotating spacetimes are widely studied because of their simplicity yet it is believed that for a spacetime to be astrophysically viable or relevant the inclusion of rotation in the non-rotating spacetime is very crucial. Motivated by this in 1965, Newman and Janis, using a complex coordinate transformation [23, 418] showed that one can obtain a rotating spacetime from non-rotating one. They were able to obtain the Kerr metric from the Schwarzschild metric. Using the same method the authors of [418] derived the Kerr-Newman metric, which represents a spacetime geometry of the electrically charged and rotating BH from a static Reissner-Nordström metric. Thus in general, the Newman-Janis algorithm (NJA) is used to construct a stationary and axisymmetric spacetime from a static and spherically symmetric one having the form (4.4). The steps involved in the algorithm have been discussed in Appendix (A). This formalism has been successfully used in several cases to find the rotating counter part of the static spherically symmetric metric[23, 418–420]. So, applying NJA to the metric (4.4), one can in principle obtain the rotating counterpart of the same. However, in course of applying the algorithm to the static case, the job of choosing the exact complexified form of the metric functions is a tedious one because there are various ways in which this can be done and it also needs to be chosen in such a way that the transformation (A.11) is allowed i.e., $\chi_1(r)$ and $\chi_2(r)$ must be functions of r only and not any other coordinates because only then these equations will be integrable. However it is found that the usual procedure fails to satisfy this for our present metric (4.4) (for details see Appendix (A)).

To do away with this, we resort to the modified version of NJA as was proposed by Azreg-Aïnou's non-complexification procedure [24], where the modification is incorporated in the third step (rest all steps are same). As per this new procedure, the complexification of the radial coordinate r is simply dropped and instead of that

we consider δ^{μ}_{ν}, in Eq. (A.6), transform as a vector under the transformation (A.7). In that case the metric coefficients $f(r), g(r)$ and $h(r)$ transform to $F = F(r, a, \theta)$, $G = G(r, a, \theta)$ and $H = H(r, a, \theta)$, respectively where a is the spin parameter in length dimension and is defined corresponding to the total angular momentum J as $a = \frac{J}{M}$ (the dimensionless spin parameter can be written as $\frac{J}{M^2}$) and θ is the angular coordinate in Boyer-Lindquist coordinates (BLC). The difference from the original NJA is that earlier, since the exact complexified form of r was known, so the exact expressions of F, G and H were also known, however now, in the modified version one does not come up with a predefined complexified form of r, rather one simply assumes that F,G and H are the complex forms (without knowing their exact expressions) of the original metric $f(r), g(r)$ and $h(r)$ respectively and then continues on with the rest of the steps. The final form of the rotating metric in BLC after applying the modified NJA becomes (see Appendix (A.2)):

$$\begin{aligned} ds^2 = &-F dt^2 - 2a\sin^2\theta\left(\sqrt{\frac{F}{G}} - F\right) dt d\phi + \frac{H}{\Delta(r)} dr^2 \\ &+ H d\theta^2 + \sin^2\theta\left[H + a^2\sin^2\theta\left(2\sqrt{\frac{F}{G}} - F\right)\right] d\phi^2 \ , \end{aligned} \tag{4.9}$$

where

$$\Delta(r) = GH + a^2\sin^2\theta = g(r)h(r) + a^2 \ ; \tag{4.10}$$

and F, G are given by (A.16) and (A.17), respectively while H remains undetermined (its expression is however obtained by comparing the quantum case with classical counterpart - see (B.1.1)). The above one represents the rotating AOS BH where we have calculated the shadow contour and super-radiance.

4.3 Finding the shadows

As already disussed in the introduction of the thesis, shadows can be studied both analytically and numerically. In our thesis we have adopted the analytical method. We have used the Hamilton-Jacobi separation method to study the general expressions for lightlike geodesics to find the nature and shape of shadows. Also for the calculations related to shadows, we have not set $G = c = \hbar = 1$.

4.3.1 Working formulas

We shall now discuss the equations involved in obtaining the contour of the shadow. Since shadow contours correspond to unstable circular null geodesics, it is necessary to obtain such equations first for the metric of our case. To find the null geodesics around the AOS BH we shall use the Hamilton-Jacobi (H-J) equation. We give here the required expression for rotating case, given by metric (4.9). After some calculations (see Appendix (A.3)), the separated geodesic equations for the photon are found to be

$$\frac{F}{G}\Delta(r)\frac{dt}{d\lambda} = \left[H + a^2\sin^2\theta\left(2\sqrt{\frac{F}{G}} - F\right)\right] E - a\left(\sqrt{\frac{F}{G}} - F\right) L \ ; \tag{4.11}$$

$$\frac{F}{G}\Delta(r)\sin^2\theta\frac{d\phi}{d\lambda} = a\sin^2\theta\left(\sqrt{\frac{F}{G}} - F\right)E + FL \ ; \tag{4.12}$$

and

$$H\frac{dr}{d\lambda} = \pm\sqrt{R(r)} \ ; \tag{4.13}$$

$$H\frac{d\theta}{d\lambda} = \pm\sqrt{\Theta(\theta)} \ , \tag{4.14}$$

where

$$R(r) = \left[\Sigma(r)E - aL\right]^2 - \Delta(r)\left[\mathcal{Q} + (L - aE)^2\right] \ , \tag{4.15}$$

and

$$\Theta(\theta) = \mathcal{Q} + a^2E^2\cos^2\theta - L^2\cot^2\theta \ . \tag{4.16}$$

In the above $\Sigma(r)$ symbolizes

$$\Sigma(r) = \sqrt{\frac{G}{F}}H + a^2\sin^2\theta = \sqrt{\frac{g(r)}{f(r)}}h(r) + a^2 \ . \tag{4.17}$$

Here $R(r)$ and $\Theta(\theta)$ must be non-negative; i.e., for the photon motion, we must have

$$\frac{R(r)}{E^2} = \left[\Sigma(r) - a\xi\right]^2 - \Delta(r)\left[\eta + (\xi - a)^2\right] \geq 0 \ , \tag{4.18}$$

and

$$\frac{\Theta(\theta)}{E^2} = \eta + (\xi - a)^2 - \left(\frac{\xi}{\sin\theta} - a\sin\theta\right)^2 \geq 0 \ , \tag{4.19}$$

In the above $\xi[= L/E]$ and $\eta[= \mathcal{Q}/E^2]$ are the critical impact parameters that determine the motion of the photon.

As already stated, the contour of a shadow depends on the unstable light rings. In the general rotating spacetime, these unstable circular photon orbits must satisfy $R(r_{ps}) = 0$, $R'(r_{ps}) = 0$ and $R''(r_{ps}) \geq 0$, where $r = r_{ps}$ is the radius of the unstable photon orbit. From the first two conditions we have

$$\left[\Sigma(r_{ps}) - a\xi\right]^2 - \Delta(r_{ps})\left[\eta + (\xi - a)^2\right] = 0 \ , \tag{4.20}$$

and

$$2\Sigma'(r_{ps})\left[\Sigma(r_{ps}) - a\xi\right] - \Delta'(r_{ps})\left[\eta + (\xi - a)^2\right] = 0 \ . \tag{4.21}$$

The valid solution for ξ for describing a BH shadow that is found from above is

$$\xi = \frac{\Sigma(r_{ps})\Delta'(r_{ps}) - 2\Delta(r_{ps})\Sigma'(r_{ps})}{a\Delta'(r_{ps})} \ . \tag{4.22}$$

Using this and solving for η we have,

$$\eta = \frac{4a^2\Sigma'^2_{ps}\Delta_{ps} - \left[\left(\Sigma_{ps} - a^2\right)\Delta'_{ps} - 2\Sigma'_{ps}\Delta_{ps}\right]^2}{a^2\Delta'^2_{ps}} \ . \tag{4.23}$$

where the subscript "ps" indicates that the quantities are evaluated at $r = r_{ps}$. The general expressions for the critical impact parameters ξ and η of the unstable

photon orbits are given by equations (4.22) and (4.23). In order to obtain the apparent shape of a shadow, the celestial coordinates α and β which lie in the celestial plane perpendicular to the line joining the observer and the center of the spacetime geometry are used. If the observer is situated at (r_0, θ_0), r_0 being the radial coordinate of the observer, i.e., the distance of the observer from the BH and θ_0 being the inclination angle of the observer which is the angle that the line joining the observer and the BH makes with the direction of axis of rotation of the BH, then the celestial coordinates are defined as [421]

$$\alpha = -r_0^2 \sin\theta_0 \frac{d\phi}{dr}\Big|_{(r_0,\theta_0)} , \tag{4.24}$$

and

$$\beta = r_0^2 \frac{d\theta}{dr}\Big|_{(r_0,\theta_0)} , \tag{4.25}$$

If the general metric is asymptotically flat, then the above equations reduce to

$$\alpha = -\frac{\xi}{\sin\theta_0} , \tag{4.26}$$

and

$$\beta = \pm\sqrt{\eta + a^2\cos^2\theta_0 - \xi^2\cot^2\theta_0} . \tag{4.27}$$

Using Eqs. (4.22), (4.23), (4.26) and (4.27), parametric plots of α and β are obtained by using the unstable photon orbit radius r_{ps} as a parameter that define the contour of the shadow. It is to be mentioned here that the expressions for $\Sigma(r)$ (4.17) and $\Delta(r)$ (4.10) contain the spherically symmetric static metric functions $f(r)$, $g(r)$ and $h(r)$. So to obtain the shadow for rotating metric, the information from the non-rotating spacetime will be used.

4.3.2 Shadow for non rotating case

In this section we shall discuss how the shadow contour looks for the case of a non-rotating AOS BH i.e., for $a = 0$ as described by the metric (4.4). Also since the underlying metric now is spherically symmetric, so the shadow to an observer seems the same whatever be the value of θ_0. Hence we can take up the simple case of $\theta_0 = \frac{\pi}{2}$. Equation (4.26) and (4.27) then reduces to

$$\alpha = -\xi \; ; \quad \beta = \pm\sqrt{\eta} , \tag{4.28}$$

and so we have

$$\alpha^2 + \beta^2 = \xi^2 + \eta . \tag{4.29}$$

With the spin parameter a set to zero we have $\Delta(r) = G(r)H(r) = g(r)h(r)$ and $\Sigma(r) = k(r) = \sqrt{\frac{g(r)}{f(r)}}h(r) = \sqrt{\frac{G(r)}{F(r)}}H(r)$ and, from the conditions $R(r_{ps}) = 0$ and $R'(r_{ps}) = 0$ we obtain the following equations

$$\eta + \xi^2 = \frac{h(r_{ps})}{f(r_{ps})} , \tag{4.30}$$

and

$$f'(r_{ps})h(r_{ps}) - f(r_{ps})h'(r_{ps}) = 0 . \tag{4.31}$$

Solving equation (4.31) we get the value of radius of the photon sphere r_{ps}. Putting this value in (4.30) gives the value of R_{sh}, the radius of the shadow contour:

$$R_{sh} = \sqrt{\alpha^2 + \beta^2} = \sqrt{\xi^2 + \eta} = \sqrt{\frac{h(r_{ps})}{f(r_{ps})}} \ . \tag{4.32}$$

The shadows for the non-rotating AOS BH along with the Schwarzschild one is plotted in Fig. (4.2) for different values of m and the quantum parameters δ_c and ϵ as mentioned in Table (4.1). It is immediately seen that the shadow radius for the quantum corrected AOS BHs are always small for a whole range of mass, starting from $1\ell_{Pl}$ to $10\ell_{Pl}$, with l_{Pl} being the Planck's length, compared to the shadow radius of the Schwarzschild BH. As the mass of the AOS BH increases from $1\ell_{Pl}$ to $10\ell_{Pl}$, the radii also increase accordingly.

m	$\tilde{\gamma}$	δ_c	δ_b	ϵ	r_{ps}	R_{sh}
$1\ell_{Pl}$	-	0	0	0	4.84×10^{-35}	8.39×10^{-35}
$1\ell_{Pl}$	0.2375	$2.92\times\ 10^{-36}$	2.52	0.16	4.99×10^{-35}	8.17×10^{-35}
$2\ell_{Pl}$	0.2375	$2.32\times\ 10^{-36}$	2.01	0.11	9.87×10^{-35}	1.6×10^{-34}
$10\ell_{Pl}$	0.2375	$1.35\times\ 10^{-36}$	1.17	0.03	4.87×10^{-34}	8.34×10^{-34}

Table 4.1: The table shows the values of different parameters for the non-rotating case. The first row contains the numbers for Schwarzschild BH with mass $m = 1\ell_{Pl}$ and the corresponding rows contain the values for the AOS BH with masses $1\ell_{Pl}$, $2\ell_{Pl}$ and $10\ell_{Pl}$ respectively.

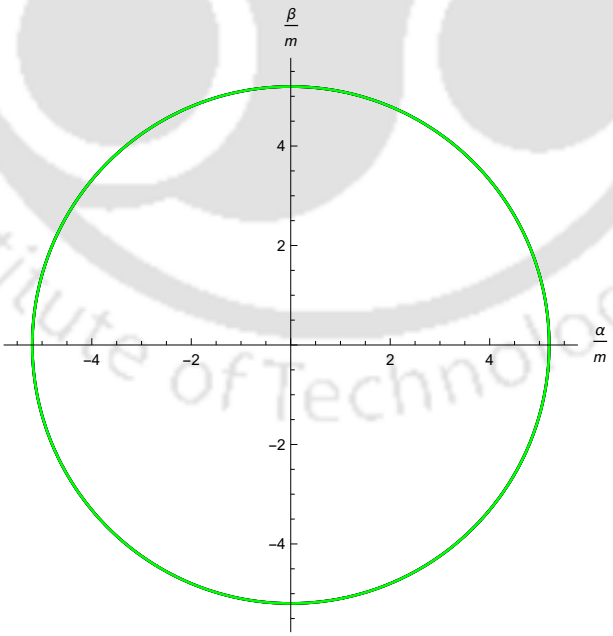

Figure 4.1: Shadows for the classical Schwarzchild BHs for different valued masses. Note that all the plots coincide since the ratios $\frac{\alpha}{m}, \frac{\beta}{m}$ scale uniformly, independent of the mass. As in Fig. (4.2), the red, blue and black lines correspond to masses $m = 1\ell_{Pl}, m = 2\ell_{Pl}$ and $m = 10\ell_{Pl}$

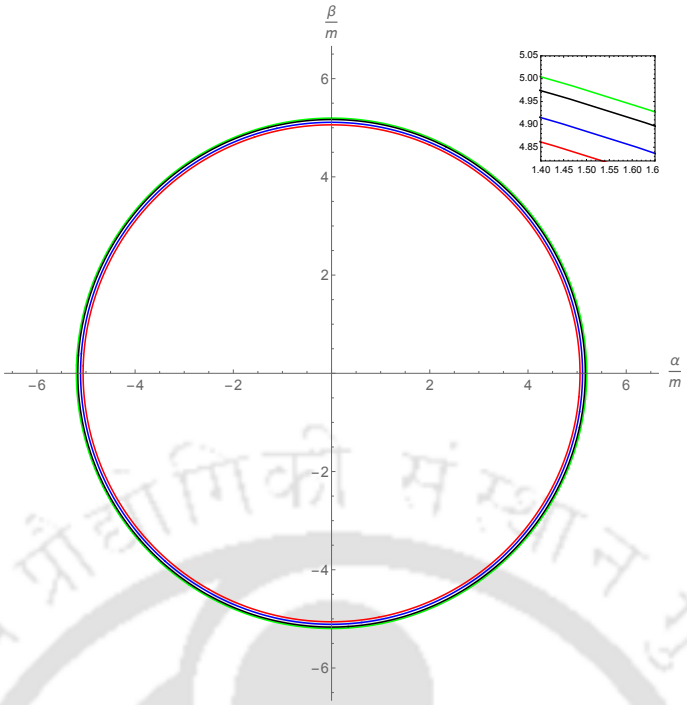

Figure 4.2: Shadows for the non rotating AOS BH for different values of the quantum parameters δ_c and ϵ. The green circle corresponds to the standard Schwarzschild BH shadow with $m = 1\ell_{Pl}$. The red, blue and black circles correspond to the quantum case with masses $m = 1\ell_{Pl}$, $m = 2\ell_{Pl}$ and $m = 10\ell_{Pl}$ respectively. A partly zoomed plot of the shadow contour in the first quadrant is plotted in the inset for understanding the difference between the standard Schwarzschild case with the non-rotating AOS one.

4.3.3 Shadow for the rotating AOS BH

We shall now apply the above formulae to obtain the contour of the shadow of a rotating AOS BH (which is physically more relevant owing to its rotation) whose corresponding non-rotating counterpart is represented by the metric (4.4) with the metric coefficients given by (4.6), (4.7) and (4.8). Also we want to compare and see how the shadow contour for quantum case varies with that of Kerr case i.e., upto what extent the quantum parameters leave its imprint on the shadows. The classical Kerr results can be obtained by setting the quantum parameters δ_c and ϵ in (4.6), (4.7) and (4.8) to zero.

In Fig. (4.3), the contours of the shadow are shown for the rotating AOS and Kerr BHs for different values of m and spin parameter a.

Also the shape of shadows at different inclination angles θ_0 for spin parameter $a = 0.9m$ ($m = 1\ell_{Pl}$) has been shown in Fig. (4.4) to see the variation in shadow with varying inclination angles.

It is observed after comparing the Quantum and Kerr case in Fig. (4.3) that the presence of quantum parameters tends to shrink the shadow i.e., the size of the shadow decreases due to quantum effect. Note that in Fig. (4.3) the dashed contours represent the Kerr case while the solid contours represent the rotating AOS BH. As the quantum parameters δ_c and ϵ are increased(i.e. for the smaller masses), both the photon sphere radius and shadow radius decreases. In Figs. (4.1)

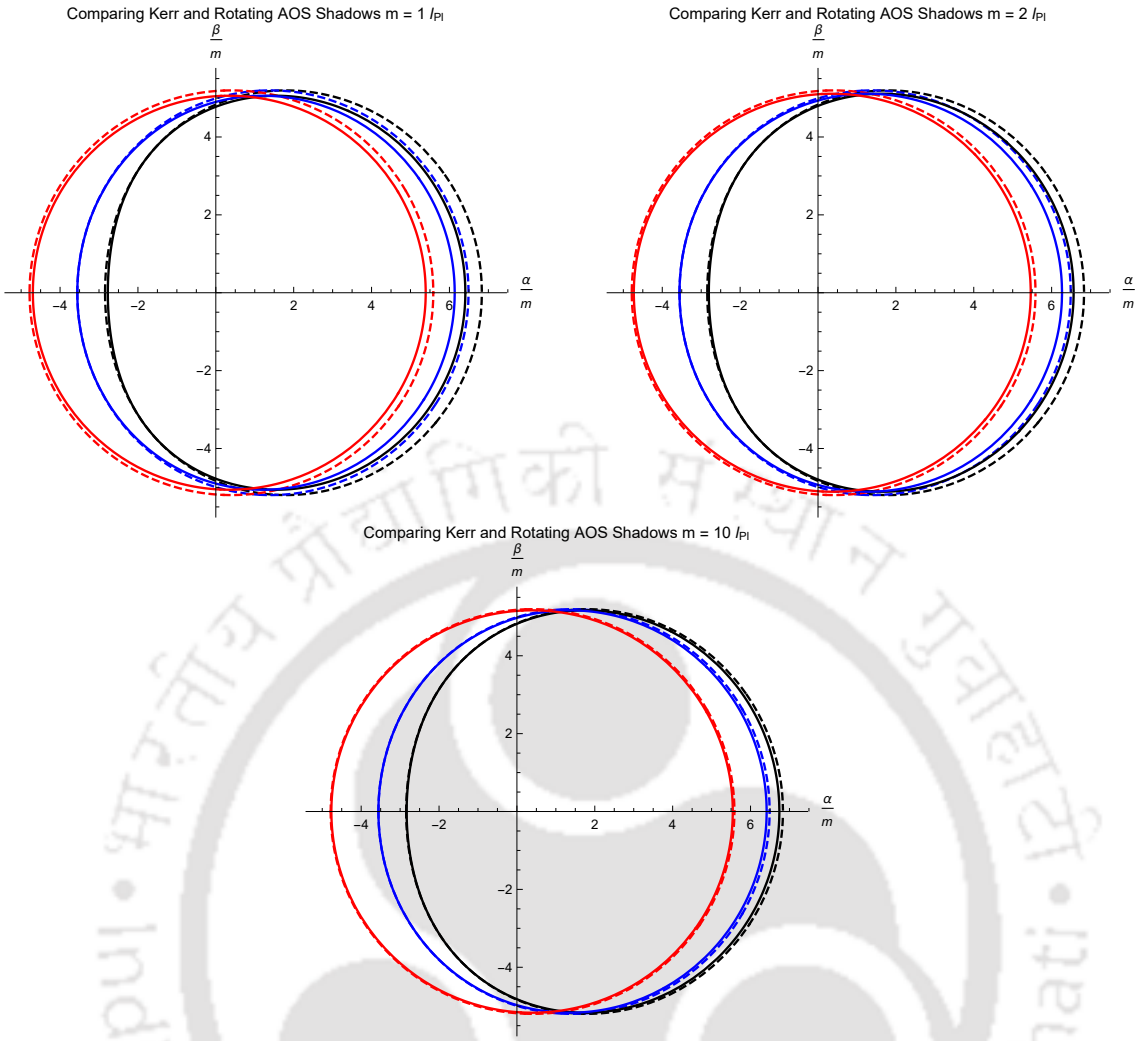

Figure 4.3: The figure shows the contours of shadow for different values spin parameter a with $m = 1\ell_{Pl}, 2\ell_{Pl}, 10\ell_{Pl}$. Color codes: Red ($a = 0.2m$), Blue ($a = 0.7m$) and Black ($a = 0.9m$). The dashed contours represent the Kerr case while the solid contours represent the rotating AOS BH.

to (4.5), we are plotting $\frac{\alpha}{m}$ and $\frac{\beta}{m}$. In the Kerr (see first figure of Fig. (4.5)) and Schwarzchild (see Fig. (4.1)) cases, this quantity scales uniformly, and hence we do not see a difference with changing mass. However, in the AOS case (see second figure of Fig. (4.5)), since the masses are a function of the quantum parameters, the scaling of these ratios are not uniform, which lead to the corrections observed in the plots. Observing these figures, it can be inferred that for a fixed mass, the shadow shrinks more on the right hand side than on the left hand due to quantum effect when compared with the Kerr case and as the mass is increased, there is not much variation in the shadows of Kerr case and quantum AOS case.This happens because the quantum parameters δ_c and ϵ are inversely proportional to m as can be seen from Eq. (4.3), so their values decrease when mass is increased and hence their impact on the shadow also reduces. With increasing values of a, not only the shadow size decreases but also the shape gets distorted. As can be seen, this distortion is more on the left part of the plot than on the right. While classically as well the asymmetry can be explained by frame dragging, the quantum corrections

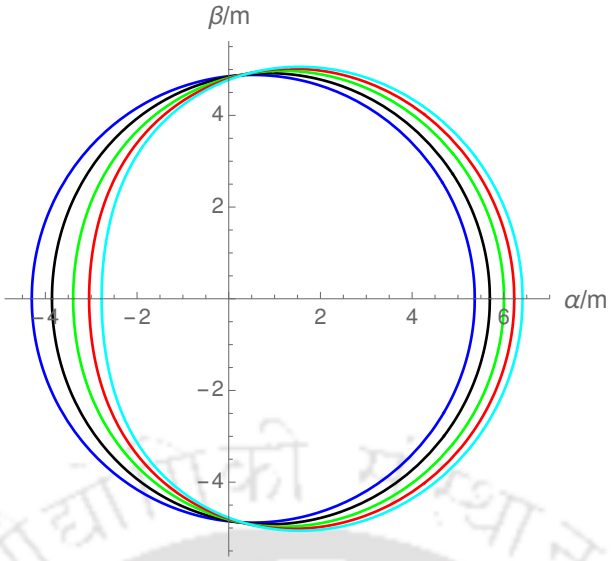

Figure 4.4: Shadows for the effective quantum metric with various values of inclination angles θ_0 for $a = 0.9m$ with $m = 1\ell_{Pl}$. Color codes: (Blue $\theta_0 = 17^0$), (Black $\theta_0 = 30^0$), (Green$\theta_0 = 45^0$), (Red $\theta_0 = 60^0$), (Cyan $\theta_0 = 90^0$).

affect the rotating AOS BH differently compared to a simple mass scaling. For a fixed value of the rotation parameter a, if we compare the change in mass of Kerr to that of rotating AOS as in Fig. (4.5), we find that there is a non-trivial difference in the shadow curvature at the left and right points in AOS while in Kerr, the shadow contours are unaffected. As noted earlier, we see that the deviation from the mass is more on the right side. This can be explained by looking at how the quantum corrections affect the curvature of the shadow at the left and right points. The two sides in the shadow contour generally reflect the prograde and retrograde orbits around the BH. We can compare the curvature at the two extreme points for the Kerr and AOS case, as is done in Fig. (4.6). Further we wish to point out that the left curvature for the AOS rotating BH, falls faster than that of Kerr for larger $\frac{a}{M}$. In Fig. (4.6), the curvature on the left crossing point crosses the X axis before $a = M$, indicated by the dashed black line. This has to do with the horizon structure of the rotating AOS BHs in this regime, and will be studied in detail in (4.4.2.1). Also from Fig. (4.4), it is seen that for a fixed value of m and a, if the inclination angle is increased, then the deviation from circularity increases and the shadow size also becomes smaller.

Thus we see that in case of shadows, the quantum effects are more prominent in the regime of small mass and high value of spin parameter. We now move on to see if the same feature is exhibited in case of super-radiance as well.

4.4 Super-radiance phenomena

We have already discussed about this phenomenon in chapter (1). Here, we will be dealing with the scattering of massless scalar fields off the rotating AOS BH wherein we study the super-radiance effect and how it is affected in presence of quantum parameters.

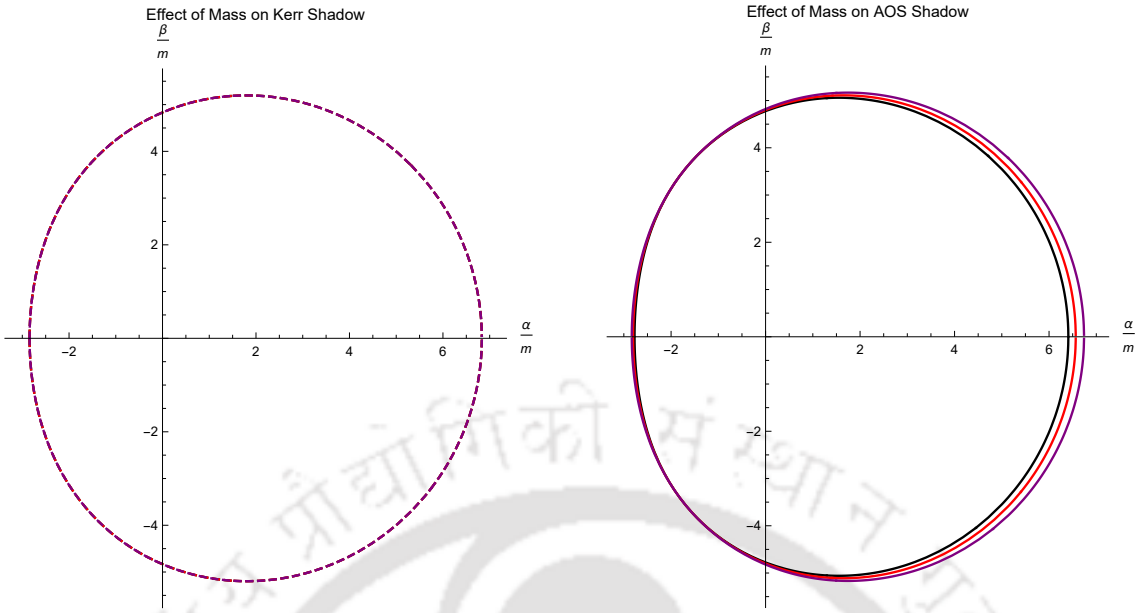

Figure 4.5: The figure shows the contours of shadow for a fixed spin parameter $a = 0.9m$ with varying masses. Color codes: Black ($m = 1\ell_{Pl}$), Red ($m = 2\ell_{Pl}$) and Purple ($m = 10\ell_{Pl}$).

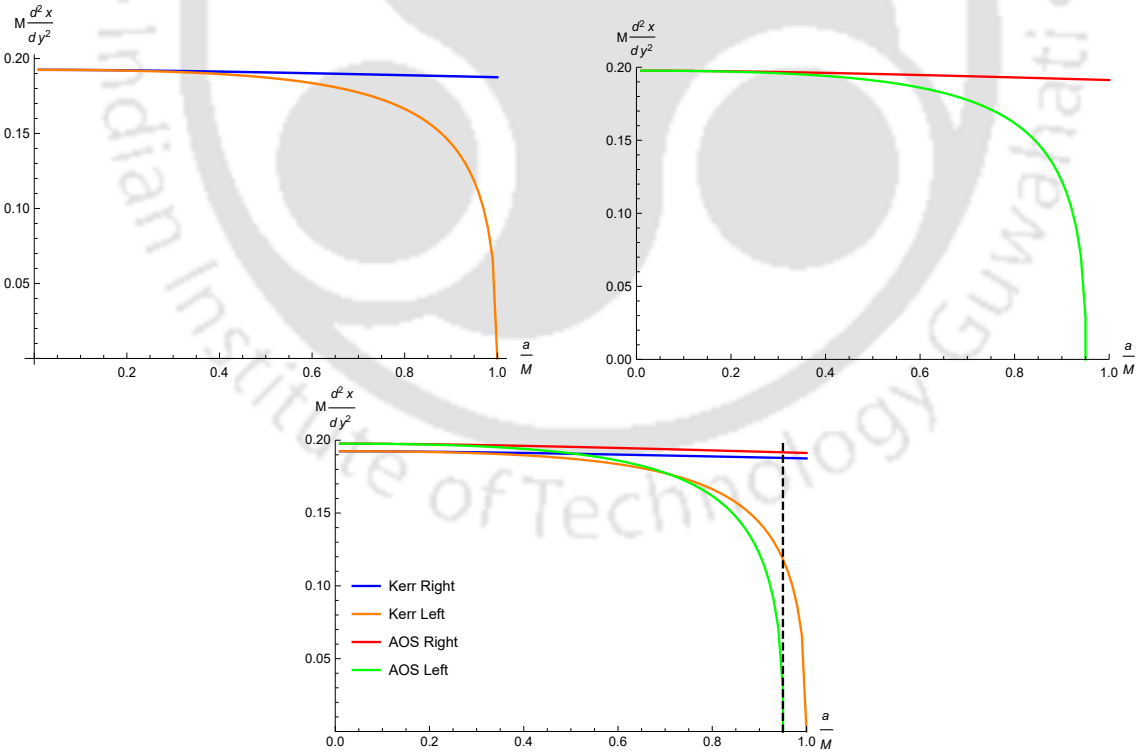

Figure 4.6: Comparing the curvature for the Kerr and AOS case at the right and left points of the shadow contour. The region to the left of the dashed black line indicates the allowed region for the horizon in the AOS case (see discussion in Sec. (4.4.2.1)).

4.4.1 Condition for super-radiance

For super-radiance one needs to concentrate on the near horizon field modes which are radially in going. In the semi-classical level the modes can be taken as the following form

$$\Phi \sim e^{iS(t,r,\theta,\phi)} \ . \tag{4.33}$$

In the above, the action $S(t,r,\theta,\phi)$, for our rotating metric (4.9) can be considered of the form (A.22) with $\mu = 0$. The radial part can be determined from the solution of (A.24). Since we are interested in near horizon regime, this equation will be solved after reducing it in the near horizon form. Note that the horizon is determined by the vanishing of $\Delta(r)$, given in (4.10). Using the tortoise coordinate r_*, defined as $dr_*/dr = (k(r)+a^2)/\Delta(r)$, Eq. (A.24) can be expressed as

$$-\Big(\frac{dS_r}{dr_*}\Big)^2 + \left[\frac{\Big(\sqrt{\frac{G}{F}}H + a^2\sin^2\theta\Big)E - aL}{k(r)+a^2}\right]^2 - \frac{(L-aE)^2+\mathcal{Q}}{(k(r)+a^2)^2}\Delta = 0 \ . \tag{4.34}$$

In the near horizon limit as $\Delta \to 0$, the above can be written approximately as

$$\Big(\frac{dS_r}{dr_*}\Big) \simeq \pm\Big[E - \frac{aL}{k(r_H)+a^2}\Big] \ , \tag{4.35}$$

where $k(r)$ is given in (A.15). The solution is found out to be as

$$S_r \sim \pm\Big[E - \frac{aL}{k(r_H)+a^2}\Big] r_* \ . \tag{4.36}$$

Therefore, by (4.33) the near horizon mode solution comes out to be

$$\Phi \sim \mathcal{S}_\theta e^{-iEt} e^{iL\phi} e^{\pm i\left[E - \frac{aL}{k(r_H)+a^2}\right] r_*} \ , \tag{4.37}$$

where we denote e^{iS_θ} by $\mathcal{S}_\theta$, as explicit expression of S_θ is unimportant for the present purpose. The value of $k(r_H)$ reduces to a very simple form:

$$k(r_H) = 4r_H^2\Big(1 + \frac{\tilde{\gamma}^2 L_0^2 \delta_c^2 r_S^2}{16 r_H^4}\Big) \frac{(1+\epsilon)^2\big(\frac{r_H}{r_S}\big)^{2+\epsilon}}{\Big(\epsilon + (2+\epsilon)\big(\frac{r_H}{r_S}\big)^{1+\epsilon}\Big)^2} \ . \tag{4.38}$$

In (4.37), negative (positive) sign corresponds to the ingoing (outgoing) mode. Since we are interested for the super-radiant modes, we will concentrate on the ingoing mode solution.

In order to find the condition for ingoing mode to be super-radiant one can follow the usual procedure (e.g. see the analysis in Section 8.6 of [422]). Since rest of the analysis is identical to the usual one, without going into the details we just give the final condition for finding super-radiant mode. Following [422] one finds the expression for energy flux through the horizon for massless scalar field as

$$\frac{d\mathcal{E}}{dt} = C_1 E\Big(E - \frac{aL}{k(r_H)+a^2}\Big) \ , \tag{4.39}$$

where C_1 is a positive constant, whose value is not important here. Then the condition for massless scalar field super-radiance in the present situation turns out to be $\left(E - \frac{aL}{k(r_H)+a^2}\right) < 0$; i.e.

$$0 < E < \frac{aL}{k(r_H) + a^2} \ , \tag{4.40}$$

where $k(r_H)$ is given by (4.38).

Let us now concentrate to find the angular velocity of the rotating AOS BH. This can be easily found out by considering $\theta = \pi/2$ in metric (4.9). Under this circumstances, for the null geodesics, the metric reduces to

$$\left[H + a^2\left(2\sqrt{\frac{F}{G}} - F\right)\right]\left(\frac{d\phi}{dt}\right)^2 - 2a\left(\sqrt{\frac{F}{G}} - F\right)\left(\frac{d\phi}{dt}\right) - F = 0 \ . \tag{4.41}$$

Remember that in the above all the function are defined at $\theta = \pi/2$. The solutions are

$$\left(\frac{d\phi}{dt}\right)_{\pm} = \frac{a\left(\sqrt{\frac{F}{G}} - F\right) \pm \sqrt{a^2\left(\sqrt{\frac{F}{G}} - F\right)^2 + F\left[H + a^2\left(2\sqrt{\frac{F}{G}} - F\right)\right]}}{H + a^2\left(2\sqrt{\frac{F}{G}} - F\right)} \ . \tag{4.42}$$

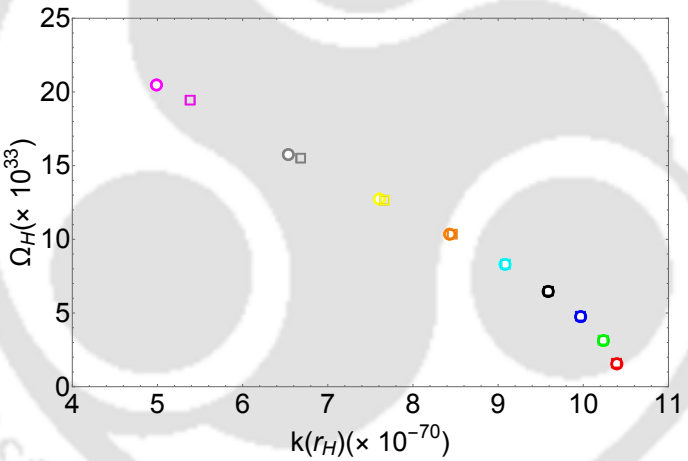

Figure 4.7: Behaviour of the horizon angular velocity (Ω_H) of the rotating AOS and the Kerr BH with respect to $k(r_H)$ with mass $m = 1\ell_{Pl}$ and for different values of the spin parameter a. The open circles are for the AOS BH and the open squares are for the Kerr case. Different colours of the legends imply different spin parameters for the BH, viz., Red: $a = 0.1m$, Green: $a = 0.2m$, Blue: $a = 0.3m$, Black: $a = 0.4m$, Cyan: $a = 0.5m$, Orange: $a = 0.6m$, Yellow: $a = 0.7m$, Grey: $a = 0.8m$ and Magenta: $a = 0.9m$ respectively. For smaller values of a, there is an overlap between the rotating AOS and Kerr results.

The horizon angular velocity is given by the minimum value of $\left(\frac{d\phi}{dt}\right)$, calculated at the horizon. For $\theta = \pi/2$, from (A.16) and (A.17) we have $F = (gh/k^2)H$ and $G = gh/H$. Substituting these in the negative sign solution in (4.42) one finds

$$\left(\frac{d\phi}{dt}\right)_{-} = \frac{a\left(\frac{1}{k} - \frac{gh}{k^2}\right) - \frac{1}{k}\sqrt{a^2 + gh}}{1 + a^2\left(\frac{2}{k} - \frac{gh}{k^2}\right)} \ . \tag{4.43}$$

Now at the horizon we have $\Delta(r_H) = 0$ which, from (4.10), yields $g(r_H)h(r_H)+a^2 = 0$. Using this in the above we find the angular velocity of the BH as

$$\Omega_H = \frac{a}{k(r_H) + a^2} \ . \tag{4.44}$$

Then in terms of the horizon angular velocity, the condition for massless scalar field super-radiance take the following form:

$$0 < E < L\Omega_H \ , \tag{4.45}$$

which is similar in form for the usual Kerr BH. In this case only Ω_H has been modified which incorporates all the quantum effects. A behaviour of the angular velocity of the horizon with respect to $k(r_H)$ for the AOS BH with mass $1\ell_{Pl}$ and for different values of the spin parameters (starting from $a = 0.1m$ to $a = 0.9m$ is plotted in Fig. (4.7). We have also plotted the respective Kerr angular velocity in the same plot for the same value of mass. It turns out that the behaviour of the horizon angular velocity of the Kerr BHs and the rotating AOS BHs are very similar and almost exactly matches for small values of the spin parameter a, while, as the spin parameter increases, the value of the angular velocity starts to change significantly i.e., the rotation of the AOS BH becomes more than Kerr in the low mass regime. This implies that for low mass and high 'a' AOS BH, the window for energy of scalar field to perform super-radiance is larger than higher mass system and this behaviour is evident from Eq. (4.45), as one can see that for high 'a', Ω_H for AOS is greater than Kerr and so the maximum value E can take also increases which means that the window for super-radiance phenomenon has increased. Further as increase in mass reduces the effect of the quantum parameters, so this window will become narrower and ultimately for large mass the window will coincide with Kerr value.

Thus the quantum parameters tend to modify the super-radiance condition by affecting the horizon angular velocity. We shall now study the effect quantum parameters have on the amplification factor.

4.4.2 Amplification factor: scalar field scattering and the Teukolsky formalism

The calculation of super-radiance amplification factors can be done using the Teukolsky formalism. The approach is discussed in detail in the recent review [423]. In the Kerr geometry (stationary and axisymmetric spacetime) various types of perturbations propagating on fixed BH metrics can be expressed in the form of the Teukolsky master equation after a Fourier-decomposition and harmonic expansion of the time-domain fields [424, 425]. For scalar perturbation, the dynamical equation is given by the Klein-Gordon equation in this curved spacetime. Here we consider massless scalar field Φ propagating in the rotating AOS background (4.9). Thus, the Klein-Gordon equation is given by $\Box\Phi = 0$. Using the symmetry in (t, ϕ), we consider the ansatz

$$\Phi(t, r, \theta, \phi) = e^{-i(\omega t+q\phi)}S(\theta)J(r) \ , \tag{4.46}$$

where q is the azimuthal number. Under the above form of solution, in tortoise coordinate we can then write the radial part of the Klein-Gordon equation in the

following Schrödinger like form (see Appendix (B.1)):

$$\frac{\mathrm{d}^2\varphi}{\mathrm{d}r_*^2} + V_{\text{eff}}\,\varphi = 0\ , \tag{4.47}$$

where function φ is related to the radial function $J(r)$ as $\varphi = \sqrt{k(r)+a^2}J$ and the potential V_{eff} encodes the curvature of the background and the properties of the test field and is of the form

$$V_{\text{eff}} = \left(\frac{K^2 - \Delta(\varrho + a^2\omega^2 - 2aq\omega)}{(k+a^2)^2} - u(r)^2 - \tau u'(r)\right)\ , \tag{4.48}$$

which is implicitly a function of r_* and $u(r) = \frac{\tau k'}{2(k+a^2)^2}$. The solutions of Eq. (4.47) is obtained under a boundary condition such that their asymptotic form must satisfy

$$\varphi = \begin{cases} Te^{-ik_H r_*} & \text{for } r \to r_H \\ Ie^{-ik_\infty r_*} + Re^{ik_\infty r_*} & \text{for } r \to \infty\ , \end{cases} \tag{4.49}$$

where I,R and T are the incident, reflection and transmission coefficients respectively. These boundary conditions correspond to an incident wave of amplitude I from spatial infinity giving rise to a reflected wave of amplitude R and a transmitted wave of amplitude T at the horizon. The wave numbers k_H and k_∞ are given by $k_H^2 = V_{\text{eff}}(r \to r_H)$ and $k_\infty^2 = V_{\text{eff}}(r \to \infty)$, respectively. Since the background is stationary, the field equations are invariant under the transformations $t \to -t$ and $\omega \to -\omega$. Thus, there exists another solution $\bar{\varphi}$ to Eq. (4.47) which satisfies the complex conjugate boundary conditions. The solutions φ and $\bar{\varphi}$ are linearly independent and standard theory of ODEs tells us that their Wronskian is independent of r_*. Thus, the Wronskian evaluated near the horizon,$W = -2\imath k_H|T|^2$, must equal the one evaluated at infinity, $W = 2ik_\infty(|R|^2 - |I|^2)$, so that [423]

$$|R|^2 = |I|^2 - \frac{k_H}{k_\infty}|T|^2\ . \tag{4.50}$$

For super-radiant amplification, we must have $|R|^2 > |I|^2$. It will be satisfied if one has $\frac{k_H}{k_\infty} < 0$. For scalar fields, the amplification factor is defined as [423]

$$Z_{slq} = Z_{0lq} = \left|\frac{R}{I}\right|^2 - 1\ . \tag{4.51}$$

Using the above one we will find the amplification factor for AOS BH.

To obtain the coefficients R, I, we need to solve the radial part (4.47). In terms of J variable and r coordinate this takes the form

$$\frac{\mathrm{d}}{\mathrm{d}r}\left(\Delta\frac{\mathrm{d}J}{\mathrm{d}r}\right) + \left(\frac{K^2}{\Delta} - \varrho\right)J = 0\ , \tag{4.52}$$

where $K = (k(r)+a^2)\omega - qa$ and $\varrho = A_{0lq} + a^2\omega^2 - 2aq\omega$ is the constant of separation. A_{0lq} are the angular eigenvalues (see Appendix (B.1)). To solve it we consider the small rotation approximation, as adopted in [423]. For sufficiently small rotation i.e $a\omega << 1$, the angular eigenvalues are given by $A_{0lq} = l(l+1) + \mathcal{O}(a^2\omega^2)$. In what follows, we set $\hbar = 1$ (in addition to $G = c = 1$) and take $E = \omega, L = q$ and take

$m = GM/c^2 \equiv M$ as the BH mass. Note that solving (4.52) is equivalent to solving (4.47) since one can derive (4.47) from (4.52) as shown in Appendix (B.1).

We solve this using matching asymptotic techniques, which is discussed in detail in Appendix (B). It must be noted to obtain the solution one should have the knowledge of the outer horizon. In the case of AOS, we have not yet considered the structure of the horizon. But in the regime where quantum corrections are small, we demand that the outer horizon of AOS be obtained by finding the quantum corrections to the outer horizon of Kerr. In the following section, we discuss in detail how to obtain these roots, upto first order in ϵ.

4.4.2.1 Horizon Structure

For the rotating AOS BH, we do not yet have an analytical expression for the horizon. This is difficult since the roots of $\Delta = 0$ generally give the horizon, but here, the quantum parameters are found in the exponent of the variable r in the function, if one explicitly writes it down. In this context, we consider 'small' quantum corrections such that one can expand Δ about the Kerr outer horizon. That is, we will consider a Taylor's expansion of Δ upto 2nd order about $r = r_+^{\text{Kerr}}$ and up to first order about $\epsilon = 0$, which gives us two roots for Δ. On considering the classical limit, we find that one of the roots reduces to r_+^{Kerr}. We denote this root as r_+ in what follows, and is (up to first order in ϵ) the outer horizon of the rotating AOS metric. The other root represents some other surface which does not have the interpretation of the horizon, and we shall denote this by r'. Thus, around $r = r_+^{\text{Kerr}}$, we can approximately write Δ in the form $\Delta = (r - r_+)(r - r')$, upto first order in ϵ. The actual expressions are included in a Mathematica notebook [426].

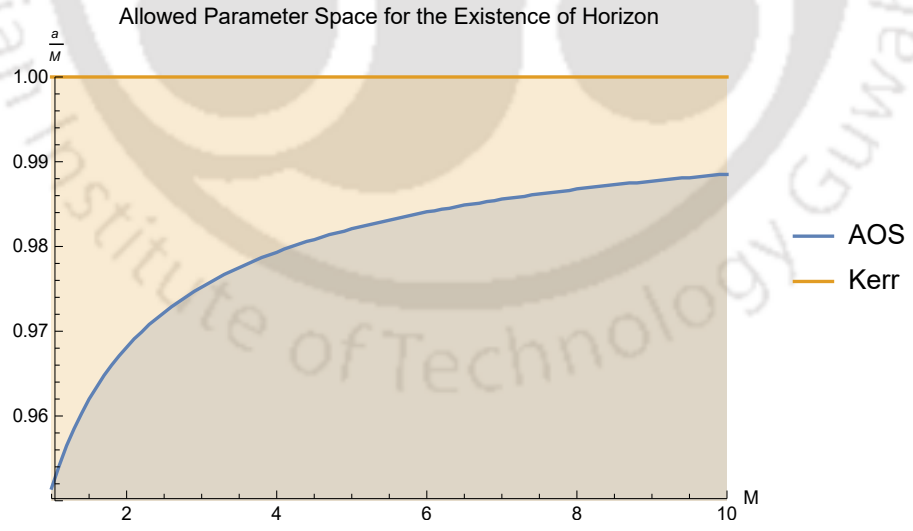

Usually, demanding that $\Delta = 0$ has real roots is used to find the location of the horizon and to avoid an NS. For the Kerr BH, this is achieved by the condition $M > a$. In the AOS case, this is modified. Given the form of Δ, one can check whether roots to this equation exist, in the region where the classical condition holds. That is, we want to check the horizon structure of the rotating AOS BH, inside the classically allowed region. In doing so, we find the following parameter space. We see that even with maintaining $M > a$, certain values of a are only

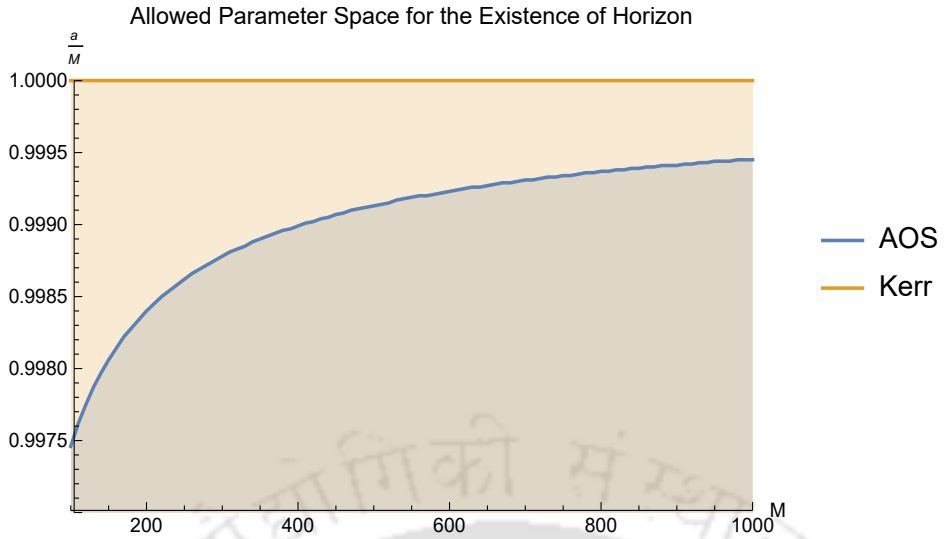

Figure 4.8: Comparing allowed parameter space in $\frac{a}{M}$ vs M plane for Kerr and AOS.

available to BHs with higher masses since Δ becomes completely positive and hence has no roots, when $\frac{a}{m}$ is high. The precise threshold of $\frac{a}{m}$ past which Δ fails to have roots depends on the value of M and is seen to increase, for increasing M. This can be observed from the parameter space plot, shown in Fig. (4.8). The complete region represents the classically allowed region of parameters. The blue curve and the region under the curve represents the threshold at which the rotating AOS BH horizon ceases to exist since Δ ceases to have roots beyond the threshold value of $\frac{a}{M}$. Therefore, even in the classically allowed region, the quantum corrections play a role so as to further restrict the parameter space under which the rotating AOS BH horizon is well defined. Note that this does not require the first order expansion in ϵ, δ since this is obtained directly from the function Δ. A simulation showing the change in the function Δ is included in the Mathematica notebook attached [426].

4.4.2.2 Estimation of amplification factor

We can now solve the radial equation, (see Appendix (B.1)) and obtain the amplification factors. The amplification factors Z_{011} and Z_{033} are plotted as a function of ωM in Fig. (4.9) and Fig. (4.10). We look at the effect of the rotation parameter a and the effect of the mass of the BH in Fig. (4.9) and (4.10) respectively. We observe from Fig. (4.9) that for BHs of a constant mass, an increase in the rotation parameter 'a' increases the separation between the AOS and Kerr super-radiance amplification factor with AOS having the greater value of Z. In this mass regime, super-radiant amplification in AOS starts out lower than that of Kerr, but increases and exceeds Kerr with an increase in a. Fig. (4.10) points out the fact that by varying the mass with a constant rotation parameter, the opposite effect is observed. The amplification factor now is much more closer between Kerr and AOS. This can be understood by noting that an increase in mass corresponds to a decrease in quantum correction effects and so these two cases approach. Thus, the large mass limit and the classical limit, are identical.

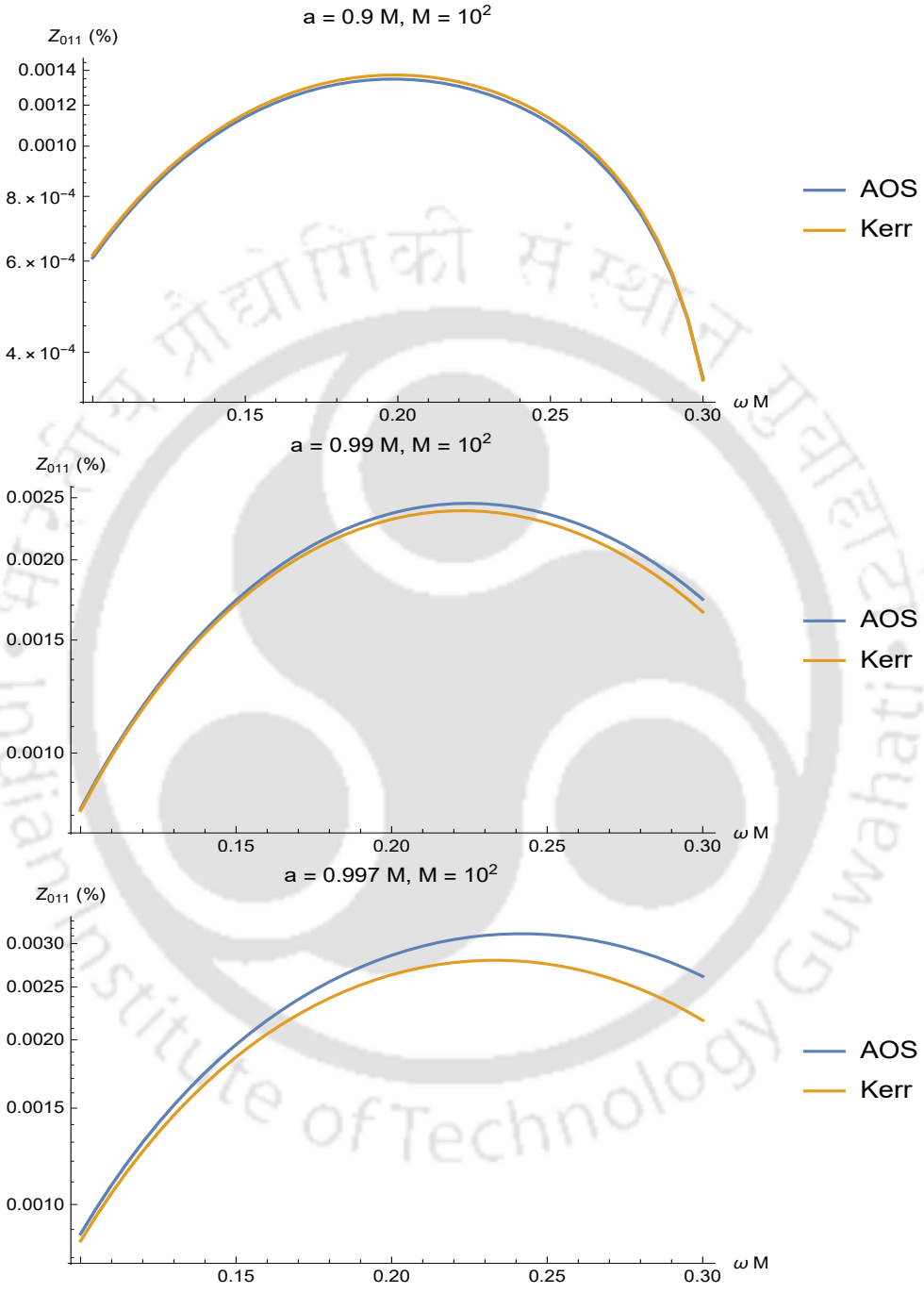

Figure 4.9: Comparing the effect of the rotation parameter a for Z_{011} with $M = 10^2$ (in units of l_{Pl}).

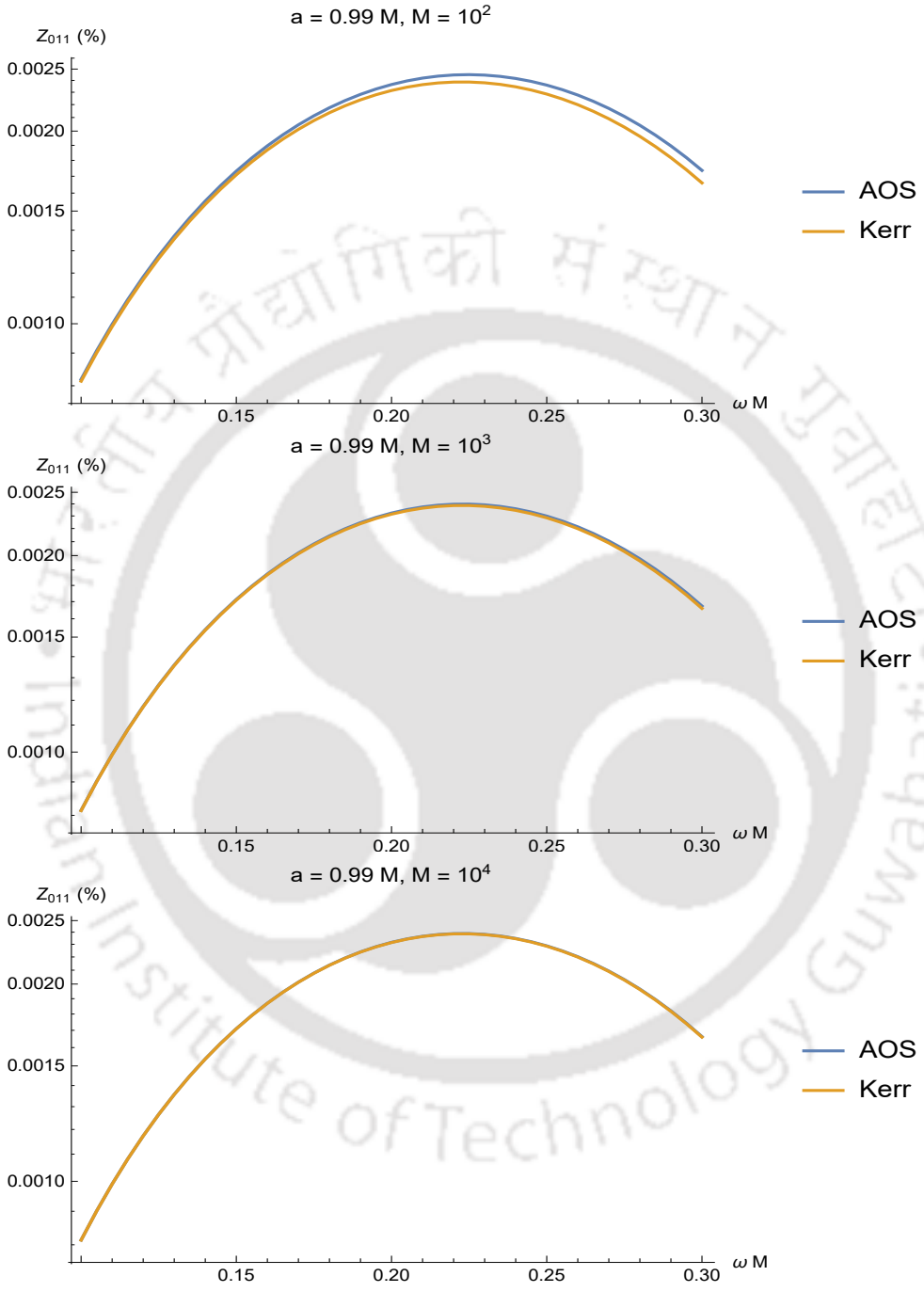

Figure 4.10: Comparing the effect of increasing mass M on Z_{011} with $a = 0.99M$ (with M in units of l_{Pl}).

4.5 Conclusion and discussions

We investigated the properties of the shadow of a recently obtained regular BH known as AOS BH. The spacetime is being modified from the LQG inspired theory. It is found that the singularity $r = 0$ is now hidden by a lowest possible value of the area element. We studied shadows for both non-rotating and as well rotating cases. It is being found that the quantum corrections can put significant signature in shadow when the BH size is of the Planck order. We noticed that although the shape of the shadows, comparing with those for Schwarzschild BH, do not change in non-rotating case in presence of the quantum corrections, but the area of the shadow decreases. The shadow radius increases as we increase mass of the BH and after certain value of mass both are indistinguishable. This shows that the quantum correction makes prominent signature on shadow for a very small Planck mass BH.

The rotating counterpart also behaves similarly. Here also the area of the shadow decreases due to quantum effect. Moreover, the contraction is less on the left hand side compared to the other side in rotating AOS BH shadow when compared with its classical counterpart, i.e. the Kerr BH. As we increase the mass of the BH, the distortion from Kerr starts to reduce. Increase of the rotation also imparts more distortion on the right side while the same decreases on the left part.

It needs to be mentioned here that the NJA is known to give rotating BH solutions within the context of Einstein gravity. However, in other theories, the NJA or its modifications is not guaranteed to give a rotating BH solution of the underlying theory [427]. The AOS BHs are not derived from an underlying physical theory, nor are they required to satisfy Einstein's field equations from classical general relativity. These are BH models which serve as possible quantum corrections to classical solutions. It is well known that in loop quantum cosmology (LQC), the full quantum evolution is extremely well approximated by certain quantum-corrected, 'effective equations'. Just as these effective equations provided a powerful tool in providing guidance for full quantum theory beyond the FLRW models, the hope is that effective equations in LQG would serve the same purpose for the ongoing efforts (see, e.g. [428–430]) to construct a more complete quantum description of the singularity resolution for BHs. Although the NJA is used to obtain the rotating solution, we make modifications to this procedure to account for the differences in the AOS metric and follow the revised procedure as outlined in [24]. We believe that the solution thus obtained is simply one possible model for capturing quantum corrections to the classical Kerr metric, and we note that this quantum-corrected rotating solution derived in this manner does reduce to the classical Kerr metric under the appropriate limit as mentioned before.

We also studied the super-radiance phenomenon for the rotating AOS BH. We observed that the condition for massless scalar field super-radiance is identical to that of the Kerr case except for the fact that it now incorporates the quantum effects. The quantum parameters further restrict the parameter space under which the rotating AOS BH horizon is well defined.

The amplification factors also exhibit trends similar to that observed in case of shadows i.e., the quantum signatures are more prominent for small mass and high spin parameter valued BHs. A natural next step would be to understand super-radiant scattering of other spin fields (in this work we only consider $s = 0$) in this background. This can be done by looking at the perturbations using the Newman-

Penrose formalism [431], as done by Teukolsky, Press and others [424, 425, 432] for the Kerr geometry. One can make a straightforward generalisation of the Kinnersely tetrad in the Kerr case, to look at other spin fields in AOS.

Finally, it may be worth mentioning that the primordial BHs (PBHs) are microscopic in size and therefore the quantum effects at this scale are not going to be negligible. Since AOS BH shows significant quantum effects at the Planck scale it may model these PBHs. Therefore investigation of these quantum induced spacetime can be useful to understand the nature of PBH. It is our belief that the present study will illuminate the properties of Planck scale physics.

भारतीय प्रौद्योगिकी संस्थान गुवाहाटी
Indian Institute of Technology Guwahati

Chapter 5

Conclusion and Future prospects

5.1 Conclusion

Although the present observations complement the status of GR as a strong contender to explain gravitational physics and it is considered as one of the pillars of modern physics, yet one should not be biased and should always remain open to look out for alternatives to GR for reasons discussed earlier in the thesis. The introduction of GW astronomy via the GW detectors along with the imaging of BH via EHT has helped to gather immense information about the extreme compact objects in the universe in the electromagnetic as well as in the gravitational domain. This has provided the platforms to test the predictions of GR and also to look out for alternatives to GR. It is therefore imperative to say that these recent observational advancements have spurred a renewed interest in finding possible deviations from GR. A number of alternatives to GR have been the context of study among a large number of researchers. One such alternative is the Einstein-Gauss-Bonnet theory that incorporates higher order curvature corrections in the action in addition to the Einstein-Hilbert term. However it is well known that such a theory can have sensible dynamical contribution in $4D$ only if there is a scalar field minimally coupled to gravity. Recently, a proposal in [10] has triggered the study in this theory by claiming that one can still get a contribution to dynamics from the Gauss-Bonnet term in the action without the need for extra degrees of freedom by simply considering a proper rescaling of the Gauss-Bonnet coupling constant α as $\frac{\alpha}{D-4}$. This proposal was subsequently criticised by a number of authors for the regularization scheme adopted in the original work. In [132] it was shown that the novel $4D$-EGB theory lacks tensorial description. In [134], the nonlinear perturbations of the metric were studied and it was found that they cannot be regularized by taking the limit $D \to 4$ as divergent terms appear in the corresponding equations of the Gauss–Bonnet theory. Again in [136] it was pointed out that in four dimensions, there is no four-point graviton scattering tree amplitudes other than those leading to the Einstein theory, so that additional degrees of freedom, for instance, a scalar field $(\partial\phi)^4$, should be added for consistency. Following this debate, few different consistent theories in $4D$ came up as an attempt to circumvent the ill-behaviour exhibited by this proposal. A scalar-tensor approach was proposed in [91, 141] where the authors first assume a particular ansatz in a higher dimensional spacetime and then take the limit $D \to 4$. However the scalar field is found to be infinitely strongly coupled. These works clarify the essential problem of the original regularization

scheme as well as the scalar–tensor approach is the infinitely strong coupling [91, 136]. A consistent description of the 4D theory was later on suggested in [144], where the authors constructed the Hamiltonian theory using the ADM decomposition and showed that the well-defined theory does not have an extra scalar degrees of freedom and therefore is free of the problem of infinite coupling. The beauty that was seen in all such various approaches was that the final solution in all these theories were same as that in [10]. In our thesis, in chapter (2) and chapter (3) respectively, we have considered the BH and NS solution of this novel $4D$-EGB theory and probed them via the technique of perturbation theory.

It is known that in spite of its success, GR has a number of loopholes of which singularity poses as one of the major loopholes as all the laws of physics break down here. For more than 80 years, theoretical physicists have been trying to develop a complete and consistent theory of quantum gravity which would successfully combine the tenets of Einstein's theory of GR together with those of QFT in a bid to check if this attempt could help get rid of the singularity problem. One such attempt at the canonical quantisation of gravity is LQG. In LQG, the spacetime is rendered regular as the theory admits the minimum eigenvalue of the area operator to be non-zero. In chapter (4), we have chosen one of the quantum-corrected BH solutions in this theory, viz. the AOS BH as proposed in [56] and made an attempt to study the imprints that quantum parameter leaves on the shadow and super-radiance in this background. We shall now provide below a brief conclusion about the different studies we have done in the above mentioned areas in different chapters.

The thesis starts with a brief overview of the alternatives to GR, that we have worked on. Different astrophysical processes that we have analysed in the BH and NS solutions of the novel $4D$-EGB and LQG theories along with the motivation behind studying them has been outlined in chapter (1). In the same chapter, we also provide the methodologies to study the astrophysical processes, such as calculations of QNMs, greybody factors, echoes, shadows and super-radiance.

In chapter (2), we have studied the asymptotically de Sitter branch of the novel $4D$-EGB BH solution's response to test fields: scalar, electromagnetic and Dirac perturbations and computed the QNFs using the 3rd order WKB approximation. To further improve the accuracy we have used Padé approximations as well. The greybody factors γ_l have also been computed and the effect of α and Λ on the QNFs and γ_l have been discussed. It is found that for all the three types of perturbations, as Λ increases, the oscillation frequency and the damping time decreases. Also, as α decreases and eventually crosses over to negative values, the real part of the frequency starts decreasing whereas the imaginary part also starts to become more negative, implying that the damping increases. However, when α increases in the positive side, the real part of the frequency increases. On the other hand, the greybody factors decrease with an increase in α and increase with an increase in Λ. Similar trend is seen in all the three types of perturbations. Along with these, the eikonal limits have also been explored for the three cases.

Chapter (3) discusses the NS solution in the novel $4D$-EGB theory of gravity that is obtained when $\alpha > M^2$. The underlying spacetime is globally non-hyperbolic, which however, does not pose a problem in our case as we have seen, following Wald's prescription, that one can still have an essentially self-adjoint operator in such a background. This statement loosely translates into the fact that in spite of the singularity being naked, dynamics can still be defined by imposing suitable

boundary conditions near the singularity. We have studied how the NS solution responds to scalar, electromagnetic and Dirac perturbations and checked for stability from time-domain evolution technique. It is found from the time evolution profile of the test fields that, for higher multipole modes, all the three types of perturbation grows unbounded with time, suggesting an instability. This further restricts the parameter space of α. Also the major finding in this chapter was that for values of $\frac{\alpha}{M^2}$ slightly greater than unity, the time domain profile shows a distinctive feature for the NS case in the form of echoes which are absent in case of BHs. This distinct feature serves the purpose of a signature that one can search for in the detectors or in the available data that might throw light on alternatives to BHs (BH mimickers or BH impostors) or some quantum modifications near the horizon. As $\frac{\alpha}{M^2}$ further increases, the echoes align to yield QNMs which we have computed using Prony's method for $l = 1$ mode of massless scalar and electromagnetic perturbations and $l = 0, 1$ modes of massless Dirac perturbations.

Finally, chapter (4) discusses a BH solution obtained in [56] and termed as AOS BH, which is the Kruskal extension of the quantum-corrected Schwarzschild BH solution. It is an LQG-motivated regular BH solution. Here, we have tried to obtain the imprints of the quantum parameters of the theory on the shadow and super-radiance in the AOS background. For the very first time, we have obtained the rotating AOS BH by applying the modified Newman-Janis Algorithm. Accordingly, we studied the shadow of the non-rotating AOS BH and shadow and super-radiance of the rotating AOS BH. The important features that we found in this chapter were that the general shape of the shadow for non-rotating AOS BH is circular in shape as is expected for its classical counter part too, but the presence of loop quantum gravity inspired modification contracts the shadow radius. This effect is found to reduce with the increase in the mass of the BH which scales inversely with the quantum parameters. On a similar note, in the rotating situation, we found contraction in shadow contours due to quantum effects. The tapered nature of the shadow contour was also seen as expected from the classical Kerr case which is one of the most paradigmatic solutions in GR, having a major potential for astrophysical relevance [433]. Also, instead of the symmetrical contraction, like non-rotating one, we found more contraction on one side relative to the other when we compared our result with the shadow of the Kerr BH. This asymmetry further increases with increase in the value of the spin parameter. However the difference that we noted was that for a fixed mass, the quantum parameters tend to shrink the right hand side contour of the shadow more than the left hand side as compared to Kerr. From this, one can infer that the quantum effects are pronounced differently on the prograde and retrograde orbits around the BH. One salient feature noted for super-radiance effect was that the condition for massless scalar field super-radiance in rotating AOS BH remains identical to that of the Kerr case. However, since the angular velocity of the horizon of the rotating AOS BH was found to be more as compared to Kerr in the low mass regime, so in case of rotating AOS BH, the massless scalar field now, has a wide range of allowed energy values to perform super-radiance. Apart from this, we also noticed that the parameter space under which the rotating AOS BH horizon is well-defined, gets restricted in the presence of the quantum parameters. From our investigation we can infer that the quantum parameters can exhibit their effects on shadows and super-radiance amplification factors more strongly as long as we are dealing with small mass BHs with high spin parameter values. As the mass

is increased, one approaches results similar to the classical case.

In the section that follows, some potential avenues for research in future are mentioned that are consistent with the above methodology and could, at most, be instructive or fascinating.

5.2 Scope for future works

We are entering into an era of precision GW astronomy. This, in turn, will help us to place stronger constraints on the limits of GR and parameters of alternative theories of gravity because of the increase in the sensitivity and the number of ground-based observatories, the development of third-generation gravitational-wave observatories like the Einstein Telescope [434], and the upcoming building of the Laser Interferometer Space Antenna (LISA) [435]. Along with this, we now, also have access to the electromagnetic domain that holds within it, the capability to provide important observations regarding BHs and other exotic compact objects. There are a good number of such exotic compact objects, which has been widely discussed in the literature for decades, that could potentially mimic BHs and thereby create degeneracy in observations from these detectors. Thus, access to the electromagnetic domain, might provide us with a direct method to actually obtain the images of these compact objects whose existence have remained a question since long. The classical and quantum conceptual issues related to the existence of an event horizon and of a curvature singularity further motivates one to look out for such mimickers. Since, in this thesis, we have focused on ringdown phase of perturbed backgrounds containing BHs and NSs, we will first mention a few possible future extensions of our works related to this aspect.

In order to understand the behaviour of BHs, one generally studies the test field perturbations as a toy model. However, in order to have a complete understanding of the underlying spacetime and to connect to the real physical observable effects, it is crucial to understand metric perturbation. Therefore, it is absolutely essential to study the full gravitational perturbation of the 4D-EGB BH and NS in different versions of the (consistent) $4D$-EGB theory. Such an analysis will provide an opportunity to put constraints on the parameter space of the Gauss-Bonnet coupling constant α. It can also help to predict direct observational distinctions, if any, between the different versions of the $4D$-EGB theories. Further as an extension to our work, rotating solutions in EGB gravity can be constructed and a possible study of the super-radiance phenomenon in such case will provide many interesting information.

Wormholes are extensively studied (especially the traversable ones) and it also poses as one of the BH mimickers. QNMs of different wormhole solutions serve as a tool for testing specific wormhole models with GW data [436]. Hence the subject calls for further research. Along this line, the Dirac and electromagnetic perturbation in wormhole backgrounds can be studied and one can check for the signature of echoes. As an extension to this work, a study on the background in presence of plasma and finding out the modifications induced due to the presence of plasma can serve as a tool to understand environmental effects near such exotic compact object backgrounds.

On the other hand, in this thesis, we also have focused on shadows. From that perspective, one can look at the following future directions:

Some spherically symmetric NS models viz: Janis-Newman-Winicour [271] and Joshi-Malafarina-Narayan NSs [63], for some particular values of theory parameters, possess photon spheres and cast shadows much similar to Schwarzschild BHs. However in the absence of photon spheres, the images of NS differ from those of BHs [437]. Along this line, a detailed investigation of other possibilities of the no-horizon cases of rotating spacetimes, resembling the BH shadows can be carried out.

It is important to mention here that recently, it was hypothesized that some galactic nuclei may not be the supermassive BHs, but entrances to wormholes [438, 439]. This has attracted the attention of the researchers towards the study of issues related to the physics of wormholes. However, this hypothesis, calls for a test. One way to do so is to study the behavior of light rays in the vicinity of the entrance of a wormhole, as well as to analyse the possibility of the appearance of a shadow, similar to the case of BH, where shadow formation does take place.

Some of the above-mentioned works are presently in progress.

भारतीय प्रौद्योगिकी संस्थान गुवाहाटी
Indian Institute of Technology Guwahati

Appendix A

Derivation of metric for rotating BH through Newman-Janis algorithm (NJA) and the photon trajectories

A.1 Original NJA

The NJA, originally proposed in [23, 418], helps to construct a stationary and axisymmetric metric from a static and spherically symmetric metric of the form

$$ds^2 = -f(r)dt^2 + \frac{dr^2}{g(r)} + h(r)\left(d\theta^2 + \sin^2\theta d\phi^2\right) \ . \tag{A.1}$$

To find the required result there are certain prescribed steps to be followed. Without going into the details, let us here just follow the prescribed steps.

The *first step* of the algorithm is to write down the metric (A.1) in the advanced null (Eddington-Finkelstein) coordinates (u, r, θ, ϕ). This is achieved by using the following transformation:

$$du = dt - \frac{dr}{\sqrt{fg}} \ . \tag{A.2}$$

The non-rotating metric in the advance null coordinates then becomes

$$ds^2 = -f(r)du^2 - 2\sqrt{\frac{f}{g}}dudr + h(r)\left(d\theta^2 + \sin^2\theta d\phi^2\right) \ . \tag{A.3}$$

The *second step* is to use a null tetrad $Z^\mu_\alpha = (l^\mu, n^\mu, m^\mu, \bar{m}^\mu)$ to express the inverse metric $g^{\mu\nu}$ in the form

$$g^{\mu\nu} = -l^\mu n^\nu - l^\nu n^\mu + m^\mu \bar{m}^\nu + m^\nu \bar{m}^\mu \ . \tag{A.4}$$

Here, the tetrad vectors satisfy the relations

$$\begin{aligned} &l_\mu l^\mu = n_\mu n^\mu = m_\mu m^\mu = l_\mu m^\mu = n_\mu m^\mu = 0 \ ; \\ &l_\mu n^\mu = -m_\mu \bar{m}^\mu = -1 \ , \end{aligned} \tag{A.5}$$

and $\bar{m}^\mu$ is the complex conjugate of m^μ.

The tetrad vectors satisfying the above relations are found to be

$$l^{\mu}=\delta^{\mu}_{r},\;\; n^{\mu}=\sqrt{\frac{g}{f}}\delta^{\mu}_{u}-\frac{g}{2}\delta^{\mu}_{r},\quad m^{\mu}=\frac{1}{\sqrt{2h}}\left(\delta^{\mu}_{\theta}+\frac{i}{\sin\theta}\delta^{\mu}_{\phi}\right)\;. \tag{A.6}$$

The *third step* is to perform the complex coordinate transformations in the (u,r) plane,

$$u'=u-ia\cos\theta;\quad r'=r+ia\cos\theta\;, \tag{A.7}$$

where $a=\frac{J}{m}$ will be identified as the specific angular momentum or spin parameter of the BH, and m, J are the mass and the angular momentum of the BH, respectively. Under these transformations the new null tetrads are

$$\begin{aligned} l'^{\mu} &= \delta^{\mu}_{r}\,; \\ n'^{\mu} &= \sqrt{\frac{G(r,\theta)}{F(r,\theta)}}\delta^{\mu}_{u}-\frac{G(r,\theta)}{2}\delta^{\mu}_{r}\,; \\ m'^{\mu} &= \frac{1}{\sqrt{2H(r,\theta)}}\left(ia\sin\theta(\delta^{\mu}_{u}-\delta^{\mu}_{r})+\delta^{\mu}_{\theta}+\frac{i}{\sin\theta}\delta^{\mu}_{\phi}\right), \end{aligned} \tag{A.8}$$

where $F(r,\theta)=f(r')$, $G(r,\theta)=g(r')$ and $H(r,\theta)=h(r')$ are respectively, the complexified form of $f(r)$, $g(r)$ and $h(r)$. Using the new tetrad, the new inverse metric is found to be

$$g'^{\mu\nu}=-l'^{\mu}n'^{\nu}-l'^{\nu}n'^{\mu}+m'^{\mu}\bar{m}'^{\nu}+m'^{\nu}\bar{m}'^{\mu}\;. \tag{A.9}$$

Then the new metric in the advanced null coordinates becomes

$$\begin{aligned} ds^{2} &= -Fdu^{2}-2\sqrt{\frac{F}{G}}dudr+2a\sin^{2}\theta\left(F-\sqrt{\frac{F}{G}}\right)dud\phi+2a\sqrt{\frac{F}{G}} \\ &\times\;\sin^{2}\theta drd\phi+Hd\theta^{2}+\sin^{2}\theta\left[H+a^{2}\sin^{2}\theta\left(2\sqrt{\frac{F}{G}}-F\right)\right]d\phi^{2}\;. \end{aligned} \tag{A.10}$$

The *final step* of the algorithm is to rewrite the above metric in Boyer-Lindquist form (where the only nonzero off-diagonal term is $g_{t'\phi'}$) using the global coordinate transformations of the form

$$du=dt'+\chi_{1}(r)dr,\qquad d\phi=d\phi'+\chi_{2}(r)dr\;. \tag{A.11}$$

In the above $\chi_1(r)$ and $\chi_2(r)$ are chosen in such a way that the metric will have only $g_{t'\phi'}$ non-vanishing off-diagonal term in (t',r,θ,ϕ') coordinates. Substitution of (A.11) in (A.10) and then demanding the above criterion one finds the metric of the form (4.9) with the following choices of $\chi_1(r)$ and $\chi_2(r)$:

$$\chi_{1}(r) = -\frac{\sqrt{\frac{G(r,\theta)}{F(r,\theta)}}H(r,\theta)+a^{2}\sin^{2}\theta}{G(r,\theta)H(r,\theta)+a^{2}\sin^{2}\theta}\equiv-\frac{A(r)}{B(r)}\;, \tag{A.12}$$

$$\chi_{2}(r) = -\frac{a}{G(r,\theta)H(r,\theta)+a^{2}\sin^{2}\theta}\equiv-\frac{a}{B(r)}\;. \tag{A.13}$$

In (4.9) we dropped the prime in time and azimuthal coordinates. This line element represents the desired metric for stationary, axisymmetric spacetime.

It must be mentioned that the transformations in (A.11) are possible (i.e. these have to be integrable) only when $\chi_1(r)$ and $\chi_2(r)$ are functions of only r and not θ. This implies that the denominator in (A.13) must be a function of r only, which we call as $B(r)$. Consequently, the numerator in (A.12) must be again a function of r only (we call this as $A(r)$). This is a very non-trivial restriction and may not be always satisfied for any value of $f(r), g(r)$ and $h(r)$ under the complexification (A.7). Incidentally for Schwarzschild BH, this is satisfied and one obtains the Kerr metric from (4.9). Whereas our present static, spherically symmetric metric coefficients, given in (4.6), (4.7) and (4.8), do not satisfy these conditions. Therefore the above ditto procedure fails to provide the rotating solution for AOS BH.

A.2 Modified NJA

We see that the original NJA may fail for some spherically symmetric static metric, like the present one. A little modification in the approach, as shown in [24], successfully overcomes this difficulty. For that, it is assumed that we have somehow obtained a metric of the form (A.10). In this case, we do not know the exact form of G, F and H; i.e. we are not using the specific complexification, given in (A.7). But the null tetrads are of the form (A.8) so that we have a rotating metric, given by (A.10). Then in the *final step* of the earlier subsection, take again the transformations of u and ϕ coordinates similar in form as (A.11):

$$du = dt' + \varsigma(r)dr, \qquad d\phi = d\phi' + \chi(r)dr \ . \tag{A.14}$$

But here, unlike before, instead of substituting these values in (A.10) and then finding the values of $\varsigma(r)$ and $\chi(r)$, we choose these unknown functions as

$$\varsigma(r) = -\frac{k(r)+a^2}{g(r)h(r)+a^2} \ ; \quad \chi(r) = -\frac{a}{g(r)h(r)+a^2} \ ; \quad k(r) = \sqrt{\frac{g(r)}{f(r)}}h(r) \ . \tag{A.15}$$

Note that the above choice is inspired by the forms (A.12) and (A.13). Since ς and χ have to be a function of r only, the original metric coefficients of (A.1) are intentionally positioned at the places where, in (A.12) and (A.13), we had the complexified versions of them. Also, $\sin^2\theta$ has been removed. This guarantees only radial dependence of our unknown functions for any given static, spherically symmetric metric which is exactly what we want.

To find F, G and H we will use the earlier trick. Since we want the metric to be in Boyer-Lindquist form, after inserting (A.14) with (A.15) in (A.10), set $g_{t'r}$ and $g_{r\phi'}$ to be zero. This will give us the relations among F, G, H and known functions $f(r), g(r), h(r)$. But since we have only two equations corresponding to the vanishing of two off-diagonal metric coefficients, one function among F, G, H will remain undetermined. This yields

$$F = \frac{g(r)h(r)+a^2\cos^2\theta}{(k(r)+a^2\cos^2\theta)^2}H \ ; \tag{A.16}$$

$$G = \frac{g(r)h(r)+a^2\cos^2\theta}{H} \ , \tag{A.17}$$

where we choose H to be undetermined. In this case the metric (A.10) takes the form

$$\begin{aligned} ds^2 &= -Fdt^2 - 2a\sin^2\theta\left(\sqrt{\frac{F}{G}} - F\right)dtd\phi + \frac{H}{g(r)h(r)+a^2}dr^2 + Hd\theta^2 \\ &+ \sin^2\theta\left[H + a^2\sin^2\theta\left(2\sqrt{\frac{F}{G}} - F\right)\right]d\phi^2 \ , \end{aligned} \tag{A.18}$$

where we have dropped the primes in t and ϕ. Now as from (A.17) we have

$$GH + a^2\sin^2\theta = g(r)h(r) + a^2 \ , \tag{A.19}$$

the metric (A.18) reduces to our desired form (4.9). Remember that in this case, H remains undetermined, whereas F and G are given by (A.16) and (A.17), respectively.

A.3 Photon trajectories

The Hamilton-Jacobi (H-J) equation in GR is given by

$$\begin{aligned} \frac{\partial S}{\partial\lambda} + \mathcal{H} &= 0\,; \\ \frac{\partial S}{\partial\lambda} + \frac{1}{2}g^{\mu\nu}p_\mu p_\nu &= 0 \ , \end{aligned} \tag{A.20}$$

where S is the Jacobi action of the photon, λ is the affine parameter of the null geodesic, $\mathcal{H}$ is the Hamiltonian and p_μ is the momentum given by

$$p_\mu = \frac{\partial S}{\partial x^\mu} = g_{\mu\nu}\frac{dx^\nu}{d\lambda} \ . \tag{A.21}$$

Now from (4.9) one can see that the metric $g_{\mu\nu}$ is independent of t and ϕ. Therefore we have two constants of motion – the conserved energy (E) and the angular momentum of the photon in the direction of the rotation axis (L). In that case, the ansatz for S is taken as

$$S = \frac{1}{2}\mu^2\lambda - Et + L\phi + S_r(r) + S_\theta(\theta) \ , \tag{A.22}$$

where μ is the rest mass of the particle moving in the BH spacetime. For photons, we have $\mu = 0$. In the above choice, the radial and θ dependence are taken to be separated as we have another conserved quantity, known as Carter constant $\mathcal{Q}$, for our metric. Putting Eq. (A.22) in the Hamilton-Jacobi equation (A.20), we obtain after some simplifications

$$\begin{aligned} -\left(GH + a^2\sin^2\theta\right)\left(\frac{dS_r}{dr}\right)^2 + \frac{\left[\left(\sqrt{\frac{G}{F}}H + a^2\sin^2\theta\right)E - aL\right]^2}{\left(GH + a^2\sin^2\theta\right)} - (L - aE)^2 \\ = \left(\frac{dS_\theta}{d\theta}\right)^2 + L^2\cot^2\theta - a^2E^2\cos^2\theta \ . \end{aligned} \tag{A.23}$$

Now, since the quantities $\left(GH + a^2\sin^2\theta\right) = g(r)h(r) + a^2 = \Delta(r)$ and $\left(\sqrt{\frac{G}{F}}H + a^2\sin^2\theta\right) = k(r) + a^2 = \sqrt{\frac{g(r)}{f(r)}}h(r) + a^2 = \Sigma(r)$ are functions of r only, the left- and right-hand side of Eq. (A.23) are only functions of r and θ respectively. Therefore, each side of this equation must be equal to some separation constant. Thus introducing the Carter constant $\mathcal{Q}$ as the separation constant we have after separation

$$-\left(GH + a^2\sin^2\theta\right)\left(\frac{dS_r}{dr}\right)^2 + \frac{\left[\left(\sqrt{\frac{G}{F}}H + a^2\sin^2\theta\right)E - aL\right]^2}{\left(GH + a^2\sin^2\theta\right)} - (L - aE)^2 = \mathcal{Q}\ , \tag{A.24}$$

and

$$\left(\frac{dS_\theta}{d\theta}\right)^2 + L^2\cot^2\theta - a^2E^2\cos^2\theta = \mathcal{Q}\ . \tag{A.25}$$

The geodesic equations (4.11), (4.12), (4.13) and (4.14) are then obtained from (A.21) by making use of (A.24) and (A.25).

Appendix B

Obtaining the super-radiance amplification factors from the Klein-Gordon equation in rotating AOS spacetime

B.1 Klein-Gordon equation in rotating AOS spacetime

B.1.1 Deriving the Schrödinger like form

We want to solve $\Box\Phi = 0$. From the line element (4.9), the inverse metric elements are given by:

$$g^{tt} = -\frac{\rho^4 + 2a^2\sin^2\theta\rho^2 + a^4\sin\theta^4 - a^2\sin^2\theta}{\Delta H} \; ; \tag{B.1}$$

$$g^{t\phi} = \frac{a\Delta - a^3\sin^2\theta - a\rho^2}{\Delta H} \; ; \tag{B.2}$$

$$g^{rr} = \frac{\Delta}{H} \; ; \tag{B.3}$$

$$g^{\theta\theta} = \frac{1}{H} \; ; \tag{B.4}$$

$$g^{\phi\phi} = \frac{\Delta - a^2\sin^2\theta}{\Delta H\sin^2\theta} \; . \tag{B.5}$$

Using these the Klein-Gordon equation can be expanded as:

$$\left(\frac{(k+a^2)^2 - \Delta a^2\sin^2\theta}{\Delta}\right)\frac{\partial^2\Phi}{\partial t^2} - \frac{2a\,(gh-k)}{\Delta}\frac{\partial^2\Phi}{\partial t\partial\phi} - \left(\frac{\Delta - a^2\sin^2\theta}{\Delta\sin^2\theta}\right)\frac{\partial^2\Phi}{\partial\phi^2} - \frac{\rho^2}{H}\frac{\partial}{\partial r}\left(\frac{H\Delta}{\rho^2}\frac{\partial\Phi}{\partial r}\right) - \frac{\rho^2}{H\sin\theta}\frac{\partial}{\partial\theta}\left(\frac{H\sin\theta}{\rho^2}\frac{\partial\Phi}{\partial\theta}\right) = 0 \; . \tag{B.6}$$

Note that the form of H is still unknown to us. Without this, the solution can not be obtained. We proceed in the following way to encounter the situation.

Under the classical limit the functions k, f, g, h have the limits given by: $h(r) \to r^2$, $\sqrt{\frac{g(r)}{f(r)}} \to 1$, $k(r) \to r^2$. Thus, if we take the classical limit of (B.6), demanding

that this must be the Klein-Gordon equation for a massless scalar field in Kerr, we can fix the form for the so far undetermined function H. This turns out to be $H = \rho^2 = k(r) + a^2\cos^2\theta$. Substituting this into the Klein-Gordon equation, we have:

$$\left(\frac{(k+a^2)^2 - \Delta a^2\sin^2\theta}{\Delta}\right)\frac{\partial^2\Phi}{\partial t^2} - \frac{2a\,(gh-k)}{\Delta}\frac{\partial^2\Phi}{\partial t\partial\phi} - \left(\frac{\Delta - a^2\sin^2\theta}{\Delta\sin^2\theta}\right)\frac{\partial^2\Phi}{\partial\phi^2} - \frac{\partial}{\partial r}\left(\Delta\frac{\partial\Phi}{\partial r}\right) - \frac{1}{\sin\theta}\frac{\partial}{\partial\theta}\left(\sin\theta\frac{\partial\Phi}{\partial\theta}\right) = 0\ . \quad \text{(B.7)}$$

Now, we consider the ansatz given in (4.46). Using this in the above equation we can separate (B.7) into radial and angular parts given by the following equations:

$$\frac{d}{dr}\left(\Delta\frac{\mathrm{d}J}{\mathrm{d}r}\right) + \left(\frac{\omega^2(k+a^2)^2 + 2q\omega a\,(gh-k) + q^2a^2}{\Delta} - a^2\omega^2 - A_{0lq}\right)J = 0\ ; \quad \text{(B.8)}$$

and

$$\frac{1}{\sin\theta}\frac{d}{d\theta}\left(\sin\theta\frac{\mathrm{d}S}{\mathrm{d}\theta}\right) + \left(\omega^2a^2\cos^2\theta - \frac{q^2}{\sin^2\theta} + A_{0lq}\right)S = 0\ , \quad \text{(B.9)}$$

where $A_{0lq} = \varrho - a^2\omega^2 + 2aq\omega$, with ϱ being the constant of separation and A_{0lq} being the angular eigenvalues. Comparing the angular equation (B.9) with what one would obtain in Kerr, we can see that they are identical. This is to be expected since, the quantum corrections are only found in the functions of the metric that depend on r and do not have any pure angular dependence. Consequently, the solution to $S(\theta)$ is the spin-weighted spheroidal harmonics (with spin $s = 0$ for scalar fields).

The radial equation (B.8) is rewritten as

$$\frac{\mathrm{d}}{\mathrm{d}r}\left(\Delta\frac{\mathrm{d}J}{\mathrm{d}r}\right) + \left(\frac{K^2}{\Delta} - \varrho\right)J = 0\ , \quad \text{(B.10)}$$

where $K = (k(r)+a^2)\omega - qa$ and $H = \rho^2$. We solve this using matching asymptotic technique, which is explained below.
First, we write it in a Schrödinger like form in the tortoise coordinate:

$$\frac{\mathrm{d}r}{\mathrm{d}r_*} = \frac{\Delta}{k(r)+a^2} \equiv \tau(r)\ . \quad \text{(B.11)}$$

Using this, and rewriting (B.10), we have:

$$\frac{\mathrm{d}^2J}{\mathrm{d}r_*^2} + \frac{k'\Delta}{(k+a^2)^2}\frac{\mathrm{d}J}{\mathrm{d}r_*} + \left(\frac{K^2 - \Delta(\varrho + a^2\omega^2 - 2aq\omega)}{(k(r)+a^2)^2}\right)J = 0\ . \quad \text{(B.12)}$$

Now, we take a transformation to define a new function: $\varphi = \sqrt{k+a^2}J$. Using this, we can write down the final Schrödinger like equation as:

$$\frac{\mathrm{d}^2\varphi}{\mathrm{d}r_*^2} + V_{\text{eff}}\,\varphi = 0\ , \quad \text{(B.13)}$$

where the form of the effective potential is given by Eq. (4.48).

B.1.2 Solving for amplification Factors

To obtain the coefficients R, I, we solve (B.10). As noted earlier, this is equivalent to solving the Schrödinger like equation (B.13). We now consider only the slowly rotating approximation $a\omega << 1$. Defining a new coordinate x given by

$$x = \frac{r - r_+}{r_+ - r'} \ , \tag{B.14}$$

the radial equation (B.10) can be approximately written as:

$$x^2(x+1)^2\frac{\mathrm{d}^2 J}{\mathrm{d}x^2} + x(x+1)\frac{\mathrm{d}J}{\mathrm{d}x} + \left[\tilde{k}^2 x^4 - \varrho x(x+1) + Q^2\right] J = 0 \ . \tag{B.15}$$

In the above different constants are defined as

$$Q = \frac{\omega - q\Omega_H}{4\pi\sigma_H}; \quad 4\pi\sigma_H = \frac{(r_+ - r')}{k(r_+) + a^2}; \quad \tilde{k} = \frac{1}{2}\frac{\partial^2 K}{\partial r^2}\bigg|_{r_+} \ , \tag{B.16}$$

with σ_H being associated with the temperature of the BH. Next, we will follow the conventional steps which are mentioned below (see e.g. [423]):

(1) Obtain the near horizon solution of Eq. (B.15); i.e. the solution for the regime $x << 1$.

(2) Obtain the far horizon limit of Eq. (B.15); i.e. in the regime $x >> 1$.

(3) Compare the large x limit of the solution obtained in step 1 and the small x limit of the solution obtained in step 2 with the demand that these solutions must be equal due to the continuity of Φ. This will fix the integration constants.

(4) Finally demand that the obtained solutions are asymptotically of the form given in (4.49). This will lead to the identification of the coefficients T, I, R.

For the amplification factor (see Eq. (4.51)) we need only I and R. Following the above steps these coefficients will be obtained below.

In the near horizon regime $x << 1$ the equation (B.15) becomes:

$$x^2(x+1)^2\frac{\mathrm{d}^2 J}{\mathrm{d}x^2} + x(x+1)\frac{\mathrm{d}J}{\mathrm{d}x} + \left[Q^2 - \varrho x(x+1)\right] J = 0 \ . \tag{B.17}$$

This has a solution given by:

$$J(x) = A_1 x^{-iQ}(x+1)^{-iQ} F\left(-l, l+1, 1-2iQ, -x\right) \ , \tag{B.18}$$

where F is the hypergeometric function. In the above, we have used the ingoing boundary condition at the horizon. Following the slowly rotating approximation, we have also used $A_{lq} = l(l+1)$. In the far region limit $x >> 1$ Eq. (B.15) becomes:

$$\frac{\mathrm{d}^2 J}{\mathrm{d}x^2} + \frac{2}{x}\frac{\mathrm{d}J}{\mathrm{d}x} + \left[\tilde{k}^2 - \frac{\varrho}{x^2}\right] J = 0 \ . \tag{B.19}$$

This has a solution of the form:

$$J(x) = C_1 e^{-i\tilde{k}x} x^l U\left(1-l, 2l+2, 2i\tilde{k}x\right) + C_2 e^{-i\tilde{k}x} x^{-l-1} U\left(-l, -2l, 2i\tilde{k}x\right) \ , \tag{B.20}$$

where U is the confluent hypergeometric function. Next, follow step 3. Matching the cross limits of (B.18) and (B.20) we find the integration constants C_1 and C_2 in terms of A_1 as

$$C_1 = A_1 \frac{\Gamma(1-2iQ)\,\Gamma(2l+1)}{\Gamma(l+1)\,\Gamma(l+1-2iQ)} \quad ; \tag{B.21}$$

and

$$C_2 = A_1 \frac{\Gamma(1-2iQ)\,\Gamma(-1-2l)}{\Gamma(-l-2iQ)\,\Gamma(-l)} \quad . \tag{B.22}$$

Finally comparing the far solution with the asymptotic solution at infinity (given in (4.49)) we have the required coefficients:

$$I = \frac{1}{\omega}\left[\tilde{k}^{l+1}\frac{C_2\,(-2i)^l\,\Gamma(-2l)}{\Gamma(-l)} + \tilde{k}^{-l}\frac{C_1\,(-2i)^{-l-1}\,\Gamma(2l+2)}{\Gamma(l+1)}\right] \quad ; \tag{B.23}$$

and

$$R = \frac{1}{\omega}\left[\tilde{k}^{l+1}\frac{C_2\,(2i)^l\,\Gamma(-2l)}{\Gamma(-l)} + \tilde{k}^{-l}\frac{C_1\,(2i)^{-l-1}\,\Gamma(2l+2)}{\Gamma(l+1)}\right] \quad . \tag{B.24}$$

Using this form for R, I we calculate the amplification factor from (4.51).

It must be mentioned that we encounter Γ functions with negative arguments in the amplification factors of both the Kerr and AOS BHs. To circumvent this, we can manipulate the functions using the Γ function reflection formula [440]:

$$\frac{\Gamma(s-a+1)}{\Gamma(s-b+1)} = (-1)^{b-a}\frac{\Gamma(b-s)}{\Gamma(a-s)} \quad . \tag{B.25}$$

for $a, b \in Z$ and complex s. This is a very standard technique in this context.

भारतीय प्रौद्योगिकी संस्थान गुवाहाटी
Indian Institute of Technology Guwahati

Bibliography

1. Guevara, A. & Kol, U. Self Dual Black Holes as the Hydrogen Atom. arXiv: 2311.07933 [hep-th] (2023).
2. Berti, E., Cardoso, V. & Starinets, A. O. Quasinormal modes of black holes and black branes. *Class. Quant. Grav.* **26,** 163001. arXiv: 0905.2975 [gr-qc] (2009).
3. Konoplya, R. A. & Zhidenko, A. Quasinormal modes of black holes: From astrophysics to string theory. *Rev. Mod. Phys.* **83,** 793–836. arXiv: 1102.4014 [gr-qc] (2011).
4. Hod, S. Bohr's correspondence principle and the area spectrum of quantum black holes. *Phys. Rev. Lett.* **81,** 4293. arXiv: gr-qc/9812002 (1998).
5. Hawking, S. W. *Particle Creation by Black Holes* 167–188. https://doi.org/10.1142/9789814539395_0011 (1993).
6. Andersson, N. & Jensen, B. P. Scattering by black holes. Chapter 0.1 (eds Pike, R. & Sabatier, P.) 1607–1626. arXiv: gr-qc/0011025 (2000).
7. Cardoso, V. & Pani, P. Testing the nature of dark compact objects: a status report. *Living Rev. Rel.* **22,** 4. arXiv: 1904.05363 [gr-qc] (2019).
8. Devi, S., Roy, R. & Chakrabarti, S. Quasinormal modes and greybody factors of the novel four dimensional Gauss–Bonnet black holes in asymptotically de Sitter space time: scalar, electromagnetic and Dirac perturbations. *Eur. Phys. J. C* **80,** 760. arXiv: 2004.14935 [gr-qc] (2020).
9. Chowdhury, A., Devi, S. & Chakrabarti, S. Naked singularity in 4D Einstein-Gauss-Bonnet novel gravity: Echoes and instability. *Phys. Rev. D* **106,** 024023. arXiv: 2202.13698 [gr-qc] (2022).
10. Glavan, D. & Lin, C. Einstein-Gauss-Bonnet Gravity in Four-Dimensional Spacetime. *Phys. Rev. Lett.* **124,** 081301. arXiv: 1905.03601 [gr-qc] (2020).
11. Cunha, P. V. P. & Herdeiro, C. A. R. Shadows and strong gravitational lensing: a brief review. *Gen. Rel. Grav.* **50,** 42. arXiv: 1801.00860 [gr-qc] (2018).
12. Perlick, V. & Tsupko, O. Y. Calculating black hole shadows: Review of analytical studies. *Phys. Rept.* **947,** 1–39. arXiv: 2105.07101 [gr-qc] (2022).
13. Shaikh, R. Testing black hole mimickers with the Event Horizon Telescope image of Sagittarius A*. *Mon. Not. Roy. Astron. Soc.* **523,** 375–384. arXiv: 2208.01995 [gr-qc] (2023).
14. Brito, R., Cardoso, V. & Pani, P. Superradiance: New Frontiers in Black Hole Physics. *Lect. Notes Phys.* **906,** pp.1–237. arXiv: 1501.06570 [gr-qc] (2015).

15. Devi, S., Nagarajan, A. S., Chakrabarti, S. & Majhi, B. R. Shadow of quantum extended Kruskal black hole and its super-radiance property. *Phys. Dark Univ.* **39,** 101173. arXiv: 2105.11847 [gr-qc] (2023).

16. Ashtekar, A., Olmedo, J. & Singh, P. Quantum extension of the Kruskal spacetime. *Phys. Rev. D* **98,** 126003. arXiv: 1806.02406 [gr-qc] (2018).

17. Konoplya, R. A. & Zinhailo, A. F. Quasinormal modes, stability and shadows of a black hole in the 4D Einstein–Gauss–Bonnet gravity. *Eur. Phys. J. C* **80,** 1049. arXiv: 2003.01188 [gr-qc] (2020).

18. Churilova, M. S. Quasinormal modes of the Dirac field in the consistent 4D Einstein–Gauss–Bonnet gravity. *Phys. Dark Univ.* **31,** 100748. arXiv: 2004.00513 [gr-qc] (2021).

19. Mishra, A. K. Quasinormal modes and strong cosmic censorship in the regularised 4D Einstein–Gauss–Bonnet gravity. *Gen. Rel. Grav.* **52,** 106. arXiv: 2004.01243 [gr-qc] (2020).

20. Cuyubamba, M. A. Stability of asymptotically de Sitter and anti-de Sitter black holes in 4D regularized Einstein–Gauss–Bonnet theory. *Phys. Dark Univ.* **31,** 100789. arXiv: 2004.09025 [gr-qc] (2021).

21. Ashtekar, A. & Olmedo, J. Properties of a recent quantum extension of the Kruskal geometry. *Int. J. Mod. Phys. D* **29,** 2050076. arXiv: 2005.02309 [gr-qc] (2020).

22. Ashtekar, A., Olmedo, J. & Singh, P. Quantum Transfiguration of Kruskal Black Holes. *Phys. Rev. Lett.* **121,** 241301. arXiv: 1806.00648 [gr-qc] (2018).

23. Newman, E. T. & Janis, A. I. Note on the Kerr spinning particle metric. *J. Math. Phys.* **6,** 915–917 (1965).

24. Azreg-Aïnou, M. Generating rotating regular black hole solutions without complexification. *Phys. Rev. D* **90,** 064041. https://link.aps.org/doi/10.1103/PhysRevD.90.064041 (2014).

25. Will, C. M. The Confrontation between General Relativity and Experiment. *Living Rev. Rel.* **17,** 4. arXiv: 1403.7377 [gr-qc] (2014).

26. Ishak, M. Testing General Relativity in Cosmology. *Living Rev. Rel.* **22,** 1. arXiv: 1806.10122 [astro-ph.CO] (2019).

27. Collaboration, T. E. H. T. & Akiyama, K. First M87 Event Horizon Telescope Results. I. The Shadow of the Supermassive Black Hole. *The Astrophysical Journal Letters* **875,** L1. https://dx.doi.org/10.3847/2041-8213/ab0ec7 (2019).

28. Abbott, B. P. *et al.* Observation of Gravitational Waves from a Binary Black Hole Merger. *Phys. Rev. Lett.* **116,** 061102. https://link.aps.org/doi/10.1103/PhysRevLett.116.061102 (2016).

29. Adamek, J., Daverio, D., Durrer, R. & Kunz, M. General relativity and cosmic structure formation. *Nature Phys.* **12,** 346–349. arXiv: 1509.01699 [astro-ph.CO] (2016).

30. Penrose, R. Gravitational Collapse: the Role of General Relativity. *Nuovo Cimento Rivista Serie* **1,** 252 (1969).

31. Curiel, E. in *The Stanford Encyclopedia of Philosophy* (eds Zalta, E. N. & Nodelman, U.) Summer 2023 (Metaphysics Research Lab, Stanford University, 2023). https://plato.stanford.edu/archives/sum2023/entries/spacetime-singularities/.
32. Zwicky, F. Die Rotverschiebung von extragalaktischen Nebeln. *Helv. Phys. Acta* **6,** 110–127 (1933).
33. Bertone, G., Hooper, D. & Silk, J. Particle dark matter: Evidence, candidates and constraints. *Phys. Rept.* **405,** 279–390. arXiv: hep-ph/0404175 (2005).
34. Peebles, P. J. E. & Ratra, B. The Cosmological Constant and Dark Energy. *Rev. Mod. Phys.* **75** (eds Hsu, J.-P. & Fine, D.) 559–606. arXiv: astro-ph/0207347 (2003).
35. Frieman, J., Turner, M. & Huterer, D. Dark Energy and the Accelerating Universe. *Ann. Rev. Astron. Astrophys.* **46,** 385–432. arXiv: 0803.0982 [astro-ph] (2008).
36. Bambi, C., Malafarina, D. & Modesto, L. Non-singular quantum-inspired gravitational collapse. *Phys. Rev. D* **88,** 044009. arXiv: 1305.4790 [gr-qc] (2013).
37. Tavakoli, Y., Marto, J. & Dapor, A. Semiclassical dynamics of horizons in spherically symmetric collapse. *Int. J. Mod. Phys. D* **23,** 1450061. arXiv: 1303.6157 [gr-qc] (2014).
38. Goswami, R., Joshi, P. S. & Singh, P. Quantum evaporation of a naked singularity. *Phys. Rev. Lett.* **96,** 031302. arXiv: gr-qc/0506129 (2006).
39. Bojowald, M., Goswami, R., Maartens, R. & Singh, P. Black Hole Mass Threshold from Nonsingular Quantum Gravitational Collapse. *Phys. Rev. Lett.* **95,** 091302. https://link.aps.org/doi/10.1103/PhysRevLett.95.091302 (2005).
40. Abbott, R. *et al.* Tests of general relativity with binary black holes from the second LIGO-Virgo gravitational-wave transient catalog. *Phys. Rev. D* **103,** 122002. arXiv: 2010.14529 [gr-qc] (2021).
41. Abbott, R. *et al.* Tests of General Relativity with GWTC-3. arXiv: 2112.06861 [gr-qc] (2021).
42. Abuter, R. *et al.* Detection of the gravitational redshift in the orbit of the star S2 near the Galactic centre massive black hole. *Astron. Astrophys.* **615,** L15. arXiv: 1807.09409 [astro-ph.GA] (2018).
43. Abuter, R. *et al.* Detection of the Schwarzschild precession in the orbit of the star S2 near the Galactic centre massive black hole. *Astron. Astrophys.* **636,** L5. arXiv: 2004.07187 [astro-ph.GA] (2020).
44. Wex, N. & Kramer, M. Gravity Tests with Radio Pulsars. *Universe* **6,** 156 (2020).
45. Bambi, C. Testing black hole candidates with electromagnetic radiation. *Rev. Mod. Phys.* **89,** 025001. arXiv: 1509.03884 [gr-qc] (2017).
46. Abbott, B. P. *et al.* GW151226: Observation of Gravitational Waves from a 22-Solar-Mass Binary Black Hole Coalescence. *Phys. Rev. Lett.* **116,** 241103. arXiv: 1606.04855 [gr-qc] (2016).

47. Abbott, B. P. *et al.* GW170817: Observation of Gravitational Waves from a Binary Neutron Star Inspiral. *Phys. Rev. Lett.* **119,** 161101. https://link.aps.org/doi/10.1103/PhysRevLett.119.161101 (2017).

48. Clifton, T., Ferreira, P. G., Padilla, A. & Skordis, C. Modified Gravity and Cosmology. *Phys. Rept.* **513,** 1–189. arXiv: 1106.2476 [astro-ph.CO] (2012).

49. Baker, T. *et al.* Strong constraints on cosmological gravity from GW170817 and GRB 170817A. *Phys. Rev. Lett.* **119,** 251301. arXiv: 1710.06394 [astro-ph.CO] (2017).

50. Stelle, K. S. Classical Gravity with Higher Derivatives. *Gen. Rel. Grav.* **9,** 353–371 (1978).

51. Capozziello, S. & De Laurentis, M. Extended Theories of Gravity. *Phys. Rept.* **509,** 167–321. arXiv: 1108.6266 [gr-qc] (2011).

52. Sotiriou, T. P. & Faraoni, V. f(R) Theories Of Gravity. *Rev. Mod. Phys.* **82,** 451–497. arXiv: 0805.1726 [gr-qc] (2010).

53. Damour, T. & Esposito-Farese, G. Tensor multiscalar theories of gravitation. *Class. Quant. Grav.* **9,** 2093–2176 (1992).

54. De Rham, C., Gabadadze, G. & Tolley, A. J. Resummation of Massive Gravity. *Phys. Rev. Lett.* **106,** 231101. arXiv: 1011.1232 [hep-th] (2011).

55. Brans, C. & Dicke, R. H. Mach's principle and a relativistic theory of gravitation. *Phys. Rev.* **124** (eds Hsu, J.-P. & Fine, D.) 925–935 (1961).

56. Ashtekar, A. Gravity and the quantum. *New J. Phys.* **7** (eds Calcagni, G., Papantonopoulos, L., Siopsis, G. & Tsamis, N.) 198. arXiv: gr-qc/0410054 (2005).

57. Rovelli, C. Loop quantum gravity. *Living Rev. Rel.* **1,** 1. arXiv: gr-qc/9710008 (1998).

58. Polchinski, J. *String theory. Vol. 1: An introduction to the bosonic string* ISBN: 978-0-511-25227-3, 978-0-521-67227-6, 978-0-521-63303-1 (Cambridge University Press, 2007).

59. Polchinski, J. *String theory. Vol. 2: Superstring theory and beyond* ISBN: 978-0-511-25228-0, 978-0-521-63304-8, 978-0-521-67228-3 (Cambridge University Press, 2007).

60. Lovelock, D. The Einstein tensor and its generalizations. *J. Math. Phys.* **12,** 498–501 (1971).

61. Padmanabhan, T. & Kothawala, D. Lanczos-Lovelock models of gravity. *Phys. Rept.* **531,** 115–171. arXiv: 1302.2151 [gr-qc] (2013).

62. Bhattacharya, K., Dey, D., Mazumdar, A. & Sarkar, T. New class of naked singularities and their observational signatures. *Phys. Rev. D* **101,** 043005. arXiv: 1709.03798 [gr-qc] (2020).

63. Joshi, P. S., Malafarina, D. & Narayan, R. Equilibrium configurations from gravitational collapse. *Class. Quant. Grav.* **28,** 235018. arXiv: 1106.5438 [gr-qc] (2011).

64. Hooft, G. On the Quantum Structure of a Black Hole. *Nuclear Physics* **256,** 727–745. https://api.semanticscholar.org/CorpusID:11180484 (1985).

65. Modesto, L. Disappearance of black hole singularity in quantum gravity. *Phys. Rev. D* **70,** 124009. arXiv: gr-qc/0407097 (2004).

66. Modesto, L. Loop quantum black hole. *Class. Quant. Grav.* **23,** 5587–5602. arXiv: gr-qc/0509078 (2006).

67. Peltola, A. & Kunstatter, G. A Complete, Single-Horizon Quantum Corrected Black Hole Spacetime. *Phys. Rev. D* **79,** 061501. arXiv: 0811.3240 [gr-qc] (2009).

68. Modesto, L. & Premont-Schwarz, I. Self-dual Black Holes in LQG: Theory and Phenomenology. *Phys. Rev. D* **80,** 064041. arXiv: 0905.3170 [hep-th] (2009).

69. Caravelli, F. & Modesto, L. Spinning Loop Black Holes. *Class. Quant. Grav.* **27,** 245022. arXiv: 1006.0232 [gr-qc] (2010).

70. Jha, S. K. Shadow, quasinormal modes, greybody bounds, and Hawking sparsity of loop quantum gravity motivated non-rotating black hole. *Eur. Phys. J. C* **83,** 952. arXiv: 2310.04759 [gr-qc] (2023).

71. Liu, C. *et al.* Shadow and quasinormal modes of a rotating loop quantum black hole. *Phys. Rev. D* **101,** 084001. https://link.aps.org/doi/10.1103/PhysRevD.101.084001 (2020).

72. Donoghue, J. F. General relativity as an effective field theory: The leading quantum corrections. *Phys. Rev. D* **50,** 3874–3888. arXiv: gr-qc/9405057 (1994).

73. Burgess, C. P. Quantum gravity in everyday life: General relativity as an effective field theory. *Living Rev. Rel.* **7,** 5–56. arXiv: gr-qc/0311082 (2004).

74. Fernandes, P. G. S., Carrilho, P., Clifton, T. & Mulryne, D. J. The 4D Einstein-Gauss-Bonnet theory of gravity: a review. *Classical and Quantum Gravity* **39,** 063001. https://dx.doi.org/10.1088/1361-6382/ac500a (2022).

75. Zwiebach, B. Curvature squared terms and string theories. *Physics Letters B* **156,** 315–317. ISSN: 0370-2693. https://www.sciencedirect.com/science/article/pii/0370269385916168 (1985).

76. Sen, A. Entropy function for heterotic black holes. *Journal of High Energy Physics* **2006,** 008. https://dx.doi.org/10.1088/1126-6708/2006/03/008 (2006).

77. Moura, F. & Schiappa, R. Higher-derivative corrected black holes: Perturbative stability and absorption cross-section in heterotic string theory. *Class. Quant. Grav.* **24,** 361–386. arXiv: hep-th/0605001 (2007).

78. Boulware, D. G. & Deser, S. String-Generated Gravity Models. *Phys. Rev. Lett.* **55,** 2656–2660. https://link.aps.org/doi/10.1103/PhysRevLett.55.2656 (1985).

79. Wheeler, J. T. Symmetric solutions to the maximally Gauss-Bonnet extended Einstein equations. *Nuclear Physics B* **273,** 732–748. ISSN: 0550-3213. https://www.sciencedirect.com/science/article/pii/0550321386903883 (1986).

80. Wiltshire, D. L. Black holes in string-generated gravity models. *Phys. Rev. D* **38,** 2445–2456. https://link.aps.org/doi/10.1103/PhysRevD.38.2445 (1988).

81. Meissner, K. A. & Olechowski, M. Brane localization of gravity in higher derivative theory. *Phys. Rev. D* **65,** 064017. https://link.aps.org/doi/10.1103/PhysRevD.65.064017 (2002).

82. Barrau, A., Grain, J. & Alexeyev, S. O. Gauss-Bonnet black holes at the LHC: Beyond the dimensionality of space. *Phys. Lett. B* **584,** 114. arXiv: hep-ph/0311238 (2004).

83. Odintsov, S. D., Oikonomou, V. K. & Fronimos, F. P. Rectifying Einstein-Gauss-Bonnet Inflation in View of GW170817. *Nucl. Phys. B* **958,** 115135. arXiv: 2003.13724 [gr-qc] (2020).

84. Oikonomou, V. K. & Fronimos, F. P. Reviving non-minimal Horndeski-like theories after GW170817: kinetic coupling corrected Einstein–Gauss–Bonnet inflation. *Class. Quant. Grav.* **38,** 035013. arXiv: 2006.05512 [gr-qc] (2021).

85. Oikonomou, V. K. A refined Einstein–Gauss–Bonnet inflationary theoretical framework. *Class. Quant. Grav.* **38,** 195025. arXiv: 2108.10460 [gr-qc] (2021).

86. Fernandes, P. G. Charged black holes in AdS spaces in 4D Einstein Gauss-Bonnet gravity. *Physics Letters B* **805,** 135468. ISSN: 0370-2693. https://www.sciencedirect.com/science/article/pii/S0370269320302720 (2020).

87. Ghosh, S. G. & Kumar, R. Generating black holes in 4*D* Einstein-Gauss-Bonnet gravity. *Class. Quant. Grav.* **37,** 245008. arXiv: 2003.12291 [gr-qc] (2020).

88. Lovelock, D. The four-dimensionality of space and the Einstein tensor. *J. Math. Phys.* **13,** 874–876 (1972).

89. Lanczos, C. A Remarkable Property of the Riemann-Christoffel Tensor in Four Dimensions. *Annals of Mathematics* **39,** 842–850. https://doi.org/10.2307/1968467 (1938).

90. Li, S.-L., Wu, P. & Yu, H. Stability of the Einstein Static Universe in 4*D* Gauss-Bonnet Gravity. arXiv: 2004.02080 [gr-qc] (2020).

91. Kobayashi, T. Effective scalar-tensor description of regularized Lovelock gravity in four dimensions. *Journal of Cosmology and Astroparticle Physics* **2020,** 013. https://dx.doi.org/10.1088/1475-7516/2020/07/013 (2020).

92. Kumar, A., Walia, R. K. & Ghosh, S. G. Bardeen Black Holes in the Regularized 4D Einstein-Gauss-Bonnet Gravity. *Universe* **8,** 232. arXiv: 2003.13104 [gr-qc] (2022).

93. Kumar, R. & Ghosh, S. G. Rotating black holes in 4*D* Einstein-Gauss-Bonnet gravity and its shadow. *JCAP* **07,** 053. arXiv: 2003.08927 [gr-qc] (2020).

94. Doneva, D. D. & Yazadjiev, S. S. Relativistic stars in 4D Einstein-Gauss-Bonnet gravity. *Journal of Cosmology and Astroparticle Physics* **2021,** 024. https://dx.doi.org/10.1088/1475-7516/2021/05/024 (2021).

95. Ghosh, S. G. & Maharaj, S. D. Radiating black holes in the novel 4D Einstein–Gauss–Bonnet gravity. *Phys. Dark Univ.* **30,** 100687. arXiv: 2003.09841 [gr-qc] (2020).

96. Malafarina, D., Toshmatov, B. & Dadhich, N. Dust collapse in 4D Einstein-Gauss-Bonnet gravity. *Phys. Dark Univ.* **30,** 100598. arXiv: 2004.07089 [gr-qc] (2020).

97. Konoplya, R. A. & Zhidenko, A. Black holes in the four-dimensional Einstein-Lovelock gravity. *Phys. Rev. D* **101,** 084038. https://link.aps.org/doi/10.1103/PhysRevD.101.084038 (2020).

98. Eslam Panah, B., Jafarzade, K. & Hendi, S. H. Charged 4D Einstein-Gauss-Bonnet-AdS black holes: Shadow, energy emission, deflection angle and heat engine. *Nucl. Phys. B* **961,** 115269. arXiv: 2004.04058 [hep-th] (2020).

99. Hosseini Mansoori, S. A. Thermodynamic geometry of the novel 4-D Gauss-Bonnet AdS black hole. *Phys. Dark Univ.* **31,** 100776. arXiv: 2003.13382 [gr-qc] (2021).

100. Konoplya, R. A. & Zinhailo, A. F. Grey-body factors and Hawking radiation of black holes in 4*D* Einstein-Gauss-Bonnet gravity. *Phys. Lett. B* **810,** 135793. arXiv: 2004.02248 [gr-qc] (2020).

101. Hegde, K., Naveena Kumara, A., Rizwan, C. L. A. & Ajith, K. M. Thermodynamics, Phase Transition and Joule Thomson Expansion of novel 4-D Gauss Bonnet AdS Black Hole. arXiv: 2003.08778 [gr-qc] (2020).

102. Guo, M. & Li, P.-C. Innermost stable circular orbit and shadow of the 4*D* Einstein–Gauss–Bonnet black hole. *Eur. Phys. J. C* **80,** 588. arXiv: 2003.02523 [gr-qc] (2020).

103. Zhang, Y.-P., Wei, S.-W. & Liu, Y.-X. Spinning Test Particle in Four-Dimensional Einstein-Gauss-Bonnet Black Holes. *Universe* **6,** 103. arXiv: 2003.10960 [gr-qc] (2020).

104. Roy, R. & Chakrabarti, S. Study on black hole shadows in asymptotically de Sitter spacetimes. *Phys. Rev. D* **102,** 024059. arXiv: 2003.14107 [gr-qc] (2020).

105. Naveena Kumara, A., Rizwan, C. L. A., Hegde, K., Ali, M. S. & Ajith, K. M. Rotating 4D Gauss–Bonnet black hole as a particle accelerator. *Annals Phys.* **434,** 168599. arXiv: 2004.04521 [gr-qc] (2021).

106. Liu, C., Zhu, T. & Wu, Q. Thin Accretion Disk around a four-dimensional Einstein-Gauss-Bonnet Black Hole. *Chin. Phys. C* **45,** 015105. arXiv: 2004.01662 [gr-qc] (2021).

107. Heydari-Fard, M., Heydari-Fard, M. & Sepangi, H. R. Bending of light in novel 4D Gauss-Bonnet-de Sitter black holes by the Rindler-Ishak method. *Europhysics Letters* **133,** 50006. https://dx.doi.org/10.1209/0295-5075/133/50006 (2021).

108. Kumar, R., Islam, S. U. & Ghosh, S. G. Gravitational lensing by charged black hole in regularized 4*D* Einstein–Gauss–Bonnet gravity. *Eur. Phys. J. C* **80,** 1128. arXiv: 2004.12970 [gr-qc] (2020).

109. Islam, S. U., Kumar, R. & Ghosh, S. G. Gravitational lensing by black holes in the 4D Einstein-Gauss-Bonnet gravity. *Journal of Cosmology and Astroparticle Physics* **2020,** 030. https://dx.doi.org/10.1088/1475-7516/2020/09/030 (2020).

110. Churilova, M. S. Quasinormal modes of the test fields in the consistent 4D Einstein–Gauss-Bonnet–(anti)de Sitter gravity. *Annals Phys.* **427,** 168425. arXiv: 2004.14172 [gr-qc] (2021).

111. Konoplya, R. Quasinormal modes of the charged black hole in Gauss-Bonnet gravity. *Phys. Rev. D* **71,** 024038. arXiv: hep-th/0410057 (2005).

112. Abdalla, E., Konoplya, R. A. & Molina, C. Scalar field evolution in Gauss-Bonnet black holes. *Phys. Rev. D* **72,** 084006. https://link.aps.org/doi/10.1103/PhysRevD.72.084006 (2005).

113. Chakrabarti, S. K. & Gupta, K. S. Asymptotic Quasinormal modes of d-dimensional Schwarzschild black hole with Gauss-Bonnet correction. *International Journal of Modern Physics A* **21,** 3565–3574. ISSN: 1793-656X. http://dx.doi.org/10.1142/S0217751X06031612 (2006).

114. Grain, J., Barrau, A. & Kanti, P. Exact results for evaporating black holes in curvature-squared lovelock gravity: Gauss-Bonnet greybody factors. *Phys. Rev. D* **72,** 104016. arXiv: hep-th/0509128 (2005).

115. Chakrabarti, S. K. Quasinormal modes for tensor and vector type perturbation of Gauss Bonnet black hole using third order WKB approach. *General Relativity and Gravitation* **39,** 567–582. ISSN: 1572-9532. http://dx.doi.org/10.1007/s10714-007-0404-8 (2007).

116. Daghigh, R. G., Kunstatter, G. & Ziprick, J. The Mystery of the asymptotic quasinormal modes of Gauss-Bonnet black holes. *Class. Quant. Grav.* **24,** 1981–1992. arXiv: gr-qc/0611139 (2007).

117. Konoplya, R. A. & Zhidenko, A. (In)stability of D-dimensional black holes in Gauss-Bonnet theory. *Physical Review D* **77.** ISSN: 1550-2368. http://dx.doi.org/10.1103/PhysRevD.77.104004 (2008).

118. Zhidenko, A. Quasinormal modes of brane-localized standard model fields in Gauss-Bonnet theory. *Phys. Rev. D* **78,** 024007. https://link.aps.org/doi/10.1103/PhysRevD.78.024007 (2008).

119. Chakrabarti, S. K. A comparative study of Dirac quasinormal modes of charged black holes in higher dimensions. *Eur. Phys. J. C* **61,** 477–488. arXiv: 0809.1004 [gr-qc] (2009).

120. Konoplya, R. A. & Zhidenko, A. Long life of Gauss-Bonnet corrected black holes. *Phys. Rev. D* **82,** 084003. arXiv: 1004.3772 [hep-th] (2010).

121. Sadeghi, J., Banijamali, A., Setare, M. R. & Vaez, H. Asymptotic quasinormal modes in Einstein-Gauss-Bonnet gravity. *Int. J. Mod. Phys. A* **26,** 2783–2794 (2011).

122. Blázquez-Salcedo, J. L. *et al.* Perturbed black holes in Einstein-dilaton-Gauss-Bonnet gravity: Stability, ringdown, and gravitational-wave emission. *Phys. Rev. D* **94,** 104024. arXiv: 1609.01286 [gr-qc] (2016).

123. Morais Graça, J. P., Salako, G. I. & Bezerra, V. B. Quasinormal modes of a black hole with a cloud of strings in Einstein–Gauss–Bonnet gravity. *Int. J. Mod. Phys. D* **26,** 1750113. arXiv: 1604.04734 [gr-qc] (2017).

124. Maselli, A., Gualtieri, L., Pani, P., Stella, L. & Ferrari, V. Testing gravity with quasi-periodic oscillations from accreting black holes:The case of the Einstein-Dilaton-Gauss-Bonnet theory. *The Astrophysical Journal* **801,** 115. https://dx.doi.org/10.1088/0004-637X/801/2/115 (2015).

125. Konoplya, R. A. & Zhidenko, A. Eikonal instability of Gauss-Bonnet–(anti-)–de Sitter black holes. *Phys. Rev. D* **95,** 104005. https://link.aps.org/doi/10.1103/PhysRevD.95.104005 (2017).

126. González, P. A., Konoplya, R. A. & Vásquez, Y. Quasinormal modes of a scalar field in the Einstein-Gauss-Bonnet-AdS black hole background: Perturbative and nonperturbative branches. *Phys. Rev. D* **95,** 124012. https://link.aps.org/doi/10.1103/PhysRevD.95.124012 (2017).

127. Konoplya, R. & Zhidenko, A. Quasinormal modes of Gauss-Bonnet-AdS black holes: towards holographic description of finite coupling. *Journal of High Energy Physics* **2017.** ISSN: 1029-8479. http://dx.doi.org/10.1007/JHEP09(2017)139 (2017).

128. Takahashi, T. & Soda, J. Catastrophic Instability of Small Lovelock Black Holes. *Prog. Theor. Phys.* **124,** 711–729. arXiv: 1008.1618 [gr-qc] (2010).

129. Takahashi, T. & Soda, J. Master Equations for Gravitational Perturbations of Static Lovelock Black Holes in Higher Dimensions. *Prog. Theor. Phys.* **124,** 911–924. arXiv: 1008.1385 [gr-qc] (2010).

130. Konoplya, R. A. & Zhidenko, A. (In)stability of black holes in the 4*D* Einstein–Gauss–Bonnet and Einstein–Lovelock gravities. *Phys. Dark Univ.* **30,** 100697. arXiv: 2003.12492 [gr-qc] (2020).

131. Vieira, H. S. Quasibound States, Stability and Wave Functions of the Test Fields in the Consistent 4D Einstein–Gauss–Bonnet Gravity. *Universe* **9,** 205. arXiv: 2107.02065 [gr-qc] (2023).

132. Gürses, M., Şişman, T. c. & Tekin, B. Is there a novel Einstein–Gauss–Bonnet theory in four dimensions? *Eur. Phys. J. C* **80,** 647. arXiv: 2004.03390 [gr-qc] (2020).

133. Gürses, M., Şişman, T. C. & Tekin, B. Comment on "Einstein-Gauss-Bonnet Gravity in Four-Dimensional Spacetime". *Phys. Rev. Lett.* **125,** 149001. https://link.aps.org/doi/10.1103/PhysRevLett.125.149001 (2020).

134. Arrechea, J., Delhom, A. & Jiménez-Cano, A. Inconsistencies in four-dimensional Einstein-Gauss-Bonnet gravity *. *Chinese Physics C* **45,** 013107. https://dx.doi.org/10.1088/1674-1137/abc1d4 (2021).

135. Arrechea, J., Delhom, A. & Jiménez-Cano, A. Comment on "Einstein-Gauss-Bonnet Gravity in Four-Dimensional Spacetime". *Phys. Rev. Lett.* **125,** 149002. https://link.aps.org/doi/10.1103/PhysRevLett.125.149002 (2020).

136. Bonifacio, J., Hinterbichler, K. & Johnson, L. A. Amplitudes and 4D Gauss-Bonnet theory. *Phys. Rev. D* **102,** 024029. https://link.aps.org/doi/10.1103/PhysRevD.102.024029 (2020).

137. Ai, W.-Y. A note on the novel 4D Einstein–Gauss–Bonnet gravity. *Communications in Theoretical Physics* **72,** 095402. https://dx.doi.org/10.1088/1572-9494/aba242 (2020).

138. Mahapatra, S. A note on the total action of 4D Gauss–Bonnet theory. *Eur. Phys. J. C* **80,** 992. arXiv: 2004.09214 [gr-qc] (2020).

139. Hohmann, M., Pfeifer, C. & Voicu, N. Canonical variational completion and 4D Gauss-Bonnet gravity. *Eur. Phys. J. Plus* **136,** 180. arXiv: 2009.05459 [gr-qc] (2021).

140. Cao, L.-M. & Wu, L.-B. On the "Einstein–Gauss–Bonnet gravity in four dimension". *Eur. Phys. J. C* **82,** 124. arXiv: 2103.09612 [gr-qc] (2022).

141. Lu, H. & Pang, Y. Horndeski gravity as $D \to 4$ limit of Gauss-Bonnet. *Phys. Lett. B* **809,** 135717. arXiv: 2003.11552 [gr-qc] (2020).

142. Fernandes, P. G. S., Carrilho, P., Clifton, T. & Mulryne, D. J. Derivation of Regularized Field Equations for the Einstein-Gauss-Bonnet Theory in Four Dimensions. *Phys. Rev. D* **102,** 024025. arXiv: 2004.08362 [gr-qc] (2020).

143. Hennigar, R. A., Kubizňák, D., Mann, R. B. & Pollack, C. On taking the D $\to$ 4 limit of Gauss-Bonnet gravity: theory and solutions. *JHEP* **07,** 027. arXiv: 2004.09472 [gr-qc] (2020).

144. Aoki, K., Gorji, M. A. & Mukohyama, S. A consistent theory of $D \to 4$ Einstein-Gauss-Bonnet gravity. *Phys. Lett. B* **810,** 135843. arXiv: 2005.03859 [gr-qc] (2020).

145. Fernandes, P. G. S. Gravity with a generalized conformal scalar field: Theory and solutions. *Phys. Rev. D* **103,** 104065. https://link.aps.org/doi/10.1103/PhysRevD.103.104065 (2021).

146. Rovelli, C. *Quantum Gravity* (Cambridge University Press, 2004).

147. Thiemann, T. *Modern Canonical Quantum General Relativity* (Cambridge University Press, 2007).

148. Gambini, R. & Pullin, J. *A First Course in Loop Quantum Gravity* (Oxford University Press, 2011).

149. Ashtekar, A. New Variables for Classical and Quantum Gravity. *Phys. Rev. Lett.* **57,** 2244–2247. https://link.aps.org/doi/10.1103/PhysRevLett.57.2244 (1986).

150. Ashtekar, A. & Singh, P. Loop Quantum Cosmology: A Status Report. *Class. Quant. Grav.* **28,** 213001. arXiv: 1108.0893 [gr-qc] (2011).

151. Thebault, K. P. Y. Big bang singularity resolution in quantum cosmology. *Class. Quant. Grav.* **40,** 055007. arXiv: 2209.05905 [gr-qc] (2023).

152. Perez, A. The Spin Foam Approach to Quantum Gravity. *Living Rev. Rel.* **16,** 3. arXiv: 1205.2019 [gr-qc] (2013).

153. Baratin, A. & Oriti, D. Ten questions on Group Field Theory (and their tentative answers). *J. Phys. Conf. Ser.* **360** (eds Mena Marugan, G. A., Barbero, J. F. G., Garay, L. J., Villasenor, E. J. S. & Olmedo, J.) 012002. arXiv: 1112.3270 [gr-qc] (2012).

154. Modesto, L. The Kantowski-Sachs space-time in loop quantum gravity. *Int. J. Theor. Phys.* **45,** 2235–2246. arXiv: gr-qc/0411032 (2006).

155. Ashtekar, A. & Bojowald, M. Quantum geometry and the Schwarzschild singularity. *Class. Quant. Grav.* **23,** 391–411. arXiv: gr-qc/0509075 (2006).

156. Modesto, L. Black hole interior from loop quantum gravity. *Adv. High Energy Phys.* **2008,** 459290. arXiv: gr-qc/0611043 (2008).

157. Dreyer, O. *et al.* Black hole spectroscopy: Testing general relativity through gravitational wave observations. *Class. Quant. Grav.* **21,** 787–804. arXiv: gr-qc/0309007 (2004).

158. Regge, T. & Wheeler, J. A. Stability of a Schwarzschild singularity. *Phys. Rev.* **108,** 1063–1069 (1957).

159. Zerilli, F. J. Gravitational Field of a Particle Falling in a Schwarzschild Geometry Analyzed in Tensor Harmonics. *Phys. Rev. D* **2,** 2141–2160. https://link.aps.org/doi/10.1103/PhysRevD.2.2141 (1970).

160. Vishveshwara, C. V. Scattering of Gravitational Radiation by a Schwarzschild Black-hole. *Nature* **227,** 936–938 (1970).

161. Kokkotas, K. D. & Schmidt, B. G. Quasinormal modes of stars and black holes. *Living Rev. Rel.* **2,** 2. arXiv: gr-qc/9909058 (1999).

162. Nollert, H.-P. Quasinormal modes: the characteristic 'sound' of black holes and neutron stars. *Classical and Quantum Gravity* **16,** R159 –R216. https://api.semanticscholar.org/CorpusID:123577194 (1999).

163. Pani, P. Advanced Methods in Black-Hole Perturbation Theory. *Int. J. Mod. Phys. A* **28** (eds Cardoso, V., Gualtieri, L., Herdeiro, C. & Sperhake, U.) 1340018. arXiv: 1305.6759 [gr-qc] (2013).

164. Cardoso, V., Dias, O. J. C. & Lemos, J. P. S. Nariai, Bertotti-Robinson and anti-Nariai solutions in higher dimensions. *Phys. Rev. D* **70,** 024002. arXiv: hep-th/0401192 (2004).

165. Vanzo, L. & Zerbini, S. Asymptotics of quasinormal modes for multihorizon black holes. *Phys. Rev. D* **70,** 044030. arXiv: hep-th/0402103 (2004).

166. Poschl, G. & Teller, E. Bemerkungen zur Quantenmechanik des anharmonischen Oszillators. *Z. Phys.* **83,** 143–151 (1933).

167. Burgess, C. P. & Lutken, C. A. Propagators and Effective Potentials in Anti-de Sitter Space. *Phys. Lett. B* **153,** 137–141 (1985).

168. Natario, J. & Schiappa, R. On the classification of asymptotic quasinormal frequencies for d-dimensional black holes and quantum gravity. *Adv. Theor. Math. Phys.* **8,** 1001–1131. arXiv: hep-th/0411267 (2004).

169. Cardoso, V. & Lemos, J. P. S. Scalar, electromagnetic and Weyl perturbations of BTZ black holes: Quasinormal modes. *Phys. Rev. D* **63,** 124015. arXiv: gr-qc/0101052 (2001).

170. Aros, R., Martinez, C., Troncoso, R. & Zanelli, J. Quasinormal modes for massless topological black holes. *Phys. Rev. D* **67,** 044014. arXiv: hep-th/0211024 (2003).

171. Birmingham, D. & Mokhtari, S. Exact Gravitational Quasinormal Frequencies of Topological Black Holes. *Phys. Rev. D* **74,** 084026. arXiv: hep-th/0609028 (2006).

172. Schutz, B. F. & Will, C. M. Black hole normal modes - A semianalytic approach. **291,** L33–L36 (1985).

173. Iyer, S. & Will, C. M. Black-hole normal modes: A WKB approach. I. Foundations and application of a higher-order WKB analysis of potential-barrier scattering. *Phys. Rev. D* **35,** 3621–3631. https://link.aps.org/doi/10.1103/PhysRevD.35.3621 (1987).

174. Iyer, S. Black-hole normal modes: A WKB approach. II. Schwarzschild black holes. *Phys. Rev. D* **35,** 3632–3636. https://link.aps.org/doi/10.1103/PhysRevD.35.3632 (1987).

175. Konoplya, R. A. Quasinormal behavior of the d-dimensional Schwarzschild black hole and higher order WKB approach. *Phys. Rev. D* **68,** 024018. arXiv: gr-qc/0303052 (2003).

176. Matyjasek, J. & Opala, M. Quasinormal modes of black holes: The improved semianalytic approach. *Phys. Rev. D* **96,** 024011. https://link.aps.org/doi/10.1103/PhysRevD.96.024011 (2017).

177. Andersson, N. On the asymptotic distribution of quasinormal-mode frequencies for Schwarzschild black holes. *Classical and Quantum Gravity* **10,** L61. https://dx.doi.org/10.1088/0264-9381/10/6/001 (1993).

178. Andersson, N. & Linnæus, S. Quasinormal modes of a Schwarzschild black hole: Improved phase-integral treatment. *Phys. Rev. D* **46,** 4179 (1992).

179. Andersson, N. Scattering of massless scalar waves by a Schwarzschild black hole: A Phase integral study. *Phys. Rev. D* **52,** 1808–1820 (1995).

180. Froeman, N., Froeman, P. O., Andersson, N. & Hoekback, A. Black hole normal modes: Phase integral treatment. *Phys. Rev. D* **45,** 2609–2616 (1992).

181. Motl, L. & Neitzke, A. Asymptotic black hole quasinormal frequencies. *Adv. Theor. Math. Phys.* **7,** 307–330. arXiv: hep-th/0301173 (2003).

182. Keshet, U. & Neitzke, A. Asymptotic spectroscopy of rotating black holes. *Phys. Rev. D* **78,** 044006. arXiv: 0709.1532 [hep-th] (2008).

183. Kao, H.-c. & Tomino, D. Quasinormal Modes of Kerr Black Holes in Four and Higher Dimensions. *Phys. Rev. D* **77,** 127503. arXiv: 0801.4195 [gr-qc] (2008).

184. Cardoso, V., Natario, J. & Schiappa, R. Asymptotic quasinormal frequencies for black holes in nonasymptotically flat space-times. *J. Math. Phys.* **45,** 4698–4713. arXiv: hep-th/0403132 (2004).

185. Horowitz, G. T. & Hubeny, V. E. Quasinormal modes of AdS black holes and the approach to thermal equilibrium. *Phys. Rev. D* **62,** 024027. arXiv: hep-th/9909056 (2000).

186. Cardoso, V. & Lemos, J. P. S. Quasinormal modes of Schwarzschild anti-de Sitter black holes: Electromagnetic and gravitational perturbations. *Phys. Rev. D* **64,** 084017. arXiv: gr-qc/0105103 (2001).

187. Starinets, A. O. Quasinormal modes of near extremal black branes. *Phys. Rev. D* **66,** 124013. arXiv: hep-th/0207133 (2002).

188. Berti, E., Cardoso, V. & Pani, P. Breit-Wigner resonances and the quasinormal modes of anti-de Sitter black holes. *Phys. Rev. D* **79,** 101501. arXiv: 0903.5311 [gr-qc] (2009).

189. Leaver, E. W. An Analytic representation for the quasi normal modes of Kerr black holes. *Proc. Roy. Soc. Lond. A* **402,** 285–298 (1985).

190. Leaver, E. W. Solutions to a generalized spheroidal wave equation: Teukolsky's equations in general relativity, and the two-center problem in molecular quantum mechanics. *J. Math. Phys.* **27,** 1238 (1986).

191. Leaver, E. W. Spectral decomposition of the perturbation response of the Schwarzschild geometry. *Phys. Rev. D* **34,** 384–408 (1986).

192. Goebel, C. J. Comments on the "vibrations" of a Black Hole. *ApJ172* (L95 1972).

193. Ferrari, V. & Mashhoon, B. New approach to the quasinormal modes of a black hole. *Phys. Rev. D* **30,** 295–304 (1984).

194. Ferrari, V. & Mashhoon, B. Oscillations of a Black Hole. *Phys. Rev. Lett.* **52,** 1361 (1984).

195. Mashhoon, B. Stability of charged rotating black holes in the eikonal approximation. *Phys. Rev. D* **31,** 290–293 (1985).

196. Yang, H. *et al.* Quasinormal-mode spectrum of Kerr black holes and its geometric interpretation. *Phys. Rev. D* **86,** 104006. arXiv: 1207.4253 [gr-qc] (2012).

197. Dolan, S. R. The Quasinormal Mode Spectrum of a Kerr Black Hole in the Eikonal Limit. *Phys. Rev. D* **82,** 104003. arXiv: 1007.5097 [gr-qc] (2010).

198. Cardoso, V., Miranda, A. S., Berti, E., Witek, H. & Zanchin, V. T. Geodesic stability, Lyapunov exponents and quasinormal modes. *Phys. Rev. D* **79,** 064016. arXiv: 0812.1806 [hep-th] (2009).

199. Bryant, A., Silva, H. O., Yagi, K. & Glampedakis, K. Eikonal quasinormal modes of black holes beyond general relativity. III. Scalar Gauss-Bonnet gravity. *Phys. Rev. D* **104,** 044051. arXiv: 2106.09657 [gr-qc] (2021).

200. Glampedakis, K., Pappas, G., Silva, H. O. & Berti, E. Post-Kerr black hole spectroscopy. *Phys. Rev. D* **96,** 064054. arXiv: 1706.07658 [gr-qc] (2017).

201. Glampedakis, K. & Silva, H. O. Eikonal quasinormal modes of black holes beyond General Relativity. *Phys. Rev. D* **100,** 044040. arXiv: 1906.05455 [gr-qc] (2019).

202. Silva, H. O. & Glampedakis, K. Eikonal quasinormal modes of black holes beyond general relativity. II. Generalized scalar-tensor perturbations. *Phys. Rev. D* **101,** 044051. arXiv: 1912.09286 [gr-qc] (2020).

203. Kimura, M. Note on the parametrized black hole quasinormal ringdown formalism. *Phys. Rev. D* **101,** 064031. arXiv: 2001.09613 [gr-qc] (2020).

204. Konoplya, R. A. Further clarification on quasinormal modes/circular null geodesics correspondence. *Phys. Lett. B* **838,** 137674. arXiv: 2210.08373 [gr-qc] (2023).

205. Konoplya, R. A. & Stuchlík, Z. Are eikonal quasinormal modes linked to the unstable circular null geodesics? *Phys. Lett. B* **771,** 597–602. arXiv: 1705.05928 [gr-qc] (2017).

206. Matamala, A., Gutierrez, F. & Díaz-Valdés, J. A connection between the asymptotic iteration method and the continued fractions formalism. *Physics Letters A* **361,** 16–17. ISSN: 0375-9601. https://www.sciencedirect.com/science/article/pii/S0375960106014101 (2007).

207. Barakat, T., Abodayeh, K., Abdallah, B. & Al-Dossary, O. M. The asymptotic iteration method for the angular spheroidal eigenvalues with arbitrary complex size parameter c. *Canadian Journal of Physics* **84,** 121–129. https://doi.org/10.1139/p06-007 (2006).

208. Cho, H. T., Cornell, A. S., Doukas, J. & Naylor, W. Black hole quasinormal modes using the asymptotic iteration method. *Class. Quant. Grav.* **27,** 155004. arXiv: 0912.2740 [gr-qc] (2010).

209. Saad, N., Hall, R. L. & Ciftci, H. Asymptotic iteration method for eigenvalue problems. *J. Phys. A* **36,** 11807 (2003).

210. Özer, O. & Roy, P. The asymptotic iteration method applied to certain quasinormal modes and non Hermitian systems. *Central European Journal of Physics* **7,** 747–752 (2009).

211. Cho, H. T., Cornell, A. S., Doukas, J., Huang, T. R. & Naylor, W. A New Approach to Black Hole Quasinormal Modes: A Review of the Asymptotic Iteration Method. *Adv. Math. Phys.* **2012,** 281705. arXiv: 1111.5024 [gr-qc] (2012).

212. Ciftci, H., Hall, R. L. & Saad, N. Perturbation theory in a framework of iteration methods. *Phys. Lett. A* **340,** 388–396. arXiv: math-ph/0504056 (2005).

213. Ciftci, H., Hall, R. L. & Saad, N. Asymptotic iteration method for eigenvalue problems. *Journal of Physics A: Mathematical and General* **36,** 11807. https://dx.doi.org/10.1088/0305-4470/36/47/008 (2003).

214. Chandrasekhar, S. & Detweiler, S. L. The quasi-normal modes of the Schwarzschild black hole. *Proc. Roy. Soc. Lond. A* **344,** 441–452 (1975).

215. Davis, M., Ruffini, R., Press, W. H. & Price, R. H. Gravitational radiation from a particle falling radially into a schwarzschild black hole. *Phys. Rev. Lett.* **27,** 1466–1469 (1971).

216. Bachelot, A. & Motet-Bachelot, A. The Resonances of a Schwarzschild black hole. (In French). *Ann. Inst. H. Poincare Phys. Theor.* **59,** 3–68 (1993).

217. Krivan, W., Laguna, P. & Papadopoulos, P. Dynamics of scalar fields in the background of rotating black holes. *Phys. Rev. D* **54,** 4728–4734. arXiv: gr-qc/9606003 (1996).

218. Krivan, W., Laguna, P., Papadopoulos, P. & Andersson, N. Dynamics of perturbations of rotating black holes. *Phys. Rev. D* **56,** 3395–3404. arXiv: gr-qc/9702048 (1997).

219. Pretorius, F. Evolution of binary black hole spacetimes. *Phys. Rev. Lett.* **95,** 121101. arXiv: gr-qc/0507014 (2005).

220. Baker, J. G., Centrella, J., Choi, D.-I., Koppitz, M. & van Meter, J. Gravitational wave extraction from an inspiraling configuration of merging black holes. *Phys. Rev. Lett.* **96,** 111102. arXiv: gr-qc/0511103 (2006).

221. Campanelli, M., Lousto, C. O., Marronetti, P. & Zlochower, Y. Accurate evolutions of orbiting black-hole binaries without excision. *Phys. Rev. Lett.* **96,** 111101. arXiv: gr-qc/0511048 (2006).

222. Dorband, E. N., Berti, E., Diener, P., Schnetter, E. & Tiglio, M. A Numerical study of the quasinormal mode excitation of Kerr black holes. *Phys. Rev. D* **74,** 084028. arXiv: gr-qc/0608091 (2006).

223. Cook, G. B. Aspects of multimode Kerr ringdown fitting. *Phys. Rev. D* **102,** 024027. arXiv: 2004.08347 [gr-qc] (2020).

224. Giesler, M., Isi, M., Scheel, M. A. & Teukolsky, S. Black Hole Ringdown: The Importance of Overtones. *Phys. Rev. X* **9,** 041060. arXiv: 1903.08284 [gr-qc] (2019).

225. Jiménez Forteza, X., Bhagwat, S., Pani, P. & Ferrari, V. Spectroscopy of binary black hole ringdown using overtones and angular modes. *Phys. Rev. D* **102,** 044053. arXiv: 2005.03260 [gr-qc] (2020).

226. Forteza, X. J., Bhagwat, S., Kumar, S. & Pani, P. Novel Ringdown Amplitude-Phase Consistency Test. *Phys. Rev. Lett.* **130,** 021001. arXiv: 2205.14910 [gr-qc] (2023).

227. Berti, E., Cardoso, V., González, J. A. & Sperhake, U. Mining information from binary black hole mergers: A comparison of estimation methods for complex exponentials in noise. *Phys. Rev. D* **75,** 124017. https://link.aps.org/doi/10.1103/PhysRevD.75.124017 (2007).

228. Cardoso, V., Lemos, J. P. S. & Yoshida, S. Quasinormal modes and stability of the rotating acoustic black hole: Numerical analysis. *Phys. Rev. D* **70,** 124032. https://link.aps.org/doi/10.1103/PhysRevD.70.124032 (2004).

229. Matyjasek, J. & Telecka, M. Quasinormal modes of black holes. II. Padé summation of the higher-order WKB terms. *Phys. Rev. D* **100,** 124006. arXiv: 1908.09389 [gr-qc] (2019).

230. Konoplya, R. A., Zhidenko, A. & Zinhailo, A. F. Higher order WKB formula for quasinormal modes and grey-body factors: recipes for quick and accurate calculations. *Class. Quant. Grav.* **36,** 155002. arXiv: 1904.10333 [gr-qc] (2019).

231. Chirenti, C. B. M. H. & Rezzolla, L. How to tell a gravastar from a black hole. *Class. Quant. Grav.* **24,** 4191–4206. arXiv: 0706.1513 [gr-qc] (2007).

232. Fernando, S. Bardeen-de Sitter black holes. *Int. J. Mod. Phys. D* **26,** 1750071. arXiv: 1611.05337 [gr-qc] (2017).

233. Toshmatov, B., Stuchlík, Z., Schee, J. & Ahmedov, B. Quasinormal frequencies of black hole in the braneworld. *Phys. Rev. D* **93,** 124017. arXiv: 1605.02058 [gr-qc] (2016).

234. Konoplya, R. A. & Zhidenko, A. Passage of radiation through wormholes of arbitrary shape. *Phys. Rev. D* **81,** 124036. https://link.aps.org/doi/10.1103/PhysRevD.81.124036 (2010).

235. Konoplya, R. A. & Zhidenko, A. Holographic conductivity of zero temperature superconductors. *Phys. Lett. B* **686,** 199–206. arXiv: 0909.2138 [hep-th] (2010).

236. Mazur, P. O. & Mottola, E. Gravitational vacuum condensate stars. *Proc. Nat. Acad. Sci.* **101,** 9545–9550. arXiv: gr-qc/0407075 (2004).

237. Lunin, O. & Mathur, S. D. AdS / CFT duality and the black hole information paradox. *Nucl. Phys. B* **623,** 342–394. arXiv: hep-th/0109154 (2002).

238. Skenderis, K. & Taylor, M. The fuzzball proposal for black holes. *Phys. Rept.* **467,** 117–171. arXiv: 0804.0552 [hep-th] (2008).

239. Almheiri, A., Marolf, D., Polchinski, J. & Sully, J. Black Holes: Complementarity or Firewalls? *JHEP* **02,** 062. arXiv: 1207.3123 [hep-th] (2013).

240. Saravani, M., Afshordi, N. & Mann, R. B. Empty black holes, firewalls, and the origin of Bekenstein–Hawking entropy. *Int. J. Mod. Phys. D* **23,** 1443007. arXiv: 1212.4176 [hep-th] (2015).

241. Cardoso, V., Franzin, E. & Pani, P. Is the gravitational-wave ringdown a probe of the event horizon? *Phys. Rev. Lett.* **116.** [Erratum: Phys.Rev.Lett. 117, 089902 (2016)], 171101. arXiv: 1602.07309 [gr-qc] (2016).

242. Cardoso, V., Hopper, S., Macedo, C. F. B., Palenzuela, C. & Pani, P. Gravitational-wave signatures of exotic compact objects and of quantum corrections at the horizon scale. *Phys. Rev. D* **94,** 084031. arXiv: 1608.08637 [gr-qc]. https://link.aps.org/doi/10.1103/PhysRevD.94.084031 (2016).

243. Cardoso, V. & Pani, P. Tests for the existence of black holes through gravitational wave echoes. *Nature Astron.* **1,** 586–591. arXiv: 1709.01525 [gr-qc] (2017).

244. Saraswat, K. & Afshordi, N. Quantum Nature of Black Holes: Fast Scrambling versus Echoes. *JHEP* **04,** 136. arXiv: 1906.02653 [hep-th] (2020).

245. Maggio, E., Buoninfante, L., Mazumdar, A. & Pani, P. How does a dark compact object ringdown? *Phys. Rev. D* **102,** 064053. https://link.aps.org/doi/10.1103/PhysRevD.102.064053 (2020).

246. Mark, Z., Zimmerman, A., Du, S. M. & Chen, Y. A recipe for echoes from exotic compact objects. *Phys. Rev. D* **96,** 084002. https://link.aps.org/doi/10.1103/PhysRevD.96.084002 (2017).

247. Konoplya, R. A., Stuchlík, Z. & Zhidenko, A. Echoes of compact objects: New physics near the surface and matter at a distance. *Phys. Rev. D* **99,** 024007. https://link.aps.org/doi/10.1103/PhysRevD.99.024007 (2019).

248. Micchi, L. F. L. & Chirenti, C. Spicing up the recipe for echoes from exotic compact objects: Orbital differences and corrections in rotating backgrounds. *Phys. Rev. D* **101,** 084010. https://link.aps.org/doi/10.1103/PhysRevD.101.084010 (2020).

249. Bronnikov, K. A. & Konoplya, R. A. Echoes in brane worlds: Ringing at a black hole-wormhole transition. *Phys. Rev. D* **101,** 064004. https://link.aps.org/doi/10.1103/PhysRevD.101.064004 (2020).

250. Dong, R. & Stojkovic, D. Gravitational wave echoes from black holes in massive gravity. *Phys. Rev. D* **103,** 024058. https://link.aps.org/doi/10.1103/PhysRevD.103.024058 (2021).

251. Dey, R., Chakraborty, S. & Afshordi, N. Echoes from braneworld black holes. *Phys. Rev. D* **101,** 104014. https://link.aps.org/doi/10.1103/PhysRevD.101.104014 (2020).

252. Dey, R., Biswas, S. & Chakraborty, S. Ergoregion instability and echoes for braneworld black holes: Scalar, electromagnetic, and gravitational perturbations. *Phys. Rev. D* **103,** 084019. https://link.aps.org/doi/10.1103/PhysRevD.103.084019 (2021).

253. Agullo, I., Cardoso, V., del Rio, A., Maggiore, M. & Pullin, J. Potential Gravitational Wave Signatures of Quantum Gravity. *Phys. Rev. Lett.* **126,** 041302. https://link.aps.org/doi/10.1103/PhysRevLett.126.041302 (2021).

254. Chakravarti, K., Ghosh, R. & Sarkar, S. Signature of nonuniform area quantization on black hole echoes. *Phys. Rev. D* **105,** 044046. https://link.aps.org/doi/10.1103/PhysRevD.105.044046 (2022).

255. Coates, A., Völkel, S. H. & Kokkotas, K. D. On black hole area quantization and echoes. *Class. Quant. Grav.* **39,** 045007. arXiv: 2201.03245 [gr-qc] (2022).

256. Abedi, J., Dykaar, H. & Afshordi, N. Echoes from the Abyss: Tentative evidence for Planck-scale structure at black hole horizons. *Phys. Rev. D* **96,** 082004. arXiv: 1612.00266 [gr-qc] (2017).

257. Abedi, J. & Afshordi, N. Echoes from the Abyss: A Status Update. arXiv: 2001.00821 [gr-qc] (2020).

258. Holdom, B. Not quite black holes at LIGO. *Phys. Rev. D* **101,** 064063. arXiv: 1909.11801 [gr-qc] (2020).

259. Conklin, R. S., Holdom, B. & Ren, J. Gravitational wave echoes through new windows. *Phys. Rev. D* **98,** 044021. arXiv: 1712.06517 [gr-qc] (2018).

260. Abedi, J., Dykaar, H. & Afshordi, N. Comment on: "Low significance of evidence for black hole echoes in gravitational wave data". arXiv: 1803.08565 [gr-qc]. 10.48550/arXiv.1803.08565 (2018).

261. Abedi, J., Dykaar, H. & Afshordi, N. Echoes from the Abyss: The Holiday Edition! arXiv: 1701.03485 [gr-qc] (2017).

262. Abedi, J. & Afshordi, N. Echoes from the Abyss: A highly spinning black hole remnant for the binary neutron star merger GW170817. *JCAP* **11,** 010. arXiv: 1803.10454 [gr-qc] (2019).

263. Westerweck, J. *et al.* Low significance of evidence for black hole echoes in gravitational wave data. *Phys. Rev. D* **97,** 124037. arXiv: 1712.09966 [gr-qc] (2018).

264. Wang, Y.-T. & Piao, Y.-S. Searching for gravitational wave echoes in GWTC-1 and O3 events. arXiv: 2010.07663 [gr-qc] (2020).

265. Tsang, K. W. *et al.* A morphology-independent search for gravitational wave echoes in data from the first and second observing runs of Advanced LIGO and Advanced Virgo. *Phys. Rev. D* **101,** 064012. arXiv: 1906.11168 [gr-qc] (2020).

266. Lo, R. K. L., Li, T. G. F. & Weinstein, A. J. Template-based Gravitational-Wave Echoes Search Using Bayesian Model Selection. *Phys. Rev. D* **99,** 084052. arXiv: 1811.07431 [gr-qc] (2019).

267. Synge, J. L. The Escape of Photons from Gravitationally Intense Stars. *Monthly Notices of the Royal Astronomical Society* **131,** 463–466. ISSN: 0035-8711. eprint: https://academic.oup.com/mnras/article-pdf/131/3/463/8076763/mnras131-0463.pdf (1966).

268. Luminet, J. P. Image of a spherical black hole with thin accretion disk. *Astronomy and Astrophysics* **75,** 228–235. https://adsabs.harvard.edu/full/1979A%26A....75..228L (1979).

269. Bardeen, J. M. Timelike and null geodesics in the Kerr metric. *Proceedings, Ecole d'Eté de Physique Théorique: Les Astres Occlus : Les Houches, France, August, 1972, 215-240* (eds DeWitt, C. & DeWitt, B. S.) 215–240 (1973).

270. Bisnovatyi-Kogan, G. S. & Tsupko, O. Y. Gravitational Lensing in Presence of Plasma: Strong Lens Systems, Black Hole Lensing and Shadow. *Universe* **3.** ISSN: 2218-1997. https://www.mdpi.com/2218-1997/3/3/57 (2017).

271. Janis, A. I., Newman, E. T. & Winicour, J. Reality of the Schwarzschild Singularity. *Phys. Rev. Lett.* **20,** 878–880 (1968).

272. Chakraborty, M. & Chakraborty, S. Traversable Wormholes and their shadows in 4D Einstein–Gauss–Bonnet Gravity: An analytic description. *Phys. Dark Univ.* **47,** 101793 (2025).

273. Dey, D., Shaikh, R. & Joshi, P. S. Perihelion precession and shadows near black holes and naked singularities. *Phys. Rev. D* **102,** 044042. arXiv: 2003.06810 [gr-qc] (2020).

274. Dey, D., Shaikh, R. & Joshi, P. S. Shadow of nulllike and timelike naked singularities without photon spheres. *Phys. Rev. D* **103,** 024015. arXiv: 2009.07487 [gr-qc] (2021).

275. Sakai, N., Saida, H. & Tamaki, T. Gravastar Shadows. *Phys. Rev. D* **90,** 104013. arXiv: 1408.6929 [gr-qc] (2014).

276. Rosa, J. a. L. & Rubiera-Garcia, D. Shadows of boson and Proca stars with thin accretion disks. *Phys. Rev. D* **106,** 084004. arXiv: 2204.12949 [gr-qc] (2022).

277. Carter, B. Global structure of the Kerr family of gravitational fields. *Phys. Rev.* **174,** 1559–1571 (1968).

278. Chandrasekhar, S. *The mathematical theory of black holes* ISBN: 978-0-19-850370-5 (1985).

279. Glampedakis, K. & Pappas, G. Modification of photon trapping orbits as a diagnostic of non-Kerr spacetimes. *Phys. Rev. D* **99,** 124041. arXiv: 1806.09333 [gr-qc] (2019).

280. Cunha, P. V. P. & Herdeiro, C. A. R. Stationary Black Holes and Light Rings. *Phys. Rev. Lett.* **124,** 181101. https://link.aps.org/doi/10.1103/PhysRevLett.124.181101 (2020).

281. Wang, M., Chen, S. & Jing, J. Kerr black hole shadows in Melvin magnetic field with stable photon orbits. *Phys. Rev. D* **104,** 084021. arXiv: 2104.12304 [gr-qc] (2021).

282. Cunha, P. V. P., Herdeiro, C. A. R., Radu, E. & Runarsson, H. F. Shadows of Kerr black holes with scalar hair. *Phys. Rev. Lett.* **115,** 211102. arXiv: 1509.00021 [gr-qc] (2015).

283. Vincent, F. H., Gourgoulhon, E., Herdeiro, C. & Radu, E. Astrophysical imaging of Kerr black holes with scalar hair. *Phys. Rev. D* **94,** 084045. arXiv: 1606.04246 [gr-qc] (2016).

284. Cunha, P. V. P. *et al.* Chaotic lensing around boson stars and Kerr black holes with scalar hair. *Phys. Rev. D* **94,** 104023. arXiv: 1609.01340 [gr-qc] (2016).

285. Johannsen, T. Photon Rings around Kerr and Kerr-like Black Holes. *Astrophys. J.* **777,** 170. arXiv: 1501.02814 [astro-ph.HE] (2013).

286. James, O., von Tunzelmann, E., Franklin, P. & Thorne, K. S. Gravitational Lensing by Spinning Black Holes in Astrophysics, and in the Movie Interstellar. *Class. Quant. Grav.* **32,** 065001. arXiv: 1502.03808 [gr-qc] (2015).

287. Doeleman, S. S. *et al.* Reference Array and Design Consideration for the Next-Generation Event Horizon Telescope. *Galaxies* **11.** https://www.mdpi.com/2075-4434/11/5/107 (2023).

288. https://blackholecam.org/.

289. Joshi, A. B., Dey, D., Joshi, P. S. & Bambhaniya, P. Shadow of a Naked Singularity without Photon Sphere. *Phys. Rev. D* **102,** 024022. arXiv: 2004.06525 [gr-qc] (2020).

290. Paul, S. Strong gravitational lensing by a strongly naked null singularity. *Phys. Rev. D* **102,** 064045. arXiv: 2007.05509 [gr-qc] (2020).

291. O, K. Die Reflexion von Elektronen an einem Potentialsprung nach der relativistischen Dynamik von Dirac. *Zeitschrift für Physik* **53,** 157–165. https://doi.org/10.1007/BF01339716 (1929).

292. Penrose, R. & Floyd, R. M. Extraction of Rotational Energy from a Black Hole. *Nature Physical Science* **229,** 177–179. https://doi.org/10.1038/physci229177a0 (1971).

293. Zel'dovich, Y. B. Generation of Waves by a Rotating Body. **14,** 180. https://api.semanticscholar.org/CorpusID:116979665 (1971).

294. Zel'dovich, Y. B. Amplification of Cylindrical Electromagnetic Waves Reflected from a Rotating Body. **35,** 1085–1087. https://api.semanticscholar.org/CorpusID:117203235 (1972).

295. Starobinsky, A. A. Amplification of waves reflected from a rotating "black hole". *Sov. Phys. JETP* **37,** 28–32 (1973).

296. Press, W. H. & Teukolsky, S. A. Floating Orbits, Superradiant Scattering and the Black-hole Bomb. *Nature* **238,** 211–212 (1972).

297. Bekenstein, J. D. & Schiffer, M. The Many faces of superradiance. *Phys. Rev. D* **58,** 064014. arXiv: gr-qc/9803033 (1998).

298. Yagi, K. & Stein, L. C. Black Hole Based Tests of General Relativity. *Class. Quant. Grav.* **33,** 054001. arXiv: 1602.02413 [gr-qc] (2016).

299. Barceló, C., Carballo-Rubio, R. & Garay, L. J. Gravitational wave echoes from macroscopic quantum gravity effects. *JHEP* **05,** 054. arXiv: 1701.09156 [gr-qc] (2017).

300. Oshita, N., Wang, Q. & Afshordi, N. On Reflectivity of Quantum Black Hole Horizons. *JCAP* **04,** 016. arXiv: 1905.00464 [hep-th] (2020).

301. Chakraborty, S., Maggio, E., Mazumdar, A. & Pani, P. Implications of the quantum nature of the black hole horizon on the gravitational-wave ringdown. *Phys. Rev. D* **106,** 024041. arXiv: 2202.09111 [gr-qc] (2022).

302. Wei, S.-W. & Liu, Y.-X. Testing the nature of Gauss-Bonnet gravity by four-dimensional rotating black hole shadow. *Eur. Phys. J. Plus* **136,** 436. arXiv: 2003.07769 [gr-qc] (2021).

303. Kumar, A., Baboolal, D. & Ghosh, S. G. Nonsingular Black Holes in 4D Einstein-Gauss-Bonnet Gravity. *Universe* **8,** 244. arXiv: 2004.01131 [gr-qc] (2022).

304. York Jr., J. W. Dynamical Origin of Black Hole Radiance. *Phys. Rev. D* **28,** 2929 (1983).

305. Dreyer, O. Quasinormal Modes, the Area Spectrum, and Black Hole Entropy. *Phys. Rev. Lett.* **90,** 081301. https://link.aps.org/doi/10.1103/PhysRevLett.90.081301 (2003).

306. Corichi, A. On quasinormal modes, black hole entropy, and quantum geometry. *Phys. Rev. D* **67,** 087502. arXiv: gr-qc/0212126 (2003).

307. Oppenheim, J. The Spectrum of quantum black holes and quasinormal modes. *Phys. Rev. D* **69,** 044012. arXiv: gr-qc/0307089 (2004).

308. Ling, Y. & Zhang, H.-b. Quasinormal modes prefer supersymmetry? *Phys. Rev. D* **68,** 101501. arXiv: gr-qc/0309018 (2003).

309. Wei, S.-W., Li, R., Liu, Y.-X. & Ren, J.-R. Quantization of Black Hole Entropy from Quasinormal Modes. *JHEP* **03,** 076. arXiv: 0901.0587 [hep-th] (2009).

310. Medved, A. J. M. On the Kerr Quantum Area Spectrum. *Class. Quant. Grav.* **25,** 205014. arXiv: 0804.4346 [gr-qc] (2008).

311. Vagenas, E. C. Area spectrum of rotating black holes via the new interpretation of quasinormal modes. *JHEP* **11,** 073. arXiv: 0804.3264 [gr-qc] (2008).

312. Koutsoumbas, G., Musiri, S., Papantonopoulos, E. & Siopsis, G. Quasi-normal Modes of Electromagnetic Perturbations of Four-Dimensional Topological Black Holes with Scalar Hair. *JHEP* **10,** 006. arXiv: hep-th/0606096 (2006).

313. Shen, J., Wang, B., Lin, C.-Y., Cai, R.-G. & Su, R.-K. The phase transition and the Quasi-Normal Modes of black Holes. *JHEP* **07,** 037. arXiv: hep-th/0703102 (2007).

314. Rao, X.-P., Wang, B. & Yang, G.-H. Quasinormal modes and phase transition of black holes. *Phys. Lett. B* **649,** 472–477. arXiv: 0712.0645 [gr-qc] (2007).

315. Myung, Y. S. Phase transition for black holes with scalar hair and topological black holes. *Phys. Lett. B* **663,** 111–117. arXiv: 0801.2434 [hep-th] (2008).

316. Koutsoumbas, G., Papantonopoulos, E. & Siopsis, G. Phase Transitions in Charged Topological-AdS Black Holes. *JHEP* **05,** 107. arXiv: 0801.4921 [hep-th] (2008).

317. Koutsoumbas, G., Papantonopoulos, E. & Siopsis, G. Discontinuities in Scalar Perturbations of Topological Black Holes. *Class. Quant. Grav.* **26,** 105004. arXiv: 0806.1452 [hep-th] (2009).

318. Kay, B. S. & Wald, R. M. Linear Stability of Schwarzschild Under Perturbations Which Are Nonvanishing on the Bifurcation Two Sphere. *Class. Quant. Grav.* **4,** 893–898 (1987).

319. Whiting, B. F. Mode Stability of the Kerr Black Hole. *J. Math. Phys.* **30,** 1301 (1989).

320. Maldacena, J. M. & Strominger, A. Black hole grey body factors and d-brane spectroscopy. *Phys. Rev. D* **55,** 861–870. arXiv: hep-th/9609026 (1997).

321. Kanti, P. & March-Russell, J. Calculable corrections to brane black hole decay. 2. Greybody factors for spin 1/2 and 1. *Phys. Rev. D* **67,** 104019. arXiv: hep-ph/0212199 (2003).

322. Chowdhury, A. & Banerjee, N. Echoes from a singularity. *Phys. Rev. D* **102,** 124051. https://link.aps.org/doi/10.1103/PhysRevD.102.124051 (2020).

323. Liu, Q.-X., Hu, Y.-P., Sui, T.-T. & An, Y.-S. Superradiance of rotating black holes surrounded by dark matter. *Phys. Dark Univ.* **46,** 101624. arXiv: 2406.04611 [gr-qc] (2024).

324. Hod, S. Bohr's Correspondence Principle and the Area Spectrum of Quantum Black Holes. *Phys. Rev. Lett.* **81,** 4293–4296. https://link.aps.org/doi/10.1103/PhysRevLett.81.4293 (1998).

325. Maggiore, M. Physical Interpretation of the Spectrum of Black Hole Quasinormal Modes. *Phys. Rev. Lett.* **100,** 141301. https://link.aps.org/doi/10.1103/PhysRevLett.100.141301 (2008).

326. Abbott, B. P. *et al.* Tests of General Relativity with GW150914. *Phys. Rev. Lett.* **116,** 221101. https://link.aps.org/doi/10.1103/PhysRevLett.116.221101 (2016).

327. Konoplya, R. & Zhidenko, A. Detection of gravitational waves from black holes: Is there a window for alternative theories? *Phys. Lett. B* **756,** 350–353. arXiv: 1602.04738 [gr-qc] (2016).

328. Berti, E., Yagi, K., Yang, H. & Yunes, N. Extreme gravity tests with gravitational waves from compact binary coalescences: (II) ringdown. *General Relativity and Gravitation* **50.** ISSN: 1572-9532. http://dx.doi.org/10.1007/s10714-018-2372-6 (2018).

329. Miskovic, O. & Olea, R. Topological regularization and self-duality in four-dimensional anti-de Sitter gravity. *Phys. Rev. D* **79,** 124020. arXiv: 0902.2082 [hep-th] (2009).

330. Araneda, R., Aros, R., Miskovic, O. & Olea, R. Magnetic Mass in 4D AdS Gravity. *Phys. Rev. D* **93,** 084022. arXiv: 1602.07975 [hep-th] (2016).

331. Shu, F.-W. Vacua in novel 4D Einstein-Gauss-Bonnet Gravity: pathology and instability? *Phys. Lett. B* **811,** 135907. arXiv: 2004.09339 [gr-qc] (2020).

332. Sengupta, S. 4D Einstein-Gauss-Bonnet gravity from non-Einsteinian phase. *JCAP* **02,** 020. arXiv: 2109.10388 [gr-qc] (2022).

333. Riess, A. G. *et al.* Observational Evidence from Supernovae for an Accelerating Universe and a Cosmological Constant. **116,** 1009–1038. arXiv: astro-ph/9805201 [astro-ph] (1998).

334. Riess, A. G. *et al.* Observational evidence from supernovae for an accelerating universe and a cosmological constant. *Astron. J.* **116,** 1009–1038. arXiv: astro-ph/9805201 (1998).

335. Zehavi, I. & Dekel, A. Constraints on the cosmological constant from flows and supernovae. *Nature* **401,** 252. arXiv: astro-ph/9904221 (1999).

336. Brill, D. R. & Wheeler, J. A. Interaction of Neutrinos and Gravitational Fields. *Rev. Mod. Phys.* **29,** 465–479. https://link.aps.org/doi/10.1103/RevModPhys.29.465 (1957).

337. Darboux, G. On a proposition relative to linear equations. *arXiv e-prints,* physics/9908003. arXiv: physics/9908003 [physics.hist-ph] (1999).

338. Glampedakis, K., Johnson, A. D. & Kennefick, D. Darboux transformation in black hole perturbation theory. *Phys. Rev. D* **96,** 024036. arXiv: 1702.06459 [gr-qc] (2017).

339. Kodama, H. Uniqueness and stability of higher dimensional black holes. *J. Korean Phys. Soc.* **45,** S68–S76. arXiv: hep-th/0403030 (2004).

340. Zinhailo, A. F. Quasinormal modes of Dirac field in the Einstein-Dilaton-Gauss-Bonnet and Einstein-Weyl gravities. *Eur. Phys. J. C* **79,** 912. arXiv: 1909.12664 [gr-qc] (2019).

341. Konoplya, R. A. & Churilova, M. S. Non-evident stability of a Dirac field in Schwarzschild-de Sitter spacetime. arXiv: 2004.05879 [gr-qc] (2020).

342. Kodama, H. & Ishibashi, A. Master equations for perturbations of generalized static black holes with charge in higher dimensions. *Prog. Theor. Phys.* **111,** 29–73. arXiv: hep-th/0308128 (2004).

343. Jansen, A. Overdamped modes in Schwarzschild-de Sitter and a Mathematica package for the numerical computation of quasinormal modes. *Eur. Phys. J. Plus* **132,** 546. arXiv: 1709.09178 [gr-qc] (2017).

344. Lopez-Ortega, A. Quasinormal modes of D-dimensional de Sitter spacetime. *Gen. Rel. Grav.* **38,** 1565–1591. arXiv: gr-qc/0605027 (2006).

345. Aragón, A., González, P. A., Papantonopoulos, E. & Vásquez, Y. Anomalous decay rate of quasinormal modes in Schwarzschild-dS and Schwarzschild-AdS black holes. *JHEP* **08,** 120. arXiv: 2004.09386 [gr-qc] (2020).

346. Datt, B. On a Class of Solutions of the Gravitation Equations of Relativity. *General Relativity and Gravitation* **31,** 1619–1627. https://doi.org/10.1023/A:1026742707143 (1999).

347. Oppenheimer, J. R. & Snyder, H. On Continued Gravitational Contraction. *Phys. Rev.* **56,** 455–459. https://link.aps.org/doi/10.1103/PhysRev.56.455 (1939).

348. Joshi, P. S. *Gravitational Collapse and Spacetime Singularities* ISBN: 978-1-107-40536-3, 978-0-521-87104-4, 978-0-511-37283-4 (Cambridge University Press, 2012).

349. Joshi, P. S. *The Story of Collapsing Stars: Black Holes, Naked Singularities, and the Cosmic Play of Quantum Gravity* ISBN: 978-0-19-968676-6, 978-0-19-881887-8, 978-0-19-927233-4 (Oxford University Press, 2018).

350. Gyulchev, G., Nedkova, P., Vetsov, T. & Yazadjiev, S. Image of the thin accretion disk around compact objects in the Einstein–Gauss–Bonnet gravity. *Eur. Phys. J. C* **81,** 885. arXiv: 2106.14697 [gr-qc] (2021).

351. Cai, R.-G., Cao, L.-M. & Ohta, N. Black Holes in Gravity with Conformal Anomaly and Logarithmic Term in Black Hole Entropy. *JHEP* **04,** 082. arXiv: 0911.4379 [hep-th] (2010).

352. Cognola, G., Myrzakulov, R., Sebastiani, L. & Zerbini, S. Einstein gravity with Gauss-Bonnet entropic corrections. *Phys. Rev. D* **88,** 024006. https://link.aps.org/doi/10.1103/PhysRevD.88.024006 (2013).

353. Fernandes, P. G. S., Carrilho, P., Clifton, T. & Mulryne, D. J. Black holes in the scalar-tensor formulation of 4D Einstein-Gauss-Bonnet gravity: Uniqueness of solutions, and a new candidate for dark matter. *Phys. Rev. D* **104,** 044029. https://link.aps.org/doi/10.1103/PhysRevD.104.044029 (2021).

354. Virbhadra, K. S. & Ellis, G. F. R. Gravitational lensing by naked singularities. *Phys. Rev. D* **65,** 103004. https://link.aps.org/doi/10.1103/PhysRevD.65.103004 (2002).

355. Wald, R. M. Dynamics in nonglobally hyperbolic static space-times. *J. Math. Phys.* **21** (1980).

356. Ishibashi, A. & Hosoya, A. Who's afraid of naked singularities? Probing timelike singularities with finite energy waves. *Phys. Rev. D* **60,** 104028. https://link.aps.org/doi/10.1103/PhysRevD.60.104028 (1999).

357. Ishibashi, A. & Wald, R. M. Dynamics in non-globally-hyperbolic static spacetimes: II. General analysis of prescriptions for dynamics. *Classical and Quantum Gravity* **20,** 3815. https://dx.doi.org/10.1088/0264-9381/20/16/318 (2003).

358. Ishibashi, A. & Wald, R. M. Dynamics in non-globally-hyperbolic static spacetimes: III. Anti-de Sitter spacetime. *Classical and Quantum Gravity* **21,** 2981. https://dx.doi.org/10.1088/0264-9381/21/12/012 (2004).

359. Cardoso, V. & Cavaglià, M. Stability of naked singularities and algebraically special modes. *Phys. Rev. D* **74,** 024027. https://link.aps.org/doi/10.1103/PhysRevD.74.024027 (2006).

360. Horowitz, G. T. & Marolf, D. Quantum probes of spacetime singularities. *Phys. Rev. D* **52,** 5670–5675. https://link.aps.org/doi/10.1103/PhysRevD.52.5670 (1995).

361. Svítek, O., Tahamtan, T. & Zampeli, A. Quantum fate of timelike naked singularity with scalar hair. *Annals of Physics* **418,** 168195. ISSN: 0003-4916. https://www.sciencedirect.com/science/article/pii/S0003491620301287 (2020).

362. Gundlach, C., Price, R. H. & Pullin, J. Late-time behavior of stellar collapse and explosions. I. Linearized perturbations. *Phys. Rev. D* **49,** 883–889. https://link.aps.org/doi/10.1103/PhysRevD.49.883 (1994).

363. Gleiser, R. J. & Dotti, G. Instability of the negative mass Schwarzschild naked singularity. *Classical and Quantum Gravity* **23,** 5063. https://dx.doi.org/10.1088/0264-9381/23/15/021 (2006).

364. Dotti, G. & Gleiser, R. J. The initial value problem for linearized gravitational perturbations of the Schwarzschild naked singularity. *Classical and Quantum Gravity* **26,** 215002. https://dx.doi.org/10.1088/0264-9381/26/21/215002 (2009).

365. Cardoso, V., Crispino, L. C. B., Macedo, C. F. B., Okawa, H. & Pani, P. Light rings as observational evidence for event horizons: Long-lived modes, ergoregions and nonlinear instabilities of ultracompact objects. *Phys. Rev. D* **90,** 044069. https://link.aps.org/doi/10.1103/PhysRevD.90.044069 (4 2014).

366. Harada, T. *et al.* Naked singularities and quantum gravity. *Phys. Rev. D* **64,** 041501. https://link.aps.org/doi/10.1103/PhysRevD.64.041501 (2001).

367. Liu, Y., Malafarina, D., Modesto, L. & Bambi, C. Singularity avoidance in quantum-inspired inhomogeneous dust collapse. *Phys. Rev. D* **90,** 044040. https://link.aps.org/doi/10.1103/PhysRevD.90.044040 (2014).

368. Kiefer, C. & Schmitz, T. Singularity avoidance for collapsing quantum dust in the Lemaître-Tolman-Bondi model. *Phys. Rev. D* **99,** 126010. https://link.aps.org/doi/10.1103/PhysRevD.99.126010 (2019).

369. Chirenti, C., Saa, A. & Skákala, J. No asymptotically highly damped quasinormal modes without horizons? *Phys. Rev. D* **87,** 044034. https://link.aps.org/doi/10.1103/PhysRevD.87.044034 (2013).

370. Akiyama, K. *et al.* First Sagittarius A* Event Horizon Telescope Results. I. The Shadow of the Supermassive Black Hole in the Center of the Milky Way. *Astrophys. J. Lett.* **930,** L12. arXiv: 2311.08680 [astro-ph.HE] (2022).

371. Hioki, K. & Maeda, K.-i. Measurement of the Kerr spin parameter by observation of a compact object's shadow. *Phys. Rev. D* **80,** 024042. https://link.aps.org/doi/10.1103/PhysRevD.80.024042 (2009).

372. Virbhadra, K. S. Relativistic images of Schwarzschild black hole lensing. *Phys. Rev. D* **79,** 083004. https://link.aps.org/doi/10.1103/PhysRevD.79.083004 (2009).

373. Amir, M. & Ghosh, S. G. Shapes of rotating nonsingular black hole shadows. *Phys. Rev. D* **94,** 024054. https://link.aps.org/doi/10.1103/PhysRevD.94.024054 (2016).

374. Perlick, V., Tsupko, O. Y. & Bisnovatyi-Kogan, G. S. Black hole shadow in an expanding universe with a cosmological constant. *Phys. Rev. D* **97,** 104062. arXiv: 1804.04898 [gr-qc] (2018).

375. Khodadi, M. Shadow of black hole surrounded by magnetized plasma: Axion-plasmon cloud. *Nucl. Phys. B* **985,** 116014. arXiv: 2211.00300 [gr-qc] (2022).

376. Amarilla, L., Eiroa, E. F. & Giribet, G. Null geodesics and shadow of a rotating black hole in extended Chern-Simons modified gravity. *Phys. Rev. D* **81,** 124045. https://link.aps.org/doi/10.1103/PhysRevD.81.124045 (2010).

377. Grenzebach, A., Perlick, V. & Lämmerzahl, C. Photon regions and shadows of Kerr-Newman-NUT black holes with a cosmological constant. *Phys. Rev. D* **89,** 124004. https://link.aps.org/doi/10.1103/PhysRevD.89.124004 (2014).

378. Atamurotov, F., Abdujabbarov, A. & Ahmedov, B. Shadow of rotating non-Kerr black hole. *Phys. Rev. D* **88,** 064004. https://link.aps.org/doi/10.1103/PhysRevD.88.064004 (2013).

379. Papnoi, U., Atamurotov, F., Ghosh, S. G. & Ahmedov, B. Shadow of five-dimensional rotating Myers-Perry black hole. *Phys. Rev. D* **90,** 024073. https://link.aps.org/doi/10.1103/PhysRevD.90.024073 (2014).

380. Konoplya, R. A., Pappas, T. & Zhidenko, A. Einstein-scalar–Gauss-Bonnet black holes: Analytical approximation for the metric and applications to calculations of shadows. *Phys. Rev. D* **101,** 044054. https://link.aps.org/doi/10.1103/PhysRevD.101.044054 (2020).

381. Antoniou, G., Papageorgiou, A. & Kanti, P. Probing Modified Gravity Theories with Scalar Fields Using Black-Hole Images. *Universe* **9,** 147. arXiv: 2210.17533 [gr-qc] (2023).

382. Zakharov, A. F. Constraints on a charge in the Reissner-Nordström metric for the black hole at the Galactic Center. *Phys. Rev. D* **90,** 062007. https://link.aps.org/doi/10.1103/PhysRevD.90.062007 (2014).

383. Tamburini, F., Thidé, B. & Della Valle, M. Measurement of the spin of the M87 black hole from its observed twisted light. *Monthly Notices of the Royal Astronomical Society: Letters* **492,** L22–L27. ISSN: 1745-3925. https://doi.org/10.1093/mnrasl/slz176 (2019).

384. Vagnozzi, S. *et al.* Horizon-scale tests of gravity theories and fundamental physics from the Event Horizon Telescope image of Sagittarius A. *Class. Quant. Grav.* **40,** 165007. arXiv: 2205.07787 [gr-qc] (2023).

385. Afrin, M., Vagnozzi, S. & Ghosh, S. G. Tests of Loop Quantum Gravity from the Event Horizon Telescope Results of Sgr A*. *Astrophys. J.* **944,** 149. arXiv: 2209.12584 [gr-qc] (2023).

386. Vagnozzi, S. & Visinelli, L. Note on Fundamental Physics Tests from Black Hole Imaging: Comment on. *Research Notes of the AAS* **6,** 106. https://dx.doi.org/10.3847/2515-5172/ac7331 (2022).

387. Mishra, A. K., Chakraborty, S. & Sarkar, S. Understanding photon sphere and black hole shadow in dynamically evolving spacetimes. *Phys. Rev. D* **99,** 104080. arXiv: 1903.06376 [gr-qc] (2019).

388. Vagnozzi, S. & Visinelli, L. Hunting for extra dimensions in the shadow of M87*. *Phys. Rev. D* **100,** 024020. arXiv: 1905.12421 [gr-qc] (2019).

389. Bambi, C., Freese, K., Vagnozzi, S. & Visinelli, L. Testing the rotational nature of the supermassive object M87* from the circularity and size of its first image. *Phys. Rev. D* **100,** 044057. arXiv: 1904.12983 [gr-qc] (2019).

390. Psaltis, D. Testing General Relativity with the Event Horizon Telescope. *Gen. Rel. Grav.* **51,** 137. arXiv: 1806.09740 [astro-ph.HE] (2019).

391. Younsi, Z., Zhidenko, A., Rezzolla, L., Konoplya, R. & Mizuno, Y. New method for shadow calculations: Application to parametrized axisymmetric black holes. *Phys. Rev. D* **94,** 084025. https://link.aps.org/doi/10.1103/PhysRevD.94.084025 (2016).

392. Chang, Z. & Zhu, Q.-H. Revisiting a rotating black hole shadow with astrometric observables. *Phys. Rev. D* **101,** 084029. https://link.aps.org/doi/10.1103/PhysRevD.101.084029 (2020).

393. Konoplya, R. Quantum corrected black holes: Quasinormal modes, scattering, shadows. *Physics Letters B* **804,** 135363. ISSN: 0370-2693. https://www.sciencedirect.com/science/article/pii/S0370269320301672 (2020).

394. Liu, C. *et al.* Shadow and quasinormal modes of a rotating loop quantum black hole. *Phys. Rev. D* **101.** [Erratum: Phys.Rev.D 103, 089902 (2021)], 084001. arXiv: 2003.00477 [gr-qc] (2020).

395. Kumar Walia, R. Observational predictions of LQG motivated polymerized black holes and constraints from Sgr A* and M87*. *JCAP* **03,** 029. arXiv: 2207.02106 [gr-qc] (2023).

396. Tsupko, O. Y., Fan, Z. & Bisnovatyi-Kogan, G. S. Black hole shadow as a standard ruler in cosmology. *Class. Quant. Grav.* **37,** 065016. arXiv: 1905.10509 [gr-qc] (2020).

397. Vagnozzi, S., Bambi, C. & Visinelli, L. Concerns regarding the use of black hole shadows as standard rulers. *Class. Quant. Grav.* **37,** 087001. arXiv: 2001.02986 [gr-qc] (2020).

398. Gyulchev, G., Nedkova, P., Vetsov, T. & Yazadjiev, S. Image of the Janis-Newman-Winicour naked singularity with a thin accretion disk. *Phys. Rev. D* **100,** 024055. arXiv: 1905.05273 [gr-qc] (2019).

399. Abdikamalov, A. B. *et al.* Black hole mimicker hiding in the shadow: Optical properties of the γ metric. *Phys. Rev. D* **100,** 024014. arXiv: 1904.06207 [gr-qc] (2019).

400. Bardeen, J. M. *Proceedings of the International Conference GR5* 1968.

401. Dymnikova, I. Vacuum nonsingular black hole. *Gen. Rel. Grav.* **24,** 235–242 (1992).

402. Mars, M., Martín-Prats, M. M. & Senovilla, J. M. M. Models of regular Schwarzschild black holes satisfying weak energy conditions. *Classical and Quantum Gravity* **13,** L51. https://dx.doi.org/10.1088/0264-9381/13/5/003 (1996).

403. Bogojević, A. & Stojković, D. Nonsingular black hole. *Phys. Rev. D* **61,** 084011. https://link.aps.org/doi/10.1103/PhysRevD.61.084011 (2000).

404. Hayward, S. A. Formation and Evaporation of Nonsingular Black Holes. *Phys. Rev. Lett.* **96,** 031103. https://link.aps.org/doi/10.1103/PhysRevLett.96.031103 (2006).

405. Daghigh, R. G., Green, M. D. & Kunstatter, G. Scalar Perturbations and Stability of a Loop Quantum Corrected Kruskal Black Hole. *Phys. Rev. D* **103,** 084031. arXiv: 2012.13359 [gr-qc] (2021).

406. Khodadi, M., Talebian, A. & Firouzjahi, H. Black Hole Superradiance in f(R) Gravities. arXiv: 2002.10496 [gr-qc] (2020).

407. Franzin, E., Liberati, S. & Oi, M. Superradiance in Kerr-like black holes. *Phys. Rev. D* **103,** 104034. arXiv: 2102.03152 [gr-qc] (2021).

408. Khodadi, M. & Pourkhodabakhshi, R. Superradiance and stability of Kerr black hole enclosed by anisotropic fluid matter. *Phys. Lett. B* **823,** 136775. arXiv: 2111.03316 [gr-qc] (2021).

409. Richarte, M. G., Martins, E. L. & Fabris, J. C. Scattering and absorption of a scalar field impinging on a charged black hole in the Einstein-Maxwell-dilaton theory. *Phys. Rev. D* **105,** 064043. arXiv: 2111.01595 [gr-qc] (2022).

410. Alexander, S., Gabadadze, G., Jenks, L. & Yunes, N. Black hole superradiance in dynamical Chern-Simons gravity. *Phys. Rev. D* **107,** 084016. arXiv: 2201.02220 [gr-qc] (2023).

411. Mascher, G., Destounis, K. & Kokkotas, K. D. Charged black holes in de Sitter space: Superradiant amplification of charged scalar waves and resonant hyperradiation. *Phys. Rev. D* **105,** 084052. arXiv: 2204.05335 [gr-qc] (2022).

412. Ishii, T., Kaku, Y. & Murata, K. Energy extraction from AdS black holes via superradiance. *JHEP* **10,** 024. arXiv: 2207.03123 [hep-th] (2022).

413. Jha, S. K. & Rahaman, A. Superradiance scattering off rotating Simpson-Visser black hole and its shadow in the non-commutative setting. arXiv: 2208.13176 [gr-qc] (2022).

414. Chen, Y., Roy, R., Vagnozzi, S. & Visinelli, L. Superradiant evolution of the shadow and photon ring of Sgr A⋆. *Phys. Rev. D* **106,** 043021. arXiv: 2205.06238 [astro-ph.HE] (2022).

415. Chen, W.-X. & Zheng, Y.-G. The superradiant stability of Kerr-Newman black holes. arXiv: 2103.04239 [gr-qc] (2021).

416. Cuadros-Melgar, B., Fontana, R. D. B. & de Oliveira, J. Superradiance and instabilities in black holes surrounded by anisotropic fluids. *Phys. Rev. D* **104,** 104039. arXiv: 2108.04864 [gr-qc] (2021).

417. Vyas, R. P. & Joshi, M. J. The Barbero–Immirzi Parameter: An Enigmatic Parameter of Loop Quantum Gravity. *Physics* **4,** 1094–1116. arXiv: 2206.00458 [gr-qc] (2022).

418. Newman, E. T. *et al.* Metric of a Rotating, Charged Mass. *J. Math. Phys.* **6,** 918–919 (1965).

419. Canonico, R., Parisi, L. & Vilasi, G. The Newman Janis Algorithm: A Review of Some Results. *Proc. Geom. Int. Quant.* **12** (eds Mladenov, I., Vilasi, G. & Yoshiokoa, A.) 159–169 (2011).

420. Drake, S. P. & Turolla, R. The Application of the Newman-Janis algorithm in obtaining interior solutions of the Kerr metric. *Class. Quant. Grav.* **14,** 1883–1897. arXiv: gr-qc/9703084 (1997).

421. Frolov, V. & Zelnikov, A. *Introduction to Black Hole Physics* (Oxford University Press, UK, 2011).

422. T.Padmanabhan. *Gravitation* ISBN: 9780511807787 (Cambridge University Press, 2010).

423. Brito, R., Cardoso, V. & Pani, P. *Superradiance* (Springer, 2020).

424. Teukolsky, S. A. Rotating Black Holes: Separable Wave Equations for Gravitational and Electromagnetic Perturbations. *Phys. Rev. Lett.* **29,** 1114–1118. https://link.aps.org/doi/10.1103/PhysRevLett.29.1114 (1972).

425. Teukolsky, S. A. Perturbations of a rotating black hole. 1. Fundamental equations for gravitational electromagnetic and neutrino field perturbations. *Astrophys. J.* **185,** 635–647. https://ui.adsabs.harvard.edu/abs/1973ApJ...185..635T (1973).

426. *Mathematica Notebook on horizons and allowed parameter space* https://www.dropbox.com/sh/t1v9wqs2hdzkr10/AADdd8OGLzmGcNnOavQhr4OMa?dl=0.

427. Hansen, D. & Yunes, N. Applicability of the Newman-Janis Algorithm to Black Hole Solutions of Modified Gravity Theories. *Phys. Rev. D* **88,** 104020. arXiv: 1308.6631 [gr-qc] (2013).

428. Gambini, R., Olmedo, J. & Pullin, J. Quantum black holes in Loop Quantum Gravity. *Class. Quant. Grav.* **31,** 095009. arXiv: 1310.5996 [gr-qc] (2014).

429. Haggard, H. M. & Rovelli, C. Quantum-gravity effects outside the horizon spark black to white hole tunneling. *Phys. Rev. D* **92,** 104020. arXiv: 1407.0989 [gr-qc] (2015).

430. Gambini, R. & Pullin, J. Hawking radiation from a spherical loop quantum gravity black hole. *Class. Quant. Grav.* **31,** 115003. arXiv: 1312.3595 [gr-qc] (2014).

431. Newman, E. & Penrose, R. An Approach to gravitational radiation by a method of spin coefficients. *J. Math. Phys.* **3,** 566–578 (1962).

432. Press, W. H. & Teukolsky, S. A. Perturbations of a Rotating Black Hole. II. Dynamical Stability of the Kerr Metric. *Astrophys. J.* **185,** 649–674 (1973).

433. Kerr, R. P. Gravitational Field of a Spinning Mass as an Example of Algebraically Special Metrics. *Phys. Rev. Lett.* **11,** 237–238. https://link.aps.org/doi/10.1103/PhysRevLett.11.237 (1963).

434. Maggiore, M. *et al.* Science Case for the Einstein Telescope. *JCAP* **03,** 050. arXiv: 1912.02622 [astro-ph.CO] (2020).

435. Amaro-Seoane, P. *et al.* Laser Interferometer Space Antenna. arXiv: 1702.00786 [astro-ph.IM] (2017).

436. Bambi, C. & Stojkovic, D. Astrophysical Wormholes. *Universe* **7,** 136. arXiv: 2105.00881 [gr-qc] (2021).

437. Shaikh, R., Kocherlakota, P., Narayan, R. & Joshi, P. S. Shadows of spherically symmetric black holes and naked singularities. *Mon. Not. Roy. Astron. Soc.* **482,** 52–64. arXiv: 1802.08060 [astro-ph.HE] (2019).

438. Kardashev, N. S., Novikov, I. & Shatskiy, A. Astrophysics of Wormholes. *International Journal of Modern Physics D* **16,** 909–926. https://doi.org/10.1142/S0218271807010481 (2007).

439. Nandi, K. K., Zhang, Y.-Z. & Zakharov, A. V. Gravitational lensing by wormholes. *Phys. Rev. D* **74,** 024020. https://link.aps.org/doi/10.1103/PhysRevD.74.024020 (2006).

440. *Wolfram Mathworld - Binomial Coefficient (Equation 5)* https://mathworld.wolfram.com/BinomialCoefficient.html.